



TESIS DOCTORAL

2019

NANOSCALE HYDRODYNAMICS  
NEAR SOLIDS

DIEGO DUQUE ZUMAJO

PROGRAMA DE DOCTORADO EN CIENCIAS

DIRECTOR: DR. PEP ESPAÑOL GARRIGÓS





DOCTORAL DISSERTATION AT THE DEPARTMENT OF FUNDAMENTAL PHYSICS IN THE FACULTY OF SCIENCE, UNIVERSIDAD NACIONAL DE EDUCACIÓN A DISTANCIA.

**Title:** Nanoscale hydrodynamics near solids.

**Author:** Diego Duque Zumajo.

**Director:** Dr. Pep Español Garrigós.

TESIS DOCTORAL PRESENTADA EN EL DEPARTAMENTO DE FÍSICA FUNDAMENTAL DE LA UNIVERSIDAD NACIONAL DE EDUCACIÓN A DISTANCIA.

**Título:** Hidrodinámica cerca de sólidos en la nanoescala.

**Autor:** Diego Duque Zumajo.

**Director:** Dr. Pep Español Garrigós.



*To those who in the last months perceived my loneliness as my absence,  
and my self-absortion as my presence.*



# Acknowledgments

Only when you finish the job to which you have dedicated the last four years, is the moment to look back and remember why you are in front of a laptop writing these lines. I would like to show my gratitude to the people who not only have supported me but also inspired me to start and end this dissertation.

To my parents and my sister for respecting my independence and encouraging me when I needed to change the direction my life was going in. Thank you for giving me that little book of astronomy which sparked my curiosity about space and, years later, my love for physics. Thanks to my father for taking my messy ideas and putting them in the cover of this dissertation. To my family for being an example of humility and critical thinking.

I would like to express my particular thanks to my thesis supervisor, Pep Español, for giving me the opportunity to live not only a period of incredible learning but also one of the most exciting of my life. Without your work, patience and persistency this dissertation would have never been finished. Thank you for transmitting your ideas about how science must be done and for pushing until the end even though the results seemed to turn against us.

My appreciation to Arturo for keeping the door of his office always open to my concerns and technical issues. Thank you for understanding my priorities as if they were your own. Without your “sons”, Bruno and Grodd, I would still be waiting for the simulations to be completed.

To Manu because he phoned me when he saw the FPI grant in the lift of the faculty. Thank you very much for helping me to take my first steps with Python and for our conversations about books, politics, films and series that dressed lunchtime along the first three years.

I would like to show my gratitude to my colleagues of the Fundamental Physics department, especially to those who covered me the last February when I was totally absorbed in this dissertation. To the heterogeneous group of the canteen because our discussions about any topic helped me to forget the troubles that awaited me in the office.

## VIII

---

Thanks to Marc for all his suggestions and English corrections in the Introduction and Chapter 1.

To my friends. From the first day they have followed the progress of my thesis despite the distance that modern life imposes. It has been said that real friends are made before your thirties [1]. I am very glad to have met you before.

To the people who have enjoyed the mountains with me. To those who were before and the ones who are now. To La Pedriza, my playground at weekends; to your slab walls and your approaches between rock roses and psychedelic granite stones; to the intricate paths which have been witnesses of innumerable races, running days and some falls. To the music bands that have made milder *the loneliness of the long distance runner*.

To my cats, Yuri and Igor, whose unconditional love and mischiefs made me happier in the sleepless nights and the crazy days.

Finally, to Claudia. Thanks not only for being by my side in the good moments but also for encouraging me in the bad ones. Thank you very much for being my partner in this life, the biggest and most beautiful mountain we have ever climbed. Now it is time for another adventure that I hope will make us have such a good time as all those we have lived together.

# Contents

<b>0</b>	<b>Introduction</b>	<b>1</b>
<b>1</b>	<b>Nonequilibrium Statistical Mechanics</b>	<b>9</b>
1.1	Introduction . . . . .	9
1.2	Hamilton's equations and the evolution of the microstates . . . . .	11
1.2.1	Hamilton's equations in operator form . . . . .	12
1.3	The Liouville theorem . . . . .	13
1.4	The Theory of Coarse-Graining and the CG variables . . . . .	15
1.4.1	Quasi-equilibrium and separation of timescales . . . . .	16
1.5	Molecular Dynamics simulations . . . . .	17
1.6	The entropy . . . . .	18
1.7	The dynamics . . . . .	21
1.7.1	The Kawasaki-Gunton projection operator . . . . .	22
1.7.2	Mori's Generalized Langevin equation . . . . .	24
1.8	Summary . . . . .	30
<b>2</b>	<b>Nanoscale hydrodynamics theory for liquids near solids</b>	<b>31</b>
2.1	Introduction . . . . .	31
2.1.1	Nonlocal hydrodynamics . . . . .	33
2.1.2	Fluid-solid interactions . . . . .	33
2.2	The system and the relevant variables . . . . .	35
2.2.1	The relevant variables . . . . .	36
2.2.2	The time derivatives of the relevant variables . . . . .	36
2.3	The relevant ensemble and the grand potential . . . . .	39
2.4	The free energy . . . . .	42
2.5	The transport equations . . . . .	45
2.5.1	Exact reversible dynamics . . . . .	46

2.5.2	Markovian irreversible dynamics . . . . .	48
2.6	The final equations of nanohydrodynamics . . . . .	51
2.6.1	Conserved quantities, $H$ -theorem and the equilibrium state . .	52
2.6.2	Approximating the relevant ensemble averages and projected currents . . . . .	54
2.7	Summary . . . . .	55
<b>3</b>	<b>Discrete hydrodynamics near solids for planar flows</b>	<b>59</b>
3.1	Introduction . . . . .	59
3.2	Simpler theory . . . . .	60
3.3	The discrete basis function set . . . . .	62
3.4	The discrete hydrodynamics equations derived with the Kawasaki-Gunton projector . . . . .	65
3.4.1	The time derivatives . . . . .	66
3.4.2	Exact reversible part of the dynamics . . . . .	69
3.4.3	Approximate reversible dynamics . . . . .	70
3.4.4	Irreversible part of the dynamics . . . . .	72
3.4.5	The final discretized equations . . . . .	74
3.4.6	Symmetry assumptions . . . . .	74
3.4.7	Normal and tangent evolution . . . . .	75
3.5	A finite element discretization . . . . .	76
3.5.1	The free energy . . . . .	78
3.5.2	The transport kernels . . . . .	79
3.6	Summary . . . . .	81
<b>4</b>	<b>Space and time locality for unconfined fluids</b>	<b>83</b>
4.1	Introduction . . . . .	83
4.2	A corrected Green-Kubo formula with no plateau problem . . . . .	86
4.3	Mori theory for shear hydrodynamics . . . . .	89
4.3.1	The CG variables . . . . .	89
4.3.2	The Green-Kubo running integral $M(t)$ . . . . .	90
4.3.3	The friction matrix $M^*$ and the nonlocal shear viscosity matrix	92
4.3.4	Fourier space . . . . .	93
4.3.5	The nonlocal kinematic viscosity matrix $\nu^*$ . . . . .	96
4.3.6	The equations for the average . . . . .	97
4.3.7	The local in time prediction . . . . .	98
4.3.8	The local in space prediction . . . . .	99
4.4	Summary of the theory and strategy in the simulations . . . . .	100
4.5	Simulations . . . . .	101

4.5.1	Simulation set up . . . . .	101
4.5.2	The correlation matrix $C(t)$ . . . . .	102
4.5.3	Validation of the Markov property . . . . .	105
4.5.4	The Green-Kubo nonlocal viscosity matrix . . . . .	108
4.6	Summary . . . . .	112
<b>5</b>	<b>Markovian behaviour near solids</b>	<b>115</b>
5.1	Introduction . . . . .	115
5.2	The CG variables and its dynamics . . . . .	116
5.3	Simulations . . . . .	119
5.3.1	Simulation set up . . . . .	119
5.3.2	Thin bins with $\Delta z = 0.5\sigma$ . . . . .	120
5.3.3	Thick bins with $\Delta z = 2\sigma$ . . . . .	124
5.4	Summary . . . . .	129
<b>6</b>	<b>The slip boundary condition</b>	<b>133</b>
6.1	Introduction . . . . .	133
6.2	The CG variables . . . . .	134
6.2.1	Time derivatives . . . . .	135
6.2.2	Correlation matrices . . . . .	135
6.3	The dynamics of the discrete transverse momentum . . . . .	136
6.4	Simulation setup . . . . .	140
6.5	The transport matrices . . . . .	141
6.6	Evolution of the flow in NEMD simulations . . . . .	143
6.7	The slip boundary condition . . . . .	147
6.7.1	Mechanical balance on a slab near wall . . . . .	147
6.7.2	The boundary condition . . . . .	150
6.7.3	The microscopic expression for the slip length . . . . .	153
6.7.4	Validation of the slip boundary condition . . . . .	158
6.8	A local hydrodynamic model with boundary conditions . . . . .	160
6.9	Summary . . . . .	164
<b>7</b>	<b>Conclusions</b>	<b>169</b>
<b>8</b>	<b>Future Directions</b>	<b>173</b>
<b>Appendix A</b>	<b>Contributions</b>	<b>187</b>
<b>Appendix B</b>	<b>Forces</b>	<b>189</b>

<b>Appendix C The projected currents</b>	<b>193</b>
<b>Appendix D Details of the derivation of discrete hydrodynamics</b>	<b>199</b>
D.1 The relevant ensemble and the entropy . . . . .	199
D.2 Momentum integration . . . . .	201
D.3 The exact reversible part of the dynamics . . . . .	203
D.4 The approximate form of the reversible part of the dynamics . . . . .	206
D.5 The connection between the free energy functional and the free energy function . . . . .	209
<b>Appendix E Isotropic fourth order tensors</b>	<b>213</b>
<b>Appendix F The covariance</b>	<b>215</b>
<b>Appendix G The continuum and thermodynamic limits</b>	<b>217</b>
<b>Appendix H Force on the boundary slab</b>	<b>219</b>
<b>Appendix I List of Acronyms</b>	<b>221</b>
<b>Appendix J List of symbols and variables</b>	<b>223</b>
<b>List of figures</b>	<b>225</b>
<b>List of tables</b>	<b>229</b>

# Abstract

This dissertation studies the behaviour of a fluid in contact with a solid in the nanoscale. Theoretical formulations of non-local continuum and discrete hydrodynamics are presented in which the interaction of the solid with the fluid appears explicitly in terms of extended forces on the fluid, confined to the vicinity of the solid object. The discrete theory is validated through MD simulations, where we encounter the plateau problem in the determination of the transport coefficients. We offer a method that solves the problem and allows us to evaluate the transport coefficients unambiguously. In the course of the MD investigation we find that the Markovian assumption implicit in the theoretical derivations is not satisfied near the wall when the hydrodynamics is resolved at molecular scales. However, for sufficiently large bins in which the discrete hydrodynamic variables are defined the behaviour is fully Markovian. The final outcome of the present dissertation is the derivation of the slip boundary condition from the microscopically formulated discrete hydrodynamic theory. The slip length and the position of the wall are defined through Green-Kubo formulas and seen to coincide with the original proposal of Bocquet and Barrat. We test the validity of the slip boundary condition thus obtained in a particularly challenging flow, an initial plug flow that is discontinuous near the wall at initial stages of the flow. We observe that the slip boundary condition is violated at the initial stages of the flow and we explain the reasons for this failure.

More specifically, we derive, using the Theory of Coarse-Graining (ToCG), the equations of motion of a fluid in contact with a solid sphere of large dimensions compared to molecular scales. We use the Kawasaki-Gunton projection operator technique which leads to a set of nonlinear equations for the relevant variables of the system. We assume the Markovian approximation in order to obtain a set of memoryless equations. We address the well-known plateau problem that appears in the expressions of the transport coefficients present in the equations of motion of the fluid in contact with a solid. We solve this problem and we obtain an alternative expression for the transport coefficients without the plateau problem.

In order to validate the theory and measure the transport coefficients with Molecular

Dynamics (MD) simulations, we derive the discrete equations of motion for a set of discrete hydrodynamic variables. These variables are defined in terms of finite element basis functions based on regular bins constructed by dividing the domain of the fluid with equiespaced parallel planes. The discrete set of hydrodynamic equations are shown to be identical to a Petrov-Galerkin discretization of the continuum equations.

The only assumption made in order to derive the equations of motion of the fluid is the Markovian hypothesis. In order to validate it, we use Mori theory which let us obtain the time evolution of the correlation of the relevant variables of the system. The equations are linear, implying an exponential behaviour of the correlation. We take deviations from exponential decay as an indication of the violation of the Markovian hypothesis.

As a first step to address the problem of Markovianity we study the simpler case of a fluid in periodic boundary conditions (PBC) by performing MD simulations. We monitor the relevant variables of the system and compute their correlations. We realize that is necessary to move to the reciprocal space (i.e. the Fourier space for unconfined fluids) in order to validate the Markovian hypothesis. Only for an exponential decay of the modes of the matrix of correlations we can expect the hypothesis to be valid.

Once the methodology is well established we address the more complicated case of a confined fluid between two solid slabs. We show that if the size of the bin is of the order of the molecular length the Markovian hypothesis fails for modes near the walls. Nevertheless, for large bins the hypothesis is satisfied but the nonlocal effect of layering is lost.

Finally, we derive the slip boundary condition from the theory proposed, by considering mechanical balance within a slab of fluid near the wall, and assuming that the flow field inside this slab is linear. This allows to infer the slip length and the position of the wall where the boundary condition is to be satisfied in microscopic terms, through Green-Kubo expressions. The microscopic expression obtained coincides with the original proposal by Bocquet and Barrat [2]. We demonstrate that the friction coefficient is an intrinsic property of the surface of the solid as it does not depend on the width of the channel.

# Resumen

Esta tesis aborda el estudio del comportamiento de un fluido en contacto con un sólido en la nanoescala. Se presenta una formulación teórica continua no local, así como su versión discreta, en la que la interacción del sólido con el fluido aparece explícitamente en términos de fuerzas confinadas cerca del sólido. La teoría discreta es validada a través de simulaciones de dinámica molecular, en donde nos encontramos con el problema del *plateau* a la hora de determinar los coeficientes de transporte. Con el fin de obtener dichos coeficientes sin el problema del *plateau*, ofrecemos un método alternativo para su obtención. A través de simulaciones de dinámica molecular mostramos que la hipótesis de Markovianidad implícita en la derivación teórica no es satisfecha cerca de la pared del sólido cuando la hidrodinámica es resuelta a escalas moleculares. Sin embargo, para celdas de discretización mayores, en los cuales están definidas las variables de la hidrodinámica discreta, el comportamiento es perfectamente Markoviano. Por último, derivamos la condición de contorno de *slip* partiendo de la formulación microscópica de la teoría hidrodinámica discreta. La longitud de *slip* y la posición de la pared son definidas a través de las fórmulas de Green-Kubo y coincide con la propuesta original de Bocquet y Barrat. Validamos la condición de contorno de *slip* en un fluido tipo *plug flow* que es discontinuo cerca de la pared en sus primeras etapas. Observamos que la condición de contorno de *slip* no se cumple para etapas iniciales del fluido y explicamos las razones de esa inconsistencia.

Más específicamente, empleando la Teoría del *Coarse-Graining* derivamos las ecuaciones de movimiento de un fluido en contacto con una esfera sólida de grandes dimensiones comparada con escalas moleculares. Empleamos la técnica de los operadores de proyección de Kawasaki-Gunton junto con la aproximación Markoviana para obtener un conjunto de ecuaciones no lineales de las variables relevantes del sistema sin términos de memoria. Abordamos el problema del *plateau* que sufren las fórmulas de Green-Kubo presentes en los coeficientes de transporte de las ecuaciones de movimiento del fluido ofreciendo una expresión alternativa de dichas fórmulas sin el problema del *plateau*.

Para validar la teoría y poder medir los coeficientes de transporte mediante simulaciones de dinámica molecular, derivamos las ecuaciones de la nanohidrodinámica a partir de un conjunto de variables hidrodinámicas discretas. Estas variables son definidas en términos de funciones base de elemento finito definidas en celdas regulares construidas mediante la división del dominio del fluido en planos paralelos equiespaciados. El conjunto de ecuaciones discretas obtenido es idéntico al que se obtiene mediante el método de Petrov-Galerkin.

La hipótesis de Markovianidad es la única aproximación realizada para derivar las ecuaciones de la hidrodinámica. Para validarla empleamos la teoría de Mori que nos ofrece una expresión de la evolución temporal de las correlaciones de las variables relevantes del sistema. Se muestra que la hipótesis Markoviana es válida siempre y cuando las correlaciones decaigan de forma exponencial.

Como primer paso para abordar el problema de la Markovianidad estudiamos el caso más sencillo posible, realizando simulaciones de dinámica molecular de un fluido no confinado en las cuales se monitorizan las variables relevantes del sistema con el fin de calcular sus correlaciones temporales. Observamos que para el estudio de la Markovianidad es conveniente trasladarse al espacio recíproco (en el caso de un fluido en condiciones de contorno periódicas se trata del espacio de Fourier) y comprobar si los modos de la matriz de correlaciones decaen o no de forma exponencial.

Tras establecer la metodología adecuada para tratar el problema, realizamos simulaciones de dinámica molecular de un fluido confinado entre dos paredes sólidas. Mostramos que para una anchura de celda del orden de la distancia molecular la hipótesis de Markovianidad no se cumple para los modos cercanos a la pared. Sin embargo, para celdas más anchas la hipótesis es validada a expensas de perder efectos de *layering*.

Finalmente, medimos la condición de contorno de *slip* a partir de una definición microscópica de la longitud de *slip* y de la posición hidrodinámica de la pared atómica. Comprobamos que la expresión obtenida es la ofrecida por Bocquet y Barrat [2] y demostramos que el coeficiente de fricción es una propiedad intrínseca de la superficie puesto que la distancia de *slip* no depende del tamaño del canal empleado.

# Notation, conventions and quotes

Functions of microstates  $z$  in phase space are denoted with a hat as in  $\hat{A}(z)$ . We follow this convention except for probability densities, as in  $\rho_t(z)$ . Operators are denoted with *CALLIGRAPHIC* symbols. Vectors and matrices are denoted with **boldfaces**.

Although we will notice when we use it, we follow Einstein summation convention in which, for example the product of two matrices in components is written as

$$(AB)_{\mu\nu} = A_{\mu\nu}B_{\nu\sigma} = \sum_{\nu} A_{\mu\nu}B_{\nu\sigma}$$

---

The quotes in the beginning of each chapter are taken from books I read over the time I have spent working in this dissertation, the last four years. I have respected the language in which the writer wrote the book.



# **Chapter 0**

## **Introduction**

It was in the December of 1959 when Richard Feynman gave a lecture at the annual American Physical Society meeting at Caltech with the name *There's Plenty of Room at the bottom: An Invitation to Enter a New Field of Physics* [3]. Although there is not unanimity in the scientific community about the real impact of this lecture in the development of the nanotechnology [4], it is considered its date of birth [5]. In the lecture Feynman expresses his intuitive ideas about the world of opportunities that exists when one descents to the micro and nanoscale.

Seven years later, in 1966, Richard Fleischer directed the science fiction film *Fantastic voyage*, based on an original idea of Otto Klement and Jerome Bixby. Six month before the release of the film, Isaac Asimov published the homonymous book [6] inspired by the screenplay of the movie. In both book and movie, a group of scientists, one American intelligence agent, and a pilot are placed inside a submarine called Proteus before being miniaturized to the size of a microbe ( $\sim 0.5\mu m$ ). The objective is to inject Proteus into the body of an important scientist affected by a clot blood in his brain that no traditional surgery can remove. The group will have only one hour before the effect of the miniaturization passes.

As well as in other areas, reality outdoes fiction. Nanothechnology applied to medical devices is a reality. In the last 20 years there has been a rapid increase in the number of nanotechnology patents [7] and there is a huge interest in the development of new nanomaterials to treat and diagnose cancer [8–10].

These advances in miniaturization and the development of new experimental techniques have increased the interest in the theoretical understanding of the behaviour of fluids in the nano [11, 12] and micro [12–14] scales because at nanoscales the structure of the fluid starts to play an important role.

The nanoscale can be studied with Molecular Dynamics (MD) simulations and there is a wealth of literature addressing the behaviour of fluids near walls with MD [15, 16]. The standard description of structured fluids is based on the (classic) Density Functional Theory (DFT) [17], with the density functional capturing all the relevant information about the *equilibrium* state of the fluid. In recent years, there has been a great interest in obtaining *dynamic* versions of the DFT (DDFT) that would allow one to discuss not only equilibrium structured fluids and its correlations but also their dynamic behaviour [18, 19]. Since the pioneering work by Marconi and Tarazona [20] for Brownian dynamics, several approaches have been considered for the formulation of DDFT, ranging from kinetic theory [21], to projection operators [22], and variational approaches [23]. Most existing works deal with colloidal suspensions [19, 24]. However, there still exists a gap in the treatment of the dynamics of *simple* fluids *near solids* at scales where the structure of the fluid is relevant. In particular, two phenomena are observed near walls at the nanoscale. First, the appearance of the density layering capturing the excluded volume effects of single molecules. For equilibrium liquids near walls, DFT has been an exceptionally good theoretical tool for the prediction of these layering effects [25]. Second, the observation that the velocity of fluids may be nonzero near the wall surface. A quite remarkable assumption in macroscopic hydrodynamics is the no slip boundary condition that states that the velocity of the fluid vanishes at the surface of fixed solid walls [26]. This assumption gives the correct predictions for macroscopic flows of Newtonian fluids. However, as the length scale of observation is reduced toward the micro and nanoscale, a large number of experimental [13] and computer simulation studies [15] have shown that the fluid may actually slip along the container walls [12]. The first consideration of this possibility was made by Navier [27], who proposed a boundary condition in which the shear stress is balanced by a friction due to the wall on the fluid, leading to the slip boundary condition. To fix ideas, consider a planar wall at rest in contact with a flowing fluid in a steady state. If there is some slip velocity  $v_{\text{slip}}$  at the wall then the friction force on the wall is assumed to be of the form

$$F^x = -\gamma v_{\text{slip}} \quad (1)$$

The average force  $F^x$  is the total tangential force exerted by the wall on the liquid (equal and opposite to the force that the liquid exerts on the wall). The interfacial friction coefficient  $\gamma$  is a phenomenological transport coefficient. The force  $F^x$ , in turn, is due to the tangential viscous stress due to the fluid  $F^x = -\eta \frac{\partial v}{\partial z}$ , where  $\eta$  is the shear viscosity of the fluid. From the combination of these two equations we obtain the Navier slip boundary condition

$$\delta \frac{\partial v}{\partial z} = v_{\text{slip}}, \quad (2)$$

where the slip length is defined as

$$\delta = \eta / \gamma \quad (3)$$

The slip boundary condition (2) relates the gradient of the velocity field with the velocity field, both evaluated at the surface of the solid. This phenomenological equation introduces both the viscosity and the friction coefficient as parameters to be fitted from experiments.

Of course, one would like to find microscopic expressions for both coefficients that would allow to compute in advance these parameters for the specific fluid and wall interaction of the system. The first calculation from first principles of the friction coefficient between a fluid and a solid wall was undertaken by Bocquet and Barrat in 1994 [2]. These authors used linear response theory in order to derive a Green-Kubo expression for the slip length. Later on, the same authors revisited the problem and offered an argument based on the generalized Langevin equation (GLE), leading to the same expression obtained earlier [28]. Bocquet and Barrat proposed the following expression for the friction coefficient

$$\gamma = \frac{1}{Sk_B T} \int_0^\tau dt \langle \hat{F}^x(t) \hat{F}^x \rangle \quad (4)$$

in terms of the equilibrium autocorrelation function of the parallel component of the microscopic fluctuating force  $\hat{F}^x(t)$  that the liquid exerts on a planar wall of area  $S$ . Equation (4) represents an important step in offering a statistical mechanics foundation of a boundary condition, with a caveat: the friction coefficient as a function of the upper limit of integration does not have a plateau and it decays to zero for large  $\tau$ . However, the formula is still useful when one expresses the force-force correlation in terms of density-density correlations, which are then treated with the well-known hydrodynamic theory of fluctuations. In that case, the hydrodynamic exponential decay assumed for the density-density correlation makes the integral non-vanishing and allows one to get explicit analytical estimates for the slip length [29–32].

The validity of the Bocquet and Barrat approach has been a subject of an ongoing debate [33–35] that we believe has not yet been concluded (see the recent account of the situation of this debate by Ramos-Alvaro et al. [36]). Petravic and Harrowell [33] argued that the Green-Kubo expression given by Bocquet and Barrat is not an intrinsic property of the surface of solid-liquid interaction but rather contains also information about the bulk friction between two parallel plates. It was further argued that the Bocquet and Barrat Green-Kubo formula gives, in fact, the friction force between two parallel plates with a liquid in between and, therefore, depends on the separation between the plates. In this way, the transport coefficient (4) would not be an interfacial friction

coefficient tied to interfacial properties alone. Petravic and Harrowell conclude “that the Navier friction coefficient cannot, in general, be obtained from the surface force time correlation function alone since these fluctuations are coupled to stress fluctuation throughout the entire system”. While Petravic and Harrowell present an indirect Green-Kubo expression for the slip length (for the case of identical parallel walls), the problem was reconsidered by Hansen, Todd, Davis [34] by looking at a GLE involving the force on a fluid slab of width  $\Delta$  near the wall and relating it with the center of mass velocity of the slab through a friction coefficient (a memory kernel in a non-steady state in general). The method is extended to cylindrical geometries also [37]. By running equilibrium molecular dynamics (MD) simulations one can get the friction coefficient and the slip length through the correlation functions of the variables involved. Hansen et al. propose a GLE of the form

$$F'^x(t) = - \int_0^t \zeta(t-\tau) u_{\text{slab}}(\tau) d\tau + F'_r(t) \quad (5)$$

where  $F'^x(t)$  is the force that the solid exerts on the fluid slab,  $u_{\text{slab}}$  is the velocity of the slab (the wall is assumed at rest here),  $\zeta(t-\tau)$  is a memory kernel and  $F'_r(t)$  is a random force. For a steady state, one obtains the average result  $\langle F'^x \rangle = -\zeta_0 \langle u_{\text{slab}} \rangle$ , where  $\zeta_0$  is the zero frequency friction coefficient which is a parameter that can be explicitly measured in MD simulations by comparing correlations inferred from (5). By solving Navier-Stokes equations with integral boundary conditions, Hansen et al. obtain an explicit form for the slip length in terms of  $\zeta_0$ . This coefficient is shown to be independent of channel width and, therefore, it is an intrinsic surface property, as expected for the interfacial friction coefficient.

More recently, Huang and Szufraska propose an *alternative* definition of a friction coefficient [35]. In this case, a GLE for the velocity of a *single liquid particle* is constructed with the Mori projection operator. While comparisons are made with the Bocquet and Barrat expression, claiming superior performance, the truth is that no connection between the obtained friction coefficient of a single particle and the slip length is made in Ref. [35]. The single particle friction coefficient, while interesting for its own sake, does not inform us about the parameter that is crucial in the boundary condition, which is the slip length. However, Bhaduria et al. [38] have used the model in Ref. [35] in order to study parallel flow of water in a confined slit made of graphene and silico. It is obvious that what is called “friction coefficient” depends very much on the variables that are connected with the force on the wall due to the fluid, be it the velocity difference between parallel walls [2, 33], the velocity of a fluid slab [34], or the velocity of a single particle of the fluid [35].

Recently, Chen et al. have revisited the problem of looking at the hydrodynamic modes of a channel between parallel walls [39]. By comparing results of MD simula-

tions and predictions of hydrodynamics they were able to locate the plane of slip, as well as measuring the slip length in the problem as in [2]. In addition, they formulated a Green-Kubo expression for both bulk viscosity and interfacial friction coefficient that, in the limit of very wide channels coincides with Bocquet and Barrat expression. The size dependence of the Bocquet and Barrat Green-Kubo expression disappears in this limit.

In summary, there seem to be three different ways of looking at the derivation of the slip boundary condition from Non Equilibrium Statistical Mechanics (NESM):

1. Through the measurement of the correlation of the transverse momentum and comparison with the predictions of continuum (local) hydrodynamics [39, 40].
2. Through linear response theory relating the force on the walls with the velocity of the fluid [33, 40].
3. By formulating linear, in general non-Markovian, connections between friction forces and velocities [34], where the meaning of these quantities is often understood implicitly.

Given the unclear state of affairs in the derivation of the slip boundary condition, in this dissertation we address the slip problem from first principles. Following the work by Robertson [41] and Piccirelli [42], who derived the hydrodynamic equations from the microscopic dynamics of a fluid, we obtain a set of continuum equations which describe the behaviour of a fluid in contact with a solid with the Markovian approximation as the only assumption. Because the validation of the theory is only possible through MD simulations, we derive the discrete equations with the same methodology as in continuum theory. A cross-check is given using a Petrov-Galerkin finite element discretization method in order to obtain from the continuum equations the resulting discrete equations previously derived. Once we have the discrete equations, we address the study of the Markovian behaviour of the simplest case (i.e. a fluid in periodic boundary conditions). We restrict the study to planar dynamics monitoring only the transverse momentum component. We use the same methodology to study the Markovian behaviour of a confined fluid between two parallel solid slabs and we show how the Markovian approximation is only valid when the size of the bin is bigger than the molecular length. Finally, we measure the transport coefficients that appear in the hydrodynamic equations in order to validate the theory. After that, the slip boundary condition is measured from a microscopic definition of the slip length and the position of the atomic wall. In contrast with the conclusion of Petracic and Harrowell [33], we obtain, as Bocquet and Barrat [2], that the slip length is an intrinsic surface property. That means that it does not depend on the geometry of the channel.

This dissertation is structured as follows. In the Chapter 1 we review NESM in order to state the foundations in which the following chapters are based. We introduce two projection operators that allows us to obtain hydrodynamic equations: the Kawasaki-Gunton projector [43] and the Mori projector [44]. The first one allows one to obtain nonlinear closed equations for the averages of the selected variables of the system, while under the Mori theory one obtains simple linear equations not only for the averages of the relevant variables, but also for their correlation functions.

In Chapter 2, we derive the hydrodynamic equations of a fluid in contact with a solid. In order to discuss total momentum conservation we choose a macroscopic solid sphere. To do so, we derive DDFT for a simple fluid including the mass and the momentum density field. We use the Kawasaki-Gunton operator technique to obtain the equations of motion of the time dependent average of these fields assuming the Markovian approximation. The resulting equations contain transport coefficients given by Green-Kubo formulas, which suffer from the plateau problem when the separation of timescales is not large. This well-known problem arises because the Green-Kubo running integral appearing in the expressions of the tranport coefficients decays as the correlation of the selected coarse-grained (CG) variables when the projected dynamics is approximated by the unprojected Hamiltonian dynamics.

Chapter 3 contains the derivation from microscopic principles of the discrete equations of hydrodynamics in the presence of a planar wall. We bin the system in slabs as is shown in Figure 1. The yellow planes are called *nodes* and they separated the *bins* into which the system is classified. We start from discrete mass and momentum densities field defined at the nodal planes in order to derive the hydrodynamic equations with the Kawasaki-Gunton projector. Also we observe that the final discrete equations are identical to a discretization of the continuum hydrodynamic equations using the Petrov-Galerkin finite element discretization method. The main objective of this chapter is to obtain the discrete transport coefficients in order to compute them with MD simulations.

In the first part of Chapter 4 the plateau problem is adressed in order to obtain, within Mori projection operator formulation, an alternative expression for the transport coefficients with a corrected Green-Kubo expression with no plateau problem. The corrected Green-Kubo expression is crucial for this dissertation because the results of Chapters 4, 5 and 6 are based on this new corrected Green-Kubo expresion.

In the second part of Chapter 4 the correlation matrix of the discrete transverse momentum density field is studied through MD simulations in order to determine to what extent the Markovian approximation is valid with a nonlocal space description of hydrodynamics. The goal is to understand a simpler case before moving to the more complicated case of a fluid confined between two solid walls. One important lesson from this chapter is that we have to consider the reciprocal space (i.e. the Fourier space

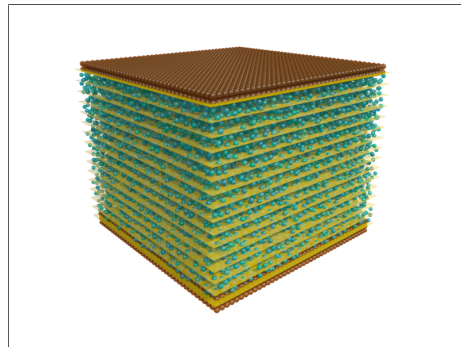


**Figure 1:** A visual representation of a MD simulation with a sketch of the binning used. In yellow are depicted the nodal planes used.

in the case of unconfined systems) to unambiguously discuss the Markov property. The method followed in this chapter will be also used for the study of confined fluids.

In Chapter 5 MD simulations are performed to compute the correlation matrix of the discrete transverse momentum density field of a fluid between two solid slabs. Because the objective of this chapter is to study the effect of the size of the bin on the Markovian behaviour near the solid walls, the system is discretized using two sizes of the bins. We realize that for bins smaller than the molecular size the description near the walls can not be Markovian, while for larger bins the description can be deemed Markovian.

Finally, in Chapter 6 the nonlocal transport kernels that appear in the discrete theory presented in Chapter 3 are measured through MD simulations. We use the corrected Green-Kubo expression in order to avoid the plateau problem. The main result of this chapter is the calculation of the slip length and the location of the hydrodynamic position of the atomic wall. We conclude that the slip length does not depend on the size of the channel and, therefore, it is an intrinsic surface property.



# Chapter 1

# Nonequilibrium Statistical Mechanics

*There is no future. There is no past. Do you see? Time is simultaneous, an intricately structured jewel that humans insist on viewing one edge at a time, when the whole design is visible in every facet.*

---

Watchmen  
ALAN MOORE

## 1.1 Introduction

It was in the nineteenth century when Statistical Mechanics was born mainly because of the work of Ludwig Boltzmann and Josiah Willard Gibbs. The goal was to reconcile Thermodynamics with the microscopic laws known at that time.

Thermodynamics was well-established because it draws its concepts from experiments while the attempts to understand it from Newton's laws collided with problems such as the impossibility of taking into account the interactions between all the particles of a thermodynamic system, the highly nontrivial form of these interactions, the huge number of degrees of freedom, or the Loschmidt paradox<sup>i</sup>. To avoid these problems

---

<sup>i</sup>The second law of thermodynamics establishes that the entropy of an isolated system increases with

physicists realized that the macro properties of a thermodynamic system do not strongly depend on the exact dynamics of every particle, but more on the averages that eventually erode the details of the behaviour of the particles. Thus, the link between the microscopic and macroscopic theory of matter can be stated through statistical assumptions in the microscopical mechanics laws. The connection is possible thanks to the notion of *ensemble*, which is a collection of imaginary replicas of the system with a set of common macroscopic properties.

Statistical Mechanics is a theoretical framework which allows one to study the macro-properties of a many-body system from the dynamics of its microscopic constituents. Therefore, we may roughly say that Statistical Mechanics acts as a bridge between two levels of description: A *microscopic level* governed by the Newton's laws of motion and the *macroscopic level* in which the knowledge is adquired from the experiments. A beautiful but rough example about how Statistical Mechanics works can be found in the book of Dean Rickles *Philosophy of Physics* [45]. He imagines a large musical ensemble playing in concert. The “global” sound produced by the musicians is analogous to the thermodynamic variables obtained from the colisions between the particles in the system. The music can be analized from two levels: the global level, where the harmony and the musical form take an important role, and the individual level, in which we focus on what the musicians are playing to produce the global sound. “It is this zooming in and out”, in words of Rickles, “from the whole system to its parts, that characterizes the relationship between statistical mechanics and thermodynamics: you won't see harmonies in a single bassoon; likewise, you won't see pressure or temperature in an individual molecule.”

The equilibrium theory of Statistical Mechanics provides an interpretation for the equilibrium thermodynamic systems from a molecular point of view. The models that allow us to reproduce real systems are the well-known microcanonical, canonical, and grand canonical ensembles. These ensembles are idealizations. They do not reproduce exactly real experiments, but give us useful information about them. However, most of the phenomena present in the Nature are out of equilibrium in the timescale of our observation. A nonequilibrium system may be modeled perturbating an equilibrium ensemble that forces the system out of equilibrium. Einstein [46], Onsager [47] and Kirkwood [48] made important contributions to NESM years before Green [49, 50], in the fifties, formulated the theory as we know it nowadays. It was in the 60's when Zwanzig [51] and Mori [44] reformulated the theory using the technique of the projection operators [52].

---

time. This can be understood as a time direction imposed by the increasing of the entropy. Furthermore, Newton's laws are reversible. According to Josef Loschmidt this apparent conflict could be the responsible for the impossibility to derive the laws of the thermodynamics from the microscopic laws. Boltzman refuted the argument brilliantly.

## 1.2 Hamilton's equations and the evolution of the microstates

We assume Classical Mechanics expressed in terms of Hamilton's equations. As opposed to Newton's equations of motion, Hamilton's are first order differential equations. As emphasized by Gibbs, statistical assumptions on initial conditions are conveniently expressed in the Hamiltonian language of phase space.

Consider a system consisting of  $N$  particles of mass  $m$  in a volume  $V$ . In Classical Mechanics the positions of the particles  $\mathbf{q}^N \equiv (\mathbf{q}_1, \dots, \mathbf{q}_N)^T$  and their  $3N$  momenta  $\mathbf{p}^N \equiv (\mathbf{p}_1, \dots, \mathbf{p}_N)^T$  specify the state of the system at any time. The collection of the positions and momenta of the particles defines the microscopic state of the system,  $z = (q, p)^T$ , which is a *phase point* in the *phase space*  $\Gamma$  of  $6N$  dimensions. The notation emphasizes that  $z$  is a column vector, where  $T$  is the transpose. Therefore, the time evolution of a phase point  $z_t$  is called the *phase trajectory* and it is determined by Hamilton's equations of motion

$$\dot{\mathbf{q}}_i = \frac{\partial \hat{H}}{\partial \mathbf{p}_i}, \quad \dot{\mathbf{p}}_i = -\frac{\partial \hat{H}}{\partial \mathbf{q}_i} \quad (1.1)$$

Typically the Hamiltonian has the form

$$\hat{H}(z) = \sum_{i=1}^N \frac{\mathbf{p}_i^2}{2m} + \hat{U}(\mathbf{q}_1, \dots, \mathbf{q}_N) + \sum_{i=1}^N \Phi(\mathbf{q}_i), \quad (1.2)$$

where the first sum is the kinetic energy of the system, the potential of interaction between particles is  $\hat{U}(\mathbf{q}_1, \dots, \mathbf{q}_N)$  and  $\Phi(\mathbf{r})$  is a time-independent external potential.

Hamilton's equations can be written in compact form as

$$\dot{z}_t = J \cdot \frac{\partial \hat{H}}{\partial z}(z_t) \equiv \hat{v}(z_t), \quad (1.3)$$

where we have defined the Hamiltonian vector field  $\hat{v}(z_t)$  and  $J$  is the symplectic matrix<sup>ii</sup> with the form

$$\begin{pmatrix} 0 & +1_{3N} \\ -1_{3N} & 0 \end{pmatrix},$$

where  $1_{3N}$  is the identity matrix of dimension  $3N \times 3N$ .

Hamilton's equation (1.3) indicates that the trajectory of  $z_t$  in phase space is an integral curve of the velocity field. Therefore, if we follow the direction given by the velocity field we can figure out which microstate will be the next one.

---

<sup>ii</sup> $J$  is an orthogonal matrix,  $J^T J = 1 \rightarrow J^T = J^{-1}$ , and its square is the minus the identity matrix  $J^2 = -1$

### 1.2.1 Hamilton's equations in operator form

Hamilton's equations are in general a *set of nonlinear ordinary differential equations*. However, in the language of linear operators we may obtain linear equations that are amenable to theoretical treatment.

We consider all functions  $\hat{B}(z)$  in phase space as vectors in infinite-dimensional vector space. The identity function in phase space is denoted as  $\hat{z}$ . It takes any microstate  $z$  into  $\hat{z}(z) = z$ . We carefully distinguish the argument  $z$ , which is a point in the phase space, from the vector of the Hilbert space  $\hat{z}$ , which represents the identity function.

The Liouville operator  $i\mathcal{L}$  is an important operator in the dynamics of the microstates. It has the following explicit form

$$i\mathcal{L} = - \sum_i \left[ \frac{\partial \hat{H}}{\partial \mathbf{q}_i} \frac{\partial}{\partial \mathbf{p}_i} - \frac{\partial \hat{H}}{\partial \mathbf{p}_i} \frac{\partial}{\partial \mathbf{q}_i} \right] \quad (1.4)$$

In order to give a more compact form of the action of the Liouville operator on a phase function we introduce the *Poisson bracket*

$$\{\hat{A}, \hat{B}\} \equiv \left( \frac{\partial \hat{A}}{\partial z} \right)^T \cdot J \cdot \frac{\partial \hat{B}}{\partial z} = \sum_i \left[ \frac{\partial \hat{A}}{\partial \mathbf{q}_i} \frac{\partial \hat{B}}{\partial \mathbf{p}_i} - \frac{\partial \hat{A}}{\partial \mathbf{p}_i} \frac{\partial \hat{B}}{\partial \mathbf{q}_i} \right] \quad (1.5)$$

Therefore, taking an arbitrary phase function  $\hat{B}(z)$  the Liouville operator acts on it in this way

$$i\mathcal{L}\hat{B} = -\{\hat{H}, \hat{B}\} \quad (1.6)$$

The action of the Liouville operator on the identity function  $\hat{z}$  is

$$i\mathcal{L}\hat{z} = \hat{v} \quad (1.7)$$

Therefore, in the language of the Liouville operator we can transform a complicated nonlinear function  $\hat{v}$  into the action of a linear operator  $i\mathcal{L}$  on the identity function  $z$ .

With the equation (1.7) Hamilton's equations (1.3) can be written in terms of the Liouville operator as

$$\frac{d}{dt} z_t = i\mathcal{L}\hat{z}(z_t) \quad (1.8)$$

In order to obtain an expression for  $z_t$ , we consider a Taylor expansion of the trajectory  $z_t$  around  $t = 0$ , that is,

$$z_t = z_0 + \frac{dz_t}{dt}(0)t + \frac{1}{2!} \frac{d^2 z_t}{dt^2}(0)t^2 + \dots \quad (1.9)$$

From (1.8) we have the first order derivative. All the high order time derivatives are given by

$$\begin{aligned}\frac{d^2 z_t}{dt^2} &= \frac{d}{dt} i \mathcal{L} \hat{z}(z_t) = \hat{v}^T(z_t) \cdot \frac{\partial i \mathcal{L} \hat{z}}{\partial z}(z_t) = (i \mathcal{L})^2 \hat{z}(z_t) \\ &\vdots \\ \frac{d^n z_t}{dt^n} &= (i \mathcal{L})^n \hat{z}(z_t)\end{aligned}\quad (1.10)$$

Evaluating all these time derivatives at  $t = 0$ , the equation (1.9) becomes

$$z_t = \hat{z}(z_0) + i \mathcal{L} \hat{z}(z_0)t + \frac{1}{2!}(i \mathcal{L}^2) \hat{z}(z_0) + \dots = \exp\{i \mathcal{L} t\} \hat{z}(z_0), \quad (1.11)$$

where the exponential operator is defined through a Taylor expansion

$$\exp(i \mathcal{L} t) \equiv \mathcal{I} + i \mathcal{L} t + \frac{1}{2!}(i \mathcal{L} t)^2 + \frac{1}{3!}(i \mathcal{L} t)^3 + \frac{1}{4!}(i \mathcal{L} t)^4 + \dots, \quad (1.12)$$

where  $\mathcal{I}$  is the identity operator. The notation of the time evolution equation (1.11) is usually simplified in this way

$$z_t = \exp\{i \mathcal{L} t\} z_0 \quad (1.13)$$

without forgetting that what we are doing is to apply an operator  $\exp\{i \mathcal{L} t\}$  to a phase function  $\hat{z}$ , giving as a result  $\exp\{i \mathcal{L} t\} \hat{z}$ , and then evaluating this result at the value  $z_0$ .

One important property of the Hamiltonian flow in phase space is that it is incompressible. This is illustrated in Figure ???. This implies that if we consider the change of variable from  $z_0$  to  $z_t$  it necessarily has a unit Jacobian.

### 1.3 The Liouville theorem

We have seen that Hamilton's equations (1.3) are first order differential equations governing the deterministic evolution of the system. These equations need an initial condition  $z_0$ , which is impossible to know in practice because in general we do not have access to the position and momenta of every single particle in the system. Usually, a system is prepared under identical macroscopic conditions that do not allow to fix the value of the initial condition. Different configurations of the particles can give an identical macroscopic condition. This enforces the introduction of a *probability density*

$\rho_0(z)$  which let us express our knowledge about the initial microscopic of the system in a statistical way. The probability distribution in phase space is usually referred to as an *ensemble*. One can imagine an ensemble as a collection of systems with equal macroscopic properties but different microscopic configurations. Note that even though the evolution of  $z_t$  is deterministic, the introduction of a probability density converts the evolution in phase space into a stochastic process. The lack of knowledge of the initial condition and the introduction of the initial probability density propagates the uncertainty regarding the exact microstate of the system to subsequent times. Therefore, we introduce the probability distribution function at a subsequent time  $\rho_t(z)$ . This allows us to know at any point in time how the systems of an ensemble are distributed in the phase space.

The probability that a system is in a microscopic state at a time  $t$  represented by a  $6N$ -dimensional phase point  $dz$  is  $\rho_t(z)dz$ . And  $\rho_t(z)$  satisfies:

$$\begin{aligned} \rho_t(z) &\geq 0 \\ \int dz \rho_t(z) &= 1 \end{aligned} \quad (1.14)$$

The equation that governs the evolution of the probability density is the *Liouville equation*

$$\frac{\partial \rho_t(z)}{\partial t} + \sum_{i=1}^N \left( \frac{\partial \rho_t(z)}{\partial \mathbf{q}_i} \cdot \dot{\mathbf{q}}_i + \frac{\partial \rho_t(z)}{\partial \mathbf{p}_i} \cdot \dot{\mathbf{p}}_i \right) = 0 \quad (1.15)$$

We may express this equation in a more compact way by using the Liouville operator (1.6)

$$\frac{\partial \rho_t(z)}{\partial t} = -i\mathcal{L}\rho_t(z) \quad (1.16)$$

Therefore, the time evolution of the probability density is

$$\rho_t(z) = \exp\{-i\mathcal{L}t\}\rho_0(z) \quad (1.17)$$

Note that we may express the Liouville equation (1.16) in the following form

$$\frac{d\rho_t(z)}{dt} = 0 \quad (1.18)$$

The Liouville theorem is a direct consequence of the incompressibility of the flow in phase space as it expresses the fact that the probability (density) of a microstate at time  $t_1$  is the probability it had at time  $t_0$ .

## 1.4 The Theory of Coarse-Graining and the CG variables

The ToCG consists on eliminating the “useless” information about a system in order to have a simplified version described by a set of selected variables with timescales much larger than the typical molecular scales. We may acquire a lot of information about the system during the simplification process because we separate the essential details from the irrelevant ones.

One of the advantages of a CG description is that it allows to simulate systems with a computer that otherwise it would not be possible or would be computationally expensive. This is because we not only gain in terms of a reduction of the number of particles, but also on the possibility to explore longer timescales. Think about a system which its constituents have different scales of length and time as, for example, colloidal suspensions, which are dispersions of mesoscopic particles suspended in a molecular solvent. The dimensions of the particles are of the order of tens or hundreds nanometers and they move in timescales of nanoseconds or microseconds, whereas the dimensions of the molecules of the solvent are a fraction of a nanometer (for example, in the case of a molecule of water typically of the order of 0.21 nm) and their timescales are of the order of picoseconds. To treat this kind of asymmetric systems from a microscopic point of view is not possible with MD simulations, but if our interest resides on the mesoscopic behaviour the problem is highly simplified using coarse-graining techniques.

A system may be described at different *levels of description* depending on the amount of information which one retains macroscopically. The state of a system at a given level of description is described by a set of *coarse grained variables* (CG variables), which are functions of the microscopic state  $z$  of the system and, therefore, are phase functions  $\hat{A}(z)$ .

The identification of the CG variables is the most important step in the ToCG in order to describe macroscopically a system with many degrees of freedom. There are few guiding principles for the identification of the CG variables such as select the dynamic invariants of the system or observe the features of the system because maybe there is a variable that captures that feature [53].

Different levels of description gives us different amount of information. Coarser levels have a smaller number of variables (slow variables) and in consequence captures less information. On the other hand, in fine levels the number of variables is so high that allow to capture too much information. Therefore, depending on the interest of the researcher, she or he would use one level of description or another. A coarse level can describe phenomena that occur at timescales equal or larger than the typical timescale of the level, but it cannot reproduce the behaviour at shorter timescales.

There are two levels of description which are particularly important: the microscopic and macroscopic levels. The microscopic level has the position and momenta of all particles of the system as the set of variables characterizing the state of the system. The equation that governs the evolution of the CG variables are the Hamilton's equations (1.3) and the timescale is the typical collision or vibration time. The macroscopic level is the level of Thermodynamics. The CG variables at this level are the dynamical invariants of the system. Because these variables are constant in time and the timescale is infinite there is not a dynamic equation for them. Any other level in between can be termed as *mesoscopic level*.

The main objective of the ToCG is to derive the dynamic equations of the CG variables. Two ideas allow us for the derivation of the dynamic equations: quasi-equilibrium and separation of timescales.

### 1.4.1 Quasi-equilibrium and separation of timescales

Imagine two ice cubes melting inside a glass of water. The process is slow but not enough to let one observe how the ice cubes reduce their size. With a sip of water is possible to appreciate that the temperature of the water has decreased. After a while the ice cubes “disappear” and the glass of water becomes an homogeneous mixture apparently in equilibrium. Nevertheless, if we let the glass on a desk, the water will begin to evaporate slowly because the equilibration of the system is not a real equilibrium state. Moreover, over many years the glass itself will probably deteriorate. Further, the process will never reach an equilibrium state, but we may distinguish “different levels” of tendency towards equilibrium each governed by a characteristic time scale.

The above example shows that a system can be at a equilibrium state depending on the timescale of the observation. The degradation of the glass over the years is very slow in contrast with the melting of the ice cubes. Therefore, at the timescale of our observations we can find functions that evolve very slowly; they may be considered as dynamic invariants that determine the equilibrium properties of the system. This situation is referred to as *quasi-equilibrium*.

In this dissertation the notion of several “equilibrium timescales” is crucial because we take advantage of the partial equilibration of the system in the timescale of evolution of the CG variables. At the typical timescale of a given level of description, we will observe that the system reaches a quasi-equilibrium state in which the CG variables are dynamics invariants. The fast degrees of freedom rapidly reach the equilibrium while the CG variables evolve slowly. When quasi-equilibrium is valid, the CG variables which describe our system at this level of description evolve much slowly than the CG of the other more detailed level of description down in the hierarchy of level of descriptions. Therefore, the system is approximately described, in the appropriate

timescale, with a generalized equilibrium ensemble, called the *relevant ensemble* or quasi-equilibrium ensemble, that takes into account the CG variables in its definition as if they were dynamical invariants of the system.

Quasi-equilibrium is connected with the notion of separation of timescales. As we said, the CG variables evolve slowly compared with the rest of degrees of freedom, which is, in fact, a necessary condition to obtain differential equations for the evolution of the CG variables. If timescales are not well-separated we may obtain dynamic equations with complicated memory terms, as we will see in Chapter 2. This situation is referred to as a *non-Markovian* dynamics, to distinguish it from *Markovian* description in which the future state of the system is only determined by the present but not for the past of the system.

## 1.5 Molecular Dynamics simulations

“We may regard the present state of the universe as the effect of its past and the cause of its future. An intellect which at a certain moment would know all forces that set nature in motion, and all positions of all items of which nature is composed, if this intellect were also vast enough to submit these data to analysis, it would embrace in a single formula the movements of the greatest bodies of the universe and those of the tiniest atom; for such an intellect nothing would be uncertain and the future just like the past would be present before its eyes.” This sentence was written at the end of the 18th century by Pierre-Simon Laplace in its famous essay *A Philosophical Essay on Probabilities* [54].

The belief in the deterministic behaviour of the nature lasted for the next century until Charles-Eugène Delaunay and Henry Poincaré introduced the first notion of the effect of the initial conditions in the evolution of a system consisting on three or more bodies, the well-known three-body problem.

Delaunay wrote two volumes [55] about the three-body problem as a perturbed system in which the perturbation played the role of the third body. Years later, Poincaré thought about the stability of a three-body system introducing the first notion of chaos.

The N-body problem is crucial in real systems consisting on a huge number of particles. In the levels of description in which the particles of a system are interacting with the other, to solve the equations of motion is in the center of the problem. Let us suppose that we have a glass of water. The number of water molecules is  $N \sim 10^{24}$ . Therefore, we need  $6N$  initial conditions and  $6N$  equations of motion to be solved ( $v_x, v_y, v_z$  and  $x, y, z$  for every particle). Is obvious that is impossible to solve analytically this bunch of equations of motion.

Once we assume that we can not solve manually the equations of motion of the

molecules of a glass of water, we may use a computer to solve them. The technique to obtain approximated solutions of the time evolution equations of the molecules is called Molecular Dynamics. The idea behind this technique is to discretize the time in intervals called *timesteps* and to compute the position and velocity of every particle at every timestep. If we estimate the number of collisions per second and calculate the number of evaluations we need to compute for every particle, we conclude that to solve the equations of motion of a real system, such a glass of water, is impossible even computationally [56]. Therefore, only small or coarse systems (i.e. with a reasonable number of particles) can be addressed using MD simulations.

The pioneering work of Adler and Wainwright [57] in the fifties was a first step in the development of the MD simulations when they studied the phase transition of a system consisting on hard spheres. In the sixties Gibson et al. [58] studied the radiation damage using MD simulations and Rahman [59] simulated a system consisting on 864 particles interacting with Lennard-Jones (LJ) potential in order to study correlations in the motion of atoms in liquid argon.

MD simulations play the role of virtual experiments. They provide us the observation which precedes the comprehension, because without comprehension science would be only documentation [60]. Simulations allows us, in contrast with the theory, to assume less approximations in exchange for a computational effort. Both simulations and physical theory must coincide (i.e. the predictions of theory must coincide with the results of the simulations). If they differ, this is an indication that an error has been committed somewhere.

This dissertation rests on two pillars. The first one consists on a theoretical derivation of the equations that governs the evolution of the CG variables of a fluid in contact with a solid. Along the derivation we only assume the Markovian approximation that simplify considerably the final equations, in which the transport coefficients are included through the Green-Kubo formula. The second pillar consists on MD simulations performed to measure the selected variables of the system which we need to validate the Markovian approximation and to compute the correlations included in the Green-Kubo formulas.

## 1.6 The entropy

As well as in equilibrium, in nonequilibrium situations entropy plays a fundamental role. Suppose that we know the averages of the CG variables,  $\hat{A}(z)$ , of a given system

$$a = \text{Tr}[\hat{A}\rho], \quad (1.19)$$

where  $\rho$  satisfies

$$\text{Tr}[\rho] = 1 \quad (1.20)$$

The trace symbol denotes a macrocanonical sum over particles and an integral over the position a momentum of  $N$  particles

$$\text{Tr}[\cdots] = \sum_{N=0}^{\infty} \frac{1}{N!h^{3N}} \int dz \cdots \quad (1.21)$$

where  $h$  is the Planck constant, introduced here just for non-dimensionalization purposes. Note that

$$\text{Tr}[\hat{A}\rho] = \int dz \rho(z) \hat{A}(z) \quad (1.22)$$

There are many possible ensembles  $\rho(z)$  which can reproduce the macroscopic information given by the average  $a$ , but we would like to take the one which gives us the least biased macroscopic information. In the theory of probability this problem is solved with the *Principle of Insufficient Reason*.

Jaynes [61] proposes that the distribution of probability we should use is that which maximises the Shannon's entropy functional

$$H[\rho] = - \sum_i \rho(z_i) \ln(\rho(z_i)) \quad (1.23)$$

subject to the constraints.

Note that this functional applies to discrete distributions. However, the Gibbs-Jaynes entropy functional  $S[\rho]$  is analogous to (1.23) but for continuos set of states  $z$

$$S[\rho] = -\text{Tr} \left[ \rho \ln \frac{\rho}{\rho_0} \right], \quad (1.24)$$

where  $\rho_0 = \frac{1}{N!h^{3N}}$  is a dimensional factor that renders the argument of the logarithm dimensionless and that takes into account the proper Boltzmann counting. The normalized probability density that maximizes the entropy functional, subject to produce prescribed values of the averages (1.19) is denoted as the relevant ensemble  $\bar{\rho}$  and has the form of a generalized canonical ensemble

$$\bar{\rho}(z) = \frac{1}{Z[\lambda]} \rho_0 \exp\{-\lambda \cdot \hat{A}(z)\}, \quad (1.25)$$

where  $\lambda$  is the set of variables conjugate to the relevant variables  $\hat{A}(z)$ . The generalized partition function is given by

$$Z[\lambda] = \text{Tr}[\rho_0 \exp\{-\lambda \cdot \hat{A}(z)\}] \quad (1.26)$$

In general,  $\lambda$  will be a collection of fields and finite dimensional vectors. We use the notation  $[\dots]$ , which is typically restricted to denote a functional, also in the present mixed case. The average  $a$  of the relevant variables with respect to the relevant ensemble will be denoted by

$$a = \langle \hat{A} \rangle^\lambda = \text{Tr}[\bar{\rho} \hat{A}] \quad (1.27)$$

and can be written as

$$a = \frac{\partial \Phi}{\partial \lambda}[\lambda], \quad (1.28)$$

where the (dimensionless) thermodynamic potential  $\Phi[\lambda]$  is given by

$$\Phi[\lambda] = -\ln Z[\lambda] \quad (1.29)$$

The average  $a$  is a function/functional of  $\lambda$ . For each  $\lambda$  we have an average  $a$  given by equation (1.28). If we take the derivative of (1.28) with respect to  $\lambda$  we arrive at

$$\frac{\partial a}{\partial \lambda} = -\langle \delta \hat{A} \delta \hat{A} \rangle^\lambda \quad (1.30)$$

where  $\delta A = \hat{A}(z) - a$ . The covariance  $\langle \delta \hat{A} \delta \hat{A} \rangle^\lambda$  is a positive definite matrix and, therefore, the functional  $\Phi[\lambda]$  is convex. This implies that the Jacobian of the change of variables from  $\lambda$  to  $a$  can be inverted to provide  $\lambda[a]$ . Therefore, there is a one to one connection between the pair of conjugate variables  $\lambda$  and  $a$ .

This argument is valid for any pair of conjugate variables and it only depends on the definition of the conjugate variables introduced in equation (1.25). It constitutes the basic content of the DFT when the relevant variable is the microscopic density operator.

Because the connection is one to one, we may change variables from  $\lambda$  to  $a$ . However, the average  $a$  is given by a derivative and such a change of variables implies a loss of information. As we know from the usual treatment in Thermodynamics [62], the correct way to proceed is to introduce the dimensionless entropy function  $S[a]$  of the given level of description as the (minus) Legendre transform of the thermodynamic potential in the form

$$S[a] = -\Phi[\lambda[a]] + \lambda[a]a \quad (1.31)$$

The relation of this entropy function  $S[a]$  and the Gibbs-Jaynes entropy functional  $S[\rho]$  in (1.24) is simple. The former is just the later evaluated at its maximum, the relevant ensemble (1.25). This is

$$S[a] = S[\bar{\rho}] \quad (1.32)$$

Because the entropy  $S[a]$  is the Legendre transform of the thermodynamic potential  $\Phi[\lambda]$ , we have the relationship conjugate to (1.28)

$$\frac{\partial S}{\partial a} = \lambda \quad (1.33)$$

## 1.7 The dynamics

One important objective within NESM is the derivation of the governing dynamics of a set of CG variables that describe the system at a mesoscopic or macroscopic level of description by starting from the microscopic laws of motion of the constituent atoms and molecules of the system [63]. In this quest, the projection operator technique, as described in the textbook by Grabert [52], has proved to be an extremely useful tool. As discussed there, there are essentially three different types of projection operator theories, associated to the names of Mori [44], Zwanzig [51], and Kawasaki and Gunton [43], with increasing order of generality [52]. The Kawasaki-Gunton projection operator allows one to obtain nonlinear closed equations for the averages of the CG variables. The Zwanzig projector is a special case of the Kawasaki-Gunton projector when the selected variables are, instead of the CG variables themselves, the *distribution* of the CG variables. This results into a governing equation for the probability distribution of CG variables. Finally, Mori projector is obtained from Zwanzig projector in near equilibrium situations [52, 64]. The resulting dynamic equations in Mori theory are linear and allow one to obtain simple equations not only for the averages of the CG variables, but also for their correlation functions.

The projection operator technique provides closed and exact equations for the evolution of the averages or probabilities of the CG variables with only one assumption about the initial distribution of microstates, which are assumed to be distributed with a maximum entropy ensemble [52]. The exact equations of motion of the CG variables contain a *reversible term* which is local in time and an *irreversible integro-differential term* describing memory about the past history of the CG variables. The memory kernel is defined in microscopic terms, and it involves the so called *projected dynamics* which is different, in general, from the usual Hamiltonian dynamics of the system.

When the selected CG variables are such that they display a clear separation of time scales in its dynamics then it is possible to resort to the Markovian approximation,

in which the memory kernel becomes proportional to a Dirac  $\delta$  function in time. Such a separation of timescales happens, in general, when the evolution of the CG variables is the result of many minuscule and fast contributions. Under the Markovian approximation, the resulting governing dynamic equations are nonlinear differential equations for the nonequilibrium averages of the CG variables in the Kawasaki-Gunton projector or stochastic differential equations (SDE) in the Mori and Zwanzig projectors. Within the Markovian approximation one obtains the transport coefficients governing the irreversible part of the dynamics in terms of the time integral of correlation functions of the time derivatives of the CG variables. These formulas for transport coefficients are the celebrated Green-Kubo formulas [49, 65].

### 1.7.1 The Kawasaki-Gunton projection operator

The projection operator method can be understood, at its most fundamental level as a way to approximate the actual time dependent ensemble, which is the solution of the Liouville equation, with a relevant ensemble of the form (1.25), plus a correction, which is the responsible for the irreversible behaviour. We summarize in the rest of this section the time-dependent projection operator technique as presented in the classical textbook by Grabert [52].

The aim is to derive equations of motion for the time dependent average  $a_i(t)$  of the set of relevant variables  $\hat{A}_i(z)$ . The time dependent average is

$$a_i(t) = \text{Tr}[\rho_t \hat{A}_i], \quad (1.34)$$

where  $\rho_t$  is the nonequilibrium solution of the Liouville equation. As it is shown in [52], for isolated systems with a time-independent Hamiltonian, the averages (1.34) evolve according to the following closed exact equation

$$\frac{\partial}{\partial t} a_i(t) = v_i(t) + \int_0^t dt' \sum_j K_{ij}(t, t') \lambda_j(t') \quad (1.35)$$

The reversible term is given by

$$v_i(t) = \text{Tr}[\bar{\rho}_t i \mathcal{L} \hat{A}_i], \quad (1.36)$$

where  $i \mathcal{L}$  is the Liouville operator (1.6).

The relevant ensemble  $\bar{\rho}_t$  is of the form (1.25), with a time dependent conjugate variable  $\lambda(t)$ . The conjugate variables  $\lambda$  are selected in such a way that the averages  $a(t)$  of the real (i.e. the solution of the Liouville equation) and of the relevant ensemble coincide. Note that if only the reversible term  $v_i(t)$  would be present in equation (1.35),

we would be approximating the actual ensemble with a relevant ensemble of the form (1.25), where the conjugate field  $\lambda(t)$  is now a function of time. The error in this approximation is, in fact, the memory term which describes irreversible behaviour. The irreversible term in equation (1.35) involves the memory kernel

$$K_{ij}(t, t') = \text{Tr} \left[ \bar{\rho}_{t'} \left( Q_{t'} i \mathcal{L} \hat{A}_j \right) G_{t't} \left( Q_t i \mathcal{L} \hat{A}_i \right) \right], \quad (1.37)$$

where the Kawasaki-Gunton projection operator  $Q_{t'}$  [52, 66] applied to an arbitrary function  $\hat{F}(z)$  is

$$Q_{t'} \hat{F}(z) = \hat{F}(z) - \text{Tr}[\bar{\rho}_{t'} \hat{F}] - \sum_i (\hat{A}_i(z) - a_i(t')) \frac{\partial}{\partial a_i(t')} \text{Tr}[\bar{\rho}_{t'} \hat{F}] \quad (1.38)$$

Finally, the time ordered projected propagator  $G_{t't}$  is given by formal series

$$\begin{aligned} G_{t't} &= 1 + \sum_{n=1}^{\infty} \int_{t'}^t dt_1 \cdots \int_{t'}^{t_{n-1}} dt_n i \mathcal{L} Q_{t_n} \cdots i \mathcal{L} Q_{t_1} \\ &\equiv T_+ \exp \left\{ \int_{t'}^t dt'' i \mathcal{L} Q_{t''} \right\}, \end{aligned} \quad (1.39)$$

where  $T_+$  ensures that the operators are ordered from left to right as time increases. equation (1.35) is a closed exact equation for the time dependent averages  $a(t)$ . The only assumption taken in deriving (1.35) is that the initial ensemble to be used in the Liouville equation is of the relevant form. This is, it is assumed that the only knowledge at the initial time is the value of the average  $a(0)$  and, therefore, the least biased initial ensemble is of the relevant form (1.25). Therefore, the time dependent average  $a(t)$  of the relevant variables  $\hat{A}(z)$  is computed with the solution of the Liouville equation  $\rho_t(z)$  with an initial condition which is of the relevant form. The relevant ensemble is a functional of  $a(t)$  through  $\lambda(t)$ . The kernel becomes a functional of  $a(t)$  through the relevant ensemble.

Although equation (1.35) is a closed equation, it is an integro-differential equation which is difficult to treat in general. Nevertheless, the exact transport equation (1.35) can be approximated by a memory-less equation whenever a clear separation of timescales exists between the evolution of the averages and the decay of the memory kernel. Under this assumption and the neglect of terms of order  $O(i \mathcal{L} \hat{A}^3)$ , assumed to be small due to the slowness of the relevant variables, one obtains the Markovian equation [52]

$$\frac{\partial}{\partial t} a_i(t) = v_i(t) + \sum_j D_{ij}(t) \lambda_j(t), \quad (1.40)$$

where the dissipative matrix is given by the Green-Kubo formula

$$D_{ij}(t) = \int_0^{\Delta t} dt' \langle Q_t i \mathcal{L} \hat{A}_j \exp\{i \mathcal{L} t'\} Q_t i \mathcal{L} \hat{A}_i \rangle^{\lambda(t)} \quad (1.41)$$

Here,  $\Delta t$  is a time large compared to the decay time of the correlation integrand but short in front of the time scale of evolution of the relevant variables. The dissipative matrix depends in general on the relevant variables through the relevant ensemble and, as such, it is a function of time. The dissipative matrix is, to the extent that the Markov property holds, positive definite and satisfies Onsager's reciprocity [52].

It is straightforward to show that the dynamic equations (1.40) have as a Lyapunov function the entropy (1.31) and, therefore, the dynamics complies with the Second Law of Thermodynamics. The equations (1.40) predict the decay of any initial value of the average of the relevant variables toward its unique equilibrium values. Forced situations may be treated with the present formalism [52] but we do not consider them here for simplicity.

### 1.7.2 Mori's Generalized Langevin equation

In the last section we introduced the Kawasaki-Gunton projection operator that allows one to obtain nonlinear closed equations of motion for the averages of a set of relevant variables. It is shown that the equations consist of two terms, a reversible term and irreversible one which contains the memory kernel. In this section we present a summary of Mori's theory [44] which allows one to obtain not only linear dynamic equations for the averages of the relevant variables but also for their correlations. We will also assume the Markovian approximation as in the case of the nonlinear equations obtained with the Kawasaki-Gunton projection operator.

Without losing generality, we will assume that the equilibrium average of the CG variables vanish. By denoting  $\hat{A}(t) = \hat{A}(z_t)$ , the evolution of these functions in phase space is given by

$$\frac{d}{dt} \hat{A}(t) = \exp\{i \mathcal{L} t\} i \mathcal{L} \hat{A}(z_0) \quad (1.42)$$

Mori's exact Generalized Langevin equation (GLE) is an evolution equation for the set of CG variables given by the following theorem [44, 63, 67]

$$\frac{d}{dt} \hat{A}(t) = -L \cdot C^{-1}(0) \cdot \hat{A}(t) - \int_0^t dt' \Gamma(t-t') \cdot C^{-1}(0) \cdot \hat{A}(t') + F^+(t), \quad (1.43)$$

where the following matrices have been introduced

$$\begin{aligned} L &= \langle \hat{A}i\mathcal{L}\hat{A}^T \rangle \\ C(0) &= \langle \hat{A}\hat{A}^T \rangle \\ \Gamma(t) &= \langle F^+(t)F^{+T}(0) \rangle, \end{aligned} \quad (1.44)$$

where  $\langle \dots \rangle$  denotes an equilibrium average

$$\langle \dots \rangle \equiv \int dz \rho^{eq}(z) \dots, \quad (1.45)$$

$\rho^{eq}(z)$  is the equilibrium ensemble, and  $\hat{A}^T$  denotes the transpose of the column vector  $\hat{A}$ . The so called projected force is given by

$$F^+(t) = \exp\{Qi\mathcal{L}t\}Qi\mathcal{L}\hat{A} \quad (1.46)$$

The projection operator  $Q$  is defined as  $Q = 1 - \mathcal{P}$  where  $\mathcal{P}$  is Mori's projector whose effect on an arbitrary phase function  $\hat{F}(z)$  is

$$\mathcal{P}\hat{F}(z) = \langle \hat{F} \rangle + \langle \hat{F}\hat{A}^T \rangle \cdot C^{-1}(0) \cdot \hat{A}(z) \quad (1.47)$$

The Mori projector (1.47) satisfies that  $\mathcal{P}\hat{A} = \hat{A}$  and transforms an arbitrary function of phase space into a linear combination of the CG variables. The projected forces have zero mean and are uncorrelated from previous values of the CG variables, that is,

$$\begin{aligned} \langle F^+(t) \rangle &= 0 \\ \langle \hat{A}F^+(t) \rangle &= 0 \quad t \geq 0 \end{aligned} \quad (1.48)$$

The equilibrium time correlation matrix of the CG variables is

$$C(t) = \langle \hat{A}(t)\hat{A}^T \rangle \quad (1.49)$$

If we multiply the exact equation (1.43) with  $\hat{A}^T(z)$  and average over the equilibrium ensemble, we obtain a closed and exact equation for the correlation matrix of the CG variables

$$\frac{d}{dt}C(t) = -L \cdot C^{-1}(0) \cdot C(t) - \int_0^t dt' \Gamma(t-t') \cdot C^{-1}(0) \cdot C(t') \quad (1.50)$$

The GLE (1.43) allows one to obtain not only an equation for the correlation of the CG variables, but also an equation for their averages. If we multiply (1.43) with an initial ensemble  $\rho_0(z)$  and integrate over the microstates  $z$  we obtain

$$\frac{d}{dt}a(t) = -L \cdot C^{-1}(0) \cdot a(t) - \int_0^t dt' \Gamma(t-t') \cdot C^{-1}(0) \cdot a(t'), \quad (1.51)$$

where the time-dependent average of the CG variables is defined as

$$a(t) = \int dz \rho_0(z) \exp\{i \mathcal{L}t\} \hat{A}(z) \quad (1.52)$$

and we have assumed that the average of the projected force with respect to the initial ensemble vanishes, i.e.

$$\int dz \rho_0(z) \exp\{Qi \mathcal{L}t\} Qi \mathcal{L} \hat{A}(z) = 0 \quad (1.53)$$

Note that in deriving (1.43) one assumes that the dynamics is given by a time-independent Hamiltonian with a well-defined equilibrium ensemble  $\rho_{\text{eq}}(z)$ . Therefore, both (1.50) and (1.51) describe the evolution of correlations and averages toward their equilibrium values.

### The Markovian approximation within Mori theory

The Markovian approximation assumes that there exists a time-independent *friction matrix*  $M^*$  that contains the transport coefficients of the CG level of description such that the linear integro-differential term in equation (1.50) can be approximated by a memory-less term, also linear in the correlation matrix

$$\int_0^t dt' \Gamma(t-t') \cdot C^{-1}(0) \cdot C(t') \simeq M^* \cdot C^{-1}(0) \cdot C(t) \quad (1.54)$$

The Markov approximation (1.54) in the GLE (1.43) implies the following evolution equation for the CG variables

$$\frac{d}{dt} \hat{A}(t) = -\Lambda^* \cdot \hat{A}(t) + F^+(t), \quad (1.55)$$

where the *relaxation matrix*  $\Lambda^*$  is defined as

$$\Lambda^* \equiv (L + M^*) \cdot C^{-1}(0) \quad (1.56)$$

The approximation (1.54) is equivalent to take

$$\Gamma(t) \approx M^* \delta^+(t) \quad (1.57)$$

where the Dirac  $\delta$  function  $\delta^+(t)$  is normalized as

$$\int_0^\infty dt \delta^+(t) = 1 \quad (1.58)$$

Under the Markovian approximation, equation (1.57) implies that the projected force is  $\delta$  correlated in time. As a consequence, the ordinary differential equation (1.55) should be interpreted as a stochastic differential equation (SDE) for times larger than the correlation of  $F^+(t)$ .

By multiplying (1.55) with an initial ensemble  $\rho_0(z)$  satisfying (1.53) we obtain the following Markovian equation for the averages

$$\frac{d}{dt}a(t) = -\Lambda^* \cdot a(t) \quad (1.59)$$

By multiplying (1.55) with  $\hat{A}(0)$  and averaging over initial conditions sampled from the equilibrium ensemble, one obtains the evolution equation of the correlation matrix under the Markovian approximation

$$\frac{d}{dt}C(t) = -\Lambda^* \cdot C(t) \quad (1.60)$$

The form of (1.59) and (1.60) illustrates Onsager's regression hypothesis, that states that (correlations of) fluctuations decay in the same way as the averages. Equation (1.59), (1.60) show that the transport coefficients that appear in the transport equation for the averages are the same as the transport coefficients governing the correlations of the fluctuations in equilibrium.

The solution of (1.60) is given by the exponential matrix

$$C(t) = \exp\{-\Lambda^* t\} \cdot C(0) \quad (1.61)$$

This is the main prediction of Mori theory that states that for a linear Markovian theory the only possibility for a correlation is to decay in an exponential matrix way. This does not mean that the elements of the correlation matrix  $C(t)$  decay as  $e^{-\alpha t}$ , because they are, in fact, the sum of many exponential terms that may lead even to quasi-algebraic decays of correlations, as in the case of hydrodynamics.

We remark that the Markovian equation (1.60) cannot hold at very short times, because at  $t = 0$  the exact equation (1.50) implies

$$\frac{d}{dt}C(0) = -L \quad (1.62)$$

which is only possible in (1.60) if  $M^* = 0$ . This paradoxical result can also be obtained from equation (1.54) because if we set  $t = 0$  in that equation we obtain again  $M^* = 0$ . Therefore, we expect (1.60) to hold only after a time  $t = \tau$  larger than the decay of the memory kernel. This is a general feature of the Markovian approximation showing that

correlations will decay in an exponential, Markovian way only after the time  $\tau$  beyond which memory is lost. The value of  $\tau$  should be explicitly measured in any procedure to validate the Markovian approximation.

The usual rationale for justifying the Markovian approximation (1.54) goes as follows [52, 63]. The memory kernel  $\Gamma(t - t')$  is given in terms of a correlation function that it is assumed to decay in a typical molecular time scale. On the other hand, it is assumed that the timescale of evolution of the CG variables is much larger than this molecular time and, therefore, within the memory integral  $C(t')$  does not change appreciably and we may approximate  $C(t') \simeq C(t)$ . Therefore, we have

$$\begin{aligned} \int_0^t dt' \Gamma(t - t') \cdot c(t') &\simeq \int_0^t dt' \Gamma(t - t') \cdot c(t) \\ &\equiv M^+(t) \cdot c(t), \end{aligned} \quad (1.63)$$

where we have introduced the *projected* Green-Kubo running integral

$$\begin{aligned} M^+(t) &\equiv \int_0^t dt' \Gamma(t') \\ &= \int_0^t dt' \left\langle \left( \exp\{Qi\mathcal{L}t'\} Qi\mathcal{L}\hat{A} \right) Qi\mathcal{L}\hat{A}^T \right\rangle \end{aligned} \quad (1.64)$$

and the normalized correlation matrix as

$$c(t) = C^{-1}(0) \cdot C(t) \quad (1.65)$$

that at  $t = 0$  becomes the identity matrix. The Markovian assumption relies on a separation of time scales. For some model systems (hydrodynamics of unconfined fluids [68] or Brownian particles [69]), one can justify rigorously such a separation of timescales as some parameter becomes small (wavelength or ratio of masses) and then usually the order of the limits in the parameter, time, and system size, plays an important role. In the present dissertation, we simply assume that the Markovian approximation is a sufficiently good one.

We will also consider the *unprojected* Green-Kubo running integral

$$M(t) \equiv \int_0^t dt' \left\langle \left( \exp\{i\mathcal{L}t'\} i\mathcal{L}\hat{A} \right) Qi\mathcal{L}\hat{A}^T \right\rangle, \quad (1.66)$$

where we distinguish  $M(t)$  from  $M^+(t)$  because the former involves the unprojected Hamiltonian dynamics  $\exp\{i\mathcal{L}t\}\hat{A}$ , while the later involves the projected dynamics  $\exp\{Qi\mathcal{L}t\}\hat{A}$ . In both  $M^+(t)$  and  $M(t)$  we recognize a total time derivative that allows to perform the time integral explicitly so we have the alternative forms

$$\begin{aligned} M^+(t) &= \left\langle \left( \exp\{Qi\mathcal{L}t\}\hat{A} \right) Qi\mathcal{L}\hat{A}^T \right\rangle \\ M(t) &= \left\langle \left( \exp\{i\mathcal{L}t\}\hat{A} \right) Qi\mathcal{L}\hat{A}^T \right\rangle \end{aligned} \quad (1.67)$$

Because the projected dynamics is in general more difficult to compute than the unprojected dynamics, one usually resorts to a large separation of timescales in order to approximate the projected dynamics with the unprojected one [51, 68, 69]. For the Markovian approximation (1.54) to hold, the matrix  $M^+(t)$  in (1.63) needs to become the time-independent matrix  $M^*$ . Note that  $M^+(t)$  vanishes at  $t = 0$  and after a time  $\tau$  should plateau to a constant value. If one approximates  $M^+(t) \simeq M(t)$ , this would require that  $M(t)$  would have a plateau itself. However, this is not true because, for an ergodic system, correlations computed with the unprojected dynamics decay to zero

$$\begin{aligned} \lim_{t \rightarrow \infty} M(t) &= \lim_{t \rightarrow \infty} \left\langle \left( \exp\{i\mathcal{L}t\}\hat{A} \right) Qi\mathcal{L}\hat{A}^T \right\rangle \\ &= \langle \hat{A} \rangle \langle Qi\mathcal{L}\hat{A}^T \rangle = 0 \end{aligned} \quad (1.68)$$

This problem was recognized already by Kirkwood as the so called plateau problem [70, 71] and limits the use of the unprojected Green-Kubo formula  $M(t)$  for the calculation of transport coefficients.

While  $M(t)$  does not have a plateau,  $M^+(t)$  may actually have a plateau depending essentially on the spectrum of the projected evolution operator  $\exp\{Qi\mathcal{L}t\}$ . If  $|\hat{\psi}_\mu\rangle$  are the eigenvectors of corresponding eigenvalues  $\lambda_\mu$  of  $Qi\mathcal{L}$ , the operator  $\exp\{Qi\mathcal{L}t\}$  admits the eigendecomposition

$$\exp\{Qi\mathcal{L}t\} = \sum_{\mu} \exp\{-\lambda_{\mu}t\} |\hat{\psi}_{\mu}\rangle \langle \hat{\psi}_{\mu}| \quad (1.69)$$

in Dirac ket and bra notation, where the inner product is defined with the equilibrium ensemble. The matrix  $M^+(t)$  then has the form

$$M^+(t) = \sum_{\mu} \exp\{-\lambda_{\mu}t\} \langle \hat{A} | \hat{\psi}_{\mu} \rangle \langle \hat{\psi}_{\mu} | Qi\mathcal{L}\hat{A}^T \rangle \quad (1.70)$$

Note that the equilibrium eigenvector  $|\psi_0\rangle$  has zero eigenvalue. For the ergodic unprojected dynamics this is the only eigenvector of null eigenvalue but for the projected dynamics, the zero eigenvalue may be degenerate. In other words, the projected dynamics may have other conserved variables in addition to the Hamiltonian that render the evolution nonergodic with respect to the equilibrium measure. Assume, for example,

that there is only one eigenvector  $|\psi_1\rangle$  different from the equilibrium one  $|\psi_0\rangle$  of null eigenvalue. Then the infinite time limit is

$$M^* = \lim_{t \rightarrow \infty} M^+(t) = \langle \hat{A} |\hat{\psi}_1 \rangle \langle \hat{\psi}_1 | Q i \mathcal{L} \hat{A}^T \rangle \quad (1.71)$$

This is an expression for the transport coefficients  $M^*$  in terms of equilibrium averages. Of course, the calculation of the spectrum of  $Q i \mathcal{L}$ , or the identification of the additional conserved quantities of the projected dynamics is not an easy task in general but it has been carried out for a model system of a Brownian particle in a double well-potential [72]. Also, under a perturbation scheme, the time integral of the correlation of the projected force of a Brownian particle has been carried out showing a non-vanishing plateau [69]. It is believed that the projected Green-Kubo matrix  $M^+(t)$  has a well-defined plateau in general.

In summary, the projected Green-Kubo matrix  $M^+(t)$  may have a well-defined plateau but it is difficult to evaluate it in order to get transport coefficients from direct MD simulations, while the unprojected Green-Kubo matrix  $M(t)$  is easily obtained from MD simulations but it usually suffers from the plateau problem giving ambiguous values for the transport coefficients. In Chapter 4 we will address the plateau problem in order to offer an alternative expression of transport coefficients in terms of corrected Green-Kubo formulas with no plateau problem by construction.

## 1.8 Summary

In this chapter we have introduced two important concepts for this dissertation. The first one, quasi-equilibrium, states that what we understand as equilibrium of a system depends on the time window we take. If the time of observation is shorter than the time in which some variables evolve, we may use the variables as CG variables. Because the other variables evolve faster we may assume that are irrelevant for the selected level of description. Therefore, we say that the slow and faster variables evolve in different timescales, which is the second important concept of this chapter. Only when there is a well-separation of timescales we obtain tractable time evolution equation without memory terms. The approximation that allows one this simplification is known as the Markovian approximation. In this approximation the present does not depend on the past.

Under the Markovian approximation, we have obtained the general form of the memory-less dynamic equation of the CG variables using the Kawasaki-Gunton projection operator and the evolution equation for the correlation of the averages of the CG variables within Mori theory.

# Chapter 2

## Nanoscale hydrodynamics theory for liquids near solids

*Le temps est une invention du mouvement. Celui qui ne bouge pas ne voit pas le temps passer.*

---

Métaphysique des tubes  
AMÉLIE NOTHOMB

### 2.1 Introduction

As it was mentioned in the Introduction, Density Functional Theory (DFT) is a successful and well-established theory for the study of the structure of simple and complex fluids at equilibrium. The theory has been generalized to dynamical situations when the underlying dynamics is diffusive as in, for example, colloidal systems. However, there is no such a clear foundation for Dynamic DFT (DDFT) for the case of *simple* fluids in contact with solid walls. In this chapter, we derive DDFT for simple fluids (fluids that obey a Hamiltonian dynamics) by including not only the mass density field but also the momentum density field of the fluid. The standard projection operator method based on the Kawasaki-Gunton operator is used for deriving the equations for the average value of these fields.

We consider a fluid in contact with a large spherical solid particle in order to address fluid-solid interactions. In usual DFT approaches, a solid wall is usually represented

with an *external hard potential*. In the present description, a solid wall is treated with a coarse-grained procedure in which the atoms of the wall are eliminated from the description, under the assumption that any elastic (or any other) degree of freedom of the solid is much faster than the timescales of the surrounding fluid. The density functional that emerges now depends not only on the density field of the fluid but also on the overall CG variables that we use to describe the solid. For simplicity, we focus on a particularly simple particle shape, a solid spherical particle. By considering the interaction of a fluid with a solid sphere, we may address the issue of total momentum conservation that may become rather obscure if one considers “planar walls with infinite mass”. Of course, many of the results that we obtain will be easily transferred to planar walls, as limits in which the mass and the radius of the solid sphere are both very large. In addition, we take a spherical particle because then only the position and momentum of the center of mass of the solid particle is required in order to have a coarse-grained description of the solid. For non-spherical particles, it is necessary, in general, to include also the orientation and angular velocity of the particle, as this is expected to play an important role in the dynamics. Still, even in the spherical particle case, it may be important to introduce angular velocity in order to have accurate results. However, for the sake of simplicity and presentation of the basic results, we restrict ourselves in this chapter to the simplest case without angular variables for the solid particle. Also, and for the sake of simplicity, we do not consider the intrinsic spin of the fluid, that may become an important relevant variable at nanoscales [73, 74].

The main result of this chapter is a set of dynamic equations that govern the nonequilibrium *averages* of hydrodynamic variables and the time-dependent position and momentum of the sphere. The dynamic equations are of the form of *nonlocal* hydrodynamic equations for the mass and momentum density fields coupled with Newton’s laws for the center of mass of the solid particle. The coarse-grained forces between the fluid and the solid have reversible and dissipative contributions, both localized in a boundary region near the solid surface. The hydrodynamic equations obtained can describe the structuring of the fluid near the solid particle and nonlocal flow effects that may be important at nano scales.

The present theory is both, i) a generalization of DFT to dynamic situations *in simple fluids*, and ii) a full description, at the coarse-grained hydrodynamic level, of the solid-wall interactions. The theory describes hydrodynamics at scales where the molecular structure of the fluid is apparent. At these scales the concept of boundary condition is not applicable. Instead, the interaction of the fluid with the solid wall is described with reversible and irreversible forces confined at the vicinity of the wall.

Because of the two aspects of the present theory that have been already mentioned, i.e i) nonlocal hydrodynamics and ii) interactions with solid walls, we discuss previous work in these two areas in what follows.

### 2.1.1 Nonlocal hydrodynamics

This chapter relies on the pioneering work by Piccirelli [42] who, following Robertson [41], derived hydrodynamic equations explicitly from the microscopic dynamics of the fluid system. The resulting exact hydrodynamic equations contained nonlocal transport coefficients defined in terms of Green-Kubo formulas. In similar terms, Grossmann [75] presented a derivation of nonlocal hydrodynamics of simple fluids by using essentially the same ideas behind the projection operator technique. While the theory provided nonlocal transport coefficients, no connection was made in these early works with DFT, which was not yet developed in those days. Such nonlocal versions for hydrodynamics are necessary when the flow fields vary rapidly in space, in the range of molecular correlations. The probing of nanoscales in MD simulations has demonstrated this point very convincingly [34, 76–78].

### 2.1.2 Fluid-solid interactions

Usually, at the hydrodynamic level of description, the interaction of a fluid with a solid is described through boundary conditions. Seminal work on the understanding of boundary conditions as irreversible interfacial processes was given by Bedeaux, Albano, and Mazur, who introduced interfacial transport coefficients entering into the boundary conditions [79]. While a fluctuation-dissipation theorem was formulated for the slip coefficient [80], which could suggest a microscopic evaluation of the interfacial boundary coefficients in terms of molecular dynamics, it was not until the contribution by Bocquet and Barrat that microscopic expressions for the interfacial mechanical [2] and thermal [81] slip transport coefficients were given. This work was a conceptual breakthrough in the extensive field of flow slip at solid surfaces. However, a debate was initiated by Petravic and Harrowell [33] who pointed out that the Green-Kubo expression proposed by Bocquet and Barrat provides not an intrinsic solid-fluid property but rather it depends on the geometry of the setup. This is due, as it was mentioned in the Introduction to the fact that the original expression reflects the total fluid friction for shear flow, including the slip friction at both interfaces as well as the viscous friction in the fluid [34, 82]. Hansen et al. [34] proposed to look at a thin slab of fluid near the wall and proposed a phenomenological Langevin equation relating the velocity of the center of mass of the fluid slab and the force that the wall exerts on the slab. The friction coefficient may be computed from equilibrium MD simulations by comparing the velocity-force correlation to the velocity-velocity correlations of the slab. Another recent approach has considered a generalized Langevin equation for the velocity of a single atom of the fluid near a wall [35]. Recent work by Ramos-Alvarado et al. [36] compares the above different approaches and concludes that simulations are

very sensitive to post-processing issues, leaving the story somewhat inconclusive.

Our theoretical approach is not restricted to parallel flow (i.e. fluid slabs) as is typically considered in simulation work [2, 33, 34, 36, 82]. Most derivations of Green-Kubo expressions for friction are based on linear response theory where the Hamiltonian is slightly perturbed by an external forcing [2, 35]. We follow here a different approach in obtaining directly the full hydrodynamic equations from the microscopic dynamics. In this way, the transport coefficients that we obtain are the ones that really enter the equations of hydrodynamics in any general flow configuration, not limited to homogeneous isotropic flat walls.

Note that all the mentioned work on MD simulations is directed to compute the transport coefficients that appear in slip boundary conditions. When one descends to the nanoscale, however, the picture of the effect of the solid-fluid interactions in terms of a boundary condition on an idealized surface is questionable. For the scales in which nanostructure is visible, e.g. layering near the wall, we aim at describing the fluid-solid interaction through coarse-grained forces that extend in a short range from the solid. An early attempt to use a “friction field” appeared in Ref. [83]. Only when the fluid is macroscopic, we would expect these forces to be treated as singular forces such that its effect can be described as truly boundary conditions on the fluid. Recently, Camargo et al. [84] describe how the present theory gives rise to boundary conditions when the flows are macroscopic.

A precursor of the work presented in this chapter can be found in [85], that considered a Brownian hard sphere in a sea of small hard spheres and used both, Mori projection operator and kinetic theory, to derive hydrodynamic equations coupled to the motion of the Brownian particle (without boundary conditions). Our method is more general in that continuum pair-wise potentials are allowed for, and the nonlinear Kawasaki-Gunton projection operator [66] is used for the coarse-graining procedure instead of the simpler Mori projector [35], the latter being limited to near equilibrium linear equations of motion [52]. A theory of coarse-graining based on the Kawasaki-Gunton projector gives a universal structure based on the usual thermodynamic potentials. The use of the Kawasaki-Gunton projector allows us to express the reversible part of the dynamics in a way that generalizes DFT to moving fluids.

Finally, Cadusch et al. [86] show that the use of a nonlocal translation invariant kernel is not exempt of problems in high density fluids in strong nanoconfinement. They state: “the fundamental theoretical challenge that remains is to include the position dependence into the kernel so that it becomes a genuinely inhomogeneous function of space and also to appropriately model the boundary conditions at the fluid–wall interface, including stick/slip boundary conditions.” The present work addresses this challenge.

## 2.2 The system and the relevant variables

In this section we use the ToCG for describing hydrodynamically a liquid near a solid. Consider a liquid system of  $N$  monoatomic molecules described with the position and momenta of their center of mass. The molecules are allowed to move through space unrestrictedly. To avoid the issues of an infinite number of particles required in the thermodynamic limit, and to make closer contact with MD simulations, we simply assume that the system has periodic boundary conditions. Interacting with that sea of liquid molecules there is a group of  $N'$  bonded atoms forming what we would understand at a macroscopic level as a solid object of spherical shape. At the microscopic level the system is described by the set of all positions  $\mathbf{q}_i$  and momenta  $\mathbf{p}_i = m_i \mathbf{v}_i$  ( $i = 1, \dots, N$ ) of the liquid atoms plus the positions  $\mathbf{q}_{i'}$  and momenta  $\mathbf{p}_{i'} = m_{i'} \mathbf{v}_{i'}$  ( $i' = 1, \dots, N'$ ) of the atoms of the solid sphere. For compactness we will denote the microstate in either of the following forms  $z$  or  $q, p, q', p'$ . From now, we will distinguish with a prime the labels of the atoms of the solid sphere from the unprimed labels of the liquid atoms. The microstate of the system evolves according to Hamilton's equations with a Hamiltonian given by

$$H(z) = \sum_i^N \frac{p_i^2}{2m_i} + \sum_{i'}^{N'} \frac{p_{i'}^2}{2m_{i'}} + U(z), \quad (2.1)$$

where the potential energy  $U(z)$  is given by

$$U(z) = V^f(q) + V^{fs}(q, q') + V^s(q') \quad (2.2)$$

We assume for simplicity a pair-wise potential energy, where  $V^f(q) = \frac{1}{2} \sum_{ij}^{NN} \phi_{ij}^{ll}$  is the potential of interaction between liquid atoms,  $V^{ls}(q, q') = \sum_{ii'}^{NN'} \phi_{ii'}^{ls}$  is the potential of interaction between liquid atoms and solid atoms, and  $V^s(q') = \frac{1}{2} \sum_{i'j'}^{N'N'} \phi_{i'j'}^{ss}$  is the potential of interaction between the atoms of the solid object. Self interaction of the atoms is not considered, so  $\phi_{ii} = 0$ , etc. There are no external conservative potentials acting on the system, although they can be easily introduced. We do not consider such external potentials in order to transparently discuss the issues of momentum conservation.

Note that at a microscopic level we do not have boundaries of any kind, we only have particles interacting with particles in free (periodic) space. In lab situations, typically, liquids are contained in flasks and other type of solid objects that prevent the liquid from leaking. We could model a spherical flask containing a liquid in very much the same way as we are going to treat the solid spherical particle surrounded by the (possibly infinite in extension, or periodic) liquid. A solid is regarded as a collection of bounded

atoms (that is, their relative distances do not increase without bound) that are moving and vibrating.

### 2.2.1 The relevant variables

We describe the system at a coarse grained level by selecting as relevant variables the mass and momentum density fields of the liquid and the center of mass position and momentum of the solid sphere. These are given by the following set of phase functions

$$\begin{aligned}\hat{\rho}_r(z) &= \sum_i^N m\delta(\mathbf{r} - \mathbf{q}_i) & \hat{\mathbf{R}}(z) &= \frac{1}{N'} \sum_{i'}^{N'} \mathbf{q}_{i'} \\ \hat{\mathbf{g}}_r(z) &= \sum_i^N \mathbf{p}_i \delta(\mathbf{r} - \mathbf{q}_i) & \hat{\mathbf{P}}(z) &= \sum_{i'}^{N'} \mathbf{p}_{i'},\end{aligned}\quad (2.3)$$

where  $\delta(\mathbf{r} - \mathbf{q}_i)$  is a Dirac  $\delta$  function as, for example, a normalized Gaussian. In these phase functions, the position  $\mathbf{r}$  plays the role of a continuous index labeling the phase function. The position  $\mathbf{r}$  may take any value in  $\mathbb{R}^3$ , or its periodic counterpart, as we do not have any restriction to the possible motion of the particles. As was mentioned in Chapter 1 the hamiltonian (2.1) is also a relevant variable.

For the sake of simplicity, we do not include orientational degrees of freedom of the solid for the time being. Note that by selecting the center of mass variables of the solid as the only ones necessary to describe the state of the solid we are implicitly assuming that the remaining solid degrees of freedom are much faster than the hydrodynamic fields. In particular, we assume that any elastic behaviour of the solid is so rapidly decaying toward its equilibrium state that elastic variables do not need to be included in the description. Should this assumption be violated, the resulting dynamic equations (not including these elastic variables for the solid) would probably be non-Markovian.

A word is in order about a model for the solid that is sometimes used in simulation work, where the solid is assumed to be made of “frozen” particles that act as simple generators of forces not reacting back to the presence of the liquid. In this case, the solid should be modeled as a static external field acting on the liquid. The structure of the theory changes in this case as we will discuss later.

### 2.2.2 The time derivatives of the relevant variables

The time derivatives of the coarse variables play a fundamental role in the final structure of the dynamic equations (1.40). The time derivative  $i\hat{\mathcal{L}}$  is the result of applying the Liouville operator (1.6) to the relevant variables. In this section, we discuss the

particular form of  $i\mathcal{L}\hat{A}$  for the case of selected CG variables (2.3). The action of the Liouville operator on the CG variables gives [87]

$$\begin{aligned} i\mathcal{L}\hat{\rho}_{\mathbf{r}}(z) &= -\nabla \cdot \hat{\mathbf{g}}_{\mathbf{r}}(z) \\ i\mathcal{L}\hat{\mathbf{g}}_{\mathbf{r}}(z) &= -\nabla \cdot \hat{\mathbf{K}}_{\mathbf{r}}(z) + \hat{\mathbf{F}}_{\mathbf{r}}^l(z) \end{aligned} \quad (2.4)$$

Here, the kinetic stress tensor is

$$\hat{\mathbf{K}}_{\mathbf{r}}(z) = \sum_i^N \mathbf{p}_i \mathbf{v}_i \delta(\mathbf{r} - \mathbf{q}_i) \quad (2.5)$$

and the total force density  $\hat{\mathbf{F}}_{\mathbf{r}}^l(z)$  on the liquid is defined as

$$\hat{\mathbf{F}}_{\mathbf{r}}^l(z) = \sum_i^N -\frac{\partial U}{\partial \mathbf{q}_i} \delta(\mathbf{r} - \mathbf{q}_i) \quad (2.6)$$

We may decompose this force density into the force that the liquid exerts on the liquid plus the force that the solid exerts on the liquid, this is,

$$\begin{aligned} \hat{\mathbf{F}}_{\mathbf{r}}^l(z) &= \hat{\mathbf{F}}_{\mathbf{r}}^{l \rightarrow l}(z) + \hat{\mathbf{F}}_{\mathbf{r}}^{s \rightarrow l}(z) \\ \hat{\mathbf{F}}_{\mathbf{r}}^{l \rightarrow l}(z) &= \sum_{ij}^{NN} \hat{\mathbf{F}}_{ij} \delta(\mathbf{r} - \mathbf{q}_i) \\ \hat{\mathbf{F}}_{\mathbf{r}}^{s \rightarrow l}(z) &= \sum_{ij'}^{NN'} \hat{\mathbf{F}}_{ij'} \delta(\mathbf{r} - \mathbf{q}_i), \end{aligned} \quad (2.7)$$

where  $\hat{\mathbf{F}}_{ij'}$  is the force that atom  $j'$  of the solid exerts on atom  $i$  of the liquid. This is,  $\hat{\mathbf{F}}_{\mathbf{r}}^{l \rightarrow l}(z)$  is the microscopic force density that the liquid exerts on the liquid molecules that are around the point  $\mathbf{r}$  and  $\hat{\mathbf{F}}_{\mathbf{r}}^{s \rightarrow l}(z)$  is the microscopic force density that the solid object exerts on the liquid at the point  $\mathbf{r}$ .

We may write the force that the liquid exerts on the liquid

$$\hat{\mathbf{F}}_{\mathbf{r}}^{l \rightarrow l}(z) = \frac{1}{2} \sum_{ij}^{NN} \hat{\mathbf{F}}_{ij} (\delta(\mathbf{r} - \mathbf{q}_i) - \delta(\mathbf{r} - \mathbf{q}_j)) \quad (2.8)$$

where we have used that the indices are dummy. By using a standard trick [52, 88], we

may express the difference of the Dirac  $\delta$  functions in terms of a divergence

$$\begin{aligned}\delta(\mathbf{r} - \mathbf{q}_i) - \delta(\mathbf{r} - \mathbf{q}_j) &= \int_0^1 d\epsilon \frac{d}{d\epsilon} \delta(\mathbf{r} - \mathbf{q}_j - \epsilon \mathbf{q}_{ij}) \\ &= -\nabla \int_0^1 d\epsilon \mathbf{q}_{ij} \delta(\mathbf{r} - \mathbf{q}_j - \epsilon \mathbf{q}_{ij})\end{aligned}\quad (2.9)$$

The liquid force density  $\hat{\mathbf{F}}_{\mathbf{r}}^{l \rightarrow l}(z)$  can then be expressed as the divergence of the microscopic virial stress tensor, that is,

$$\begin{aligned}\hat{\mathbf{F}}_{\mathbf{r}}^{l \rightarrow l}(z) &= -\nabla \cdot \hat{\Pi}_{\mathbf{r}}(z) \\ \hat{\Pi}_{\mathbf{r}}(z) &\equiv \frac{1}{2} \sum_{ij}^N \mathbf{q}_{ij} \hat{\mathbf{F}}_{ij} \int_0^1 d\epsilon \delta(\mathbf{r} - \mathbf{q}_i - \epsilon \mathbf{q}_{ij})\end{aligned}\quad (2.10)$$

The time derivative of the momentum density (2.4) becomes

$$\begin{aligned}i\mathcal{L}\hat{\mathbf{g}}_{\mathbf{r}}(z) &= -\nabla \cdot \hat{\mathbf{K}}_{\mathbf{r}}(z) - \nabla \cdot \hat{\Pi}_{\mathbf{r}}(z) + \hat{\mathbf{F}}_{\mathbf{r}}^{s \rightarrow l}(z) \\ &= -\nabla \cdot (\hat{\mathbf{K}}_{\mathbf{r}}(z) + \hat{\Pi}_{\mathbf{r}}(z)) + \hat{\mathbf{F}}_{\mathbf{r}}^{s \rightarrow l} \\ &= -\nabla \cdot \hat{\sigma}_{\mathbf{r}} + \hat{\mathbf{F}}_{\mathbf{r}}^{s \rightarrow l},\end{aligned}\quad (2.11)$$

where  $\hat{\sigma}_{\mathbf{r}}(z) = \hat{\mathbf{K}}_{\mathbf{r}}(z) + \hat{\Pi}_{\mathbf{r}}(z)$  is the microscopic stress tensor of the fluid, that is,

$$\hat{\sigma}_{\mathbf{r}} = \sum_i^N \mathbf{p}_i \mathbf{v}_i \delta(\mathbf{r} - \mathbf{q}_i) + \frac{1}{2} \sum_{ij}^N \mathbf{q}_{ij} \hat{\mathbf{F}}_{ij} \int_0^1 d\epsilon \delta(\mathbf{r} - \mathbf{q}_i - \epsilon \mathbf{q}_{ij})\quad (2.12)$$

For the solid object we have that the action of the Liouville operator gives

$$\begin{aligned}i\mathcal{L}\hat{\mathbf{R}}(z) &= \frac{\hat{\mathbf{P}}(z)}{M'} \\ i\mathcal{L}\hat{\mathbf{P}}(z) &= - \int d\mathbf{r} \hat{\mathbf{F}}_{\mathbf{r}}^{s \rightarrow l}(z)\end{aligned}\quad (2.13)$$

Note that the total momentum, which is defined in terms of the CG variables as

$$\hat{\mathbf{P}}_T = \int d\mathbf{r} \hat{\mathbf{g}}_{\mathbf{r}}(z) + \hat{\mathbf{P}}(z),\quad (2.14)$$

satisfies  $i\mathcal{L}\hat{\mathbf{P}}_T = 0$  and is, therefore, a conserved quantity of the microscopic dynamics. We have used that  $\int d\mathbf{r} \nabla \cdot \hat{\boldsymbol{\sigma}} = 0$  due to Gauss theorem and the fact that at the infinite we assume there are no fluid molecules. A similar argument holds when the domain of integration is periodic.

Summarizing, the time derivatives of the relevant variables of the system are

$$\begin{aligned} i\mathcal{L}\hat{\rho}_{\mathbf{r}}(z) &= -\nabla \cdot \hat{\mathbf{g}}_{\mathbf{r}}(z) \\ i\mathcal{L}\hat{\mathbf{g}}_{\mathbf{r}}(z) &= -\nabla \cdot \hat{\boldsymbol{\sigma}}_{\mathbf{r}}(z) + \hat{\mathbf{F}}_{\mathbf{r}}^{\text{s} \rightarrow \text{l}}(z) \\ i\mathcal{L}\hat{\mathbf{R}}(z) &= \frac{\hat{\mathbf{P}}(z)}{M} \\ i\mathcal{L}\hat{\mathbf{P}}(z) &= -\int d\mathbf{r} \hat{\mathbf{F}}_{\mathbf{r}}^{\text{s} \rightarrow \text{l}}(z) \end{aligned} \quad (2.15)$$

## 2.3 The relevant ensemble and the grand potential

In Sec. 1.6 we obtained that the ensemble which maximizes the Gibbs-Jaynes entropy function (1.24) is of the type

$$\bar{\rho}(z) = \frac{1}{Z[\lambda]} \rho_0 \exp\{-\lambda \cdot \hat{A}(z)\} \quad (2.16)$$

When the CG variables are those in (2.3), the relevant ensemble  $\bar{\rho}(z)$  takes the form

$$\begin{aligned} \bar{\rho}(z) &= \frac{1}{\Xi[\lambda]} \rho_0 \exp\{-\beta H(z)\} \\ &\times \exp\left\{-\beta \int d\mathbf{r} (\lambda_{\rho}(\mathbf{r}) \cdot \hat{\rho}_{\mathbf{r}}(z) + \lambda_g(\mathbf{r}) \cdot \hat{\mathbf{g}}_{\mathbf{r}}(z))\right\} \\ &\times \exp\{-\beta \lambda_R \cdot \hat{\mathbf{R}}(z) - \beta \lambda_P \cdot \hat{\mathbf{P}}(z)\} \end{aligned} \quad (2.17)$$

The normalization factor is the  $\lambda$ -dependent grand-canonical partition function defined as

$$\begin{aligned} \Xi[\lambda] &\equiv \sum_{N=0}^{\infty} \frac{1}{N! h^{3N}} \int dq dp dq' dp' \\ &\times \exp\left\{-\beta H - \beta \sum_{i=1}^N m \lambda_{\rho}(\mathbf{q}_i) - \beta \sum_{i=1}^N \mathbf{p}_i \cdot \lambda_g(\mathbf{q}_i)\right\} \\ &\times \exp\{-\beta \lambda_R \cdot \hat{\mathbf{R}}(z) - \beta \lambda_P \cdot \hat{\mathbf{P}}(z)\}, \end{aligned} \quad (2.18)$$

where we have introduced the coarse conjugate variables as

$$\begin{aligned}\lambda_\rho(\mathbf{q}_i) &= \int d\mathbf{r} \lambda_\rho(\mathbf{r}) \delta(\mathbf{r} - \mathbf{q}_i) \\ \lambda_g(\mathbf{q}_i) &= \int d\mathbf{r} \lambda_g(\mathbf{r}) \delta(\mathbf{r} - \mathbf{q}_i)\end{aligned}\quad (2.19)$$

The conjugate fields  $\lambda$  of the CG variables (2.3) are fixed by the condition that the averages of the CG variables with the relevant ensemble coincide with the averages  $\rho(\mathbf{r}), \mathbf{g}(\mathbf{r}), \mathbf{R}, \mathbf{P}$  computed with the solution of the Liouville equation (we omit the time dependence for simplicity). This conditions can be expressed as in equation (1.28) through the followig expressions

$$\begin{aligned}\rho(\mathbf{r}) &= \frac{\delta\Phi[\lambda]}{\delta\lambda_\rho(\mathbf{r})} & \mathbf{R} &= \frac{\partial\Phi[\lambda]}{\partial\lambda_R} \\ \mathbf{g}(\mathbf{r}) &= \frac{\delta\Phi[\lambda]}{\delta\lambda_g(\mathbf{r})} & \mathbf{P} &= \frac{\partial\Phi[\lambda]}{\partial\lambda_P},\end{aligned}\quad (2.20)$$

where the  $\lambda$ -dependent *grand-canonical potential* is given, as in equation (1.29) by

$$\Phi[\lambda] \equiv -k_B T \ln \Xi[\lambda] \quad (2.21)$$

As shown in Sec. 1.6, there is a one to one connection between the CG variables and the conjugate ones becasuse the functional  $\Phi[\lambda]$  is convex. Therefore, the functionals  $\lambda_\rho[\rho, \mathbf{g}, \mathbf{R}, \mathbf{P}]$ ,  $\lambda_g[\rho, \mathbf{g}, \mathbf{R}, \mathbf{P}]$ ,  $\lambda_R[\rho, \mathbf{g}, \mathbf{R}, \mathbf{P}]$ ,  $\lambda_P[\rho, \mathbf{g}, \mathbf{R}, \mathbf{P}]$  exist and are unique. We can therefore switch from the conjugate variables to the relevant variables and construct the corresponding *hydrodynamic functional* given by the Legendre transform of the  $\lambda$ -dependent grand-canonical potential, that is,

$$\begin{aligned}\mathcal{H}[\rho, \mathbf{g}, \mathbf{R}, \mathbf{P}] &= \Phi[\lambda_\rho, \lambda_g, \lambda_R, \lambda_P] \\ &\quad - \int d\mathbf{r} \rho(\mathbf{r}) \lambda_\rho(\mathbf{r}) - \int d\mathbf{r} \mathbf{g}(\mathbf{r}) \cdot \lambda_g(\mathbf{r}) \\ &\quad - \lambda_R \cdot \mathbf{R} - \lambda_P \cdot \mathbf{P}\end{aligned}\quad (2.22)$$

Note that the hydrodynamic functional is the negative of the correspoding entropy (1.31) for the present level of description. Therefore, the equation (1.33) must be satisfied.

$$\begin{aligned}\lambda_\rho(\mathbf{r}) &= -\frac{\delta\mathcal{H}}{\delta\rho(\mathbf{r})} & \lambda_R &= -\frac{\partial\mathcal{H}}{\partial\mathbf{R}} \\ \lambda_g(\mathbf{r}) &= -\frac{\delta\mathcal{H}}{\delta\mathbf{g}(\mathbf{r})} & \lambda_P &= -\frac{\partial\mathcal{H}}{\partial\mathbf{P}}\end{aligned}\quad (2.23)$$

It is possible to find the explicit expression of  $\lambda_g(\mathbf{r})$  and  $\lambda_P$  by performing the momentum integrals in equation (2.18). Replacing in equation (2.18) the Hamiltonian (2.1) and the momentum of the solid (2.3) we obtain

$$\begin{aligned} \Xi[\lambda] \equiv & \sum_{N=0}^{\infty} \frac{1}{N!h^{3N}} \int dq dp dq' dp' \\ & \times \exp \left\{ -\beta U(z) - \beta \sum_{i=1}^N m \lambda_\rho(\mathbf{q}_i) - \beta \lambda_R \cdot \hat{\mathbf{R}}(z) \right\} \\ & \times \exp \left\{ -\beta \left( \sum_{i=1}^N \frac{\mathbf{p}_i^2}{2m_i} + \sum_{i=1}^{N'} \frac{\mathbf{p}_{i'}^2}{2m_{i'}} \right) - \beta \sum_{i=1}^N \mathbf{p}_i \cdot \lambda_g(\mathbf{q}_i) - \beta \lambda_P \sum_{i=1}^{N'} \mathbf{p}_{i'} \right\} \end{aligned} \quad (2.24)$$

We may group the terms in this way

$$\begin{aligned} \Xi[\lambda] \equiv & \sum_{N=0}^{\infty} \frac{1}{N!h^{3N}} \int dq dp dq' dp' \\ & \times \exp \left\{ -\beta U(z) - \beta \sum_{i=1}^N m \lambda_\rho(\mathbf{q}_i) - \beta \lambda_R \cdot \hat{\mathbf{R}}(z) \right\} \\ & \times \exp \left\{ -\beta \sum_{i=1}^N \left( \frac{\mathbf{p}_i^2}{2m_i} + \mathbf{p}_i \cdot \lambda_g(\mathbf{q}_i) \right) \right\} \exp \left\{ -\beta \sum_{i=1}^{N'} \left( \frac{\mathbf{p}_{i'}^2}{2m_{i'}} + \lambda_P \mathbf{p}_{i'} \right) \right\} \end{aligned} \quad (2.25)$$

We perform the Gaussian integrals over momenta by using

$$\int_{-\infty}^{\infty} dx e^{-ax^2+bx} = \sqrt{\frac{\pi}{a}} e^{b^2/4a} \quad (2.26)$$

reaching the following expression

$$\begin{aligned} \Xi[\lambda] \equiv & \sum_{N=0}^{\infty} \frac{1}{N!} \int \frac{dq}{\Lambda^{3N}} \frac{dq'}{\Lambda^{3N'}} e^{-\beta U} \\ & \times \exp \left\{ -\beta \sum_{i=1}^N \left( m \lambda_\rho(\mathbf{r}_i) - \frac{m}{2} \lambda_g^2(\mathbf{q}_i) \right) \right\} \times \exp \left\{ -\beta \left( \lambda_R \cdot \hat{\mathbf{R}} - \frac{M'}{2} \lambda_P^2 \right) \right\}, \end{aligned} \quad (2.27)$$

where we have introduced the thermal wavelength

$$\Lambda = \left( \frac{h^2 \beta}{2\pi m} \right)^{\frac{1}{2}} \quad (2.28)$$

Together with equation (2.20) and equation (2.21)

$$\begin{aligned}\rho(\mathbf{r}) &= \frac{\delta\Phi[\lambda]}{\delta\lambda_\rho(\mathbf{r})} = \frac{1}{\Xi[\lambda]} \frac{\delta\Xi[\lambda]}{\delta\lambda_\rho(\mathbf{r})} = m \\ \mathbf{g}(\mathbf{r}) &= \frac{\delta\Phi[\lambda]}{\delta\lambda_g(\mathbf{r})} = \frac{1}{\Xi[\lambda]} \frac{\delta\Xi[\lambda]}{\delta\lambda_g(\mathbf{r})} = -m \cdot \boldsymbol{\lambda}_g(\mathbf{r}) \\ \mathbf{P} &= \frac{\delta\Phi[\lambda]}{\delta\lambda_P} = \frac{1}{\Xi[\lambda]} \frac{\partial\Xi[\lambda]}{\partial\lambda_P} = -M' \cdot \boldsymbol{\lambda}_P\end{aligned}\quad (2.29)$$

This leads directly to the explicit form of the following conjugate variables

$$\begin{aligned}\boldsymbol{\lambda}_g(\mathbf{r}) &= -\frac{\mathbf{g}(\mathbf{r})}{\rho(\mathbf{r})} = -\mathbf{v}(\mathbf{r}) \\ \boldsymbol{\lambda}_P &= -\frac{\mathbf{P}}{M'} = -\mathbf{V}\end{aligned}\quad (2.30)$$

and allows one to interpret these conjugate variables as (negative) velocities.

We may express the gran potential (2.21) as a sum of two contributions

$$\Phi[\lambda] = \Phi^{\text{pos}}[\mu, \lambda_R] - \frac{M'}{2} \boldsymbol{\lambda}_P^2, \quad (2.31)$$

where we have defined the following grand potential

$$\begin{aligned}\Phi^{\text{pos}}[\mu, \lambda_R] &\equiv -k_B T \ln \sum_{N=0}^{\infty} \frac{1}{N!} \int \frac{dq}{\Lambda^{3N}} \frac{dq'}{\Lambda^{3N'}} \\ &\times \exp \left\{ -\beta \left( U - \sum_{i=1}^N \mathbf{m}_i \cdot \boldsymbol{\mu}(\mathbf{q}_i) + \lambda_R \cdot \hat{\mathbf{R}} \right) \right\}\end{aligned}\quad (2.32)$$

and the chemical potential per unit mass has been introduced as

$$\boldsymbol{\mu}(\mathbf{r}) \equiv \frac{1}{2} \boldsymbol{\lambda}_g^2(\mathbf{r}) - \boldsymbol{\lambda}_\rho(\mathbf{r}) \quad (2.33)$$

Note that the gran potential (2.32) is similar to the macrocanonical gran potential of a fluid, except for the presence of the solid degrees of freedom and the corresponding conjugate variable  $\lambda_R$ .

## 2.4 The free energy

The Legendre transform of the gran potential for a simple liquid gives the classic (free energy) density functional and we may pursue the same route in order to define the free

energy density functional of a fluid in the presence of a solid sphere. The Legendre transform of the gran potential (2.32) is

$$\mathcal{F}[\rho, \mathbf{R}] \equiv \Phi^{\text{pos}}[\mu, \lambda_R] - \mu(\mathbf{r}) \frac{\delta \Phi^{\text{pos}}}{\delta \mu(\mathbf{r})}[\mu, \lambda_R] - \lambda_R \frac{\delta \Phi^{\text{pos}}}{\delta \lambda_R}[\mu, \lambda_R] \quad (2.34)$$

The derivatives we need of the functional (2.32) are

$$\begin{aligned} \frac{\delta \Phi^{\text{pos}}}{\delta \mu(\mathbf{r})}[\mu, \lambda_R] &= -\langle \hat{\rho}_{\mathbf{r}} \rangle^{\mu, \lambda_R} \\ \frac{\delta \Phi^{\text{pos}}}{\delta \lambda_R}[\mu, \lambda_R] &= \langle \hat{\mathbf{R}} \rangle^{\mu, \lambda_R}, \end{aligned} \quad (2.35)$$

where the averages  $\langle \dots \rangle^{\mu, \lambda_R}$  are defined in these equations. The second derivatives of  $\Phi^{\text{pos}}$  are given by covariances (see equations (1.28)-(1.30)) and this implies that  $\Phi^{\text{pos}}[\mu, \lambda_R]$  is a convex function. Therefore, the connection between  $\langle \hat{\rho}_{\mathbf{r}} \rangle^{\mu, \lambda_R}$ ,  $\langle \hat{\mathbf{R}} \rangle^{\mu, \lambda_R}$  and  $\mu(\mathbf{r}), \lambda_R$  is one to one. Note also that because the phase functions  $\hat{\rho}_{\mathbf{r}}, \hat{\mathbf{R}}$  do not depend on particle's momenta, we have that the averages are given by

$$\begin{aligned} \langle \hat{\rho}_{\mathbf{r}} \rangle^{\mu, \lambda_R} &= \text{Tr}[\bar{\rho} \hat{\rho}_{\mathbf{r}}] = \rho(\mathbf{r}) \\ \langle \hat{\mathbf{R}} \rangle^{\mu, \lambda_R} &= \text{Tr}[\bar{\rho} \hat{\mathbf{R}}] = \mathbf{R} \end{aligned} \quad (2.36)$$

Therefore, we have a one to one connection between the conjugate variables  $\mu(\mathbf{r}), \lambda_R$  and the averages  $\rho(\mathbf{r}), \mathbf{R}$  of the CG variables computed with the solution of the Liouville equation.

Finally, we have the free energy functional  $\mathcal{F}[\rho, \mathbf{R}]$  of a structured fluid in the presence of a solid sphere as the following Legendre transform

$$\mathcal{F}[\rho, \mathbf{R}] \equiv \Phi^{\text{pos}}[\mu, \lambda_R] + \int d\mathbf{r} \rho(\mathbf{r}) \mu(\mathbf{r}) - \lambda_R \cdot \mathbf{R}, \quad (2.37)$$

whose derivatives are given by

$$\begin{aligned} \frac{\delta \mathcal{F}}{\delta \rho(\mathbf{r})}[\rho, \mathbf{R}] &= \mu(\mathbf{r}) \\ \frac{\delta \mathcal{F}}{\delta \mathbf{R}}[\rho, \mathbf{R}] &= -\lambda_R \end{aligned} \quad (2.38)$$

We can obtain an expression for the hydrodynamic functional (2.22) replacing the terms  $\Phi[\lambda]$ ,  $\lambda_g(\mathbf{r})$ ,  $\lambda_P$ , and  $\lambda_R \cdot \mathbf{R}$  by the equations (2.30), (2.31), and using (2.37),

respectively.

$$\begin{aligned}\mathcal{H}[\rho, \mathbf{g}, \mathbf{R}, \mathbf{P}] = & - \int d\mathbf{r} \rho(\mathbf{r}) \lambda_\rho(\mathbf{r}) + \int d\mathbf{r} \frac{\mathbf{g}^2(\mathbf{r})}{\rho(\mathbf{r})} \\ & + \mathcal{F}[\rho, \mathbf{R}] - \int d\mathbf{r} \rho(\mathbf{r}) \mu(\mathbf{r}) + \frac{\mathbf{P}^2}{2M'}\end{aligned}\quad (2.39)$$

If we replace  $\mu(\mathbf{r})$  by the equation (2.33) and use (2.30), we finally arrive to an expression of the hydrodynamic functional  $\mathcal{H}$  which is the sum of a kinetic part and a “potential” part

$$\mathcal{H}[\rho, \mathbf{g}, \mathbf{R}, \mathbf{P}] = \underbrace{\int d\mathbf{r} \frac{\mathbf{g}^2(\mathbf{r})}{2\rho(\mathbf{r})} + \frac{\mathbf{P}^2}{2M'}}_{\text{kinetic}} + \underbrace{\mathcal{F}[\rho, \mathbf{R}]}_{\text{potential}}\quad (2.40)$$

As we show in Appendix B,  $\lambda_R$  is just the average force on the solid due to the fluid. Therefore, the “potential” part  $\mathcal{F}[\rho, \mathbf{R}]$  of the hydrodynamic functional (2.40) really acts as a potential energy whose negative gradient gives the actual force on the sphere. For future reference, we may also compute the functional derivative of the hydrodynamic functional  $\mathcal{H}$  with respect to the density field with the result

$$\frac{\delta \mathcal{H}}{\delta \rho(\mathbf{r})}[\rho, \mathbf{g}, \mathbf{R}, \mathbf{P}] = \frac{\mathbf{v}^2(\mathbf{r})}{2} + \frac{\delta \mathcal{F}}{\delta \rho(\mathbf{r})}[\rho, \mathbf{R}]\quad (2.41)$$

The free energy functional is translationally invariant, that is,

$$\mathcal{F}[T_{\mathbf{u}}\rho, T_{\mathbf{u}}\mathbf{R}] = \mathcal{F}[\rho, \mathbf{R}],\quad (2.42)$$

where the translation operator applied to any function is defined as

$$T_{\mathbf{u}}f(\mathbf{r}) = f(\mathbf{r} + \mathbf{u})\quad (2.43)$$

The invariance can be shown by performing a suitable change of variables inside the phase space integrals defining the partition function. By taking the derivative with respect to  $\mathbf{u}$  in both sides of equation (2.42) and setting afterwards  $\mathbf{u} = 0$  we obtain the identity

$$\int d\mathbf{r} \frac{\delta \mathcal{F}}{\delta \rho(\mathbf{r})} \nabla \rho(\mathbf{r}) + \frac{\delta \mathcal{F}}{\delta \mathbf{R}} = 0\quad (2.44)$$

This identity will be crucial in order to show that total momentum is conserved by the reversible part of the dynamics.

The calculation of the thermodynamic potential (2.32) needed for the evaluation of the free energy functional  $\mathcal{F}[\rho, \mathbf{R}]$  is very difficult to perform in general and, therefore, one needs to model the free energy functional based on intuition and previous experience. A particularly simple model that takes into account the effect of the fluid-solid interaction is given by

$$\mathcal{F}[\rho, \mathbf{R}] = \mathcal{F}_0[\rho] + \int d\mathbf{r} \frac{1}{m} \rho(\mathbf{r}) V(\mathbf{r}, \mathbf{R}), \quad (2.45)$$

where  $\mathcal{F}_0[\rho]$  is the free energy density functional of the fluid in the absence of the solid, and all the fluid solid interaction is taken into account through the second term that involves a *coarse-grained potential*  $V(\mathbf{r}, \mathbf{R})$ . This potential captures the effective (reversible) interaction between solid and fluid atoms. Note that even for the case of an ideal gas interacting with a solid sphere the model (2.45) does not follow straightforwardly from the exact free energy (2.37) with (2.32) due to the integrals over the solid degrees of freedom of the interaction potential between ideal gas particles and solid particles. Equation (2.45) is just a natural candidate to model the free energy  $F[\rho, \mathbf{R}]$ . The potential energy  $V(\mathbf{r}, \mathbf{R})$  becomes infinite (or extremely large) for the points  $\mathbf{r}$  inside the solid sphere. Therefore, the last term in (2.45) makes impossible the realization of density fields with nonzero value inside the solid sphere (i.e. leads to impenetrability of the solid). The derivatives of the free energy model (2.45) are

$$\frac{\delta \mathcal{F}}{\delta \rho(\mathbf{r})} = \mu_0(\mathbf{r}) + \frac{V(\mathbf{r}, \mathbf{R})}{m}, \quad \frac{\delta \mathcal{F}}{\delta \mathbf{R}} = - \int d\mathbf{r} \frac{1}{m} \rho(\mathbf{r}) \mathbf{F}(\mathbf{r}, \mathbf{R}), \quad (2.46)$$

where  $\mu_0(\mathbf{r})$  is the usual chemical potential of the solvent in the absence of any solid, and  $\mathbf{F}(\mathbf{r}, \mathbf{R})$  is the effective force, deriving from the potential  $V(\mathbf{r}, \mathbf{R})$  that the solid sphere with center of mass at  $\mathbf{R}$  exerts on a fluid atom at  $\mathbf{r}$ .

## 2.5 The transport equations

In this section we obtain the transport equation for a fluid in contact with a solid sphere. In Sec. 1.7 we obtained an expression for the evolution of the selected variables using the technique of projection operators. This expression consists on two terms: the reversible part and the irreversible part.

### 2.5.1 Exact reversible dynamics

In this subsection we consider the reversible part for the case that the CG variables are those in equations (2.3). For the mass density we have

$$\partial_t \rho(\mathbf{r}, t)|_{\text{rev}} = \text{Tr}[\bar{\rho}_t i \mathcal{L} \hat{\rho}_{\mathbf{r}}] = -\nabla \cdot \mathbf{g}(\mathbf{r}, t), \quad (2.47)$$

where we have used equation (2.4) and the fact that the relevant ensemble average of  $\hat{\mathbf{g}}$  is precisely the momentum density field  $\mathbf{g}(\mathbf{r}, t)$ . On the other hand, and using again the equation (2.4), the reversible part of the momentum density evolution equation is

$$\partial_t \mathbf{g}(\mathbf{r}, t)|_{\text{rev}} = \text{Tr}[\bar{\rho}_t i \mathcal{L} \hat{\mathbf{g}}_{\mathbf{r}}] = -\nabla \cdot \text{Tr}[\bar{\rho}_t \hat{\mathbf{K}}_{\mathbf{r}}] + \text{Tr}[\bar{\rho}_t \hat{\mathbf{F}}_{\mathbf{r}}^l] \quad (2.48)$$

We will compute the terms of equation (2.48) taking advantage of the Galilean operator.

The Galilean operator changes the velocity arguments from  $\mathbf{v}_i \rightarrow \mathbf{v}_i + \mathbf{v}(\mathbf{q}_i)$  for each  $i$  fluid particle, that is,

$$\mathcal{G}\hat{F}(\mathbf{q}_1, \dots, \mathbf{q}_N; \mathbf{p}_1, \dots, \mathbf{p}_N) = \hat{F}(\mathbf{q}_1, \dots, \mathbf{q}_N; \mathbf{p}_1 + m_1 \mathbf{v}(\mathbf{q}_1), \dots, \mathbf{p}_N + m_N \mathbf{v}(\mathbf{q}_N)) \quad (2.49)$$

The intuitive meaning of the Galilean operator is that when applied to a phase function gives how it is seen in a reference frame that moves with the flow field. Within any trace this is just a change of variables. Therefore, we have the property

$$\text{Tr}[\bar{\rho}_t \hat{F}] = \text{Tr}[(\mathcal{G}\bar{\rho}_t)(\mathcal{G}\hat{F})] \quad (2.50)$$

The action of the Galilean operator on the relevant variables is

$$\begin{aligned} \mathcal{G}\hat{\rho}_{\mathbf{r}} &= \hat{\rho}_{\mathbf{r}} \\ \mathcal{G}\hat{\mathbf{g}}_{\mathbf{r}} &= \hat{\mathbf{g}}_{\mathbf{r}} + \mathbf{v}(\mathbf{r})\hat{\rho}_{\mathbf{r}} \\ \mathcal{G}\hat{\mathbf{R}}(z) &= \hat{\mathbf{R}}(z) \\ \mathcal{G}\hat{\mathbf{P}}(z) &= \hat{\mathbf{P}}(z) \end{aligned} \quad (2.51)$$

Therefore, the action of  $\mathcal{G}$  on the relevant ensemble is

$$\mathcal{G}\bar{\rho}_t = \frac{1}{\Xi[\lambda(t)]} \rho^{\text{eq}}(z) \exp \left\{ \beta \int d\mathbf{r} \mu(\mathbf{r}) \hat{\rho}_{\mathbf{r}}(z) \right\} \exp \left\{ -\beta \lambda_R(t) \cdot \hat{\mathbf{R}}(z) - \beta \lambda_P(t) \cdot \hat{\mathbf{P}}(z) \right\}, \quad (2.52)$$

where the chemical potential per unit mass has been introduced in equation (2.33). The action of the Galilean operator on the microscopic kinetic stress tensor is

$$\mathcal{G}\hat{\mathbf{K}}_{\mathbf{r}} = \hat{\mathbf{K}}_{\mathbf{r}} + \mathbf{v}(\mathbf{r})\hat{\mathbf{g}}_{\mathbf{r}} + \hat{\mathbf{g}}_{\mathbf{r}}\mathbf{v}(\mathbf{r}) + \mathbf{v}(\mathbf{r})\mathbf{v}(\mathbf{r})\hat{\rho}_{\mathbf{r}} \quad (2.53)$$

Using (2.50) we have

$$\text{Tr}[\bar{\rho}_t \hat{\mathbf{K}}_{\mathbf{r}}] = \text{Tr}[(\mathcal{G}\bar{\rho}_t)(\mathcal{G}\hat{\mathbf{K}}_{\mathbf{r}})] \quad (2.54)$$

By noting that the ensemble (2.52) is Gaussian in momenta, we have finally

$$\text{Tr}[\bar{\rho}_t \hat{\mathbf{K}}_{\mathbf{r}}] = \mathbf{v}(\mathbf{r})\mathbf{v}(\mathbf{r})\rho(\mathbf{r}) + \frac{k_B T}{m}\rho(\mathbf{r})\delta, \quad (2.55)$$

where  $\delta$  is the unit tensor. The last term  $\text{Tr}[\bar{\rho}_t \hat{\mathbf{F}}_{\mathbf{r}}^l]$  in equation (2.48) is computed in equation (B.8) of the Appendix B. By collecting (2.55) and (B.8) into the momentum density equation (2.48) we obtain

$$\partial_t \mathbf{g}(\mathbf{r}, t)|_{\text{rev}} = -\nabla \cdot (\mathbf{v}(\mathbf{r}, t)\mathbf{g}(\mathbf{r}, t)) - \rho(\mathbf{r})\nabla \frac{\delta \mathcal{F}}{\delta \rho(\mathbf{r})}[\rho, \mathbf{R}] \quad (2.56)$$

Finally, the averages with the relevant ensemble of the solid object variables are

$$\begin{aligned} \text{Tr}[\bar{\rho}_t i \mathcal{L} \hat{\mathbf{R}}] &= \frac{\mathbf{P}}{M} \\ \text{Tr}[\bar{\rho}_t i \mathcal{L} \hat{\mathbf{P}}] &= -\frac{\partial \mathcal{F}}{\partial \mathbf{R}}[\rho, \mathbf{R}], \end{aligned} \quad (2.57)$$

where we have used equation (B.10) in the Appendix B.

By collecting the above results, the reversible part of the dynamics has the form

$$\begin{aligned} \partial_t \rho(\mathbf{r})|_{\text{rev}} &= -\nabla \cdot \mathbf{g}(\mathbf{r}) \\ \partial_t \mathbf{g}(\mathbf{r})|_{\text{rev}} &= -\nabla \cdot (\mathbf{g}(\mathbf{r})\mathbf{v}(\mathbf{r})) - \rho(\mathbf{r})\nabla \frac{\delta \mathcal{F}}{\delta \rho(\mathbf{r})}[\rho, \mathbf{R}] \\ \partial_t \mathbf{R}|_{\text{rev}} &= \frac{\mathbf{P}}{M} \\ \partial_t \mathbf{P}|_{\text{rev}} &= -\frac{\partial \mathcal{F}}{\partial \mathbf{R}}[\rho, \mathbf{R}] \end{aligned} \quad (2.58)$$

These reversible equations are exact as no approximations have been made so far. We qualify these equations as reversible because, as can be explicitly shown, they conserve the hydrodynamic functional (2.22), which is minus the entropy corresponding to this level of description.

### 2.5.2 Markovian irreversible dynamics

While the reversible part of the dynamics (2.58) is exact, the irreversible part that we consider is approximate because we assume a Markovian dynamics. Under the Markovian approximation in which the memory kernel is assumed to decay in a time scale short as compared to the time scales of the hydrodynamic variables, the irreversible dynamics is given by the term  $\sum_j D_{ij} \lambda_j$  in equation (1.40). Because the time derivatives of  $\hat{\rho}(\mathbf{r})$  and  $\hat{\mathbf{R}}$  are given in terms of momenta, which are relevant variables themselves, the effect of the projection operator in (1.38) is simply  $Qi\mathcal{L}\hat{\rho}_r = 0$  and  $Qi\mathcal{L}\hat{\mathbf{R}}_\mu = 0$  resulting in a large simplification of the friction matrix. The irreversible part of the dynamics  $\sum_j D_{ij} \lambda_j$  in equation (1.40) now takes the form

$$\partial_t \begin{pmatrix} \rho(\mathbf{r}) \\ \mathbf{g}(\mathbf{r}) \\ \mathbf{R} \\ \mathbf{P} \end{pmatrix}_{\text{irr}} = - \begin{pmatrix} 0 & 0 & 0 & 0 \\ 0 & \int d\mathbf{r}' M_{\mathbf{rr}'}^{gg} & 0 & M_{\mathbf{r}}^{gP} \\ 0 & 0 & 0 & 0 \\ 0 & \int d\mathbf{r}' M_{\mathbf{r}'}^{Pg} & 0 & M^{PP} \end{pmatrix} \begin{pmatrix} \frac{\delta \mathcal{H}}{\delta \rho_{r'}} \\ \frac{\delta \mathcal{H}}{\delta \mathbf{g}_{r'}} \\ \frac{\delta \mathcal{H}}{\delta \mathbf{R}} \\ \frac{\delta \mathcal{H}}{\delta \mathbf{P}} \end{pmatrix} \quad (2.59)$$

where we have used (2.23). The sum over the continuum “index”  $\mathbf{r}$  becomes an integral. The domain of integration of this integral is  $\mathbb{R}^3$ , including the interior of the solid sphere. By using the results (2.23) and (2.30) that link the functional derivatives of the CG Hamiltonian with respect to momenta to the velocities, we obtain the following irreversible dynamics

$$\begin{aligned} \partial_t \mathbf{g}(\mathbf{r}) &= - \int d\mathbf{r}' M_{\mathbf{rr}'}^{gg} \mathbf{v}(\mathbf{r}') - M_{\mathbf{r}}^{gP} \mathbf{V} \\ \frac{d}{dt} \mathbf{P}(t) &= - \int d\mathbf{r}' M_{\mathbf{r}'}^{Pg} \mathbf{v}(\mathbf{r}') - M^{PP} \mathbf{V}, \end{aligned} \quad (2.60)$$

where the matrix elements are defined in terms of Green-Kubo formulas as

$$\begin{aligned} M_{\mathbf{r}\mathbf{r}'}^{gg} &= \frac{1}{k_B T} \int_0^{\Delta t} dt \langle Q_i \mathcal{L} \hat{\mathbf{g}}_r(t) Q_i \mathcal{L} \hat{\mathbf{g}}_{r'} \rangle^\lambda \\ M_{\mathbf{r}}^{gP} &= \frac{1}{k_B T} \int_0^{\Delta t} dt \langle Q_i \mathcal{L} \hat{\mathbf{g}}_r(t) Q_i \mathcal{L} \hat{\mathbf{P}} \rangle^\lambda \\ M_{\mathbf{r}'}^{Pg} &= \frac{1}{k_B T} \int_0^{\Delta t} dt \langle Q_i \mathcal{L} \hat{\mathbf{P}}(t) Q_i \mathcal{L} \hat{\mathbf{g}}_{r'} \rangle^\lambda \\ M^{PP} &= \frac{1}{k_B T} \int_0^{\Delta t} dt \langle Q_i \mathcal{L} \hat{\mathbf{P}}(t) Q_i \mathcal{L} \hat{\mathbf{P}} \rangle^\lambda \end{aligned} \quad (2.61)$$

Note that momentum conservation implies that the gain rate of the total momentum of the fluid is equal to the loss rate of momentum of the particle

$$\int d\mathbf{r} i \mathcal{L} \hat{\mathbf{g}}_{\mathbf{r}} = -i \mathcal{L} \hat{\mathbf{P}} \quad (2.62)$$

The conservation of momenta then implies the following relationships between elements of the dissipative matrix

$$M_{\mathbf{r}}^{gP} = - \int d\mathbf{r}' M_{\mathbf{r}\mathbf{r}'}^{gg}, \quad M^{PP} = - \int d\mathbf{r} M_{\mathbf{r}}^{Pg} \quad (2.63)$$

and this leads in equation (2.60) to

$$\begin{aligned} \partial_t \mathbf{g}(\mathbf{r}) &= - \int d\mathbf{r}' M_{\mathbf{r}\mathbf{r}'}^{gg} (\mathbf{v}(\mathbf{r}') - \mathbf{V}) \\ \frac{d}{dt} \mathbf{P}(t) &= \int d\mathbf{r} \int d\mathbf{r}' M_{\mathbf{r}\mathbf{r}'}^{gg} (\mathbf{v}(\mathbf{r}') - \mathbf{V}) \end{aligned} \quad (2.64)$$

which contain only the matrix element  $M_{\mathbf{r}\mathbf{r}'}^{gg}$  and are manifestly Galilean invariant. By using equations (2.11), (2.13) in the definition of  $M_{\mathbf{r}\mathbf{r}'}^{gg}$  in equation (2.61), and inserting the result in the equation of motion (2.60) one obtains

$$\begin{aligned} \partial_t \mathbf{g}^\alpha(\mathbf{r})|_{\text{irr}} &= \nabla_{\mathbf{r}}^\beta \Sigma^{\alpha\beta}(\mathbf{r}) + \mathcal{S}^\alpha(\mathbf{r}) \\ \left. \frac{d}{dt} \mathbf{P}^\alpha(t) \right|_{\text{irr}} &= - \int d\mathbf{r}' \mathcal{S}^\alpha(\mathbf{r}'), \end{aligned} \quad (2.65)$$

where the fluid stress tensor is

$$\Sigma^{\alpha\beta}(\mathbf{r}) = \int d\mathbf{r}' \eta_{\mathbf{rr}'}^{\alpha\beta\alpha'\beta'} \nabla_{\mathbf{r}'}^{\beta'} \mathbf{v}^{\alpha'}(\mathbf{r}') \quad (2.66)$$

and the *irreversible surface force density* on the fluid is defined as

$$\begin{aligned} S^\alpha(\mathbf{r}) = & - \int d\mathbf{r}' \mathbf{G}_{\mathbf{rr}'}^{\alpha\alpha'\beta'} \nabla_{\mathbf{r}'}^{\beta'} \mathbf{v}^{\alpha'}(\mathbf{r}') \\ & + \nabla_{\mathbf{r}}^\beta \int d\mathbf{r}' \mathbf{H}_{\mathbf{rr}'}^{\alpha\beta\alpha'} (\mathbf{v}^{\alpha'}(\mathbf{r}') - \mathbf{V}^{\alpha'}) - \int d\mathbf{r}' \gamma_{\mathbf{rr}'}^{\alpha\alpha'} (\mathbf{v}^{\alpha'}(\mathbf{r}') - \mathbf{V}^{\alpha'}) \end{aligned} \quad (2.67)$$

Note that we use Einstein's sum over repeated indices convention. In these expressions we have introduced the following *nonlocal* transport coefficients: the viscosity kernel  $\eta_{\mathbf{rr}'}$  (fourth order tensor), the slip kernels  $\mathbf{H}_{\mathbf{rr}'}, \mathbf{G}_{\mathbf{rr}'}$  (third order tensors), and the friction kernel  $\gamma_{\mathbf{rr}'}$  (second order tensor). They are defined by the Green-Kubo formulas

$$\begin{aligned} \eta_{\mathbf{rr}'} &\equiv \frac{1}{k_B T} \int_0^{\Delta t} dt' \langle Q_t \hat{\sigma}_{\mathbf{r}}(t') Q_t \hat{\sigma}_{\mathbf{r}'} \rangle^{\lambda(t)} \\ \mathbf{H}_{\mathbf{rr}'} &\equiv \frac{1}{k_B T} \int_0^{\Delta t} dt' \langle Q_t \hat{\sigma}_{\mathbf{r}}(t') Q_t \hat{\mathbf{F}}_{\mathbf{r}'}^{s \rightarrow l} \rangle^{\lambda(t)} \\ \mathbf{G}_{\mathbf{rr}'} &\equiv \frac{1}{k_B T} \int_0^{\Delta t} dt' \langle Q_t \hat{\mathbf{F}}_{\mathbf{r}}^{s \rightarrow l}(t') Q_t \hat{\sigma}_{\mathbf{r}'} \rangle^{\lambda(t)} \\ \gamma_{\mathbf{rr}'} &\equiv \frac{1}{k_B T} \int_0^{\Delta t} dt' \langle Q_t \hat{\mathbf{F}}_{\mathbf{r}}^{s \rightarrow l}(t') Q_t \hat{\mathbf{F}}_{\mathbf{r}'}^{s \rightarrow l} \rangle^{\lambda(t)} \end{aligned} \quad (2.68)$$

These transport kernels are state dependent, i.e. functions of the time dependent averages of the relevant variables, through the dependence of the relevant ensemble on these averages. The explicit form of the projected currents appearing in these expressions is given in the Appendix C.

## 2.6 The final equations of nanohydrodynamics

By collecting the reversible part of the dynamics (2.58) and the irreversible part (2.65) we obtain the final dynamic equations for the relevant variables

$$\begin{aligned}\partial_t \rho(\mathbf{r}) &= -\nabla \cdot \mathbf{g}(\mathbf{r}) \\ \partial_t \mathbf{g}(\mathbf{r}) &= -\nabla \cdot (\mathbf{g}(\mathbf{r}) \mathbf{v}(\mathbf{r})) - \rho(\mathbf{r}) \nabla \frac{\delta \mathcal{F}}{\delta \rho(\mathbf{r})} [\rho, \mathbf{R}] + \nabla \cdot \boldsymbol{\Sigma}(\mathbf{r}) + \mathbf{S}(\mathbf{r}) \\ \dot{\mathbf{R}} &= \frac{\mathbf{P}}{M} \\ \dot{\mathbf{P}} &= -\frac{\partial \mathcal{F}}{\partial \mathbf{R}} - \int d\mathbf{r} \mathbf{S}(\mathbf{r}),\end{aligned}\tag{2.69}$$

where the free energy functional  $\mathcal{F}[\rho, \mathbf{R}]$  is introduced in equation (2.37), the velocity field is  $\mathbf{v}(\mathbf{r}) = \mathbf{g}(\mathbf{r})/\rho(\mathbf{r})$ , the fluid stress tensor  $\boldsymbol{\Sigma}(\mathbf{r})$  is given in (2.66), and the irreversible force  $\mathbf{S}(\mathbf{r})$  is given in equation (2.67).

Equations (2.69), (2.68), (2.67) are the main results of the present chapter. They describe the isothermal nonlocal hydrodynamics of a simple fluid coupled with the motion of an immersed structureless solid sphere. These equations generalize equilibrium DFT for a simple fluid to nonequilibrium situations in which the fluid may be moving around a solid sphere. The only approximation that has been taken in the derivation is the Markovian approximation that neglects memory effects in the dissipative part of the dynamics.

Let us discuss the physical meaning of the different terms in equations (2.69). The equation for the evolution of the mass density field is just the continuity equation. The equation for the momentum density field involves the usual convective term plus a term involving the gradient of the functional derivative of the free energy. This term describes both, the “pressure gradient” term and the reversible coupling between the fluid and solid sphere. The viscous term  $\nabla \cdot \boldsymbol{\Sigma}$  describes the internal friction of the fluid due to its self-interaction. This viscous term involving second derivatives is the usual viscosity term of the Navier-Stokes equations, which is here expressed in a nonlocal form. The use of nonlocal viscosities has been advocated recently in the field of nano-hydrodynamics [34, 76–78]. A phenomenological alternative to address flow problems where density is inhomogeneous is to keep using local hydrodynamics with the viscosity of the bulk but evaluated at the local values of the density [89]. While this may lead to reasonable results, the present microscopically derived model seems to have a firmer basis. The fourth order viscosity tensor is given in terms of the correlation of the fluctuations of the fluid stress tensor. Away from the walls, it is expected that the viscosity tensor becomes fully isotropic and dependent only on the distance between

the points  $\mathbf{r}, \mathbf{r}'$ .

The force density  $\mathcal{S}(\mathbf{r})$  involving the nonlocal transport kernels  $\mathbf{H}_{\mathbf{rr}'}$ ,  $\mathbf{G}_{\mathbf{rr}'}$ ,  $\gamma_{\mathbf{rr}'}$  describes the irreversible interaction between the solid and the fluid. Note that these kernels are defined in (2.68) in terms of correlations involving the force density  $\hat{\mathbf{F}}_{\mathbf{r}}^{s \rightarrow l}$  that the solid sphere exerts on the liquid molecules. These terms should be understood, therefore, as the responsible for transmitting the irreversible forces that the solid sphere exerts on the fluid. The force density  $\hat{\mathbf{F}}_{\mathbf{r}}^{s \rightarrow l}(z)$  will be different from zero only for those points  $\mathbf{r}$  that are near of the solid sphere. This means that the transport kernels  $\mathbf{G}_{\mathbf{rr}'}, \mathbf{H}_{\mathbf{rr}'}, \gamma_{\mathbf{rr}'}$  are highly localized near the atoms of the solid that interact with the fluid. Note that *the concept of surface of the solid does not enter this theory*. There is no such a well-defined surface in microscopic terms. However, this surface can be defined *operationally* by looking precisely at the singular behaviour of the above transport kernels. Indeed, the force density  $\hat{\mathbf{F}}_{\mathbf{r}}^{s \rightarrow l}(z)$  will be a fluctuating vector on the surface of the solid sphere. If the interaction between fluid and solid atoms is purely repulsive, this force will be most of the time directed outwards the surface of the solid sphere. At the same time, because the interaction between solid and fluid atoms is singular as their separation vanishes, we expect that  $\hat{\mathbf{F}}_{\mathbf{r}}^{s \rightarrow l}$  will diverge as  $\mathbf{r}$  approaches the solid boundary. This divergence will be reflected in divergences of the transport kernels as  $\mathbf{r}$  or  $\mathbf{r}'$  approach the boundary of the solid. In a similar way, the stress tensor  $\hat{\sigma}_{\mathbf{r}}$  that depends only on fluid atom coordinates will be nonzero only outside the solid sphere because the interaction with the solid sphere refrains to have liquid molecules inside the solid sphere (more on this later). Therefore, the surface of the solid may be characterized by the singularity of the transport coefficients  $\mathbf{H}_{\mathbf{rr}'}, \mathbf{G}_{\mathbf{rr}'}, \gamma_{\mathbf{rr}'}$  and the vanishing of  $\eta_{\mathbf{rr}'}$ .

The force density and the stress tensor are assumed to vary in time in a time scale much shorter than the typical timescale in which the mass and momentum density of the solvent, and the position and momentum of the solid sphere particle appreciably changes. This separation of timescales is at the core of the Markovian form of the evolution of the CG dynamics in the projection operator technique. Whether the selected relevant variables do actually comply with this separation of time scales can only be assessed from the validity of the predictions of the resulting theory as compared with actual simulations or experiments. Note, however, that for slowly varying flow configurations, as those attained in steady states, the Markovian approximation should be reasonably fulfilled.

### 2.6.1 Conserved quantities, $H$ -theorem and the equilibrium state

The equations (2.69) are the equations of hydrodynamics in the presence of a solid spherical particle. We stress that the above equations conserve total mass and momentum,

given by

$$\begin{aligned} M_T &= M' + \int d\mathbf{r} \rho(\mathbf{r}) \\ \mathbf{P}_T &= \mathbf{P} + \int d\mathbf{r} \mathbf{g}(\mathbf{r}) \end{aligned} \quad (2.70)$$

Mass conservation follows immediately from the continuity equation. Momentum conservation is a consequence of the invariance under translations of the free energy functional expressed in equation (2.44) that ensures that the reversible part of the dynamics conserves momentum. The irreversible part conserves also total momentum because the momentum lost by the fluid is gained by the solid sphere.

In addition, the function  $\mathcal{H}$  evolves in time in a strictly decreasing way, that is,

$$\frac{d\mathcal{H}}{dt}(t) \leq 0, \quad (2.71)$$

where the equality sign occurs when the system has reached its equilibrium state. This is because, while the reversible part of the dynamics conserves  $\mathcal{H}$ , the irreversible part of the dynamics fulfills (2.71), due to the positive semidefinite character of the friction matrix.

As a consequence, the equilibrium state of equations (2.69) is the one that minimizes  $\mathcal{H}$  subject to the constraints of giving the actual values of the total mass and momentum. In order to obtain the equilibrium values of the relevant variables, one should minimize the following functional without constraints

$$\mathcal{H} - \mu_0 \int d\mathbf{r} \rho(\mathbf{r}) - \mathbf{V}_0 \cdot \left[ \int d\mathbf{r} \mathbf{g}(\mathbf{r}) + \mathbf{P} \right], \quad (2.72)$$

where  $\mu_0, \mathbf{V}_0$  are the corresponding Lagrange multipliers. Setting to zero the derivatives of the above functional gives

$$\begin{aligned} \frac{\mathbf{v}^2(\mathbf{r})}{2} + \frac{\delta\mathcal{F}}{\delta\rho(\mathbf{r})}[\rho, \mathbf{R}] - \mu_0 - V_0 \int d\mathbf{r} \mathbf{v}(\mathbf{t}) &= 0, & \frac{\partial\mathcal{F}}{\partial\mathbf{R}}[\rho, \mathbf{R}] &= 0 \\ \mathbf{v}(\mathbf{r}) - \mathbf{V}_0 &= 0, & \mathbf{V} - \mathbf{V}_0 &= 0 \end{aligned} \quad (2.73)$$

This means that the state of equilibrium has a constant velocity field equal to the velocity of the solid particle and, without losing generality, we may take  $\mathbf{V}_0 = 0$ . We then have the following two coupled equations for the equilibrium value that take the density field and the position of the sphere

$$\frac{\delta\mathcal{F}}{\delta\rho(\mathbf{r})}[\rho, \mathbf{R}] = \mu_0, \quad \frac{\partial\mathcal{F}}{\partial\mathbf{R}}[\rho, \mathbf{R}] = 0 \quad (2.74)$$

From equations (2.38), the first equation (2.74) simply states that the equilibrium state has a constant value of the chemical potential  $\mu(\mathbf{r}) = \mu_0$  while the second equation states that the total force on the solid sphere vanishes at equilibrium. This set of two coupled equations should be understood as a set of nonlinear equations for the equilibrium density field  $\rho(\mathbf{r})$  and the equilibrium value of the center of mass position  $\mathbf{R}$  of the sphere. Translational invariance of the system implies that if  $\mathbf{R}, \rho(\mathbf{r})$  is a solution of (2.74), then  $\mathbf{R} + \mathbf{u}, \rho(\mathbf{r} + \mathbf{u})$  is also a solution. Therefore, without loss of generality we may choose the origin of coordinates at the center of the sphere and  $\mathbf{R} = 0$ . Then the equilibrium density field is the solution of the first equation. Note that for realistic models of the free energy functional, the density field will display oscillations at short length scales due to the packing of the fluid near the solid sphere.

In the present theory, the equilibrium profile is the one that is reached at long times due to the evolution of the hydrodynamic equations. In this subsection, we have shown how the theory presented contains the usual prescription to obtain the equilibrium density profile in DFT by minimizing the free energy functional.

## 2.6.2 Approximating the relevant ensemble averages and projected currents

It should be remarked that the theory presented is valid, as the H-theorem clearly testifies, for the decaying dynamics toward the equilibrium state in isolated systems. It is, therefore, a theory that describes, given initial nonequilibrium values for the averages of the CG variables, the subsequent average evolution toward equilibrium. One situation in which we will be interested is when the solid particle is very large and massive. In these situations, we may assume that the spherical particle has initial (average) position  $\mathbf{R}_0$  and initial (average) momentum  $\mathbf{P}_0 = 0$  and that, for all the decay evolution of the hydrodynamic fields, these values do not change appreciably because the forces that the fluid exerts on the particle during its evolution are not sufficiently strong to modify these variables substantially.

In principle, the relevant ensemble depends (in a functional way) on the averages of all the relevant variables of the system. As this is unduly complicated, we take the approximation in which the transport kernels are evaluated for the *equilibrium* values of the relevant variables. In this doing, we assume that for any other value of the average value of the relevant variables obtained in the course of the dynamics, the transport kernels do not change appreciably. The equilibrium values of the average relevant variables have been obtained in equation. (2.73), (2.74) and are characterized by the following conjugate variables (see equation (2.30) and (2.38))

$$\mu(\mathbf{r}, \mathbf{R}) = \mu_0, \quad \lambda_g(\mathbf{r}) = 0, \quad \lambda_P = 0, \quad \lambda_R = 0, \quad (2.75)$$

Substitution of these conjugate variables into the relevant ensemble (2.17) shows that the relevant ensemble becomes just the equilibrium ensemble. Of course an equilibrium average of the microscopic system is one in which the sampling of the microscopic state involves states where the solid sphere may be located in any position of the physical space, due to Brownian motion. When the solid particle is infinitely massive, the position of the center of mass will not change appreciably in the time scale at which the solvent becomes equilibrated. This is, for a very massive sphere we expect that the instantaneous values of their centers of mass  $\hat{\mathbf{R}}$  is always very similar to their average values. For massive solid objects and, in particular, planar walls, we should understand the averages over the equilibrium ensemble as conditional averages where the solid object is fixed in space. These equilibrium averages can be, therefore, sampled through the ergodic hypothesis, as time averages over long MD simulations in which the solid remains fixed.

When we approximate the relevant ensemble with an equilibrium ensemble in the Green-Kubo transport coefficients, they become state independent. In this particular case, we may justify Onsager's reciprocity for the transport coefficients. As it is well-known, if two phase space variables  $\hat{A}(z), \hat{B}(z)$  transform under time reversal with the same parity, the property of microscopic reversibility together with the stationarity of the equilibrium ensemble imply

$$\langle \hat{A}(t)B \rangle^{\text{eq}} = \langle A\hat{B}(t) \rangle^{\text{eq}} \quad (2.76)$$

The microscopic reversibility property reflects into the following property of correlations

$$\langle (Q\mathbf{F}_r(t))(Q\sigma_{r'}(t)) \rangle^{\text{eq}} = \langle Q\sigma_{r'}(t)Q\mathbf{F}_r \rangle^{\text{eq}} \quad (2.77)$$

This results in the following symmetry properties (Onsager relations) for the transport kernels

$$\eta_{rr'}^{\alpha\beta\alpha'\beta'} = \eta_{r'r}^{\alpha'\beta'\alpha\beta}, \quad \mathbf{H}_{rr'}^{\alpha\beta\alpha'} = \mathbf{G}_{r'r}^{\alpha'\alpha\beta}, \quad \gamma_{rr'}^{\alpha\alpha'} = \gamma_{r'r}^{\alpha'\alpha} \quad (2.78)$$

## 2.7 Summary

In this chapter we have derived DDFT for simple fluid in contact with a solid sphere. We have taken as relevant variables the mass and momentum density fields of the fluid and the center of mass position and momentum of the solid sphere. We have used the Kawasaki-Gunton operator in order to obtain the evolution equations for the average value of these fields. A crucial assumption in the method of projection operators is that

the relevant variables should be *slow* in order to have a Markovian, memoryless equation. Equations with memory are indeed much more difficult to deal with than memoryless equations. In the former case one needs to know the specific form of the memory kernel *function* instead of just one single number, the transport *coefficient*, which in the present theory is, in fact, a nonlocal function of space. The equations (2.69) are nonlocal in space because 1) the free energy functional depends in general in a nonlocal way on the density field in order to account for the ordering of a fluid near a wall. And 2), the irreversible part of the dynamics involves transport kernels that are nonlocal. Note that we assume nonlocality in space but locality in time (no memory), and this may not be entirely consistent. However, memory kernels are typically uncomputable from MD, as they involve the projected dynamics instead of the real dynamics. The usual approximation in which the projected dynamics is substituted with the real, Hamiltonian, dynamics is only justified when, precisely, one has separation of timescales (i.e. when the Markovian dynamics holds). We take the pragmatic point of view in which we give credit to the Markovian approximation but retain spatially nonlocal hydrodynamic equations, by hoping that non-Markovian effects will not dominate the problem. In particular, we believe that for flows that vary slowly in time, the Markov approximation will hold. This excludes, perhaps, shocks or other strongly varying flows.

The theory presented in Sec. 1.7 (and in which the present chapter is based) is valid for *isolated* systems that decay toward the unique equilibrium state, abiding to the Second Law of Thermodynamics, and it does not allow to treat forced situations where there are external forces applied either to the fluid or to the solid. In this respect, no steady states can be described by the theory as it stands. However, the generalization of the framework to include external forcing is not difficult and is sketched in what follows by following Grabert's textbook [52]. For sufficiently small external forcings, the equations of motion (i.e. the transport equations and free energy function) are the same as the no forced situations, with the external forcing appearing in two places. On one hand in the fluid momentum equation a term  $\rho(\mathbf{r}, t)\mathbf{F}^{\text{ext}}(\mathbf{r}, t)$  appears, where  $\mathbf{F}^{\text{ext}}(\mathbf{r}, t)$  is any external force field acting on a molecule of fluid that happens to be at the point  $\mathbf{r}$ . On the other hand, in the particle momentum equation, an additional force term  $\mathbf{F}(\mathbf{R})$  appears, describing any external force acting on the particle.

The theory presented is isothermal. We have not considered in the description the energy density field of the fluid, nor the internal energy of the solid sphere. Instead, only the total energy has been considered as relevant variable and local transport of energy is not described by the present theory. Of course, these local energy variables can be introduced in the theory, at the expense of additional equations and terms.

A word is in order about the mathematical nature of the integro-differential equations. From a mathematical point of view, these equations require the specification of (mathematical) boundary conditions in order to have a unique solution. What are

the suitable boundary conditions to be specified for equations (2.69)? In the present situation, where only transient dynamics toward equilibrium can be investigated, these boundary conditions appear as an initial value problem. In addition, note that we have not included any external confining potential that would model the confinement of the fluid in a container. Only a sphere in an infinite fluid (or with periodic boundary conditions) has been considered. It is straightforward to include an external potential, though. These confining potential are such that, by definition, leave the fluid in a closed region of space, where outside the region there are no atoms of the fluid. In order to do so, these confining potentials need to be singular. This implies that outside the container region both the mass density and momentum densities of the fluid are zero. Note that outside the container region, both the force density  $\hat{\mathbf{F}}_r^{s \rightarrow l}(z)$  and the fluid stress tensor  $\hat{\sigma}_r(z)$  vanish, because there are no fluid particles outside. This means that the transport kernels vanish if  $\mathbf{r}$  or  $\mathbf{r}'$  are outside the container. This should tame the potentially singular presence of factors of the inverse of the density appearing in the velocity field  $\mathbf{v}(\mathbf{r}) = \mathbf{g}(\mathbf{r})/\rho(\mathbf{r})$ . The presence of the sphere produces forces that are highly localized in a narrow region around the solid particle. From a thermodynamic point of view, the issue of boundary conditions as emerging from “physics” rather than “numerical analysis” has also been considered in the past [79, 90–92]. In a fully macroscopic phenomenological theory, the effect of the irreversible surface force is taken into account through boundary conditions applied to the fluid equations. Camargo et al. discuss in Ref. [84] the emergence of boundary conditions in a macroscopic theory. They consider the conditions under which the localized irreversible surface forces produce actual boundary conditions for the hydrodynamic equations.

A general comment on the status of the present theory is in order. This theory is the natural generalization of equilibrium DFT for simple fluids, when these fluids are in motion and, therefore, out of equilibrium. It allows, in principle, to study effects like how the structuring of the fluid near a wall is modified by the flow field. While it is a coarse-grained theory where the relevant variables are the hydrodynamic fields, it captures the structure of the fluid at atomic nanoscales. The value of the present theory lies in that it provides the structure of the equations. For example, as compared with previous work, the present theory gives a neat definition of all the irreversible forces in a fluid that arise due to the interaction with solids. In particular, the distinction of the forces on the fluid due to the fluid itself and due to the solid reflects into the final structure of the irreversible forces that involve both, microscopically defined slip coefficients (due to fluid-solid interactions), as well as viscosity kernels (due to the fluid-fluid interactions). The form of these forces is such that, not only friction forces that depend on the velocity difference between the fluid and the solid appear, but also forces that depend on the gradients of the velocity field near the solid are present.

All these features are important assets of the theory. Unfortunately, in order to make

the theory predictive, it is necessary to fill in some important information. The first input element is the free energy functional (2.45) involving the standard equilibrium free energy functional  $\mathcal{F}_0[\rho]$ . One can benefit from the vast amount of work in the literature addressing the construction of very realistic models for the free energy functional. The second piece of information that is required is the dissipative matrix, that contains the *nonlocal* transport kernels, which are *tensorial* in nature. This means that in order to make dynamic predictions with this theory we have to know in advance 50 different functions (tensor elements after sorting out the corresponding symmetries of the stress tensor and Onsager reciprocity) of the six variables  $\mathbf{r}, \mathbf{r}'$ . While in principle, the Green-Kubo expressions would allow for the explicit calculation through MD simulations, it is clearly not a feasible program. In order to make any advance in the prediction of transport at the nanoscale it is necessary to make some approximations in order to reduce the large number of transport kernels. In the following chapters, we will consider situations in which symmetries of the solid surface and fluid flow can be exploited. In those situations, the number of Green-Kubo expressions is dramatically reduced and can be computed explicitly.

Finally, we remark that the present theory is concerned with the evolution of the *averages* of the relevant variables. The fact that we use a spherical solid particle is just a recourse to deal with momentum conservation, but we have in mind that the particle will be very large and massive for which Brownian motion plays no role.

# Chapter 3

## Discrete hydrodynamics near solids for planar flows

*Nothing got inside the head without becoming pictures.*

---

The corrections  
JONATHAN FRANZEN

### 3.1 Introduction

In Chapter 2 we constructed from first principles a theory for hydrodynamics in contact with solids. Based on the Kawasaki-Gunton projector [43, 52], the theory governs the average value of the hydrodynamic variables in the presence of a solid sphere. The essential ingredients of the theory are the conventional free energy functional of DFT that governs the layering of the density field, and the presence of irreversible forces that are concentrated near the solid surface and that are the responsible at the coarse-grained level of transmitting the interactions of the solid atoms to the fluid.

In spite of its elegance, the theory as presented in Chapter 2 cannot yet be validated through simulations for two reasons. First, the amount of information required in the hydrodynamic equations is exceedingly large. Nonlocal higher order tensors are required leading to an untractable number of different components. Second, in order to compare with MD simulations, one necessarily requires a discrete version of such a

theory. Particles need to be sorted into cells in order to measure “fields” in MD. The purpose of this chapter is to produce the discrete hydrodynamic equations involving a tractable amount of measurable information. The discrete quantities appearing in the theory can be measured through equilibrium MD simulations, and the theory may be then validated by comparing with nonequilibrium MD simulations. Such a comparison allows us to validate the only assumption on which the continuum hydrodynamic equations (2.69) are based, which is the Markovian assumption. This validation will be presented in the following chapters, where we have observed that only for sufficiently large discretization cells, larger than molecular sizes, one observes Markovian behaviour. In the strict continuum limit of very small cells, a Markovian theory is unable to describe the numerical results.

In this chapter we derive with the technique of projection operators the evolution equations for the nonequilibrium averages of the discrete hydrodynamic variables. The methodology follows Refs. [93–96] where a set of discrete hydrodynamic variables are introduced through a finite element basis function set. The present work is a generalization of the results of Ref. [96] in the presence of solid walls and for the particular case of parallel flows. One interesting benefit of the discretization methodology that we consider in this chapter is that the final discrete evolution equations obtained from first principles are identical to a finite element discretization of the continuum equations (2.69), once isotropy and translation invariance along the wall is assumed for the flow.

## 3.2 Simpler theory

The hydrodynamic theory (2.69) requires an extremely large amount of information in order to be predictive, which is almost a contradiction. In particular, we need to know the transport coefficients which are, in general nonlocal, but most dramatically, tensorial in character. The Green-Kubo expressions (2.68) correlate the different components of the microscopic force vector that the solid exerts on the fluid, and the microscopic stress tensor, defined both in (2.12). The number of components of the tensorial kernels is very large. The viscosity tensor, being a fourth order tensor has in principle 81 components, but the symmetry of the microscopic stress tensor reduces the number to 36 independent components. The tensors  $\mathbf{G}, \mathbf{H}$  are third order tensors and, on account of the symmetry of the microscopic stress tensor, have 21 independent components, while the number of independent components of the second order friction tensor is 9. Onsager reciprocity reduces the total number to 23 which is still a very large number of components to consider.

For this reason, we will consider a theory that is restricted to *planar walls*. Specifically, two solid walls made of atoms located at fixed lattice positions enclose our fluid

system. The concept of “surface” is subtle from a microscopic point of view. In fact, the solid is made of point particles that act like centers of force for the fluid particles. The concept of surface of a solid and its actual position needs to be, therefore, related to the interactions between fluid and solid, as discussed in [84].

In this chapter we assume that the walls, or rather the interactions felt by the fluid due to the walls, are statistically planar and isotropic, i.e. invariant under translations in the plane of the wall, and under rotations around an axis perpendicular to the walls. In addition, we will restrict ourselves to *planar flow* situations in which the hydrodynamic flow depends only on the coordinate perpendicular to the wall, i.e. it is invariant under translations tangent to the walls. In this way, the planar flows to be considered include shear flows (Poiseuille and Couette, for example) and sound wave propagation perpendicular to the walls but not, for example, sound waves that propagate parallel to the walls.

In order to validate through computer simulations a continuum theory like the one presented in Chapter 2 one needs to follow three consecutive steps that require a discrete framework. In the first step, equilibrium MD simulations should be run in order to measure the nonlocal transport kernels. In the second step, the discrete equations with the measured kernels should be solved numerically in order to predict the flow field given a certain initial velocity profile. In the third step, one should run a separate nonequilibrium MD simulation with the same initial velocity profile. By averaging over several initial microscopic configurations corresponding to this initial velocity flow one obtains the nonequilibrium average time evolution of the velocity profile as measured from MD. The comparison of the predicted time-dependent velocity profile with the result obtained directly from nonequilibrium MD simulations allows one to validate the theory.

*All these steps require the discretization of space in slabs.* In the first step, this is necessary in order to deal with the Dirac  $\delta$  functions that appear in the force density and stress tensor (2.12), whose correlations give rise to the kernels. The second step requires a discretization in order to solve numerically equations (2.69). Finally, in the third step the discretization is required in order to measure the density and velocity fields. It is important that the discretization in these three steps is done consistently. In Refs. [95, 96] is discussed how a method based on finite elements allows one to construct the CG discrete variables evolving according to dynamic equations that are consistent with a finite element discretization of the continuum equations.

### 3.3 The discrete basis function set

In this chapter, the finite elements are defined in 3D but taking into account the translation invariance of the flow field along the directions parallel to the walls, as follows.

We bin the system in layers parallel to the planar walls. The box length  $L_z$  is divided in  $N_{\text{bin}}$  bins labeled with an index  $\mu$ . Each bin is a layer or slab of dimensions  $L_x, L_y, \Delta z$  with  $\Delta z = L_z/N_{\text{bin}}$ . The bins are separated by  $N_{\text{bin}}$  nodes (actually, nodal planes) located at  $z_\mu = \mu\Delta z$  with  $\mu = 0, \dots, N_{\text{bin}} - 1$ . We assume that we have periodic boundary conditions in the  $z$  direction and, therefore, node  $\mu = 0$  is equal to the node  $N_{\text{bin}}$ . We carefully distinguish between *nodes* and *bins*: nodes are points in the  $z$  axis, while bins are segments in this axis. In 3D, nodes are planes, while bins are slabs. As it will become apparent, from a microscopic point of view, mass, momentum, and force densities are defined at the nodes, while stress is defined at the bins.

We introduce the characteristic function of the bin  $\chi_\mu(\mathbf{r})$  that takes the value 1 if  $\mathbf{r}$  is in the bin and zero otherwise. Its explicit form is given by the unit function

$$\chi_\mu(\mathbf{r}) = \theta(z_{\mu+1} - z)\theta(z - z_\mu) = \chi_\mu(z), \quad (3.1)$$

where  $\theta(x)$  is the Heaviside step function,  $z_{\mu+1}$  is the position of the upper boundary of the layer, and  $z_\mu$  is the corresponding position of the lower boundary of the layer. The set of characteristic functions form a partition of unity, i.e. by summing over all the bins we have

$$\sum_{\mu}^{N_{\text{bin}}} \chi_\mu(\mathbf{r}) = 1 \quad (3.2)$$

The volume integral of the characteristic function gives the volume  $\mathcal{V}_\mu$  of the bin

$$\mathcal{V}_\mu = \int d\mathbf{r} \chi_\mu(\mathbf{r}) = L_x L_y \Delta z \quad (3.3)$$

For each node, we introduce a finite element linear basis function  $\Phi_\mu(\mathbf{r})$

$$\Phi_\mu(\mathbf{r}) = \chi_\mu(z) \frac{z_{\mu+1} - z}{\Delta z} + \chi_{\mu-1}(z) \frac{z - z_{\mu-1}}{\Delta z}, \quad (3.4)$$

that depends only on the  $z$  component of  $\mathbf{r}$ . The finite element basis functions  $\Phi_\mu(\mathbf{r})$  also form a partition of unity, i.e.

$$\sum_{\mu}^{N_{\text{bin}}} \Phi_\mu(\mathbf{r}) = 1 \quad (3.5)$$

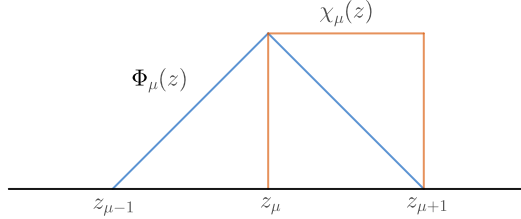


**Figure 3.1:** The basis function  $\Phi_\mu(z)$  of node  $\mu$  (blue) and the characteristic function  $\chi_\mu(z)$  of bin  $\mu$  (orange).

We plot in Fig. 3.1 the basis function  $\Phi_\mu(z)$  of node  $\mu$  and the characteristic function  $\chi_\mu(z)$  of bin  $\mu$ .

The gradient of the basis function is

$$\nabla \Phi_\mu(\mathbf{r}) = -\frac{\chi_\mu(\mathbf{r}) - \chi_{\mu-1}(\mathbf{r})}{\Delta z} \mathbf{n}, \quad (3.6)$$

where  $\mathbf{n}$  is the unit vector in the normal direction.

Following Ref. [96], we now introduce dual basis functions  $\delta_\mu(\mathbf{r})$  and  $\psi_\mu(\mathbf{r})$ . The basis function  $\delta_\mu(\mathbf{r})$  is used to discretize a continuum field  $v(\mathbf{r})$  by defining the discrete values  $v_\mu$  according to

$$v_\mu = \int d\mathbf{r} v(\mathbf{r}) \delta_\mu(\mathbf{r}) \quad (3.7)$$

On the other hand, the basis function  $\psi_\mu(\mathbf{r})$  allows one to construct a continuum field out of a discrete set of values through interpolation, that is,

$$\bar{v}(\mathbf{r}) = \sum_\mu v_\mu \psi_\mu(\mathbf{r}) \quad (3.8)$$

In this chapter, overlined fields indicate fields interpolated from a set of discrete values. The basis functions are required to satisfy the biorthonormality condition

$$\int d\mathbf{r} \delta_\mu(\mathbf{r}) \psi_\nu(\mathbf{r}) = \delta_{\mu\nu}, \quad (3.9)$$

where  $\delta_{\mu\nu}$  is the Kronecker delta. It proves convenient to introduce the following parenthetical notation for space integrals

$$(\dots) = \int d\mathbf{r} \dots \quad (3.10)$$

and the biorthonormality condition (3.9) becomes

$$(\delta_\mu \psi_\nu) = \delta_{\mu\nu} \quad (3.11)$$

We stipulate that the relation between both basis function is linear

$$\delta_\mu(\mathbf{r}) = \sum_\nu M_{\mu\nu}^\delta \psi_\nu(\mathbf{r}), \quad \psi_\mu(\mathbf{r}) = \sum_\nu M_{\mu\nu}^\psi \delta_\nu(\mathbf{r}) \quad (3.12)$$

and, then, the biorthonormality condition (3.9) implies that the matrices are given by

$$M_{\mu\nu}^\delta = (\delta_\mu \delta_\nu), \quad M_{\mu\nu}^\psi = (\psi_\mu \psi_\nu) \quad (3.13)$$

and these two matrices are inverse of each other.

The biorthonormality condition ensures the consistency property that if we discretize as in (3.7) an interpolated field like (3.8) we get

$$c_\mu = \int d\mathbf{r} \delta_\mu(\mathbf{r}) \bar{c}(\mathbf{r}) = \sum_\nu \int d\mathbf{r} \delta_\mu(\mathbf{r}) \psi_\nu(\mathbf{r}) c_\nu = c_\mu \quad (3.14)$$

Therefore, the discretization of an interpolated field gives consistently back the original discrete field, and no errors are accumulated in the process.

Let us now specify the actual form of the basis functions. The finite element basis function  $\Phi_\mu(\mathbf{r})$  has an associated volume  $\mathcal{V}_\mu$  defined as

$$\mathcal{V}_\mu = \int d\mathbf{r} \Phi_\mu(\mathbf{r}) \quad (3.15)$$

and the usual mass matrix of the finite element method is

$$M_{\mu\nu}^\Phi = (\Phi_\mu \Phi_\nu) \quad (3.16)$$

and has dimensions of volume. This matrix satisfies

$$\sum_\mu M_{\mu\nu}^\Phi = \mathcal{V}_\nu \quad (3.17)$$

and, by multiplying with the inverse on both sides

$$\sum_\mu \mathcal{V}_\mu [M^\Phi]_{\mu\nu}^{-1} = 1 \quad (3.18)$$

for all  $\nu$ .

The discrete Dirac  $\delta$  function is defined in terms of the finite element basis function according to

$$\delta_\mu(\mathbf{r}) \equiv \frac{\Phi_\mu(\mathbf{r})}{\mathcal{V}_\mu} \quad (3.19)$$

The matrices  $M_{\mu\nu}^\delta, M_{\mu\nu}^\psi$  defined in (3.13) are related to the mass matrix of the finite element basis (3.16) through

$$M_{\mu\nu}^\delta = \frac{M_{\mu\nu}^\Phi}{\mathcal{V}_\mu \mathcal{V}_\nu}, \quad M_{\mu\nu}^\psi = \mathcal{V}_\mu [M^\Phi]_{\mu\nu}^{-1} \mathcal{V}_\nu \quad (3.20)$$

Given the definition (3.19) for the discrete Dirac  $\delta$  function, the interpolant basis function given in (3.12) takes the form

$$\psi_\mu(\mathbf{r}) = \mathcal{V}_\mu \sum_\nu [M^\Phi]_{\mu\nu}^{-1} \Phi_\nu(\mathbf{r}) \quad (3.21)$$

in terms of the finite element basis function set.

### 3.4 The discrete hydrodynamics equations derived with the Kawasaki-Gunton projector

In this section, we present a derivation of the governing equations of the dynamics of the nonequilibrium average of the discrete hydrodynamic variables from first principles, i.e. based on the projection operator technique [52], summarized in Sec. 1.7 of Chapter 1. The CG variables that we consider in this chapter are the total Hamiltonian  $\hat{H}(z)$  and the discrete mass and momentum fields, which are defined according to

$$\hat{\rho}_\mu = \sum_i^N m_i \delta_\mu(\mathbf{q}_i), \quad \hat{\mathbf{g}}_\mu = \sum_i^N \mathbf{p}_i \delta_\mu(\mathbf{q}_i) \quad (3.22)$$

The phase functions (3.22), as opposed to the microscopic functions (2.3) can be measured directly in a MD simulation. The continuum (2.3) and discrete (3.22) variables are connected by

$$\hat{\rho}_\mu = \int d\mathbf{r} \delta_\mu(\mathbf{r}) \hat{\rho}_{\mathbf{r}}, \quad \hat{\mathbf{g}}_\mu = \int d\mathbf{r} \delta_\mu(\mathbf{r}) \hat{\mathbf{g}}_{\mathbf{r}} \quad (3.23)$$

The discrete mass and momentum densities are defined at the nodal planes. We see from (3.22) that the mass density at a node receives a contribution of the mass of fluid molecule  $i$  that depends on the distance of this molecule to the nodal plane  $\mu$ , and similarly for the momentum. The microscopic variables (3.22) give, essentially, the number of particles and the average velocity of the particles (per unit volume) that happen to be “around” the nodal plane  $\mu$ .

No macroscopic variables are assumed for the solid, because we assume that it is a very massive wall with definite location. By the very selection of the variables (3.22) as the CG variables, we are making a strong assumption about the situations in which the theory may be applicable. For example, the resulting theory will not be able to describe situations in which a sound wave is propagating in the direction *parallel* to the walls, because such a wave has variations in the parallel direction that cannot be captured by the CG variables. However, it will allow us to discuss sound propagation *perpendicular* to the walls. It is expected that the CG variables (3.22) will feel the effects of the walls in a very integrated form, in which the isotropy and translation invariance of the walls will be a very good approximation. In that sense, for those situations in which the resulting dynamic equations are valid (i.e. parallel flow), the assumed isotropy of the walls is expected to be valid. The calculations presented in what follows are very similar to the ones described in Ref. [97], except that the present calculation deals with “canonical” averages instead of “microcanonical” averages. They also crucially differ in that the present derivation accounts for the presence of confining walls.

### 3.4.1 The time derivatives

The time derivatives of the CG variables (3.22) are given through the action of the Liouville operator

$$i\mathcal{L}\hat{\rho}_\mu = \sum_{i=1}^N \mathbf{p}_i \cdot \nabla \delta_\mu(\mathbf{q}_i), \quad i\mathcal{L}\hat{\mathbf{g}}_\mu = \sum_{i=1}^N \mathbf{p}_i \mathbf{v}_i \cdot \nabla \delta_\mu(\mathbf{q}_i) + \hat{\mathbf{F}}_\mu \quad (3.24)$$

In the expression (3.24) we see that the momentum density changes through two different mechanism, the convective motion of the particles and the forces on the particles. The total force density  $\hat{\mathbf{F}}_\mu$  felt by the fluid particles at node  $\mu$  is

$$\hat{\mathbf{F}}_\mu = \hat{\mathbf{F}}_\mu^{s \rightarrow l} + \hat{\mathbf{F}}_\mu^{l \rightarrow l}, \quad (3.25)$$

where  $\hat{\mathbf{F}}_\mu^{s \rightarrow l}$  is the force density on the fluid at node  $\mu$  due to the solid and  $\hat{\mathbf{F}}_\mu^{l \rightarrow l}$  is the force density on the fluid at node  $\mu$  due to the fluid. These forces are defined as

$$\hat{\mathbf{F}}_\mu^{s \rightarrow l} \equiv \sum_{ij'} \hat{\mathbf{F}}_{ij'} \delta_\mu(\mathbf{q}_i), \quad \hat{\mathbf{F}}_\mu^{l \rightarrow l} \equiv \sum_{ij} \hat{\mathbf{F}}_{ij} \delta_\mu(\mathbf{q}_i) \quad (3.26)$$

Recall that solid atoms have primed indices and fluid atoms have unprimed indices.

For future reference, we express the time derivative of the discrete momentum density field in terms of a discrete stress tensor. The gradient of the discrete delta function is given, from (3.6) and (3.19), by

$$\nabla \delta_\mu(\mathbf{r}) = -\frac{1}{\mathcal{V}_\mu} \frac{\chi_\mu(z) - \chi_{\mu-1}(z)}{\Delta z} \mathbf{n} \quad (3.27)$$

This means that the convective part can be expressed in the form

$$\sum_{i=1}^N \mathbf{p}_i \mathbf{v}_i \cdot \nabla \delta_\mu(\mathbf{q}_i) = -\frac{1}{\mathcal{V}_\mu} \sum_{i=1}^N \mathbf{p}_i \mathbf{v}_i \cdot \mathbf{n} \frac{\chi_\mu(z) - \chi_{\mu-1}(z)}{\Delta z} \quad (3.28)$$

For the force due to the fluid we may use the trick

$$\begin{aligned} \hat{\mathbf{F}}_\mu^{l \rightarrow l} &= \sum_{ij}^N \hat{\mathbf{F}}_{ij} \delta_\mu(\mathbf{q}_i) = \frac{1}{2} \sum_{ij}^N \hat{\mathbf{F}}_{ij} (\delta_\mu(\mathbf{q}_i) - \delta_\mu(\mathbf{q}_j)) = \frac{1}{2} \sum_{ij}^N \hat{\mathbf{F}}_{ij} \int_0^1 d\epsilon \frac{d}{d\epsilon} \delta_\mu(\mathbf{q}_j + \epsilon \mathbf{q}_{ij}) \\ &= \frac{1}{2} \sum_{ij}^N \hat{\mathbf{F}}_{ij} \mathbf{q}_{ij} \cdot \int_0^1 d\epsilon \nabla \delta_\mu(\mathbf{q}_j + \epsilon \mathbf{q}_{ij}) \end{aligned} \quad (3.29)$$

Therefore we have

$$\begin{aligned} \sum_{ij}^N \hat{\mathbf{F}}_{ij} \delta_\mu(\mathbf{q}_i) &= \frac{1}{2} \sum_{ij}^N \hat{\mathbf{F}}_{ij} \mathbf{q}_{ij} \cdot \mathbf{n} \int_0^1 d\epsilon \frac{1}{\mathcal{V}_\mu} \frac{\chi_\mu(\mathbf{q}_j + \epsilon \mathbf{q}_{ij}) - \chi_{\mu-1}(\mathbf{q}_j + \epsilon \mathbf{q}_{ij})}{\Delta z} \\ &= \frac{1}{\mathcal{V}_\mu} \frac{1}{2} \sum_{ij}^N \hat{\mathbf{F}}_{ij} \mathbf{q}_{ij} \cdot \mathbf{n} \frac{z_\mu(i, j) - z_{\mu-1}(i, j)}{\Delta z}, \end{aligned} \quad (3.30)$$

where we have introduced the geometric factor

$$\begin{aligned} z_\mu(i, j) &= \int_0^1 d\epsilon \chi_\mu(\mathbf{q}_i - \epsilon \mathbf{q}_{ij}) \\ &= \int_0^1 d\epsilon \theta(z_{\mu+1} - z_i + \epsilon z_{ij}) \theta(z_i - \epsilon z_{ij} - z_\mu) \\ &= \frac{1}{z_{ij}} \int_0^{z_{ij}} dz \theta(z_{\mu+1} - z_i + z) \theta(z_i - z_\mu - z) \end{aligned} \quad (3.31)$$

The integral can be easily computed with the result

$$\begin{aligned} z_\mu(i, j) = & \frac{1}{z_{ij}} [(z_j - z_\mu)\theta(z_{\mu+1} - z_j, z_\mu - z_j) - (z_i - z_\mu)\theta(z_{\mu+1} - z_i, z_\mu - z_i) \\ & - (z_j - z_{\mu+1})\theta(z_{\mu+1} - z_j) + (z_i - z_{\mu+1})\theta(z_{\mu+1} - z_i)], \end{aligned} \quad (3.32)$$

where  $\theta(a, b) = \theta(a)\theta(b)$  takes the value 1 if both  $a, b > 0$ , and zero otherwise. Note that  $z_\mu(i, j) = z_\mu(j, i)$ . If both particles are within the bin, then  $z_\mu(i, j) = 1$ . If the line joining the particles does not cross the bin (for example,  $z_i, z_j < z_\mu$ ) then  $z_\mu(i, j) = 0$ . If both particles are outside the bin, but the line joining the particles crosses the bin (for example,  $z_i < z_\mu, z_j > z_{\mu+1}$ ) then  $z_\mu(i, j) = \frac{z_{\mu+1} - z_\mu}{z_j - z_i}$ . Finally, if one particle is in the bin, and the other outside (for example  $z_\mu < z_i < z_{\mu+1}, z_j > z_{\mu+1}$ ) then  $z_\mu(i, j) = \frac{z_{\mu+1} - z_i}{z_j - z_i}$ . In summary,  $z_\mu(i, j)$  is the fraction of the segment of the *vertical* distance between particles  $i, j$  that happens to be within the bin  $\mu$ . The partition of unity (3.2) implies also that

$$\sum_\mu z_\mu(i, j) = 1, \quad (3.33)$$

as can be seen easily from the definition (3.31).

By collecting the results (3.24), (3.26), (3.30) we end up with the final form of the time derivative of the discrete momentum variable

$$i\mathcal{L}\hat{\mathbf{g}}_\mu = \hat{\mathbf{F}}_\mu^{\text{s} \rightarrow \text{l}} - \frac{\hat{\boldsymbol{\sigma}}_\mu - \hat{\boldsymbol{\sigma}}_{\mu-1}}{\Delta z} \cdot \mathbf{n}, \quad (3.34)$$

where we have introduced the discrete stress tensor of bin  $\mu$  through

$$\hat{\boldsymbol{\sigma}}_\mu = \frac{1}{\mathcal{V}_\mu} \left[ \sum_i \mathbf{p}_i \mathbf{v}_i \chi_\mu(\mathbf{r}_i) + \frac{1}{2} \sum_{ij}^N \mathbf{r}_{ij} \hat{\mathbf{F}}_{ij} z_\mu(i, j) \right] \quad (3.35)$$

The form of equation (3.34) makes explicit that the momentum density changes due to the force density due to the solid wall and the discrete gradient of the fluid stress tensor. As shown in Chapter 2, this separation of the force on the fluid into solid-fluid and fluid-fluid interactions is at the basis of the final structure of the hydrodynamic equations.

Note that, while the force is discretized with the basis function  $\Phi_\mu(\mathbf{r})$ , the stress is discretized with the characteristic function  $\chi_\mu(\mathbf{r})$ . Therefore, forces are defined on nodal planes while stresses are defined on bins.

The partitions of unity (3.2) and (3.33) ensure that the arithmetic average of the stress tensor of the bins gives the total stress tensor of the system, that is,

$$\frac{1}{N_{\text{bin}}} \sum_{\mu}^{N_{\text{bin}}} \hat{\sigma}_{\mu} = \hat{\sigma}, \quad (3.36)$$

where the total fluid stress tensor of the system is defined in the usual way as

$$\hat{\sigma} = \frac{1}{V} \left[ \sum_i \mathbf{p}_i \mathbf{v}_i + \frac{1}{2} \sum_{ij} \mathbf{r}_{ij} \hat{\mathbf{F}}_{ij} \right] \quad (3.37)$$

and the total volume of the system is  $V = L_x L_y L_z$ .

### 3.4.2 Exact reversible part of the dynamics

As shown in Sec. 2.5.1 of Chapter 2, the reversible part of the dynamics is given by the average of the microscopic time derivatives with respect to the relevant ensemble. The explicit form of the relevant ensemble and the corresponding averages leading to the reversible part of the dynamics are given in the Appendix D. There it is shown that the reversible part of the dynamics is given by the *exact* equations

$$\begin{aligned} \langle i \mathcal{L} \hat{\rho}_{\mu} \rangle^{\lambda v} &= (\langle \hat{\rho}_{\mathbf{r}} \rangle^{\lambda v} \bar{\mathbf{v}} \cdot \nabla \delta_{\mu}) \\ \langle i \mathcal{L} \hat{\mathbf{g}}_{\mu} \rangle^{\lambda v} &= (\langle \hat{\rho}_{\mathbf{r}} \rangle^{\lambda v} \bar{\mathbf{v}} \mathbf{v} \cdot \nabla \delta_{\mu}) + (\delta_{\mu} \langle \hat{\rho}_{\mathbf{r}} \rangle^{\lambda v} \nabla \bar{\mu}), \end{aligned} \quad (3.38)$$

where we have used the notation (3.10) for space integrals, the notation (3.8) for interpolated fields, and  $\langle \hat{\rho}_{\mathbf{r}} \rangle^{\lambda v}$  is the average of the microscopic density field (2.3) with respect to the relevant ensemble. The chemical potential field per unit mass is defined by

$$\bar{\mu}(\mathbf{r}) = \bar{\lambda}(\mathbf{r}) - \frac{\bar{\mathbf{v}}^2(\mathbf{r})}{2}, \quad (3.39)$$

where the interpolated conjugate variables are defined as

$$\bar{\lambda}(\mathbf{r}) = \sum_{\mu} \lambda_{\mu} \psi_{\mu}(\mathbf{r}), \quad \bar{\mathbf{v}}(\mathbf{r}) = \sum_{\mu} \mathbf{v}_{\mu} \psi_{\mu}(\mathbf{r}) \quad (3.40)$$

The conjugate variables  $\lambda_{\mu}, \mathbf{v}_{\mu}$  are functions of the CG variables averages  $\rho_{\mu}, \mathbf{g}_{\mu}$ , computed with the real ensemble (i.e. the solution of the Liouville equation). In particular,

the velocity  $\mathbf{v}_\mu$  is related to the momentum density through

$$\mathbf{g}_\mu = \sum_\nu \rho_{\mu\nu} \mathbf{v}_\nu, \quad (3.41)$$

where the mass density matrix is defined by

$$\rho_{\mu\nu} = \int d\mathbf{r} \delta_\mu(\mathbf{r}) \psi_\nu(\mathbf{r}) \langle \hat{\rho}_{\mathbf{r}} \rangle^{\lambda v} \quad (3.42)$$

### 3.4.3 Approximate reversible dynamics

The reversible part of the dynamics (3.38) is not given in *explicit* form in terms of the discrete CG variables, that are hidden inside the Lagrange multipliers  $\lambda_\mu, \mathbf{v}_\mu$  and the average  $\langle \hat{\rho}_{\mathbf{r}} \rangle^{\lambda v}$ . We consider now an approximation that will make the exact equations (3.38) explicit in the CG variables. This approximation has been named as the *linear for spiky approximation* (LFSA) in Ref. [97], and consists on approximating, within ensemble averages, the “spiky” fields (3.22) with piece-wise linear functions as

$$\begin{aligned} \hat{\rho}_{\mathbf{r}} &\simeq \sum_\sigma \hat{\rho}_\sigma \psi_\sigma(\mathbf{r}) \\ \hat{\mathbf{g}}_{\mathbf{r}} &\simeq \sum_\sigma \hat{\mathbf{g}}_\sigma \psi_\sigma(\mathbf{r}) \end{aligned} \quad (3.43)$$

As illustrated in Fig. (3.2), the left hand side contains sums of singular Dirac  $\delta$  functions, while the right hand side are piece-wise linear functions given in terms of the discrete values  $\hat{\rho}_\sigma, \hat{\mathbf{g}}_\sigma$ . This approximation is expected to hold inside ensemble averages and to be a good one if there are many particles per bin.

In the LFSA, the average of the density field becomes explicit in the discrete density variables

$$\langle \hat{\rho}_{\mathbf{r}} \rangle^{\lambda v} \simeq \sum_\mu \rho_\mu \psi_\mu(\mathbf{r}) = \bar{\rho}(\mathbf{r}) \quad (3.44)$$

and the density matrix (3.42) becomes explicit in the discrete density

$$\rho_{\mu\nu} \simeq \sum_\sigma (\delta_\mu \psi_\nu \psi_\sigma) \rho_\sigma = (\delta_\mu \psi_\nu \bar{\rho}) \quad (3.45)$$

Therefore, the discrete velocity field (3.41) is given explicitly in terms of the discrete mass and momentum densities by

$$\mathbf{v}_\mu = \sum_\nu \rho_{\mu\nu}^{-1} \mathbf{g}_\nu \quad (3.46)$$

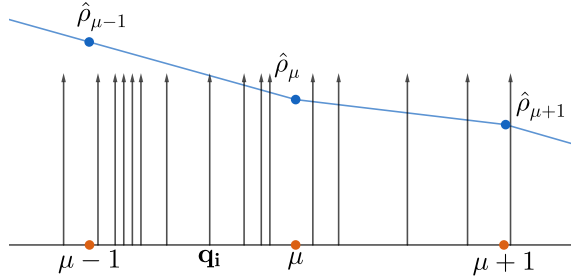


**Figure 3.2:** The microscopic density field  $\hat{\rho}_r(z)$  (black), which is a sum of Dirac  $\delta$  functions each one located at the position of the particle  $i$ , is approximated by an interpolation of the discrete microscopic density field  $\hat{\rho}_\mu(z)$  at the nodes (blue).

Under this LFSA the reversible part (3.38) takes the *explicit* form

$$\begin{aligned}\langle i \mathcal{L} \hat{\rho}_\mu \rangle^{\lambda v} &= (\bar{\rho} \bar{\mathbf{v}} \cdot \nabla \delta_\mu) \\ \langle i \mathcal{L} \hat{\mathbf{g}}_\mu \rangle^{\lambda v} &= (\bar{\rho} \bar{\mathbf{v}} \bar{\mathbf{v}} \cdot \nabla \delta_\mu) + (\delta_\mu \bar{\rho} \nabla \bar{\mu})\end{aligned}\quad (3.47)$$

These equations are explicit in the CG variables because the fields  $\bar{\rho}(\mathbf{r}), \bar{\mathbf{v}}(\mathbf{r})$  are explicit functions of the discrete CG variables  $\rho_\mu, \mathbf{v}_\mu$ . As shown in the Appendix D, the last term involving the chemical potential admits the following form

$$(\delta_\mu \bar{\rho} \nabla \bar{\mu}) = - \sum_v (\bar{\rho} \delta_\mu \nabla \delta_v) \frac{\partial F}{\partial \rho_v}(\rho), \quad (3.48)$$

where the free energy function depends only on the discrete density field.

Therefore, the final reversible part of the dynamics takes the form

$$\begin{aligned}\langle i \mathcal{L} \hat{\rho}_\mu \rangle^{\lambda v} &= (\bar{\rho} \bar{\mathbf{v}} \cdot \nabla \delta_\mu) \\ \langle i \mathcal{L} \hat{\mathbf{g}}_\mu \rangle^{\lambda v} &= (\bar{\rho} \bar{\mathbf{v}} \bar{\mathbf{v}} \cdot \nabla \delta_\mu) - \sum_v (\bar{\rho} \delta_\mu \nabla \delta_v) \frac{\partial F}{\partial \rho_v}(\rho)\end{aligned}\quad (3.49)$$

### 3.4.4 Irreversible part of the dynamics

As shown in Sec. 1.7 of Chapter 1, the irreversible part of the dynamics in the projection operator method is given by the standard form

$$\sum_j D_{ij} \frac{\partial S}{\partial a_j}, \quad (3.50)$$

where  $S$  is the entropy and the dissipative matrix is given by

$$D_{ij} = \frac{1}{k_B T} \int_0^\tau \langle Q i \mathcal{L} \hat{A}_i(t) Q i \mathcal{L} \hat{A}_j \rangle^{\lambda} \quad (3.51)$$

Therefore, the dissipative matrix depends, in general, on the state of the CG variables. In the present case, the CG variables are  $\hat{\rho}_\mu$  and  $\hat{\mathbf{g}}_\mu$ . In the LFSA (3.43) the time derivative of the density is given by

$$i \mathcal{L} \hat{\rho}_\mu = \int d\mathbf{r} \hat{\mathbf{g}}_\mu \cdot \nabla \delta_\mu(\mathbf{r}) \simeq \sum_\nu \hat{\mathbf{g}}_\nu (\psi_\nu \nabla \delta_\mu) \quad (3.52)$$

We see that this time derivative is given in terms of the discrete momentum which is a CG variable itself and, therefore, the associated projected current vanishes,  $Q i \mathcal{L} \hat{\rho}_\mu = 0$ . This leads to a much simpler dissipative matrix. The derivatives of the entropy are given in equations (D.8) in the Appendix D, and we may write the irreversible terms (3.50) in the form

$$\left. \frac{d}{dt} \begin{pmatrix} \rho_\mu \\ \mathbf{g}_\mu \end{pmatrix} \right|_{\text{irr}} = \sum_\nu \begin{pmatrix} 0 & 0 \\ 0 & \mathbf{D}_{\mu\nu} \end{pmatrix} \begin{pmatrix} \mathcal{V}_\nu \tilde{\lambda}_\nu \\ -\mathcal{V}_\nu \tilde{\mathbf{v}}_\nu \end{pmatrix}, \quad (3.53)$$

where the dissipative matrix is given by

$$\mathbf{D}_{\mu\nu} = \frac{1}{k_B T} \int_0^\tau dt \langle Q i \mathcal{L} \hat{\mathbf{g}}_\mu(t) Q i \mathcal{L} \hat{\mathbf{g}}_\nu \rangle^{\lambda \mathbf{v}} \quad (3.54)$$

and we have introduced the discrete fields

$$\tilde{\lambda}_\mu = \sum_\nu \mathcal{V}_\nu [M^\Phi]_{\mu\nu}^{-1} \lambda_\nu, \quad \tilde{\mathbf{v}}_\mu = \sum_\nu \mathcal{V}_\nu [M^\Phi]_{\mu\nu}^{-1} \mathbf{v}_\nu \quad (3.55)$$

By using now the decomposition (3.34) of the time derivative of the momentum density in the dissipative matrix (3.54), we obtain the following irreversible part of the

dynamics

$$\begin{aligned}
 \frac{d}{dt} \rho_\mu \Big|_{\text{irr}} &= 0 \\
 \frac{d}{dt} \mathbf{g}_\mu \Big|_{\text{irr}} &= - \sum_v \mathcal{V}_v \frac{\mathbf{n} \cdot [\eta_{\mu\nu} - \eta_{\mu-1\nu} - \eta_{\mu\nu-1} + \eta_{\mu-1\nu-1}]}{\Delta z^2} : \mathbf{n} \tilde{\mathbf{v}}_v \\
 &\quad + \sum_v \mathcal{V}_v \frac{[\mathbf{G}_{\mu\nu} - \mathbf{G}_{\mu\nu-1}]}{\Delta z} \cdot \mathbf{n} \tilde{\mathbf{v}}_v \\
 &\quad + \sum_v \mathcal{V}_v \frac{\mathbf{n} \cdot [\mathbf{H}_{\mu\nu} - \mathbf{H}_{\mu-1\nu}]}{\Delta z} \cdot \tilde{\mathbf{v}}_v \\
 &\quad - \sum_v \mathcal{V}_v \gamma_{\mu\nu} \cdot \tilde{\mathbf{v}}_v,
 \end{aligned} \tag{3.56}$$

where we have introduced the following tensorial transport matrices

$$\begin{aligned}
 \boldsymbol{\eta}_{\mu\nu} &= \frac{1}{k_B T} \int_0^\tau dt \langle Q \hat{\sigma}_\mu(t) Q \hat{\sigma}_\nu \rangle^{\lambda v} & \simeq \frac{1}{k_B T} \int_0^\tau dt \langle Q \hat{\sigma}_\mu(t) Q \hat{\sigma}_\nu \rangle \\
 \mathbf{G}_{\mu\nu} &= \frac{1}{k_B T} \int_0^\tau dt \langle Q \hat{\mathbf{F}}_\mu^{s \rightarrow l}(t) Q \hat{\sigma}_\nu \rangle^{\lambda v} & \simeq \frac{1}{k_B T} \int_0^\tau dt \langle Q \hat{\mathbf{F}}_\mu^{s \rightarrow l}(t) Q \hat{\sigma}_\nu \rangle \\
 \mathbf{H}_{\mu\nu} &= \frac{1}{k_B T} \int_0^\tau dt \langle Q \hat{\sigma}_\mu(t) Q \hat{\mathbf{F}}_\nu^{s \rightarrow l} \rangle^{\lambda v} & \simeq \frac{1}{k_B T} \int_0^\tau dt \langle Q \hat{\sigma}_\mu(t) Q \hat{\mathbf{F}}_\nu^{s \rightarrow l} \rangle \\
 \boldsymbol{\gamma}_{\mu\nu} &= \frac{1}{k_B T} \int_0^\tau dt \langle Q \hat{\mathbf{F}}_\mu^{s \rightarrow l}(t) Q \hat{\mathbf{F}}_\nu^{s \rightarrow l} \rangle^{\lambda v} & \simeq \frac{1}{k_B T} \int_0^\tau dt \langle Q \hat{\mathbf{F}}_\mu^{s \rightarrow l}(t) Q \hat{\mathbf{F}}_\nu^{s \rightarrow l} \rangle
 \end{aligned} \tag{3.57}$$

Note that we have approximated the relevant ensemble  $\langle \dots \rangle^{\lambda v}$  by the equilibrium ensemble  $\langle \dots \rangle$  in the calculation of the above transport coefficients. In general, the transport coefficients dependent on the CG state of the system through the average with the relevant ensemble. This poses a large complication in its actual evaluation. Assuming that we may approximate the relevant ensemble by the equilibrium ensemble in the calculation of the transport coefficients, the transport coefficients do not depend on local values of density and momenta. They depend only on the global thermodynamic point at which the equilibrium correlations are computed.

### 3.4.5 The final discretized equations

By collecting the reversible (3.49) and irreversible (3.56) parts of the dynamics we obtain the final set of discrete equations

$$\begin{aligned}
 \frac{d}{dt} \rho_\mu &= (\bar{\rho} \bar{\mathbf{v}} \nabla \delta_\mu) \\
 \frac{d}{dt} \mathbf{g}_\mu &= (\bar{\rho} \bar{\mathbf{v}} \bar{\mathbf{v}} \cdot \nabla \delta_\mu) - \sum_v (\bar{\rho} \delta_\mu \nabla \delta_v) \frac{\partial F}{\partial \rho_v}(\rho) \\
 &\quad - \sum_v \mathcal{V}_v \frac{\mathbf{n} \cdot [\eta_{\mu\nu} - \eta_{\mu-1\nu} - \eta_{\mu\nu-1} + \eta_{\mu-1\nu-1}]}{\Delta z^2} : \mathbf{n} \tilde{\mathbf{v}}_v \\
 &\quad + \sum_v \mathcal{V}_v \frac{[\mathbf{G}_{\mu\nu} - \mathbf{G}_{\mu\nu-1}]}{\Delta z} \cdot \mathbf{n} \tilde{\mathbf{v}}_v \\
 &\quad + \sum_v \mathcal{V}_v \frac{\mathbf{n} \cdot [\mathbf{H}_{\mu\nu} - \mathbf{H}_{\mu-1\nu}]}{\Delta z} \cdot \tilde{\mathbf{v}}_v \\
 &\quad - \sum_v \mathcal{V}_v \gamma_{\mu\nu} \cdot \tilde{\mathbf{v}}_v
 \end{aligned} \tag{3.58}$$

These equations are a closed system of ordinary differential equations that govern the evolution of the discrete variables  $\rho_\mu, \mathbf{g}_\mu$ . Note that the transport kernels (3.57) contain too many components. We consider next how they simplify when we assume that the walls are isotropic and traslation invariant.

### 3.4.6 Symmetry assumptions

We now take advantage of the assumption that the system is isotropic when we rotate it with respect to an axis perpendicular to the walls and reflect it with respect to a plane containing the axis. These symmetries reflect into an enormous simplification of the structure of the fourth order tensor  $\eta_{\mu\nu}$ , the third order tensors  $\mathbf{G}_{\mu\nu}, \mathbf{H}_{\mu\nu}$  and the second order tensor  $\gamma_{\mu\nu}$ . Camargo et al. discussed in Ref. [84] what are the most general forms of the tensors  $\mathbf{G}_{\mu\nu}, \mathbf{H}_{\mu\nu}, \gamma_{\mu\nu}$  satisfying the required symmetries. In Appendix E we discuss the most general fourth order tensor  $\eta_{\mu\nu}$  with the required symmetries. We introduce normal  $\mathbf{nn}$  and tangential  $\mathbf{T} = \delta - \mathbf{nn}$  projectors, where  $\delta$  is the unit matrix. We note that the tangential projector satisfies

$$\mathbf{T}^{\alpha z} = \delta^{\alpha z} - \mathbf{n}^\alpha \mathbf{n}^z = 0 \quad \forall \alpha = x, y, z \tag{3.59}$$

and, therefore, the required components of the viscosity tensor for an isotropic wall are given, from equation (E.6) in the Appendix E, by

$$\eta^{\alpha z \gamma z} = \eta^{||} \mathbf{T}^{\alpha \gamma} + \eta^{\perp} \mathbf{n}^\alpha \mathbf{n}^\gamma \quad (3.60)$$

The required components of the third order tensors are, from equations (104) and (105) of Ref. [84]

$$\begin{aligned} \mathbf{G}^{\alpha \beta z} &= G^{||} \mathbf{T}^{\alpha \beta} + G^{\perp} \mathbf{n}^\alpha \mathbf{n}^\beta \\ \mathbf{H}^{\alpha z \gamma} &= H^{||} \mathbf{T}^{\alpha \gamma} + H^{\perp} \mathbf{n}^\alpha \mathbf{n}^\gamma \end{aligned} \quad (3.61)$$

and the second order friction tensor becomes, under isotropic symmetry

$$\boldsymbol{\gamma} = \gamma^{||} \mathbf{T}^{\alpha \beta} + \gamma^{\perp} \mathbf{n}^\alpha \mathbf{n}^\beta \quad (3.62)$$

In these expressions the transport kernels are

$$\begin{aligned} \eta_{\mu\nu}^{||} &= \frac{1}{k_B T} \int_0^\tau dt \langle Q \hat{\sigma}_\mu^{xz}(t) Q \hat{\sigma}_\nu^{xz} \rangle, & \eta_{\mu\nu}^{\perp} &= \frac{1}{k_B T} \int_0^\tau dt \langle Q \hat{\sigma}_\mu^{zz}(t) Q \hat{\sigma}_\nu^{zz} \rangle \\ G_{\mu\nu}^{||} &= \frac{1}{k_B T} \int_0^\tau dt \langle Q \hat{\mathbf{F}}_\mu^x(t) Q \hat{\sigma}_\nu^{xz} \rangle, & G_{\mu\nu}^{\perp} &= \frac{1}{k_B T} \int_0^\tau dt \langle Q \hat{\mathbf{F}}_\mu^z(t) Q \hat{\sigma}_\nu^{zz} \rangle \\ H_{\mu\nu}^{||} &= \frac{1}{k_B T} \int_0^\tau dt \langle Q \hat{\sigma}_\mu^{xz}(t) Q \hat{\mathbf{F}}_\nu^x \rangle, & H_{\mu\nu}^{\perp} &= \frac{1}{k_B T} \int_0^\tau dt \langle Q \hat{\sigma}_\mu^{zz}(t) Q \hat{\mathbf{F}}_\nu^z \rangle \\ \gamma_{\mu\nu}^{||} &= \frac{1}{k_B T} \int_0^\tau dt \langle Q \hat{\mathbf{F}}_\mu^x(t) Q \hat{\mathbf{F}}_\nu^x \rangle, & \gamma_{\mu\nu}^{\perp} &= \frac{1}{k_B T} \int_0^\tau dt \langle Q \hat{\mathbf{F}}_\mu^z(t) Q \hat{\mathbf{F}}_\nu^z \rangle \end{aligned} \quad (3.63)$$

These expressions have been obtained by suitable contractions of the tensors in equations (3.60)-(3.62) with  $\mathbf{n}$  or the tracing them out, and then using the microscopic expressions given in (3.57).

### 3.4.7 Normal and tangent evolution

When we assume the above symmetries, it makes sense to look separately to the different components of the dynamic equation (3.58). The density  $\rho_\mu$  and normal component of the momentum  $\mathbf{g}_\mu^z$  evolve according to

$$\begin{aligned} \frac{d}{dt} \rho_\mu &= (\bar{\rho} \bar{v}^z \nabla^z \delta_\mu) \\ \frac{d}{dt} \mathbf{g}_\mu^z &= (\bar{\rho} \bar{v}^z \bar{v}^z \nabla^z \delta_\mu) - (\bar{\rho} \delta_\mu \nabla^z \delta_\nu) \frac{\partial F}{\partial \rho_\nu}(\rho) + M_{\mu\nu}^{\perp} \mathcal{V}_\nu \tilde{v}_\nu^z, \end{aligned} \quad (3.64)$$

where the dissipative matrix is defined as

$$M_{\mu\nu}^\perp = -\frac{\eta_{\mu\nu}^\perp - \eta_{\mu-1\nu}^\perp - \eta_{\mu\nu-1}^\perp + \eta_{\mu-1\nu-1}^\perp}{\Delta z^2} + \frac{G_{\mu\nu}^\perp - G_{\mu\nu-1}^\perp}{\Delta z} + \frac{H_{\mu\nu}^\perp - H_{\mu-1\nu}^\perp}{\Delta z} - \gamma_{\mu\nu}^\perp \quad (3.65)$$

On the other hand, the parallel component  $\mathbf{g}_\mu^\alpha$  for  $\alpha = x, y$  of the discrete momentum density evolves independently of  $\rho_\mu, \mathbf{g}_\mu^z$ , and according to

$$\frac{d}{dt} \mathbf{g}_\mu^\alpha = -M_{\mu\nu}^{||} \mathcal{V}_\nu \tilde{v}_\nu^\alpha, \quad (3.66)$$

where the dissipative matrix in this equation is

$$M_{\mu\nu}^{||} = -\frac{\eta_{\mu\nu}^{||} - \eta_{\mu-1\nu}^{||} - \eta_{\mu\nu-1}^{||} + \eta_{\mu-1\nu-1}^{||}}{\Delta z^2} + \frac{G_{\mu\nu}^{||} - G_{\mu\nu-1}^{||}}{\Delta z} + \frac{H_{\mu\nu}^{||} - H_{\mu-1\nu}^{||}}{\Delta z} - \gamma_{\mu\nu}^{||} \quad (3.67)$$

equation (3.64)-(3.67) along with the Green-Kubo integrals (3.63) are one of the main result of the present chapter. They display the discrete hydrodynamics of a fluid confined by parallel walls and moving with a flow that is translation invariant along the walls. These equations predict that the tangential component of the momentum do not depend on the free energy of the system and is uncoupled from the dynamics of the normal component and the density. This means that shearing motions do not affect the structure of the density field.

### 3.5 A finite element discretization

In this section, we show that if we discretize the continuum equations (2.69) with a Petrov-Galerkin finite element discretization method, and assume that the transport kernels are isotropic under rotations around the axis perpendicular to the slabs, we recover the discrete equations (3.58) that have been obtained directly from the projection operator technique.

The first step of the Petrov-Galerkin method to discretize the continuum equations (2.69), (2.66) and (2.67) proceeds by inserting the equations (2.66) and (2.67) into (2.69) and then multiply with  $\delta_\mu(\mathbf{r})$  and integrate over  $\mathbf{r}$ . After some integration by

parts one gets

$$\begin{aligned}
 \frac{d}{dt} \rho_\mu &= \int d\mathbf{r} \nabla \delta_\mu(\mathbf{r}) \cdot \rho(\mathbf{r}) \mathbf{v}(\mathbf{r}) \\
 \frac{d}{dt} \mathbf{g}_\mu &= \int d\mathbf{r} \nabla \delta_\mu(\mathbf{r}) \cdot \rho(\mathbf{r}) \mathbf{v}(\mathbf{r}) \mathbf{v}(\mathbf{r}) \\
 &\quad - \int d\mathbf{r} \delta_\mu(\mathbf{r}) \rho(\mathbf{r}) \nabla \frac{\delta \mathcal{F}}{\delta \rho(\mathbf{r})} \\
 &\quad - \int d\mathbf{r} \nabla \delta_\mu(\mathbf{r}) \cdot \int d\mathbf{r}' \boldsymbol{\eta}_{\mathbf{rr}'} : \nabla' \mathbf{v}(\mathbf{r}') \\
 &\quad - \int d\mathbf{r} \delta_\mu(\mathbf{r}) \int d\mathbf{r}' \mathbf{G}_{\mathbf{rr}'} : \nabla' \mathbf{v}(\mathbf{r}') \\
 &\quad - \int d\mathbf{r} \nabla \delta_\mu(\mathbf{r}) \int d\mathbf{r}' \mathbf{H}_{\mathbf{rr}'} \cdot (\mathbf{v}(\mathbf{r}') - \mathbf{V}) \\
 &\quad - \int d\mathbf{r} \nabla \delta_\mu(\mathbf{r}) \int d\mathbf{r}' \boldsymbol{\gamma}_{\mathbf{rr}'} \cdot (\mathbf{v}(\mathbf{r}') - \mathbf{V})
 \end{aligned} \tag{3.68}$$

According to equation (3.8), from the discrete values  $\rho_\mu, \mathbf{v}_\mu$  of the density and velocity of node  $\mu$  we may construct continuum fields  $\bar{\rho}(\mathbf{r}), \bar{\mathbf{v}}(\mathbf{r})$  through the interpolation with the basis functions  $\psi_\mu(\mathbf{r})$

$$\bar{\rho}(\mathbf{r}) = \sum_\mu \rho_\mu \psi_\mu(\mathbf{r}), \quad \bar{\mathbf{v}}(\mathbf{r}) = \sum_\mu \mathbf{v}_\mu \psi_\mu(\mathbf{r}) \tag{3.69}$$

In terms of the finite element basis functions  $\Phi_\mu(\mathbf{r})$  we may write (3.69) in the form

$$\bar{\rho}(\mathbf{r}) = \sum_\mu \tilde{\rho}_\mu \Phi_\mu(\mathbf{r}), \quad \bar{\mathbf{v}}(\mathbf{r}) = \sum_\mu \tilde{\mathbf{v}}_\mu \Phi_\mu(\mathbf{r}), \tag{3.70}$$

where we have used (3.21) and the discrete field  $\tilde{\mathbf{v}}_\mu$  is defined in (3.55) with a similar definition for  $\tilde{\rho}_\mu$ .

The second step in the Petrov-Galerkin approximation is to substitute the actual fields  $\rho(\mathbf{r}), \mathbf{v}(\mathbf{r})$  in the right hand side of (3.68) with the interpolated fields (3.69)

$$\rho(\mathbf{r}) \simeq \bar{\rho}(\mathbf{r}), \quad \mathbf{v}(\mathbf{r}) \simeq \bar{\mathbf{v}}(\mathbf{r}) \tag{3.71}$$

In general, we expect that the approximation (3.71) will be accurate if the bin width  $\Delta z$  is sufficiently small as compared with the length scale of variation of the hydrodynamic fields.

Because the interpolated fields are determined by the discrete CG variables, we end up with the following closed system of ordinary differential equations for the discrete CG variables

$$\begin{aligned}
\frac{d}{dt} \rho_\mu &= (\bar{\rho} \bar{\mathbf{v}} \nabla \delta_\mu) \\
\frac{d}{dt} \mathbf{g}_\mu &= (\bar{\rho} \bar{\mathbf{v}} \bar{\mathbf{v}} \cdot \nabla \delta_\mu) - \left( \delta_\mu \bar{\rho} \nabla \frac{\delta \mathcal{F}}{\delta \rho} \right) \\
&\quad - \sum_\nu \left[ \int d\mathbf{r} \int d\mathbf{r}' \nabla \delta_\mu(\mathbf{r}) \boldsymbol{\eta}_{\mathbf{r}\mathbf{r}'} : \nabla' \Phi_\nu(\mathbf{r}') \right] \bar{\mathbf{v}}_\nu \\
&\quad - \sum_\nu \left[ \int d\mathbf{r} \int d\mathbf{r}' \delta_\mu(\mathbf{r}) \mathbf{G}_{\mathbf{r}\mathbf{r}'} : \nabla' \Phi_\nu(\mathbf{r}') \right] \bar{\mathbf{v}}_\nu \\
&\quad - \sum_\nu \left[ \int d\mathbf{r} \int d\mathbf{r}' \nabla \delta_\mu(\mathbf{r}) \mathbf{H}_{\mathbf{r}\mathbf{r}'} \Phi_\nu(\mathbf{r}') \right] \cdot (\bar{\mathbf{v}}_\nu - \mathbf{V}) \\
&\quad - \sum_\nu \left[ \int d\mathbf{r} \int d\mathbf{r}' \delta_\mu(\mathbf{r}) \boldsymbol{\gamma}_{\mathbf{r}\mathbf{r}'} \Phi_\nu(\mathbf{r}') \right] (\bar{\mathbf{v}}_\nu - \mathbf{V})
\end{aligned} \tag{3.72}$$

Note that the terms

$$(\bar{\rho} \bar{\mathbf{v}} \nabla \delta_\mu) = \sum_{\nu\nu'} \bar{\rho}_\nu \bar{\mathbf{v}}_{\nu'} \cdot (\Phi_\nu \Phi_{\nu'} \nabla \delta_\mu) \tag{3.73}$$

etc, are explicit functions of the discrete variables, where the term within parenthesis in the right hand side is a purely geometric quantity.

Note that the equations (3.72) are obtained from the continuum equations presented in Chapter 2. In the continuum theory a solid sphere is moving with an average velocity  $\mathbf{V}$ . In the present case (i.e. fixed walls) this velocity must be equal to zero.

### 3.5.1 The free energy

The only term that is not explicit in the discrete variables  $\rho_\mu, \mathbf{v}_\mu$  in equations (3.72) is the term in the momentum equation involving the functional derivative of the free energy functional. In order to have an explicit expression, we need to discretize the equilibrium density *functional*  $\mathcal{F}[\rho]$  and convert it into a free energy *function*  $F(\rho)$ . The way to proceed was introduced in Ref. [95]. We define the free energy function  $F(\rho)$  as the result of evaluating the free energy functional at the interpolated field, that is,

$$F(\rho) \equiv \mathcal{F}[\rho_\mu \psi_\mu] \tag{3.74}$$

Note that we use the Einstein summation convention. In the Appendix D we demonstrate that the free energy function  $F(\rho)$  defined “numerically” in this way is, under a reasonable approximation, the free energy function that is obtained from the statistical mechanics of the level of description given by the discrete CG variables (3.22).

The partial derivative of the free energy function is

$$\frac{\partial F}{\partial \rho_\mu}(\rho) = \int d\mathbf{r}' \frac{\delta \mathcal{F}}{\delta \rho(\mathbf{r}')}[ \rho_\mu \psi_\mu ] \psi_\mu(\mathbf{r}') \quad (3.75)$$

By multiplying with respect to  $\delta_\mu(\mathbf{r})$  and summing over  $\mu$  we have

$$\sum_\mu \delta_\mu(\mathbf{r}) \frac{\partial F}{\partial \rho_\mu}(\rho) = \int d\mathbf{r}' \frac{\delta \mathcal{F}}{\delta \rho(\mathbf{r}')}[ \rho_\mu \psi_\mu ] \sum_\mu \psi_\mu(\mathbf{r}') \delta_\mu(\mathbf{r}) \quad (3.76)$$

The function

$$\Delta(\mathbf{r}, \mathbf{r}') \equiv \sum_\mu \psi_\mu(\mathbf{r}') \delta_\mu(\mathbf{r}) \quad (3.77)$$

is very similar to a Dirac  $\delta$  function (it has a width of the order of the bins and is normalized to unity). When quantities change little from bin to bin, we may approximate  $\Delta(\mathbf{r}, \mathbf{r}') \simeq \delta(\mathbf{r} - \mathbf{r}')$ , leading to

$$\frac{\delta \mathcal{F}}{\delta \rho(\mathbf{r})}[ \rho_\mu \psi_\mu ] \simeq \sum_\mu \delta_\mu(\mathbf{r}) \frac{\partial F}{\partial \rho_\mu}(\rho) \quad (3.78)$$

Therefore, the term in the momentum equation is

$$-\left( \delta_\mu \bar{\rho} \nabla \frac{\delta \mathcal{F}}{\delta \rho} \right) \simeq -\sum_\nu \left( \bar{\rho} \delta_\mu \nabla \delta_\nu \right) \frac{\partial F}{\partial \rho_\nu}(\rho) \quad (3.79)$$

which is now a term that depends explicitly on the discrete values of the density  $\rho_\mu$ .

### 3.5.2 The transport kernels

We now consider each term within square brackets in equation. (3.72). The first one is, after using the expression (3.6) for the derivatives of the basis functions

$$\begin{aligned}
& \int \frac{d\mathbf{r}}{\mathcal{V}_\mu} \int \frac{d\mathbf{r}'}{\mathcal{V}_\nu} \nabla \Phi_\mu(\mathbf{r}) \cdot \boldsymbol{\eta}_{\mathbf{rr}'} \cdot \nabla' \Phi_\nu(\mathbf{r}') \\
&= \frac{1}{\Delta z^2} \int \frac{d\mathbf{r}}{\mathcal{V}_\mu} \int \frac{d\mathbf{r}'}{\mathcal{V}_\nu} (\chi_\mu(z) - \chi_{\mu-1}(z)) \mathbf{n} \cdot \boldsymbol{\eta}_{\mathbf{rr}'} \cdot \mathbf{n} (\chi_\nu(z) - \chi_{\nu-1}(z)) \\
&= \frac{1}{\Delta z^2} \mathbf{n} \cdot [\boldsymbol{\eta}_{\mu\nu} - \boldsymbol{\eta}_{\mu-1\nu} - \boldsymbol{\eta}_{\mu\nu-1} + \boldsymbol{\eta}_{\mu-1\nu-1}] \cdot \mathbf{n},
\end{aligned} \tag{3.80}$$

where we have introduced the discrete nonlocal viscosity kernel as

$$\boldsymbol{\eta}_{\mu\nu} \equiv \int \frac{d\mathbf{r}}{\mathcal{V}_\mu} \int \frac{d\mathbf{r}'}{\mathcal{V}_\nu} \chi_\mu(\mathbf{r}) \boldsymbol{\eta}_{\mathbf{rr}'} \chi_\nu(\mathbf{r}') \tag{3.81}$$

The second square bracket in (3.72) is

$$\begin{aligned}
& \int \frac{d\mathbf{r}}{\mathcal{V}_\mu} \int \frac{d\mathbf{r}'}{\mathcal{V}_\nu} \Phi_\mu(\mathbf{r}) \mathbf{G}_{\mathbf{rr}'} \cdot \nabla' \Phi_\nu(\mathbf{r}') \\
&= -\frac{1}{\Delta z} \int \frac{d\mathbf{r}}{\mathcal{V}_\mu} \int \frac{d\mathbf{r}'}{\mathcal{V}_\nu} \Phi_\mu(\mathbf{r}) G_{\mathbf{rr}'}^{||} (\chi_\nu(\mathbf{r}') - \chi_{\nu-1}(\mathbf{r}')) \\
&= -\frac{1}{\Delta z} [\mathbf{G}_{\mu\nu} - \mathbf{G}_{\mu\nu-1}] \cdot \mathbf{n},
\end{aligned} \tag{3.82}$$

where we have introduced

$$\mathbf{G}_{\mu\nu} \equiv \int \frac{d\mathbf{r}}{\mathcal{V}_\mu} \int \frac{d\mathbf{r}'}{\mathcal{V}_\nu} \Phi_\mu(\mathbf{r}) \mathbf{G}_{\mathbf{rr}'} \chi_\nu(\mathbf{r}') \tag{3.83}$$

The third square bracket is

$$-\frac{1}{\Delta z} \int \frac{d\mathbf{r}}{\mathcal{V}_\mu} \int \frac{d\mathbf{r}'}{\mathcal{V}_\nu} (\chi_\mu(\mathbf{r}) - \chi_{\mu-1}(\mathbf{r})) \mathbf{n} \cdot \mathbf{H}_{\mathbf{rr}'} \Phi_\nu(\mathbf{r}') = -\frac{1}{\Delta z} \mathbf{n} \cdot [\mathbf{H}_{\mu\nu} - \mathbf{H}_{\mu-1\nu}], \tag{3.84}$$

where

$$\mathbf{H}_{\mu\nu} \equiv \int \frac{d\mathbf{r}}{\mathcal{V}_\mu} \int \frac{d\mathbf{r}'}{\mathcal{V}_\nu} \chi_\mu(\mathbf{r}) \mathbf{H}_{\mathbf{rr}'} \Phi_\nu(\mathbf{r}') \tag{3.85}$$

The last square bracket in (3.72) is

$$\boldsymbol{\gamma}_{\mu\nu} \equiv \int \frac{d\mathbf{r}}{\mathcal{V}_\mu} \frac{d\mathbf{r}'}{\mathcal{V}_\nu} \Phi_\mu(\mathbf{r}) \boldsymbol{\gamma}_{\mathbf{rr}'} \Phi_\nu(\mathbf{r}') \tag{3.86}$$

Once we use the microscopic expressions given in (2.68) with (2.12), the discrete kernels  $\eta_{\mu\nu}, \mathbf{G}_{\mu\nu}, \mathbf{H}_{\mu\nu}, \gamma_{\mu\nu}$  introduced in (3.80)-(3.85) turn out to be *identical* to (3.57).

In summary, by using a Petrov-Galerkin discretization of the continuum equations (2.69) we obtain a set of discrete equations that are identical to the ones obtained with the method of projection operators that starts directly from the Hamiltonian dynamics and considers the evolution of the discrete variables (3.22). This consistency property is very pleasant and is a consequence of the particular way of defining the CG variables (3.22), in terms of finite element basis functions.

### 3.6 Summary

In Chapter 2 we presented a continuum isothermal hydrodynamic theory for simple fluids in the presence of solid walls. The theory describes solid-fluid interaction through reversible repulsive forces that prevent leaking of the fluid inside the solid and irreversible forces concentrated near the walls. Camargo et al. shown in [84] that the effect of the forces that the solid exert on the fluid can be described, when flow fields and geometry are macroscopic (much larger than molecular scales), as boundary conditions.

Despite its elegance, this general theory is very complex as it involves a large number of nonlocal tensorial kernels (related to viscous and friction forces). In addition, as it is formulated at the continuum level, transport kernels involve correlations of the local stress tensor and force densities which involve delta functions and that cannot possibly be computed in MD simulations. In order to tackle these problems, in the present chapter we have derived from first principles a hydrodynamic theory for planar geometries and flows involving discrete mass and momentum density variables defined in terms of finite element basis functions. By the very selection of the CG defined in slabs, we expect to have reasonable predictions from the discrete theory only in the case that the flows are translationally invariant in the direction parallel to the walls. Only eight kernels are required in order to describe planar flows in isotropic walls,  $\eta^{\parallel}, G^{\parallel}, H^{\parallel}, \gamma^{\parallel}$  and  $\eta^{\perp}, G^{\perp}, H^{\perp}, \gamma^{\perp}$ . Onsager reciprocity reduces further the number of kernels to six, because the  $H$ 's are transposes of the  $G$ 's. The kernel  $\eta^{\parallel}$  appearing for a flow parallel to the walls (i.e. pure shear) plays the role of a nonlocal shear viscosity kernel while  $\eta^{\perp}$  can be understood as nonlocal bulk viscosity kernel needed to discuss a flow perpendicular to the walls, i.e. sound. The rest of kernels  $G, H, \gamma$  give the overall magnitude of the irreversible forces that the solid exerts on the fluid.

Even for the simplest case of a shear flow (i.e. no compression waves) in which the dynamics is linear in the velocity field and that does not require a free energy function, one obtains a nontrivial equation (3.66). This equation is not trivial as it describes the

interaction of the fluid with the solid walls not in terms of boundary condition but rather in terms of irreversible surface forces.

The discrete hydrodynamic equations obtained in this chapter are the first step toward the validation of the continuum hydrodynamic equations in the presence of walls as obtained in Chapter 2. Only discrete equations can be dealt with MD simulations.

A crucial observation is that the discrete theory has a built in length scale given by the width of the bins. The two main assumptions under which the discrete hydrodynamic theory is obtained are 1) the Markov assumption and 2) Linear for spiky assumption (LFSA). We expect that the validity of both assumptions is linked to the size of the bins used. In fact, we have conducted MD simulations in order to evaluate the kernels  $\eta^{\parallel\parallel}, G^{\parallel\parallel}, H^{\parallel\parallel}, \gamma^{\parallel\parallel}$  appearing in equation (3.66) describing shear flow. We have also compared the predictions of the discrete equations with direct measurement of the flows starting from nonequilibrium conditions. These simulations, that will be detailed in the following chapters, show that for bin sizes  $\Delta z$  smaller than the molecular size the dynamics near the walls is non-Markovian. Only for bins larger than a molecular size, the Markov approximation is shown to be valid. In this case, the resulting hydrodynamic fields vary on length scales of supramolecular size and cannot capture, for example, the density layering near walls.

# Chapter 4

## Space and time locality for unconfined fluids

*Time is longer than any distance.*

---

Absalom, Absalom!  
WILLIAM FAULKNER

### 4.1 Introduction

The well-known Navier-Stokes equations of hydrodynamics govern the behaviour of a fluid at large scales [98–100]. These equations are based on the conservation of mass, momentum and energy, and are supplemented with boundary conditions at the frontier of the fluid domain. When the scales probed are shrunked to the nanoscale as, for example, in nanochannels and nanopores, the Navier-Stokes equations are no longer appropriate. Typically, the atomic structure of the fluid starts to manifest, and this leads to a number of interesting effects, such as the layering of the density near the walls and the appearance of slip at the walls. As a general feature, the fluid starts to behave in a nonlocal way in both space and time.

For unconfined fluids at the nanoscale the methods of Generalized Hydrodynamics [25, 101–103] have been very succesfull in order to characterize the dynamics of fluids at nanoscales. These scales can be probed with neutron scattering techniques. Generalized hydrodynamics considers wavenumber and frequency dependent transport coefficients, reflecting nonlocality in space and time, respectively, in order to extend the

validity of the hydrodynamic equations to molecular scales. Correlation functions of conserved hydrodynamic and non-hydrodynamic variables are defined in Fourier space and measured in MD simulations, thus providing a wealth of information about the behaviour of fluids at small scales [104–106]. When the fluid is confined, traslation invariance is broken and Fourier techniques are no longer as useful as in unconfined fluids. One is, therefore, restricted to work in real space.

The aim in the present chapter is to reframe in real space (as opposed to Fourier space) the discussion of nonlocality in time and space of hydrodynamics in a way suitable for MD simulations. As discussed in Chapter 3, validation of a continuum theory through MD simulations requires necessarily the use of a discrete setting. This is typically done by binning space and measuring the number of particles, average velocity and energy of the particles in that bin. Alternatively, the method of planes [107, 108] has been used to define discrete hydrodynamic variables. In a number of works [93, 95, 96, 109], Español et al. have discussed refined strategies for the definition of discrete hydrodynamic variables in real space. The main objective of these strategies is to match the bottom up derivation of discrete evolution equations with the top down discretization of continuum equations. The methodology will be transferrable to confined fluids allowing us to discuss wall effects in chapters 5 and 6. More specifically, the objective here is to assess to what extent it makes sense to approximate the dynamics of discrete hydrodynamic variables in a Markovian way while, at the same time, use nonlocal transport coefficients.

In the study of shear flow of simple fluids at the nanoscale, as those occurring in nanoscale pores, there seems to be two different approaches in the literature. The first approach is the Local Average Density Model (LADM) introduced by Bitsanis et al. [89], while the second approach is the nonlocal viscosity model. The LADM assumes that the local transport coefficients of an inhomogeneous fluid can be set equal to the corresponding homogeneous transport coefficients calculated at a locally averaged density.

This somewhat heuristic idea was given a rigorous foundation from a kinetic theory for dense fluids proposed by Pozhar et al. [110]. From the computational side, Bitsanis et al. [89] used Nonequilibrium Molecular Dynamics (NEMD) to produce Couette-like flows in several external conservative fields and it was shown that the LADM gives good results. More recent work by Hoang and Galliero [111, 112] use NEMD to measure viscosity with LADM and they find good agreement for liquids but not so good for gases.

The second approach that has been used in the description of fluids at the nanoscale is based on the notion of a nonlocal (in space and time) generalization of Newton’s constitutive equation for planar shear flows. Evans and Morriss [113] proposed a nonlocal constitutive equation in which the stress is related to the strain field  $\dot{\gamma}$  in the

form

$$P^{xy}(\mathbf{r}, t) = - \int_0^t ds \int_{-\infty}^{\infty} d\mathbf{r}' \eta(\mathbf{r}, \mathbf{r}', t-s) \dot{\gamma}(\mathbf{r}', s), \quad (4.1)$$

where  $P^{xy}(\mathbf{r}, t)$  is the  $xy$  pressure tensor element and  $\eta(\mathbf{r}, \mathbf{r}', t)$  is the shear viscosity nonlocal memory kernel. This is the real-space version of the wave number and frequency dependent viscosity [113] studied in Generalized Hydrodynamics, that is

$$P^{yx}(k, t) = - \int_0^t ds \eta(k, t-s) \dot{\gamma}(k, s) \quad (4.2)$$

For steady state flows, the constitutive equation becomes

$$P^{xy}(\mathbf{r}) = - \int_{-\infty}^{\infty} d\mathbf{r}' \eta(\mathbf{r}, \mathbf{r}') \dot{\gamma}(\mathbf{r}'), \quad (4.3)$$

where the shear viscosity nonlocal kernel  $\eta(\mathbf{r}, \mathbf{r}')$  in (4.3) has different physical dimensions from the memory kernel  $\eta(\mathbf{r}, \mathbf{r}', t)$  in (4.1). For homogeneous fluids, translation invariance implies that  $\eta(\mathbf{r}, \mathbf{r}') = \eta(\mathbf{r} - \mathbf{r}')$  which is just a function of just one variable in planar flows. Under this simplifying circumstances Zhang et al. [76] considered planar Poiseuille and Couette Weeks-Chandler-Andersen (WCA) flows with NEMD and evaluated the shear viscosity nonlocal kernel. Further work in this direction was pursued in Refs. [77, 78, 86] where the wavenumber dependent shear viscosity for steady states for the WCA fluid was computed. It was shown that the nonlocality stands for 2-3 molecular diameters. Todd et al. [114] showed by using analytic arguments, that (space) nonlocality dominates transport phenomena when the variation in the strain rate is of the order of the width of the viscosity kernel. It should be emphasized that all the simulation work mentioned above in which the nonlocal viscosity kernel or the LADM viscosity have been explicitly computed deal with *steady state* situations for which the dynamic evolution of the flow plays no role. We are not aware of any study of *spontaneously* evolving hydrodynamics at nanoscale that make use of a nonlocal viscosity. Therefore, it is pertinent to question the validity of such an approach.

The strategy that we follow in order to answer the question about nonlocality of hydrodynamics is based on the study of *equilibrium time correlation functions* of the discrete hydrodynamic variables. The idea is that a constitutive equation like (4.1) should govern the nonequilibrium *averages* of the momentum density field. Through Onsager regression hypothesis, near equilibrium the correlation functions will obey the same equation as the one for the averages and, therefore, from the study of the correlation of the momentum density field we may extract information about the viscosity kernel. We pursue this route through the well-established Mori projector technique that

allows one to construct *linear* equations for the correlation functions. The technique produces formally exact governing equations for the correlation matrix of the selected CG variables. These equations are integro-differential equations that contain a memory kernel, which is not trivial to compute explicitly. Therefore, a clear separation of time scales is usually invoked in such a way that an approximate Markovian differential equation is obtained. Unfortunately, the resulting Green-Kubo expressions for the transport coefficients suffer from the well-known plateau problem [115], first described in the seminal work by Kirkwood [70]. In order to avoid the plateau problem, in Sec. 4.2 we propose an alternative formulation for the transport coefficients in terms of a *corrected* Green-Kubo formula that does not suffer from the plateau problem. We will use this expression in order to evaluate the nonlocal transport coefficients.

The distinctive feature of the Markovian approximation in Mori theory is to predict a (matrix) exponential decay of correlations. An important point of the present chapter is to compute explicitly the matrix exponential and to validate to what extent the predicted solution from the Markovian approximation describes the actual decay of the correlations.

This chapter is structured as follows. In Sec. 4.2 we obtain a corrected Green-Kubo formula which avoid the plateau problem. In Sec. 4.3 we particularize Mori theory to the discrete transverse momentum variable, both in real and Fourier space. In Sec. 4.4 we collect the relevant theoretical results and discuss the strategy in the simulations. In Sec. 4.5 we present the simulation results.

## 4.2 A corrected Green-Kubo formula with no plateau problem

In this section we address the plateau problem that appears in the expression of transport coefficient in terms of the unprojected Green-Kubo running integrals. When the dynamic of the CG variables is Markovian, but with not an extreme separation of time scales, the decay of the unprojected Green-Kubo running integral does not allow to determine unambiguously the value of the transport coefficients.

We now consider a procedure that allows one to obtain the friction matrix  $M^*$  from a modified version of the Green-Kubo formula even when no plateau exists, *provided* the dynamics is Markovian in such a way that correlations of CG variables obey (1.60).

The action of Mori projector operator on the phase function  $i\mathcal{L}\hat{A}$  is

$$\begin{aligned} Qi\mathcal{L}\hat{A} &= i\mathcal{L}\hat{A} - \langle i\mathcal{L}\hat{A}\hat{A}^T \rangle \cdot (\hat{A}\hat{A}^T)^{-1} \cdot \hat{A} \\ &= i\mathcal{L}\hat{A} + L \cdot C^{-1}(0) \cdot \hat{A} \end{aligned} \tag{4.4}$$

and therefore, the unprojected Green-Kubo matrix (1.66) becomes

$$M(t) = \int_0^t dt' \langle i\mathcal{L}\hat{A}(t')i\mathcal{L}\hat{A}^T \rangle + L \cdot C^{-1}(0) \cdot \int_0^t dt' \langle \hat{A}(t')i\mathcal{L}\hat{A}^T \rangle \quad (4.5)$$

By using the identity  $\frac{d}{dt} \hat{A}(z_t) = i\mathcal{L}\hat{A}(z_t)$  and the fact that the Liouville operator satisfies  $\langle \hat{A}(t)i\mathcal{L}\hat{A}^T \rangle = -\langle i\mathcal{L}\hat{A}(t)\hat{A}^T \rangle$  we obtain

$$M(t) = \int_0^t dt' \frac{d}{dt'} \langle \hat{A}(t')i\mathcal{L}\hat{A}^T \rangle - L \cdot C^{-1}(0) \cdot \int_0^t dt' \frac{d}{dt'} \langle \hat{A}(t')\hat{A}^T \rangle \quad (4.6)$$

We may integrate the time derivatives obtaining

$$\begin{aligned} M(t) &= \langle \hat{A}(t)i\mathcal{L}\hat{A}^T \rangle - \langle \hat{A}(0)i\mathcal{L}\hat{A}^T \rangle \\ &\quad - L \cdot C^{-1}(0) \cdot \langle \hat{A}(t)\hat{A}^T \rangle + L \cdot C^{-1}(0) \cdot \langle \hat{A}(0)\hat{A}^T \rangle \end{aligned} \quad (4.7)$$

The second and fourth terms in the right hand side cancel each other and we finally obtain

$$M(t) = -\frac{d}{dt} C(t) - L \cdot c(t), \quad (4.8)$$

where the normalized correlation matrix  $c(t)$  is defined in (1.65). This is a mathematical identity that relates the unprojected Green-Kubo matrix  $M(t)$  with the correlation matrix  $C(t)$  of the CG variables. It shows that  $M(t)$  cannot have a plateau for an ergodic system where  $\lim_{t \rightarrow \infty} C(t) = 0$ .

If we now assume that the correlation function  $C(t)$  obeys the Markovian dynamics (1.60) with (1.56), then equation (4.8) becomes

$$M(\tau) \simeq M^* \cdot c(\tau) \quad (4.9)$$

This expression shows that the unprojected Green-Kubo matrix decays as the correlation of the CG variables. Although the time integral in the left hand side of (4.9) has no plateau as it is obvious by looking at the decaying correlation in the right hand side, it is still possible to infer the friction matrix  $M^*$  by multiplying (4.9) with the inverse of the normalized correlation, leading to

$$M^* = \int_0^\tau dt \langle Q i\mathcal{L}\hat{A}(t)i\mathcal{L}\hat{A}^T \rangle \cdot c^{-1}(\tau) \quad (4.10)$$

This new corrected Green-Kubo formula (4.10) allows one to calculate the friction matrix  $M^*$  from MD simulations and does not suffer from the plateau problem by

construction, provided the dynamic is Markovian. The equation (4.10) is conceptually pleasing as it displays in very graphical terms why the unprojected Green-Kubo integral (1.66) has no plateau – in fact, it decays as the correlation matrix itself. It is obvious that (4.10) can not be true at  $\tau = 0$  as this would imply  $M^* = 0$ . However, after a time in the molecular time scales, the right hand side of equation (4.10) should be time independent provided that the Markovian description (1.60) is valid. In the limit of very large separation of time scales, when  $M(t)$  has a “fast-up, slow-down” structure, we may assume that the normalized correlation matrix is very close to its value at  $t = 0$  which is just the identity matrix, this is  $c^{-1}(\tau) \simeq 1$ . In this case, we recover from (4.10) the unprojected Green-Kubo prescription (1.66) for the transport coefficients.

In summary, equation (4.10) shows a way to infer the friction matrix  $M^*$  in the Markovian equation (1.55) from a time integral even when it is not possible to identify a well-defined plateau in the unprojected Green-Kubo formula (1.66).

The mathematics behind the derivation of (4.10) should not obscure the essential procedure that we have followed here. We have inferred  $M^*$  from the fact that the correlation matrix  $C(t)$  obeys the Markovian equation (1.60). In this respect, an alternative, *entirely equivalent*, and perhaps simpler way to obtain the friction matrix  $M^*$  is by introducing the time dependent matrix

$$\Lambda(t) \equiv -\frac{d}{dt} C(t) \cdot C^{-1}(t) \quad (4.11)$$

From equation (1.60), if the Markov assumption is correct after a molecular time  $\tau$ ,  $\Lambda(t)$  should become a time-independent matrix  $\Lambda^*$

$$\lim_{t \rightarrow \infty} \Lambda(t) = \Lambda^* \quad (4.12)$$

Therefore, from (1.56) we can obtain the friction matrix as

$$M^* = -L + \Lambda^* \cdot C(0) \quad (4.13)$$

In some situations, however, it is preferable to obtain the friction matrix  $M^*$  from the corrected Green-Kubo expression (4.10) than from (4.13) because the Green-Kubo expression involves the time derivative  $i\mathcal{L}\hat{A}$  that may induce special structure to the matrix  $M^*$ . This is the case of hydrodynamics near walls that we discuss elsewhere.

The method to obtain the matrix  $\Lambda^*$  from the plateau of  $\Lambda(t)$  in (4.11) needs high quality statistics for  $C(t)$  and  $\frac{d}{dt}C(t)$ . The same is true for the new Green-Kubo formula (4.10). In fact,  $C(t)$  is an exponentially decaying matrix, and  $C^{-1}(t)$  is an exponentially growing matrix. At very large times, any statistical error will be exponentially amplified. This means also that  $\tau$  should be, in practice, as small as possible in order to detect a plateau value for  $\Lambda(t)$ , and for which statistical errors have not yet been amplified to a catastrophic level.

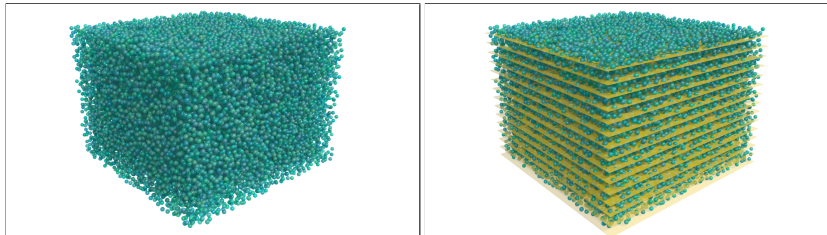


**Figure 4.1:** A visual representation of the MD simulation (left) and the same with the sketch of the binning used in yellow (right). Because of the high number of bins used, we only draw some of them.

## 4.3 Mori theory for shear hydrodynamics

In this section, we use Mori theory in the notation presented in Sec. 1.7.2 for predicting the dynamics of equilibrium time correlations of the discrete transverse momentum density in a periodic box.

### 4.3.1 The CG variables

In Chapter 3 we gave a detailed description of the definitions of the geometry and the definition of the CG variables. The simulation periodic box of dimensions  $L_x, L_y, L_z$  is divided in its  $L_z$  direction in  $N_{\text{bin}}$  nodal planes, as it shown in Fig. 4.1, labelled with an index  $\mu$  located at  $z_\mu = \mu\Delta z$ ,  $\mu = 0, \dots, N_{\text{bin}} - 1$  with  $\Delta z = L_z/N_{\text{bin}}$ . Due to periodic boundary conditions (PBC) in the  $z$  direction the node  $\mu = 1$  is equal to the node  $\mu = N_{\text{bin}} + 1$ , whereas the node  $\mu = 0$  is equal to the node  $N_{\text{bin}}$ .

As we explained in Sec. 3.3, nodes are points in the  $z$  axis, while bins are segments in this axis. In 3D, nodes are planes, while bins are slabs. From a microscopic point of view, mass, momentum, and force densities are defined at the nodes, while stress is defined at the bins. Each bin is a layer of dimensions  $L_x, L_y, \Delta z$ .

As CG variables we choose the set of discrete hydrodynamic variables, which are the mass density  $\hat{\rho}_\mu(z)$  and the momentum density  $\hat{\mathbf{g}}_\mu(z)$  defined at the nodal planes  $\mu$

$$\hat{\rho}_\mu(z) = \sum_i^N m_i \delta_\mu(\mathbf{r}_i), \quad \hat{\mathbf{g}}_\mu(z) = \sum_i^N \mathbf{p}_i \delta_\mu(\mathbf{r}_i), \quad (4.14)$$

where  $\mathbf{r}_i, \mathbf{p}_i$  are the position and momentum of particle  $i$ , and the discrete Dirac  $\delta$  was introduced in (3.19). The microscopic variables (4.14) give, essentially, the number of particles and momentum per unit volume of the particles that happen to be “around”

the nodal plane  $\mu$ . The rationale for using this definition has been discussed in Chapter 3.

Note that the discrete Dirac  $\delta$  function depends on the finite element basis function  $\Phi_\mu(\mathbf{r})$ , introduced in equation (3.4), which form a partition of unity (3.5) The partition of unity implies that if we compute the discrete integral (i.e. sum over bins times the volume of the bin) of the discrete hydrodynamic variables we obtain

$$\begin{aligned} \sum_{\mu} \mathcal{V}_{\mu} \hat{\rho}_{\mu}(z) &= mN \\ \sum_{\mu} \mathcal{V}_{\mu} \hat{\mathbf{g}}_{\mu}^x(z) &= \sum_i^N \mathbf{p}_i = \hat{\mathbf{P}}_T(z), \end{aligned} \quad (4.15)$$

where we have introduced the total mass  $mN$  and the total momentum  $\hat{\mathbf{P}}_T(z)$  of the system. These are quantities that are conserved under the Hamiltonian evolution of the microscopic state.

We will only consider the correlations of the component  $\hat{\mathbf{g}}_{\mu}^x$  of the momentum density parallel to the bins. These variables are collected into the  $N_{\text{bin}}$ -dimensional vector  $\hat{g}(z) = \{\hat{\mathbf{g}}_1^x(z), \dots, \hat{\mathbf{g}}_{N_{\text{bin}}}^x(z)\}$ . We have checked through MD simulations that the coupling between this component and the rest of hydrodynamic variables (density, other momentum components) is negligible. Therefore, we expect that a theory of just the transverse momentum is a good candidate for a Markovian theory.

### 4.3.2 The Green-Kubo running integral $M(t)$

Mori theory for correlations presented in Sec. 1.7.2 allows one to obtain the evolution of the matrix of correlations  $C(t)$  as

$$\frac{d}{dt} C(t) = -(L + M^*) \cdot c(t), \quad (4.16)$$

where we have used equations (1.60), (1.56) and the normalized correlation matrix defined as in (1.65). Note that the reversible matrix  $L$  vanishes because it involves an equilibrium average of a function that is even in the momentum variables. Therefore

$$\frac{d}{dt} C(t) = -k_B T M^* \cdot c(t), \quad (4.17)$$

where, in order to make contact with known results, we have redefined the transport matrix  $M^*$  by introducing a prefactor  $k_B T$  where  $k_B$  is Boltzman's constant and  $T$  the equilibrium temperature.

The friction matrix  $M^*$  in (4.10) is related to the standard Green-Kubo running integral

$$M(t) = \frac{1}{k_B T} \int_0^t dt' \langle i \mathcal{L}\hat{g}(t') i \mathcal{L}\hat{g}^T \rangle \quad (4.18)$$

that involves the time derivative of the momentum density which, as shown in equation (3.34), is given by

$$i \mathcal{L}\hat{g}_\mu(z) = -\frac{\hat{\sigma}_\mu^{xz} - \hat{\sigma}_{\mu-1}^{xz}}{\Delta z} \quad (4.19)$$

This is a discrete expression of the momentum balance equation in which the time rate of change of the momentum of the node  $\mu$  is due to the finite difference gradient of the stress tensor  $\hat{\sigma}_\mu^{xz}$  of the neighbour bins. The microscopic stress tensor of bin  $\mu$  is

$$\hat{\sigma}_\mu = \frac{1}{V_\mu} \left[ \sum_i \mathbf{p}_i \mathbf{v}_i \chi_\mu(\mathbf{r}_i) + \frac{1}{2} \sum_{ij}^N \mathbf{r}_{ij} \hat{\mathbf{F}}_{ij} z_\mu(i, j) \right], \quad (4.20)$$

where  $\chi_\mu(\mathbf{r})$  is the characteristic function of bin  $\mu$  and  $z_\mu(i, j)$ , introduced in equation (3.32), is the fraction of the distance between atoms  $i, j$  that happens to be within bin  $\mu$ .

We may write equation (4.19) in matrix form as

$$i \mathcal{L}\hat{g} = -B \cdot \hat{\sigma}^{xz} = F^T \cdot \hat{\sigma}^{xz}, \quad (4.21)$$

where  $\hat{\sigma}$  is a  $N_{\text{bin}}$ -dimensional column vector containing the discrete stress tensor of bin  $\mu$  and  $B$  is the backward finite difference matrix. This matrix is  $B = -F^T$ , where the matrix  $F$  is the forward finite difference operator (for PBC)

$$F = \frac{1}{\Delta z} \begin{pmatrix} -1 & 1 & 0 & \cdots & 0 \\ 0 & -1 & 1 & \cdots & 0 \\ \vdots & & \ddots & & \vdots \\ 0 & \cdots & 0 & -1 & 1 \\ 1 & \cdots & 0 & 0 & -1 \end{pmatrix} \quad (4.22)$$

By using (4.21) into the Green-Kubo integral matrix  $M(t)$  in (4.18) we have

$$M(t) = F^T \cdot \eta(t) \cdot F, \quad (4.23)$$

where the *nonlocal viscosity Green-Kubo matrix* is the running time integral of the correlation of the stress tensor at different bins,

$$\eta(t) = \frac{1}{k_B T} \int_0^t dt' \langle \hat{\sigma}^{xz}(t') \hat{\sigma}^{xz} \rangle \quad (4.24)$$

Note that for a homogeneous system (as one with PBC), the nonlocal viscosity matrix is translationally invariant, this is  $\eta_{\mu\nu} = \eta(|\mu - \nu|)$ . This kind of matrices commute with the forward differencing matrix

$$F \cdot \eta(t) = \eta(t) \cdot F \quad (4.25)$$

By using this commutation property in the Green-Kubo integral (4.23) we obtain

$$M(t) = -\Delta \cdot \eta(t), \quad (4.26)$$

where we have introduced the discrete Laplacian matrix (for PBC) as

$$\Delta \equiv B \cdot F = \frac{1}{\Delta z^2} \begin{pmatrix} -2 & 1 & 0 & \cdots & 1 \\ 1 & -2 & 1 & \cdots & 0 \\ \vdots & & \ddots & & \vdots \\ 1 & \cdots & 0 & 1 & -2 \end{pmatrix} \quad (4.27)$$

### 4.3.3 The friction matrix $M^*$ and the nonlocal shear viscosity matrix

Note that the Green-Kubo integral (4.18) can also be written in the form

$$\begin{aligned} M(t) &= \frac{1}{k_B T} \int_0^t dt' \frac{d}{dt'} \langle \hat{g}(t') i \mathcal{L} \hat{g}^T \rangle \\ &= \frac{1}{k_B T} \langle \hat{g}(t) i \mathcal{L} \hat{g}^T \rangle = -\frac{1}{k_B T} \frac{d}{dt} \langle \hat{g}(t) \hat{g}^T \rangle = -\frac{1}{k_B T} \frac{d}{dt} C(t) \end{aligned} \quad (4.28)$$

Therefore, equations (4.26), (4.28) lead to the following *rigorous and exact* result

$$\frac{d}{dt} C(t) = k_B T \Delta \cdot \eta(t) \quad (4.29)$$

that links the momentum correlation matrix with the stress correlation matrix. This equation shows that the Green-Kubo running integral (4.24) for the viscosity matrix

$\eta(t)$  cannot have a plateau, as it should decay according to the time derivative of  $C(t)$  and, hence, from (1.60) as the correlation matrix  $C(t)$  itself.

By analogy with (4.26), we assume that the friction matrix  $M^*$  in (4.17) has the structure

$$M^* = -\Delta \cdot \eta^* \quad (4.30)$$

for a certain matrix  $\eta^*$  referred to as the nonlocal shear viscosity matrix. The Markovian dynamics (4.17) becomes

$$\frac{d}{dt} C(t) = k_B T \Delta \cdot \eta^* \cdot c(t) \quad (4.31)$$

We would like to obtain the matrix  $\eta^*$  from the Green-Kubo running integral (4.24) for  $\eta(t)$ . Comparison of (4.31) and (4.29) gives

$$\Delta \cdot \eta(t) = \Delta \cdot \eta^* \cdot c(t) \quad (4.32)$$

If the two matrices  $\Delta, c(t)$  were invertible, then (4.31) would allow to obtain  $\eta^*$  from the correlation of the momentum density, while equation (4.32) would give  $\eta^*$  from the correlation of the stress. Both routes are, of course, mathematically equivalent. However, both the Laplacian matrix  $\Delta$  and the normalized correlation matrix  $c(t)$  are not invertible. The reason is that the normalized “constant” vector

$$v = \frac{1}{\sqrt{N_{\text{bin}}}} (1, 1, \dots, 1) \quad (4.33)$$

is the unique eigenvector of null eigenvalue of the Laplacian operator with periodic boundary conditions,  $\Delta \cdot v = 0$ . This vector is also eigenvector of null eigenvalue of the correlation matrix  $C(t) \cdot v = 0$  due to total momentum conservation in PBC. In the next section we take advantage of the periodicity and the translational invariance of the system in order to deal with that issue in Fourier space.

#### 4.3.4 Fourier space

Consider the unitary matrix with elements

$$E_{\mu\nu} = \frac{1}{\sqrt{N_{\text{bin}}}} \exp \left\{ i \frac{2\pi}{N_{\text{bin}}} \mu \nu \right\} \quad (4.34)$$

This matrix has the following inverse

$$E_{\mu\nu}^{-1} = \frac{1}{\sqrt{N_{\text{bin}}}} \exp \left\{ -i \frac{2\pi}{N_{\text{bin}}} \mu \nu \right\} \quad (4.35)$$

The indices are assumed to run in the range  $\mu = 0, 1, \dots, N_{\text{bin}} - 1$ . We define the Fourier transform  $\tilde{A}$  of a matrix  $A$  as

$$\tilde{A} = E^{-1} \cdot A \cdot E \quad (4.36)$$

with the inverse relation

$$A = E \cdot \tilde{A} \cdot E^{-1} \quad (4.37)$$

The discrete Laplace operator diagonalizes in Fourier space, that is,

$$E^{-1} \cdot \Delta \cdot E = \tilde{\Delta}, \quad (4.38)$$

where  $\tilde{\Delta}$  is a diagonal matrix whose diagonal elements are

$$\tilde{\Delta}_{\mu\mu} = -\frac{2}{\Delta z^2} \left( 1 - \cos \left( \frac{2\pi\mu}{N_{\text{bin}}} \right) \right) \leq 0 \quad (4.39)$$

This is the spectrum of the discrete Laplace operator  $\Delta$ .

The matrix  $E$  diagonalizes any traslation invariant and periodic matrix  $A_{\mu\nu}$  satisfying  $A_{\mu\nu} = a(|\mu - \nu|)$  and  $a(\mu) = a(N_{\text{bin}} - 1 - \mu)$  as it is easily seen

$$\begin{aligned} [E^{-1} \cdot A \cdot E]_{\mu\nu} &= \frac{1}{N_{\text{bin}}} \sum_{\mu'=0}^{N_{\text{bin}}-1} \sum_{\nu'=0}^{N_{\text{bin}}-1} e^{-i \frac{2\pi}{N_{\text{bin}}} \mu \mu'} a(|\mu' - \nu'|) e^{i \frac{2\pi}{N_{\text{bin}}} \nu' \nu} \\ &= \frac{1}{N_{\text{bin}}} \delta_{\mu\nu} \underbrace{\sum_{\sigma=0}^{N_{\text{bin}}-1} a(\sigma) e^{i \frac{2\pi}{N_{\text{bin}}} \sigma \nu}}_{\tilde{a}(\nu)} \end{aligned} \quad (4.40)$$

Because the matrix  $C(t)$  is periodic traslation invariant, the Fourier transform is a diagonal periodic matrix  $\tilde{C}_{\mu\nu}(t) = \delta_{\mu\nu} \tilde{C}_{\mu\mu}(t)$ . The two equations (4.31),(4.32) become in Fourier space

$$\begin{aligned} \frac{d}{dt} \tilde{C}(t) &= k_B T \tilde{\Delta} \cdot \tilde{\eta}^* \cdot \tilde{c}(t) \\ \tilde{\Delta} \cdot \tilde{\eta}(t) &= \tilde{\Delta} \cdot \tilde{\eta}^* \cdot \tilde{c}(t) \end{aligned} \quad (4.41)$$

All matrices appearing in these equations are diagonal. Therefore, except for  $\mu = 0$ , where  $\tilde{c}_{00} = 0$  due to total momentum conservation, we may infer the diagonal elements

of the shear viscosity matrix in Fourier space  $\tilde{\eta}^*$  from either any of these two equations

$$\begin{aligned}\tilde{\eta}_{\mu\mu}^* &= \frac{1}{k_B T \tilde{\Lambda}_{\mu\mu} \tilde{c}_{\mu\mu}(t)} \frac{d}{dt} \tilde{C}_{\mu\nu}(t) \\ \tilde{\eta}_{\mu\mu}^* &= \frac{\tilde{\eta}_{\mu\mu}(t)}{\tilde{c}_{\mu\mu}(t)}\end{aligned}\quad (4.42)$$

These two expressions are mathematically equivalent but they allow to obtain the nonlocal shear viscosity in Fourier space  $\tilde{\eta}_{\mu\mu}^*$  either from the correlation of momentum or from the correlation of stress. The existence of a plateau in the time-dependent functions of the right hand side in (4.42) constitute both, a validation of the Markovian assumption, as well as a way to compute the nonlocal shear viscosity.

If we wish to recover the nonlocal shear viscosity in real space we need to know all their eigenvalues. However, the element  $\tilde{\eta}_{00}$  cannot be computed from (4.42) because  $\tilde{c}_{00} = 0$ . Note that this value can be obtained directly by recognizing that

$$\tilde{\eta}_{00}(t) = E_{0\mu}^{-1} \cdot \eta_{\mu\nu}(t) \cdot E_{\nu 0} = \frac{1}{N_{\text{bin}}} \sum_{\mu\nu} \eta_{\mu\nu}(t) \quad (4.43)$$

From (4.20) and the fact that  $\chi_\mu(\mathbf{r}), z_\mu(i, j)$  form a partition of unity, we have that the total stress is the arithmetic average of the stress in each bin is given by

$$\hat{\sigma}_T^{xz} = \frac{1}{N_{\text{bin}}} \sum_{\mu} \hat{\sigma}_{\mu}^{xz}, \quad (4.44)$$

where the total stress  $\hat{\sigma}_T^{xz}$  is defined in the usual way

$$\hat{\sigma}_T^{xz} = \frac{1}{V_T} \left[ \sum_i \mathbf{p}_i^x \mathbf{v}_i^z + \frac{1}{2} \sum_{ij} \mathbf{r}_{ij}^x \hat{\mathbf{F}}_{ij}^z \right] \quad (4.45)$$

and  $V_T$  is the total volume of the system.

By using (4.24) in (4.43) we obtain

$$\tilde{\eta}_{00}(t) = \frac{1}{N_{\text{bin}}} \frac{1}{k_B T} \int_0^t dt' \left\langle \sum_{\mu} \hat{\sigma}_{\mu}^{xz}(t') \sum_{\nu} \hat{\sigma}_{\nu}^{xz} \right\rangle \quad (4.46)$$

Using the equation (4.44)

$$\tilde{\eta}_{00}(t) = \frac{N_{\text{bin}}}{k_B T} \int_0^t dt' \left\langle \hat{\sigma}_T^{xz}(t') \hat{\sigma}_T^{xz} \right\rangle \quad (4.47)$$

Introducing the *local* shear viscosity given by the standard Green-Kubo integral

$$\eta_0(t) \equiv \frac{V_T}{k_B T} \int_0^t dt' \langle \hat{\sigma}_T^{xz}(t') \hat{\sigma}_T^{xz} \rangle \quad (4.48)$$

we finally reach

$$\tilde{\eta}_{00}(t) = \frac{N_{\text{bin}}}{V_T} \eta_0(t) \quad (4.49)$$

Therefore, the eigenvalue  $\tilde{\eta}_{00}(t)$  can be computed independently from the local shear viscosity.

#### 4.3.5 The nonlocal kinematic viscosity matrix $\nu^*$

As we will see, the notion of locality in space is best addressed with the kinematic viscosity, which is the nonlocal shear viscosity matrix  $\eta^*$  divided by some “mass density”. In a discrete setting, the connection between the discrete momentum and the discrete velocity is slightly more involved than in the continuum for which one has the simple result  $\mathbf{g}(\mathbf{r}) = \rho(\mathbf{r})\mathbf{v}(\mathbf{r})$ . In the discrete, the proportionality between velocity and momentum is through a mass density. Let us see the details.

As shown in Appendix F, the covariance  $C(0)$  of the discrete momentum density in PBC is given by

$$C_{\mu\nu}(0) = \frac{k_B T}{\mathcal{V}_\mu} \rho_{\mu\nu}, \quad (4.50)$$

where we have introduced the mass density matrix  $\rho_{\mu\nu}$  as

$$\rho_{\mu\nu} \equiv m \mathcal{V}_\mu n \left[ M_{\mu\nu}^\delta - \frac{1}{nN} \langle \hat{n}_\mu \hat{n}_\nu \rangle \right], \quad (4.51)$$

where  $\hat{n}_\mu = \hat{\rho}_\mu/m$  is the number density of node  $\mu$  and  $n = N/V$  is the average number density. The matrix  $M_{\mu\nu}^\delta$  is given in (3.13). For a system with regular bins with constant volume  $\mathcal{V}$  each, this matrix takes the form

$$M^\delta = \frac{1}{6\mathcal{V}} \begin{pmatrix} 4 & 1 & 0 & \cdots & 0 & 1 \\ 1 & 4 & 1 & \cdots & 0 & 0 \\ \vdots & & & \ddots & & \vdots \\ 0 & 0 & 0 & \cdots & 4 & 1 \\ 1 & 0 & 0 & \cdots & 1 & 4 \end{pmatrix} \quad (4.52)$$

The last term in (4.51) scales as the inverse of the total number  $N$  of particles and it is negligible in the thermodynamic limit. However, we should keep it as it has observable consequences in our simulations. In fact, this term is responsible for total momentum conservation (4.15), that is,

$$\sum_{\mu} \mathcal{V}_{\mu} \langle \hat{g}_{\mu} \hat{g}_{\nu} \rangle = 0 \quad (4.53)$$

as it should, because the total momentum  $\sum_{\mu} \mathcal{V}_{\mu} \hat{g}_{\mu}$  vanishes in the center of mass reference frame that we take.

By using the explicit form (4.50) of the covariance matrix, we may express equation (4.31) in the form

$$\frac{d}{dt} C(t) = \Delta \cdot v^* \cdot C(t), \quad (4.54)$$

where we have introduced the nonlocal *kinematic* viscosity matrix through the matrix

$$v^* \equiv \eta^* \cdot \mathcal{V} \cdot \rho^{-1}, \quad (4.55)$$

where  $\mathcal{V}$  is a diagonal matrix that contains in the diagonal the volume  $\mathcal{V}_{\mu}$  of the bins. In Fourier space equation (4.55) takes the diagonal form

$$\tilde{v}_{\mu}^* = \frac{\mathcal{V}_{\mu} \tilde{\eta}_{\mu}^*}{\tilde{\rho}_{\mu}} \quad (4.56)$$

### 4.3.6 The equations for the average

We now show why we refer to the matrix  $\eta^*$  as the nonlocal shear viscosity and to the matrix  $v^*$  as the nonlocal kinematic viscosity. According to Mori theory, which encompass Onsager regression hypothesis, the evolution of the average value of the discrete momentum should evolve according to a vector equation analogous to (4.54) for the correlation matrix

$$\frac{d}{dt} g(t) = \mathcal{V} \cdot \Delta \cdot \eta^* \cdot v(t), \quad (4.57)$$

where we have defined the discrete velocity field  $v = (\mathbf{v}_1^x, \dots, \mathbf{v}_{N_{bin}}^x)$  according to

$$\mathbf{v}_{\mu}^x \equiv \sum_{\nu} \rho_{\mu\nu}^{-1} \mathbf{g}_{\nu}^x \quad (4.58)$$

The matrix  $\rho_{\mu\nu}$  defined in (4.51) has dimensions of a mass density and it is fairly diagonal. Its inverse  $\rho^{-1}$  is concentrated on the diagonal (in fact, it decays exponentially fast as we move out from the diagonal). Because of this, we may interpret  $v_\mu$  defined in (4.58) as a velocity that contains information about the discretization method used. The components of equation (4.57) are

$$\frac{d}{dt} \mathbf{g}_\mu^x(t) = - \sum_v \mathcal{V}_v \frac{[\eta_{\mu\nu}^* - \eta_{\mu-1\nu}^* - \eta_{\mu\nu-1}^* + \eta_{\mu-1\nu-1}^*]}{\Delta z^2} \mathbf{v}_v^x(t) \quad (4.59)$$

This equation for the non-equilibrium average is identical to the one obtained in Chapter 3 with the Kawasaki-Gunton projector.

By a suitably relabeling of indices and by using the translation invariance of the viscosity matrix we have

$$\frac{d}{dt} \mathbf{g}_\mu^x(t) = \sum_v \mathcal{V}_v \eta_{\mu\nu}^* \frac{[\mathbf{v}_{v+1}^x - 2\mathbf{v}_v^x + \mathbf{v}_{v-1}^x]}{\Delta z^2} \quad (4.60)$$

Equation (4.60) looks like a discretization of the following integro-differential equation

$$\frac{d}{dt} \mathbf{g}^x(z) = \int dz' \eta^*(z-z') \partial_z^2 \mathbf{v}^x(z') \quad (4.61)$$

This is a nonlocal generalization of the diffusion equation of the continuum transverse momentum

$$\partial_t \mathbf{g}^x(z) = v_0^* \partial_z^2 \mathbf{g}^x(z) \quad (4.62)$$

Equation (4.62) is obtained from (4.61) by setting  $\eta^*(z-z') = \eta_0^* \delta(z-z')$ , where the local kinematic viscosity is  $v_0^* = \eta_0^*/\rho$ . Therefore, it is justified to refer to the matrix  $\eta_{\mu\nu}^*$  introduced in (4.24) as the nonlocal shear viscosity matrix and to  $\mathbf{v}_\mu$  introduced in (4.58) as the velocity.

### 4.3.7 The local in time prediction

By using (4.38) and (4.39), the Fourier transform of the equation of motion (4.54) is then

$$\frac{d}{dt} \tilde{C}_\mu(t) = -\frac{1}{\tau_\mu} \tilde{C}_\mu(t), \quad (4.63)$$

where the relaxation time  $\tau_\mu$  of mode  $\mu$  satisfies

$$\frac{1}{\tau_\mu} \equiv \frac{2}{\Delta z^2} \left( 1 - \cos \left( \frac{2\pi\mu}{N_{\text{bin}}} \right) \right) \tilde{\nu}_\mu^* \quad (4.64)$$

The solution of equation (4.63) with “initial condition”  $\tilde{C}_\mu(\tau)$  at time  $\tau$  is the exponential function

$$\tilde{C}_\mu(t) = \exp \left\{ -\frac{t-\tau}{\tau_\mu} \right\} \tilde{C}_\mu(\tau), \quad (4.65)$$

The displacement of the initial condition to the time  $\tau$  is due to the fact that we know that the exponential behaviour cannot start at  $t = 0$  where the Markovian equation (1.60) (and hence (4.63)), cannot strictly hold.

The correlation matrix  $C(t)$  in real space is obtained from the correlation in Fourier space in (4.65) by equation (4.37), and leads to the result

$$C(t) = \exp \{ \Delta \cdot \nu^*(t - \tau) \} C(\tau), \quad (4.66)$$

where the exponential matrix takes the form

$$[\exp \{ \Delta \cdot \nu^* t \}]_{\mu\nu} = \frac{1}{N_{\text{bin}}} \sum_{\mu'} \exp \left\{ i \frac{2\pi}{N_{\text{bin}}} (\mu - \nu) \mu' \right\} \exp \left\{ -\frac{t}{\tau_{\mu'}} \right\} \quad (4.67)$$

In summary, the prediction of the correlation matrix in Fourier space is given by single exponentials, while in real space is given by a linear combination of single exponentials. As we will see, the later will give rise to quasi-algebraic decay of correlations in real space.

### 4.3.8 The local in space prediction

The discrete version of the local continuum hydrodynamics equation (4.62) is simply

$$\frac{d}{dt} \mathbf{g}_\mu^x(t) = \nu_0 \Delta_{\mu\nu} \mathbf{g}_\nu^x(t) \quad (4.68)$$

By comparing this discrete equation in the local approximation with the nonlocal discrete equation (4.57), we conclude that the local approximation of the nonlocal viscosity matrix  $\nu$  becomes a diagonal matrix of the form

$$\nu_{\mu\mu'} \simeq \nu_0 \delta_{\mu\mu'}, \quad (4.69)$$

where the local kinematic viscosity is given by

$$\nu_0 \equiv \sum_{\mu'} \nu_{\mu\mu'} \quad \forall \mu \quad (4.70)$$

In the local approximation, the differential equation (4.54) for the correlation matrix becomes

$$\frac{d}{dt} C(t) = \nu_0 \Delta \cdot C(t) \quad (4.71)$$

The Fourier transform of the local equation (4.71) is identical to (4.63) but with a constant value for the kinematic viscosity in (4.64)

$$\tilde{\nu}_{\mu}^* = \nu_0 \quad (4.72)$$

for all  $\mu$ . Therefore, the local hydrodynamic prediction says that the Fourier kinetic viscosity coefficients  $\tilde{\nu}_{\mu}$  take the constant value  $\nu_0$  given in (4.70). In the local approximation, the relaxation time (4.64) is given by

$$\frac{1}{\tau_{\mu}^{\text{loc}}} = \frac{2}{\Delta z^2} \left( 1 - \cos \left( \frac{2\pi\mu}{N_{\text{bin}}} \right) \right) \nu_0 \quad (4.73)$$

## 4.4 Summary of the theory and strategy in the simulations

In the previous section we have considered the theoretical results predicted from Mori's theory for the correlation matrix  $C(t)$  of the transverse momentum. The correlation matrix obeys the linear equation (4.17) where the corrected Green-Kubo matrix  $M^*$  is related to the plateau problematic Green-Kubo running integral  $M(t)$  through (4.10). By extracting the space derivatives from  $M^*$  and  $M(t)$  we relate these matrices to the corrected nonlocal viscosity matrix  $\eta^*$  in (4.30) and to the nonlocal viscosity matrix  $\eta(t)$  in (4.26), respectively. The latter has the Green-Kubo expression (4.24) in terms of the correlation of the stress tensor. The corrected  $\eta^*$  is obtained from  $\eta(t)$  through the equations (4.42) in Fourier space.

In order to discuss the local approximation in space in the equation for the average of the momentum field (4.57) it is convenient to introduce the kinematic viscosity matrix (4.55) because the local approximation is very simple in Fourier space in terms of the kinematic viscosity matrix. The local approximation amounts to set all the eigenvalues of the kinematic matrix identical to the standard kinematic viscosity of the fluid, as in (4.72).

In the next section we measure through MD simulations the two main quantities of concern in this chapter which are the correlation matrix of discrete momentum  $C(t)$  and the correlation matrix of the discrete stress that appears in the Green-Kubo running integral  $\eta(t)$ . From these primary quantities, we obtain their Fourier transforms  $\tilde{C}(t), \tilde{\eta}(t)$  which are diagonal matrices due to translation invariance.

In order to test the locality in time, we check for the simple exponential decay prediction (4.65) for the eigenvalues of the correlation matrix. In order to test the nonlocality in space, from equation (4.42) we will infer the nonlocal shear viscosity matrix  $\tilde{\eta}^*$  and, from the Fourier transform of (4.55), the nonlocal kinematic viscosity  $\tilde{\nu}^*$ . The local approximation in space will be good if we can approximate  $\tilde{\nu}^*$  as in (4.72). Once we have measured  $\Lambda^*$  or equivalently  $\eta^*$  or  $\nu^*$  we can compare the prediction (4.66) from Mori theory with the correlation matrix measured in the simulation.

## 4.5 Simulations

In Sec. 4.3 we saw that the two main quantities of concern are the correlation matrix of discrete momentum  $C(t)$  and the correlation matrix of the discrete stress that appears in the Green-Kubo running integral  $\eta(t)$ . These two matrices can be measured from MD simulations.

The objective of this section is to present the simulations conducted to measure the momentum correlation matrix  $C(t)$  and the Green-Kubo nonlocal viscosity  $\eta(t)$ . From these primary quantities, we obtain their Fourier transforms  $\tilde{C}(t), \tilde{\eta}(t)$  which are diagonal matrices due to traslation invariance.

### 4.5.1 Simulation set up

A system of particles interacting with a LJ potential truncated at  $\sigma = 2.5$  has been simulated in PBC with the LAMMPS code [116]. In Fig. 4.1 a snapshot of the simulation is showed. The box size is  $40 \times 40 \times 30$ , the number of particles is  $N = 28749$ , and the timestep is 0.002 in reduced units. After an equilibration of  $10^5$  timesteps with a Langevin thermostat to produce a microstate typical from a thermodynamic point corresponding to  $T = 2, \rho = 0.6$  in reduced units, the system is evolved under NVE microcanonical conditions for a further  $10^5$  timesteps. After this equilibration phase, production runs of  $1.5 \times 10^6$  timesteps are launched. The  $z$  axis is binned in 60 bins on which the  $x$  component of the momentum density is recorded every 10 timesteps. The width of the bin is  $\Delta z = 0.5\sigma$  which is subatomic. We will see in the next chapter that in the presence of walls, such a bin allows to capture some of the density layering. A total of  $60 \times 60$  correlations corresponding to the elements of the correlation matrix are

computed in each simulation. In order to increase statistics, we average the result of 30 simulations and exploit the translation invariance of the system by further averaging correlations between nodes at a given distance. Although computing all the correlation matrix elements may seem unnecessary, we will use the same methodology for confined fluids in the next chapter. In this later case, translation invariance is broken and we need to consider the full correlation matrix.

#### 4.5.2 The correlation matrix $C(t)$

In Fig. 4.2 we plot the correlation matrix of the transverse momentum  $C_{\mu\nu}(t) = \langle g_\mu(t) g_\nu \rangle$  at the time  $t = 0$  and  $t = 0.6$ . This matrix is periodic and translation invariant. Therefore, statistical errors have been further reduced by averaging this matrix “along diagonals”. In addition, we have taken advantage of the analytical calculation of the covariance  $\langle g_\mu g_\nu \rangle$  in the Appendix F in a manner that we describe below.

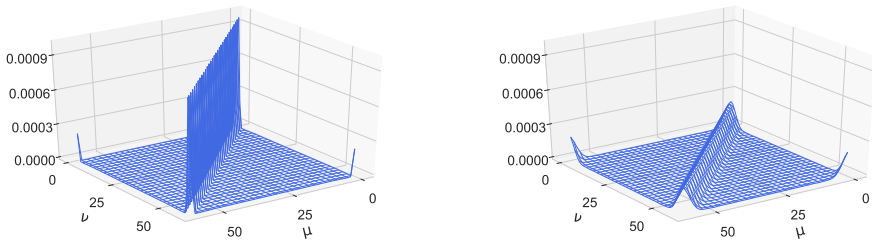


**Figure 4.2:** The correlation matrix  $C_{\mu\nu}(t) = \langle g_\mu(t) g_\nu \rangle$  for  $t = 0$  (left) and  $t = 0.6$  (right).

In Fig. 4.3 the correlations  $\langle g_\mu(t) g_\nu \rangle$  for  $\mu = 30$  and different values of  $\nu$  at  $t = 0$  (blue),  $t = 0.2$  (orange),  $t = 0.4$  (purple) and  $t = 0.6$  (green) is shown. This is the row 30 of the matrix plotted in Fig. 4.2. We observe a diffusive behaviour over a negative background. The origin of this negative global correlation for nodes that are far apart is due to total momentum conservation in PBC. If a bin has a positive momentum, the rest of bins should have an overall negative value in order for the total momentum to be zero. In order to improve the statistical quality of the matrix  $C(t)$  we have used the analytical value (F.9) for the background, as provided by the analytic calculation of the covariance in the Appendix F.

The autocorrelation  $\langle g_\mu(t) g_\mu \rangle$  (which is the same for all  $\mu$ ) is shown in Fig. 4.4 as a function of time in both linear and log scales. Also shown is a function  $\propto t^{-1/2}$ . The observed decay does not correspond to this algebraic decay. As discussed in Appendix

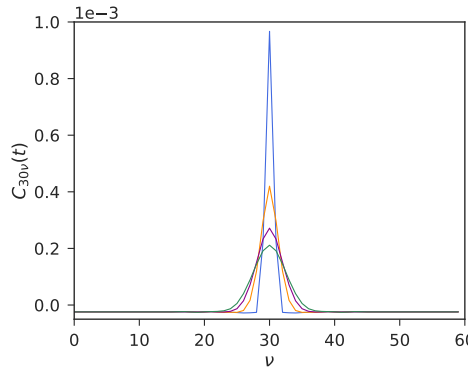


**Figure 4.3:**  $C_{\mu\nu}(t) = \langle g_\mu(t)g_\nu \rangle$  for  $\nu = 30$  as a function of node index  $\nu$  and for times  $t = 0, 0.2, 0.4, 0.6$  in descending order.

G, only in both, the continuum and thermodynamic limits, we expect the long time tail  $\propto t^{-1/2}$  behaviour predicted by continuum hydrodynamics.

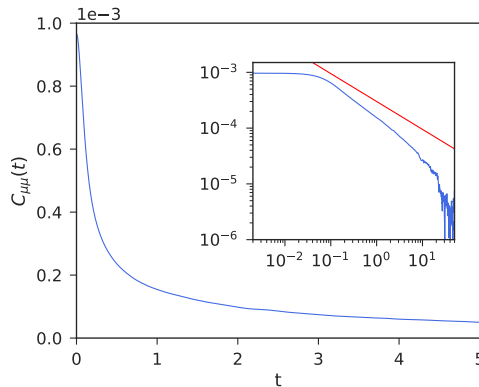


**Figure 4.4:** The autocorrelation  $\langle g_\mu(t)g_\mu \rangle$  (for any  $\mu$ ). The correlation decays very slowly, in an apparent algebraic way as can be seen in logscale in the inset.

The Fourier transform  $\tilde{C}(t)$  of the correlation matrix  $C(t)$  is a diagonal matrix. The diagonal  $\tilde{C}_{\mu\mu}(t)$  is plotted in Fig. 4.5 as a function of the mode  $\mu$  for different values of the time, from  $t = 0.10$  to  $t = 0.20$  in intervals of 0.02 in descending order. Note that the mode  $\mu = 0$  gives a vanishing value because of momentum conservation. At

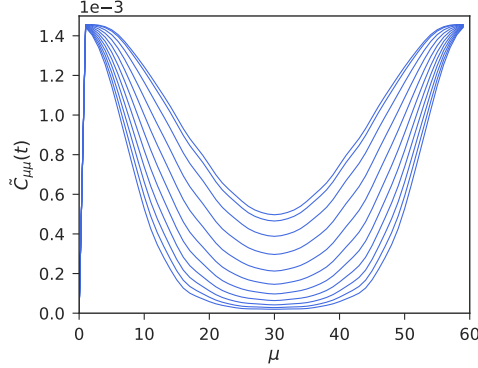


**Figure 4.5:** The diagonal  $\tilde{C}_{\mu\mu}(t)$  of the Fourier transform of the correlation matrix  $C(t)$  for different values of the time. In descending order the plotted times go from  $t = 0.10$  to  $t = 0.20$  in intervals of 0.02.

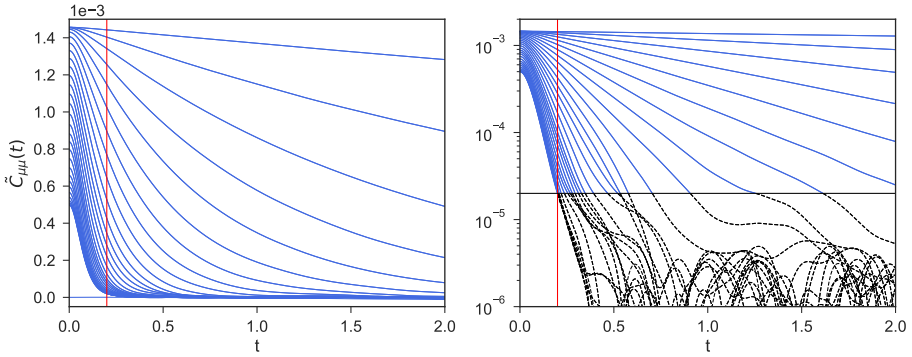


**Figure 4.6:** The evolution of the different eigenvalues  $\tilde{C}_{\mu\mu}(t)$  of the correlation matrix of momentum as a function of time in a lin-lin plot (left) and log-lin plot (right). Also plotted are a vertical line at  $t = \tau = 0.2$  and a horizontal line at the value  $2 \times 10^{-5}$ , signaling the threshold below which statistical errors give spurious results.

the largest times plotted, the value of the diagonal correlation matrix in Fourier space  $\tilde{C}_\mu(t)$  goes to zero for modes with values near  $\mu = 30$ , implying the amplification of the statistical errors in the inverse matrix in that region. In the left panel of Fig. 4.6 we plot the eigenvalues  $\tilde{C}_{\mu\mu}(t)$  as a function of time. Observe that after a time around  $\tau = 0.2$  (red line) the decay in log-lin (right panel) is approximately linear, suggesting an exponential decay. Also we have represented in black and dashed lines the values of

the eigenvalues  $\tilde{C}_{\mu\nu}$ , which statistical errors give spurious results.

### 4.5.3 Validation of the Markov property

When the Markov equation (1.60) is valid, we have that the eigenvalues of the correlation matrix decay exponentially, according to the prediction (4.63). In order to better discriminate the exponential behaviour we introduce the time-dependent matrix

$$\Lambda(t) \equiv -\frac{d}{dt} C(t) \cdot C^{-1}(t) \quad (4.74)$$

that according to the Markov equation (1.60), should evolve toward a constant time independent matrix  $\Lambda(t) \rightarrow \Lambda^*$  after certain time. In Fourier space all matrices in equation (4.74) are diagonal and, therefore

$$\tilde{\Lambda}_{\mu\mu}(t) \equiv -\frac{1}{\tilde{C}_{\mu\mu}(t)} \frac{d\tilde{C}_{\mu\mu}}{dt}(t) \quad (4.75)$$

Note that for times  $t > \tau$  we have that  $\tilde{\Lambda}_{\mu\mu}(t) \rightarrow \frac{1}{\tau_\mu}$  where the relaxation time is given in equation (4.64).

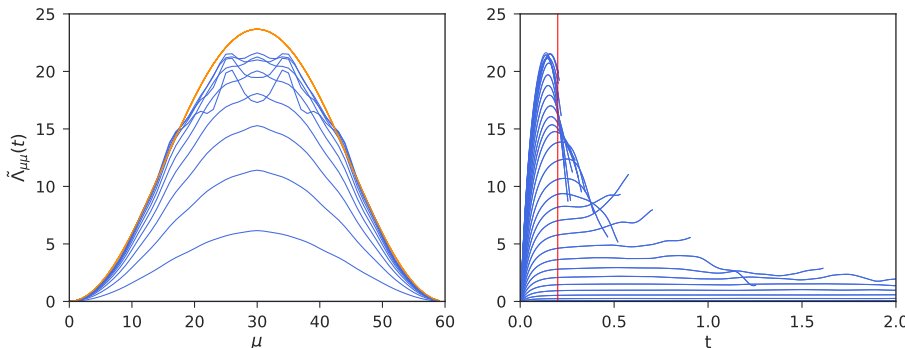


**Figure 4.7:** The diagonal elements  $\tilde{\Lambda}_{\mu\mu}(t)$  of the Fourier transform of  $\Lambda(t)$  defined in (4.74), as a function of  $\mu$  (left) and  $t$  (right). In the left panel, in ascending order the plotted times go from  $t = 0$  to  $t = 0.20$  in intervals of 0.02. The orange line is the local approximation equation (4.76) with a value of the local kinematic viscosity of  $v_0 = 1.48$ . In the right panel, we observe a clear plateau, beyond  $\tau = 0.2$  (red line) indicating the exponential behaviour of the correlations in Fig. 4.6.

In Fig. 4.7 we plot  $\tilde{\Lambda}_{\mu\mu}(t)$  as a function of  $\mu$  for different times (left) and as a function of  $t$  for the different values of  $\mu$  (right). In the left panel, the different curves correspond

to values of  $t$  from 0 to 0.20 in intervals of 0.02. The structure observed in the central region is spurious and due to statistical errors. These errors increase with time. We also plot in Fig. 4.7 the theoretical prediction of this matrix in the local approximation given in equation (4.73) for a fitted value of the local kinematic viscosity of  $\nu_0 = 1.48$ , which is the value of the kinematic viscosity for this system and thermodynamic point, as reported in the literature [117]. We observe that the local approximation (4.73) gives a fairly reasonable approximation for the converged value  $\tilde{\Lambda}^*$  of the relaxation matrix in Fourier space. In the right panel, we plot  $\tilde{\Lambda}_{\mu\mu}(t)$  for all  $\mu$  as a function of time  $t$ . We have disregarded the data points beyond times in which the statistical errors lead to meaningless results (those below the threshold in the eigenvalues in Fig 4.6). We may appreciate a very clear plateau for the modes of low  $\mu$  (large wavelengths). As the wavenumber increases, for wavenumbers  $\mu \geq 20$  the plateau disappears and this is concomitant with the appearance of great distortions that are due to the lack of statistics necessary to describe the inverse of the correlation matrix. Therefore, we cannot decide from the plots whether there is no plateau at large wavenumber or, on the contrary, there is a plateau but it is obscured by the lack of statistics. Hence, we select the time  $\tau = 0.2$  as the best compromise satisfying that  $\tilde{\Lambda}_{\mu\mu}(t)$  has attained its constant value but does not suffer from dramatic statistical errors. The existence of a plateau beyond  $\tau = 0.2$  signals to the exponential behaviour of the correlations in Fig. 4.6 beyond this time. We measure then the relaxation matrix in Fourier space through  $\tilde{\Lambda}_{\mu\mu}^* = \tilde{\Lambda}_{\mu\mu}(\tau)$ . This measured relaxation matrix is compared with its local approximation  $\tilde{\Lambda}_{\mu\mu}^{\text{loc}}$  which, from equation (4.73), is given by

$$\tilde{\Lambda}_{\mu\mu}^{\text{loc}} = \frac{2}{\Delta z^2} \left( 1 - \cos \left( \frac{2\pi\mu}{N_{\text{bin}}} \right) \right) \nu_0 \quad (4.76)$$

In Fig. 4.8 we plot  $\tilde{\Lambda}_{\mu\mu}^* = \tilde{\Lambda}_{\mu\mu}(\tau)$  for  $\tau = 0.2$  against  $\tilde{\Lambda}_{\mu\mu}^{\text{loc}}$  in (4.76) with  $\nu_0 = 1.48$ . Observe that the linear behaviour of this plot indicates that, to a very good degree, the local approximation describes well the relaxation matrix  $\Lambda^*$ . From the Fourier transform of the diagonal matrix  $\tilde{\Lambda}^*$  we may obtain the relaxation matrix  $\Lambda^*$  in real space which, by comparing (1.60) with (4.54) is given by  $\Lambda^* = \Delta v^*$ . From equation (4.66) we can now have the prediction of Mori theory for the correlation matrix  $C(t)$ . In Fig. 4.9 we compare the autocorrelation  $C_{\mu\mu}(t)$  measured in MD with the predictions of the nonlocal (orange) and local (green) theories. The arrow is at  $t = \tau$  where the three curves coincide by construction. The agreement of the three curves is excellent beyond  $\tau$ . This is best appreciated in logscale (right panel). The curving at long times, reflecting the finite size of the simulation box (see Appendix F) is captured in both theories. The inset in the left panel of Fig. 4.9 shows a zoom at short times, where one appreciates that the nonlocal theory gives a better prediction than the local prediction

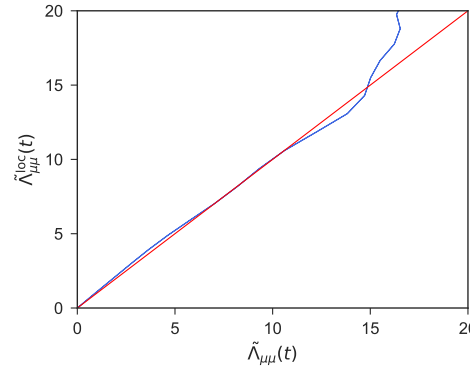


**Figure 4.8:** Comparison  $\tilde{\Lambda}_{\mu\mu}^* = \tilde{\Lambda}_{\mu\mu}(\tau)$  for  $\tau = 0.2$  with  $\tilde{\Lambda}_{\mu\mu}^{\text{loc}}$  in equation (4.76) with  $v_0 = 1.48$ . The red line has slope 1 and it is for guide the eye.

but, of course, yields poor results at very short times. Note that the Markovian theory leads to a cusp at  $t = 0$  in the correlation while the MD results have a vanishing value of the derivative of the correlation.

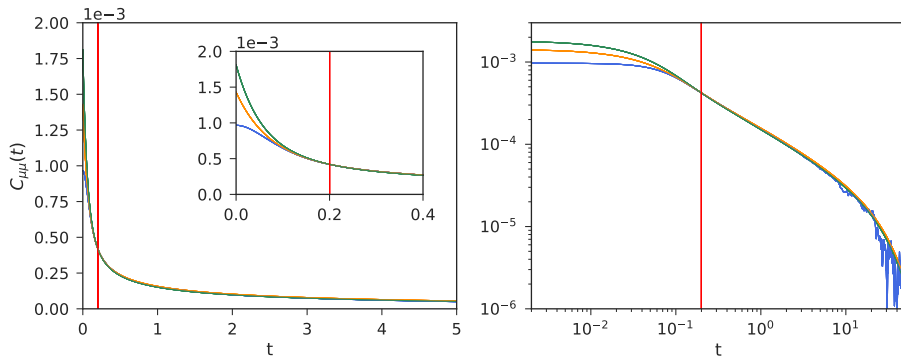


**Figure 4.9:** Comparison of autocorrelation  $C_{\mu\mu}(t)$  with the predictions of the nonlocal (orange) and local (green) theories. The left panel is in linscale and the right panel in logscale. The red line is at  $t = \tau$  where the three curves coincide by construction. The inset shows a zoom at short times.

In Fig. 4.10 we compare the cross correlation  $C_{\mu\mu+1}(t)$  in the same way as we did with the autocorrelation in Fig. 4.9. The agreement of the the three curves (predictions, nonlocal and local theories) is excellent beyond  $\tau$ .

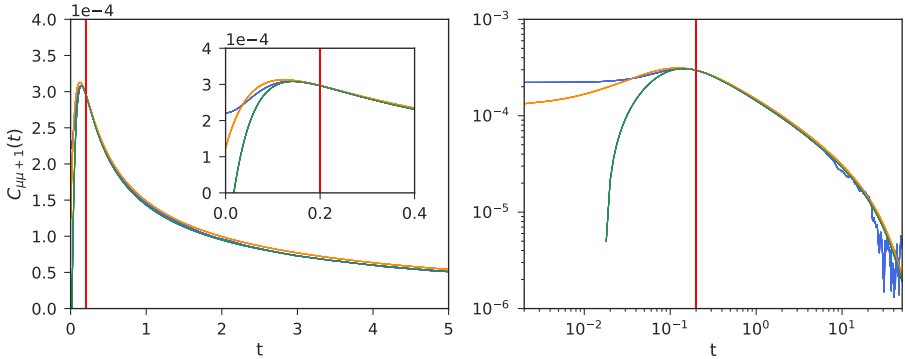


**Figure 4.10:** Comparison of cross correlation  $C_{\mu\mu+1}(t)$  with the predictions of the nonlocal (orange) and local (green) theories. The left panel is in linscale and the right panel in logscale. The red line is at  $t = \tau$  where the three curves coincide by construction. The inset shows a zoom at short times.

In summary, in the present subsection we have shown that the Markovian approximation is an excellent one for the prediction of the correlation matrix of the transverse momentum beyond a characteristic time  $\tau$ . We have also observed that, *beyond* this time  $\tau$ , a local in space approximation gives equally excellent predictions.

#### 4.5.4 The Green-Kubo nonlocal viscosity matrix

In this section, we discuss the nonlocal viscosity matrix  $\eta_{\mu\nu}(\tau)$  defined equation (4.24). To compute  $\eta_{\mu\nu}(t)$  we record the stress tensor per bin  $\hat{\sigma}_\mu$ , defined in (4.20), and compute the time integral of the equilibrium correlation  $\langle \hat{\sigma}_\mu(t) \hat{\sigma}_\nu \rangle$ . In the left panel of Fig. 4.11 we plot the nonlocal shear viscosity matrix  $\eta_{\mu\nu}(t)$  for  $\mu = 30$  and different values of  $\nu = 30 - 40$ . We observe that  $\eta_{\mu\nu}(t)$  starts from 0 at  $t = 0$  and attains a maximum at a time that increases with the separation between bins. Even though in linear scale there seem to be a plateau after the maximum, the logscale representation in the left panel of Fig. 4.11 reveals that such a plateau does not exist as a very slow algebraic decay is apparent. This result reveals strikingly that the standard Green-Kubo expression for the nonlocal viscosity has no plateau and cannot be used to define the nonlocal viscosity because there is no a priori criteria to fix the upper limit of integration  $\tau$ . Of course, from equation (4.29) we already observed that  $\eta(t)$  cannot have a plateau because the time derivative of the correlation function decays at long times. Note that the non-existence of a plateau in the nonlocal viscosity matrix  $\eta(t)$  is in clear contrast to the case of the Green-Kubo running integral for the local shear viscosity  $\eta_0(t)$  which,

according to equations (4.43) and (4.48) is proportional to the sum of all the function  $\eta_{\mu\nu}(t)$  that decay in a quasi algebraic manner.

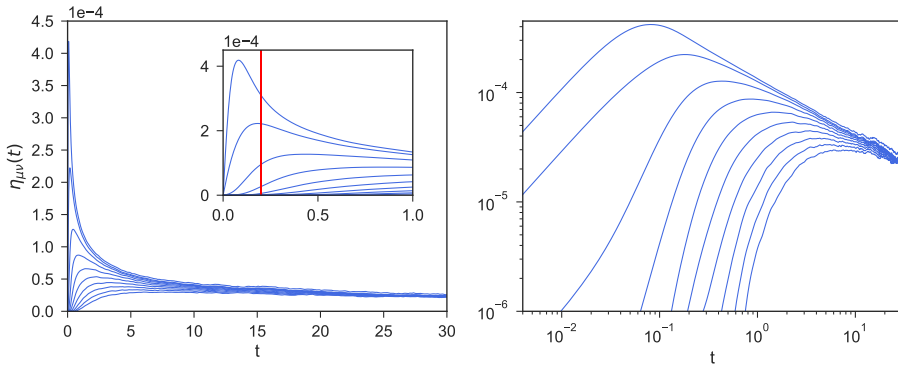


**Figure 4.11:** The nonlocal viscosity  $\eta_{\mu\nu}(t)$  as a function of time, for  $\mu = 30$  and, in descending order,  $\nu = 30 - 40$ . The left panel is in linscale, while the right panel in logscale. The inset is a zoom and the red line is at  $t = \tau$ .

In Fig. 4.12 we plot  $v_0(t)$  which we recall that is the sum of the curves in the left panel of Fig. 4.11 divided by the density. We observe a very neat plateau. Of course, the plateau cannot extend indefinitely because of the finite number of terms involved in the sum (4.43). We expect that after an estimated time of the order of  $L^2/v_0$  that takes the vorticity to diffuse the entire system size the plateau will curve down. In our system this time is  $\sim 600$ , well beyond our observation span. After this time we expect that the plateau in  $v_0(t)$  will start to decrease due to finite size effects.

We have shown in equation (4.42) how to evaluate the nonlocal shear viscosity matrix  $\tilde{\eta}_{\mu\mu}^*$  not from the standard Green-Kubo formula but rather from a corrected version of it that accounts for the fact that the Green-Kubo running integral decays as the correlation of the CG variables themselves. According to equation (4.42),  $\tilde{\eta}_{\mu\mu}^*$  should have a plateau if the Markovian approximation is appropriate.

In Fig. 4.13 we show the function  $\tilde{\eta}_{\mu\mu}^*(t)$  as a function of time for the different modes. We observe that, whenever the statistics allow for it, a reasonable plateau is obtained. Therefore, it is possible to define the nonlocal shear viscosity matrix  $\eta_{\mu\nu}^*$  in real space from the Fourier transform of the plateau value  $\tilde{\eta}_{\mu\mu}(\tau)$ . The row  $\mu = 30$  of the matrix  $\eta_{\mu\nu}^*$  is shown in Fig. (4.14). We observe that the width is about  $5\sigma$ . This is, approximately twice the cutoff distance of the LJ potential. One way to explain this width is by noting that the stress tensor of a bin, defined in (4.20) contains contributions of pairs of atoms through the fraction of the distance between the atoms. Bins which

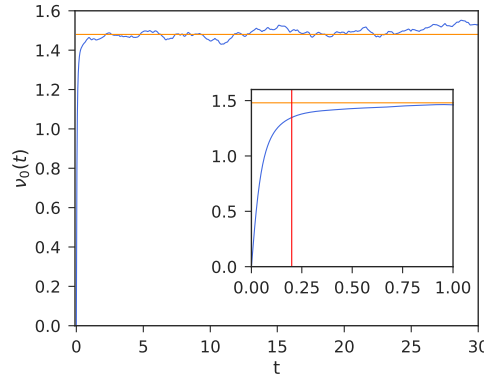


**Figure 4.12:** The local kinematic viscosity  $\nu_0(t) = \eta_0(t)/\rho^{\text{eq}}$  as a function of time where the shear viscosity is computed with the data from Fig. 4.11. A horizontal orange line at  $\nu_0 = 1.48$  from the literature [117] is also plotted in order to guide the eye in the plateau region.

are at a distance larger than twice the LJ cutoff radius do not have any atom that simultaneously contribute to the stress tensor in each bin. Therefore, it is plausible to infer that the width of the stress correlation is a consequence of the absence of correlation between the stress through atoms that contribute to the stress in both bins.

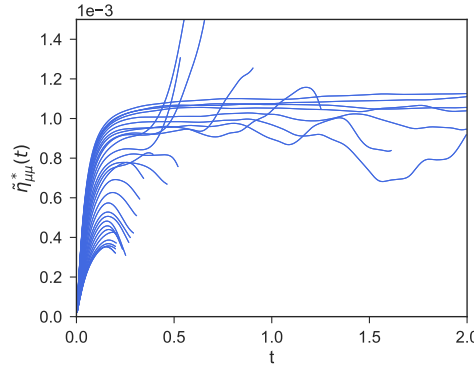


**Figure 4.13:** The eigenvalues of the nonlocal shear viscosity kernel from corrected Green-Kubo formula  $\tilde{\eta}_{\mu\mu}^* = \frac{\tilde{\eta}_{\mu\mu}(t)}{\tilde{c}_{\mu\mu}(t)}$

The kinematic viscosity in Fourier space is obtained through equation (4.56) We

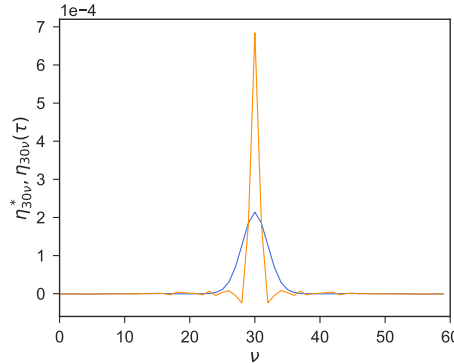


**Figure 4.14:** The row  $\mu = 30$  of the nonlocal shear viscosity matrix  $\mu_{\mu\nu}^*$  in real space obtained from the corrected Green-Kubo formula (orange). Also plot is the nonlocal shear viscosity  $\eta_{\mu\nu}$  for the Green-Kubo running integral (blue).

plot  $\tilde{v}_\mu(t)$  in Fig. (4.15) as a function of time  $t$  for different modes  $\mu$  (left) and as a function of the mode number  $\mu$  at different times from  $t = 0$  to  $t = 0.2$  in intervals of 0.01 (right). From the last plot we observe that the modes around  $\sim 30$  are subject to large statistical error because for these modes the eigenvalue  $\tilde{c}_\mu(t)$  of the correlation matrix has already taken very low values, thus amplifying through its inverse the small statistical errors present. In any case, we observe that  $\tilde{v}_\nu(t)$  is almost constant for all values of  $\mu$  and that for times larger than  $\tau = 0.2$  the kinematic viscosity of all modes is fairly constant  $\tilde{v}_\nu(\tau) \simeq v_0 = 1.48$  in reduced units. This is, another reflection of the fact that the discrete hydrodynamics in periodic boundary conditions is fairly local, and can be described with a local in space approximation, as has been corroborated in Figs. 4.9, 4.10 and 4.13.

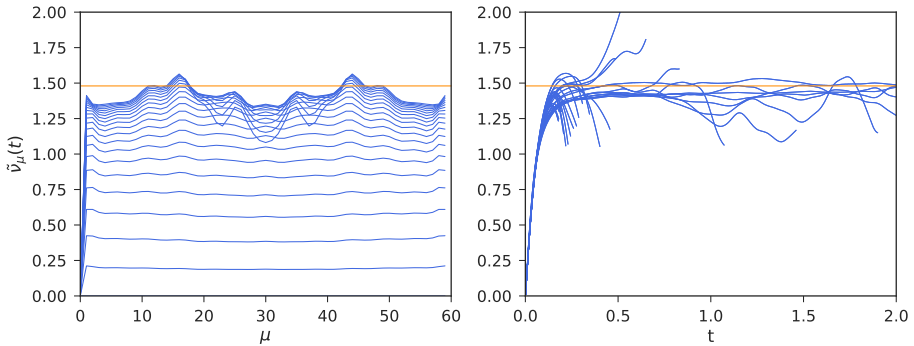


**Figure 4.15:** The eigenvalues of the nonlocal kinematic viscosity matrix as a function of time (right panel), and as a function of the mode index por times from  $t=0$  to  $t=0.2$  in ascending order in intervals of 0.01. The orange line at  $v_0 = 1.48$  is plotted in order to guide the eye in the plateau region.

## 4.6 Summary

In this chapter we have addressed the plateau problem that appears in the expression of transport coefficient in terms of the standard Green-Kubo running integrals. In the case of Markovian dynamics with not an extreme separation of time scales, the decay of the Green-Kubo running integral does not allow to determine unambiguously the value of the transport coefficients. We have shown in equation (4.8) that the Green-Kubo running integral necessarily decays to zero because it is given in terms of the correlation of the CG variables and its time derivative. With this observation, we have proposed a correction to the standard Green-Kubo expression that does has a well-defined infinite time limit.

After that we have introduced the Mori theory for discrete hydrodynamics and we have computed from MD simulations the equilibrium time-dependent correlation matrix of the discrete transverse momentum density. Under the Markovian approximation, Mori theory gives a definite prediction for the correlation matrix in terms of a decaying matrix exponential. As we have discussed, the Markovian prediction *cannot* hold for very small times, essentially because the exponential matrix decay predicts a non-zero value of the derivatives of the correlation at  $t = 0$ , while microscopic reversibility enforces a vanishing value of the derivative of the correlations at  $t = 0$ . Therefore, the initial decay of the correlation cannot be of the exponential matrix form. Only after a time  $\tau$  in which the memory has faded out one can expect a Markovian, local in time, approximation to hold. We have observed that the relaxation matrix  $\Lambda(t)$  does indeed plateau to a constant value  $\Lambda^*$ , indicating that after the time  $\tau$  the decay of

the correlation matrix is exponential and hence Markovian. At the plateau time  $\tau$  the correlation matrix has decayed already to 50% of its initial value.

The *nonlocal* shear viscosity defined in terms of the Green-Kubo formula as the time integral of the stress-stress correlation does not show a plateau. Quite remarkably, the sum of the (non-plateau) nonlocal shear viscosity matrix elements does indeed have a plateau. This plateau corresponds to the *local* viscosity computed in the usual way from its Green-Kubo formula. The existence of this plateau in the local viscosity is due to global momentum conservation. By using the nonlocal viscosity once corrected according to the method in Sec. 4.2, we observe that the predictions for the correlation matrix  $C(t)$  are quite accurate even for times smaller than the plateau time  $\tau$ . In this way, the nonlocal model describes the behaviour of the correlation matrix in real space for very small times, during the decay of the correlation from 80% its initial value on. We observe that for the times beyond  $\tau$  in which the Markovian (local in time) approximation is valid, the local in space approximation of the kinematic shear viscosity matrix gives already very accurate results. In summary, the eigenvalues of the correlation matrix decay in a strict exponential way, signaling Markovian behaviour, after a time  $\tau = 0.2$ .

One strategy to increase the validity of a purely Markovian theory for times smaller than  $\tau$  consists on including additional non-conserved variables in the list of CG variables. For example, by including the stress tensor and heat flux as additional variables, one expects to capture the viscoelastic and memory effects that are required to describe the dynamics of the conserved variables at smaller time scales [106, 118, 119].

In the present chapter we have limited ourselves to the discrete transverse momentum variable. With the same methodology, the extension to the rest of conserved hydrodynamic variables is straightforward. We have considered an unconfined simple fluid in periodic boundary conditions. In the next chapters, the same methodology used here will be used for the case of fluids confined in between parallel solid walls. The computational burden in that case is much larger because translation invariance cannot be used in order to increase statistics, as we have done in the present chapter. In addition to the nonlocal shear viscosity, new transport coefficients related to friction and slip at the wall appear in confined fluids, as has been recently described in Ref. [120] and in Chapter 3.



# Chapter 5

## Markovian behaviour near solids

*It's the things we forget about that tell us who we are.*

---

Zero K  
DON DELILLO

### 5.1 Introduction

In Chapter 4 we have demonstrated through MD simulations that the Markovian assumption is valid for the description of correlations of the discrete transverse momentum *beyond* certain time. We have shown that beyond this time, hydrodynamics is essentially local in time *and* space. In this chapter we follow the same strategy as for unconfined fluids in order to study the Markovian behaviour of a fluid in between two solid slabs.

As we mentioned in the Introduction, at nanoscopic scales, a fluid starts displaying its molecular structure in phenomena like the wall ordering. In addition, slip of the fluid at the walls becomes noticeable. The usual local hydrodynamic description with local transport coefficients and no slip boundary conditions needs to be adequately modified in order to address the peculiar fluid behaviour at nanoscales.

We have presented in Chapter 2 a derivation of the equations of hydrodynamics in the presence of solid walls that govern the averages of the mass and momentum density fields. A crucial feature of this theory is that the effect of the walls on the fluid is not

through boundary conditions but rather through forces confined to the vicinity of the solid wall. In a recent work, Camargo et al. [84] show how boundary conditions can be derived when the flows are of macroscopic character. The theory gives the usual Navier slip boundary condition with microscopically defined parameters that coincide with those of Bocquet and Barrat [2].

The only crucial assumption made in the formulation of the theory in Chapter 2 is that the dynamics is Markovian, this is, that the hydrodynamic equations do not have integral memory terms. It is, therefore, important to test through MD simulations that the Markovian approximation is correct. Comparison with MD simulation require the introduction of discrete equations. To achieve this goal, we have proposed in Chapter 3 a discrete hydrodynamic theory for planar flows near solid walls that can be understood as a finite element discretization of the continuum theory presented in Chapter 2. The size of the bins enter the discrete theory as an intrinsic length scale. The forces on fluid elements are due to the effect of nonlocal stress tensor and nonlocal surface forces due to the walls.

In the theory presented in Chapter 2, based on the projection operator technique, the Markovian approximation produces formal expressions in terms of Green-Kubo formulas for the transport coefficients. However, these expressions are formal for two reasons. First they involve the so called projected dynamics which is uncomputable from MD simulations. The usual step of substituting the projected dynamics by the real Hamiltonian dynamics is not entirely justified. The second problem is that the Green-Kubo formulas suffer from the plateau problem [70, 115]. In Sec. 4.2 we have presented a new corrected Green-Kubo expression for transport coefficients that does not suffer from the plateau problem.

The theory presented in Chapter 2 describes the evolution of nonequilibrium ensemble averages and it is based on the Kawasaki-Gunton projector [52]. It is nonlinear and involves the free energy functional familiar from DFT. For the case of the transverse momentum, the Kawasaki-Gunton projector gives a very simple linear equation that does not involve the free energy functional. A very similar linear equation can be obtained in an alternative way from the simpler Mori theory, that always produces linear equations. In order to address the plateau problem it proves very convenient to have a theory not only for averages but also for time correlation functions and both are provided in Mori theory.

## 5.2 The CG variables and its dynamics

We consider a LJ fluid system confined in between two parallel solid walls made of LJ particles fixed in a simple cubic lattice. The walls are along the directions  $x, y$ . Because

of traslational invariance along the walls, we bin the vertical direction  $z$  in layers parallel to the planar walls. The box length  $L_z$  is divided in  $N_{\text{bin}}$  bins labelled with an index  $\mu$ . The bins are separated by  $N_{\text{bin}}$  nodes (actually, nodal planes) located at  $z_\mu = \mu\Delta z$ ,  $\mu = 0, \dots, N_{\text{bin}} - 1$ , with  $\Delta z = L_z/N_{\text{bin}}$ . We assume that we have periodic boundary conditions in the  $z$  direction, albeit due to the solid walls the fluid will never cross the periodic boundary nor interact with itself through the boundary conditions as the width of the walls is larger than the cutoff of the interaction potential. The node  $\mu = 0$  is equal to the node  $N_{\text{bin}}$ .

In this chapter, we use as the only CG variable relevant to the problem the parallel component  $\hat{g}_\mu = \mathbf{g}_\mu^x$  of the momentum density field defined microscopically as

$$\hat{\mathbf{g}}_\mu = \sum_i \mathbf{p}_i \delta_\mu(\mathbf{q}_i), \quad (5.1)$$

where  $\delta$  is the discrete Dirac  $\delta$  function defined in (3.19).

We have checked that the correlations  $\langle \hat{\mathbf{g}}_\mu^x(t) \hat{\mathbf{g}}_\nu^z \rangle$ ,  $\langle \hat{\mathbf{g}}_\mu^x(t) \hat{\rho}_\nu \rangle$  are vanishingly small, corroborating the predictions of the theory. Therefore, as far as shear motion of the fluid is concerned, a level of description given by the parallel component  $\hat{\mathbf{g}}_\mu^z$  should be sufficient. We will consider elsewhere the more general situation that allows one to study compression of the fluid in the direction normal to the walls.

We will collect the CG variables into an  $N_{\text{bin}}$ -dimensional column vector  $\hat{\mathbf{g}}$  that contains as components the parallel component of the momentum density of bin  $\mu$ , this is  $\hat{\mathbf{g}}^T = (\hat{\mathbf{g}}_1^x, \dots, \hat{\mathbf{g}}_{N_{\text{bin}}}^x)$ , where the superscript  $T$  denotes the transpose. The central quantity in this chapter is the equilibrium time correlation matrix  $C(t)$  of the CG variables given by

$$C(t) = \langle \hat{\mathbf{g}}(t) \hat{\mathbf{g}}^T \rangle \quad (5.2)$$

According to Mori theory the correlation matrix decays in a linear way,

$$\frac{d}{dt} C(t) = -\Lambda^* \cdot C(t), \quad (5.3)$$

where the relaxation matrix  $\Lambda^*$  is a constant  $N_{\text{bin}} \times N_{\text{bin}}$  matrix. The relaxation matrix subsumes all the transport coefficients of the system. As shown in Chapter 4, the relaxation matrix can be decomposed into a nonlocal viscosity contribution and nonlocal friction contributions, all defined through Green-Kubo expressions, suitably corrected with the method given in Sec. 4.2. As discussed in Chapter 4 a Markovian equation like (5.3) is expected to hold only after a time  $\tau$  has elapsed. The reason is that from the time reversal properties of the CG variables we know that the time derivative of the

correlation matrix at  $t = 0$  vanishes, but equation (5.3) would imply at  $t = 0$  the absurd result  $0 = -\Lambda^* \cdot C(0)$ .

The Markovian relaxation equation (5.3) predicts the following evolution equation for correlation matrix

$$C^{\text{predict}}(t) = \exp\{-\Lambda^*(t-\tau)\}C(\tau), \quad (5.4)$$

where we have introduced the matrix exponential through its Taylor series and have taken into account that equation (5.3) can only be valid after a time  $\tau$ . The elements of the matrix exponential do not need to decay as exponential functions. As we will see, in fact, the decay is quasi-algebraic.

In order to have an easier identification of whether the evolution of the matrix exponential is described by the Markovian equation (5.3) it proves convenient to diagonalize the correlation matrix. We introduce eigenvalues  $\tilde{C}_\mu$  and eigenvectors  $u_\mu$  in such a way that the correlation matrix is given by the spectral decomposition

$$C(t) = \sum_{\mu}^{N_{\text{bin}}} \tilde{C}_\mu(t) u_\mu(t) \otimes u_\mu^T(t) \quad (5.5)$$

The unitary matrix  $E(t)$  that has as columns the eigenvectors allows to diagonalize the correlation matrix, this is

$$E^{-1}(t) \cdot C(t) \cdot E(t) = \tilde{C}(t), \quad (5.6)$$

where  $\tilde{C}(t) = \text{Diag}[\tilde{C}_1(t), \dots, \tilde{C}_{N_{\text{bin}}}(t)]$  is a diagonal matrix containing the eigenvalues in the diagonal. If the system was translation invariant in the  $z$  dimension, the matrix  $E(t)$  would be given by the time-independent discrete Fourier transform, as discussed in Sec. 4.3.4. In the present problem, where the solid walls break translation invariance, the unitary matrix  $E(t)$  is time dependent. As a consequence, the diagonal matrix  $\tilde{C}(t)$  evolves according to

$$\frac{d}{dt} \tilde{C}(t) = -\tilde{\Lambda}^* \cdot \tilde{C}(t) + \frac{d}{dt} (E^{-1}(t)) \cdot C(t) \cdot E(t) + E(t) \cdot C(t) \cdot \frac{d}{dt} E(t) \quad (5.7)$$

We have observed that the time dependence of the unitary matrix is very weak,  $\dot{E} \approx 0$  and allows one to approximate equation (5.7) as

$$\frac{d}{dt} \tilde{C}(t) \approx -\tilde{\Lambda}^* \cdot \tilde{C}(t), \quad (5.8)$$

where, consistently, the matrix  $\tilde{\Lambda}^*$  has small off-diagonal elements. Therefore, we arrive at the conclusion that the eigenvalues  $\tilde{c}_\mu(t)$  of the correlation matrix evolve according to a single exponential

$$\tilde{C}_\mu(t) = \exp\{-\tilde{\Lambda}_{\mu\mu}(t-\tau)\}\tilde{C}_\mu(\tau), \quad (5.9)$$

where we have taken into account that the Markovian approximation is valid only after the time  $\tau$ . The exponential decay is one signature of the validity of the Markovian equation (5.3). Another signature of the validity is obtained from each component of (5.8) that shows that the function defined as

$$\tilde{\Lambda}_\mu(t) \equiv -\frac{1}{\tilde{C}_\mu(t)} \frac{d\tilde{C}_\mu}{dt}(t) \quad (5.10)$$

should, after a time  $\tau$ , reach the constant plateau value  $\tilde{\Lambda}_{\mu\mu}^*$ . Note that the eigenvalues should decay exponentially and, therefore,  $\tilde{\Lambda}_\mu(t)$  in (5.10) is the product of an exponentially decaying function and an exponentially exploding function. This means that we need high quality statistics in order to have sensible values for  $\tilde{\Lambda}_\mu(t)$ . We also realize that no matter how good our statistics is, we will always encounter sufficiently large times where the exponential amplification of statistical errors render the function  $\tilde{\Lambda}_\mu(t)$  meaningless.

## 5.3 Simulations

The objective of this section is to present the simulations conducted to measure the matrix of correlations  $C(t)$  in order to validate the Markovian approximation of a confined fluid. We follow the strategy presented in Sec. 4.5. Because translational invariance is broken in a confined fluid, we use the eigenvector basis of  $C(t)$ , which is not given in this case by the Fourier basis. We deal with a system in which the space occupied by the fluid is exactly the same as in the case of an unconfined fluid. In the first part of this section the fluid region is divided in bins in which  $\Delta z$  is the same as the used in Chapter 4. In the second part, the width of the bins is twice large.

### 5.3.1 Simulation set up

A system of particles interacting with a LJ potential truncated at  $\sigma = 2.5$  has been simulated with the open source code LAMMPS code [116]. The box size is  $40 \times 40 \times 33$ , the number of fluid particles is  $N = 28175$  and the timestep is 0.002 in reduced units. Periodic boundary conditions are assumed in all directions. Two solid walls in the  $xy$

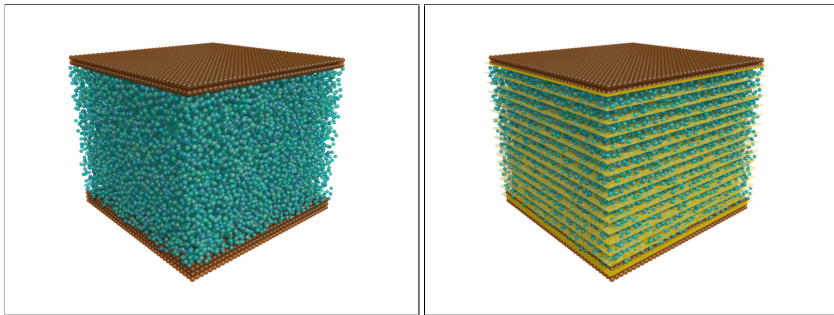


**Figure 5.1:** A visual representation of the MD simulation (left) and the same with a sketch of the binning used in yellow (right).

plane confine the fluid as is shown in Fig. 5.1. The bottom wall is made of two layers of LJ particles located in a simple cubic lattice with lattice spacing  $\sigma$ . The top wall is made of two layers of LJ particles in a similar cubic lattice. The location of the four crystalline planes are  $z = 0, 1, 31, 32$  in LJ units. Due to PBC, the distance between the layers of solid particles which are in contact with the fluid is  $3\sigma$  beyond the cutoff of the LJ potential. Therefore, the fluid particles occupy a space of  $30\sigma$  and do not interact with the periodic images in the vertical direction. Note that the space occupied by the fluid is equal to the case exposed in the previous chapter, in which the fluid is unconfined.

After an equilibration of  $10^5$  timesteps with a Langevin thermostat to produce a microstate typical from a thermodynamic point corresponding to  $T = 2, \rho = 0.6$  in reduced units, the system is evolved under NVE microcanonical conditions for a further  $10^5$  timesteps. After this equilibration phase, production runs of  $12 \times 10^6$  time steps are launched and the  $x$  component of the discrete momentum density is recorded every 2 timesteps. In order to increase statistics, we average the result of 18 simulations.

### 5.3.2 Thin bins with $\Delta z = 0.5\sigma$

The  $z$  axis is binned in 66 bins of width of half the molecular size,  $\Delta z = 0.5\sigma$ . The correlation matrix of the transverse momentum of different bins is computed, requiring a total of  $66 \times 66$  time correlations functions in each simulation. The support of the correlation matrix is extended only up to a time of  $t = 2$  in reduced units, which is sufficient to measure the relaxation matrix  $\Lambda(t)$ . A few selected elements of the correlation matrix are computed with a very long support of  $t = 30$  in reduced units, in order to test the predictions of the theory at long times.

The time correlation matrix is shown in Fig. 5.2 at two different times,  $t = 0$  and  $t = 0.6$  in reduced LJ units. For the covariance, at  $t = 0$ , we can observe the reminiscence of the density layering near the wall in the form of peaks. As time proceeds, the diagonal of the correlation widens and decreases in height. Nodes  $\mu = 0, 1, 63, 64, 65$  contain no fluid, while node  $\mu = 2, 62$  have a very small, but not negligible contribution from the fluid. This means that out of the  $66 \times 66$  correlation matrix, we strip off a band of zeros, leaving a matrix of  $61 \times 61$  nonzero elements.

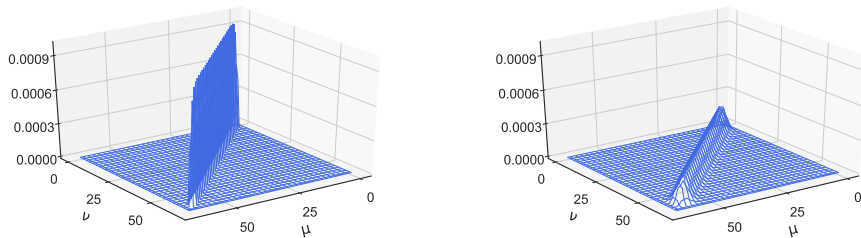


**Figure 5.2:** The correlation matrix  $C_{\mu\nu}(t) = \langle g_\mu(t)g_\nu \rangle$  for  $t = 0$  (left) and  $t = 0.6$  (right).

Next, we consider the time-dependent eigenvalues  $\tilde{C}_\mu(t)$  of the correlation matrix  $C(t)$ . The eigenvector basis depends slightly in time. We have checked that by using the matrix  $E(t)$  at the fixed times  $t = 0.15, 0.30$  instead of the time-dependent matrix  $E(t)$  in (5.6), the correlation matrix  $C(t)$  essentially diagonalizes with the same eigenvalues, therefore validating the approximation (5.8). This can be seen in Fig. 5.3, where it plotted for clarity only 15 elements of the diagonal of the matrix  $\tilde{\Lambda}(t)$  in three different basis:  $E(0.15)$ ,  $E(0.30)$  and  $E(t)$ .

We plot in Fig. 5.4 all the 61 nonzero eigenvalues, in descending order, as a function of time. Statistical errors are manifest in the log-lin plot, in spite of the overall high-quality statistics. Also clear from the log-lin plot is the linear decay of the eigenvalues beyond a certain time, signaled by the vertical red line located at  $\tau = 0.2$ . Note that at  $t = 0$  the correlation matrix has zero time derivative due to time reversal invariance, and this reflects in the parabolic, not exponential, initial decay of the eigenvalues. In Fig. 5.5 we show the function  $\tilde{\Lambda}_\mu(t)$  defined in (5.10). We only plot this function for the data where the eigenvalues  $\tilde{C}_\mu(t) > 2 \times 10^{-5}$ , which is the horizontal line plotted in the right panel in Fig. 5.4. Below this value, which is two order of magnitude smaller than the value at  $t = 0$ , the statistical errors in the inverse matrix blow up exponentially, and lead to an inverse that varies erratically and is not reliable. With this cutoff, a very nice plateau is observed for the lower modes, reflecting the exponential decay of the eigenvalues as shown in Fig. (5.5).

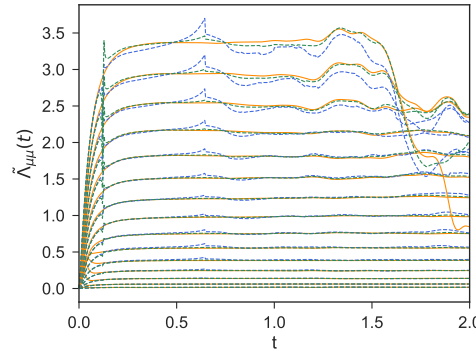


**Figure 5.3:** The diagonal elements  $\tilde{\Lambda}_{\mu\mu}(t)$  of the  $\Lambda(t)$  in three basis:  $E(0.15)$  (dashed blue lines),  $E(0.30)$  (dashed green lines) and  $E(t)$  (solid orange lines).

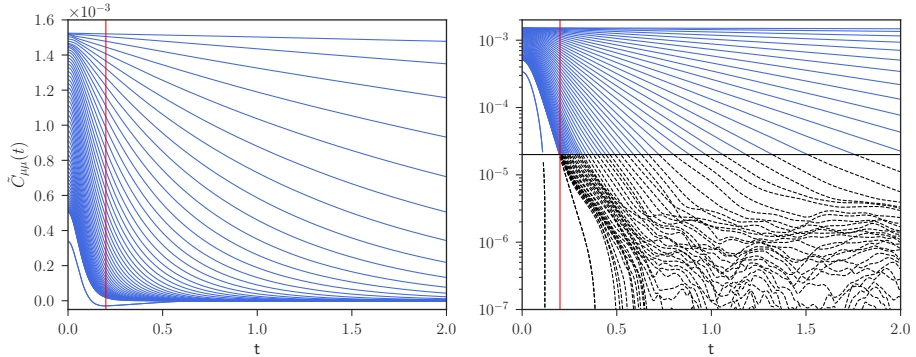


**Figure 5.4:** The evolution of the different eigenvalues  $\tilde{C}_{\mu\mu}(t)$  of the correlation matrix of momentum as a function of time in a lin-lin plot (left) and log-lin plot (right). Also plotted are a vertical line at  $t = \tau = 0.2$  and a horizontal line at the value  $2 \times 10^{-5}$ , signaling the threshold below which statistical errors give spurious results.

One interesting feature of the spectrum of the correlation matrix shown in Fig. 5.4 are the smallest two eigenvalues corresponding to  $\mu = 59, 60$  that are clearly separated from the rest. This eigenvalues are plotted in isolation for clarity in the left panel of Fig. 5.6. Note that these eigenvalues have a distinct negative tail. This implies that these modes do not decay in an exponential way at all. The corresponding eigenvectors are shown in the right panel of Fig. 5.6. Note that these eigenvectors are localised

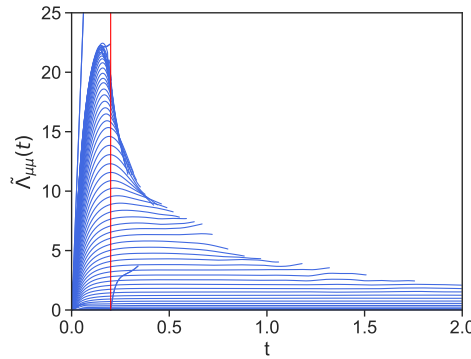


**Figure 5.5:** The diagonal elements  $\tilde{\Lambda}_{\mu\mu}(t)$  of the  $\Lambda(t)$  in the reciprocal space defined in (5.10), as a function of  $t$ .

near the walls and, therefore, the contribution of this eigenvectors into the spectral decomposition (5.5) boils down to a sort of bounce-back effect of the fluid in the direction parallel to the walls.

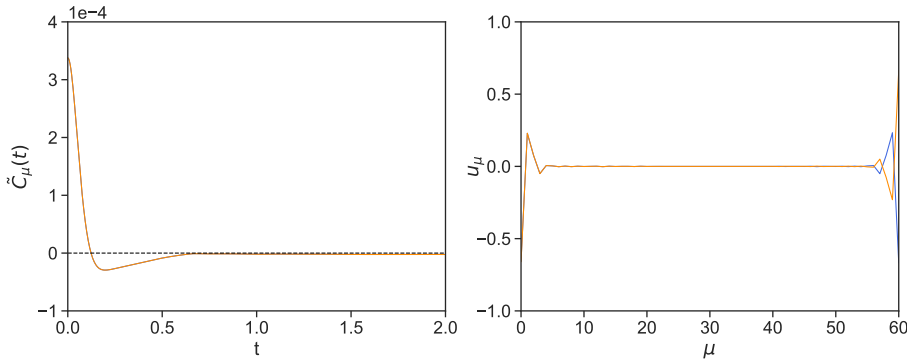


**Figure 5.6:** The eigenvalues  $\tilde{C}_\mu(t)$  of the correlation matrix  $C(t)$  for  $\mu = 59, 60$  which are identical and superimpose (left) and the corresponding eigenvectors  $u_\mu$  in blue and orange, respectively (right).

The fact that there are eigenvalues that decay in a non-exponential way indicates that the dynamics is non-Markovian, at least near the walls. The non-Markovian effects could be small, however, as only one eigenvalue is clearly non-exponential. In order to appreciate the actual effect of this non-Markovian contribution to the correlation matrix

in real space, we define the relaxation matrix in Fourier space as  $\tilde{\Lambda}^* = \tilde{\Lambda}(\tau)$  for  $\tau = 0.2$ . As appreciated in Fig. 5.5, this time  $\tau$  seems to be a compromise for the minimum time at which almost all the elements  $\tilde{\Lambda}_\mu(t)$  have reached the plateau and yet the statistical errors due to the inverse of the eigenvalues have not exploded. From  $\tilde{\Lambda}^*$  we construct the relaxation matrix  $\Lambda^*$  in real space and, from equation (5.4), we obtain the prediction  $C^{\text{predict}}(t)$  of the correlation matrix. We plot in Fig. 5.7 the comparison of the measured and the predicted correlation matrix for particular elements  $C_{\mu\mu}(t)$  of the matrix along the diagonal. In particular, we choose  $\mu = 33$  which is in the middle of the channel and  $\mu = 2, 3$  which are the two bins closer to the walls that have already fluid in it (bins  $\mu = 0, 1$  do not contain fluid particles due to the presence of the wall). In the top panel of Fig. 5.7 are the results for the autocorrelation in the middle of the channel. The inset is a zoom at short times. The right plot, in logscale, has a support up to  $t = 30$ . The agreement between predicted and measured correlations is excellent in the middle of the channel. The middle and bottom panels in Fig. 5.7 describing the comparison near the solid wall, however, show noticeable discrepancies. Very close to the wall, for  $\mu = 2$  the measured correlation displays a bump, better noticed in the logscale plot, that probably reflects the “bounce-back” contribution of the eigenvalues  $\mu = 59, 60$  in the correlation matrix (5.5). The measured autocorrelation remains positive, though, while the predicted correlation becomes negative. Therefore, we conclude that the measured relaxation matrix  $\Lambda^*$  does not allow to predict through (5.3) the correct momentum correlations near the wall. This is a clear sign that the dynamics near the wall is not Markovian.

### 5.3.3 Thick bins with $\Delta z = 2\sigma$

In order to assess the effect of the bin width on the Markovian character of the dynamics of the discrete momentum variable, we have conducted simulations of the same system but with 33 nodal planes, giving bins of a size  $\Delta z = \sigma$ , and with 17 nodal planes giving a bin width of  $\Delta z = 2\sigma$ . The phenomenology for 33 nodes is very similar to the one for 66 nodes. We still observe negative eigenvalues and non-Markovian behaviour, although the effects are not so pronounced as for 66 nodes. For this reason, we do not present the results for 33 nodes and present only the results for 17 nodes.

In Fig. 5.8 (left panel) the time dependent eigenvalues  $\tilde{C}_\mu(t)$  of the  $17 \times 17$  correlation matrix are plotted as a function of time. In the right panel, the logscale plot shows a fairly linear decay, signaling exponential behaviour. This is more clearly seen in Fig. 5.9, where the function  $\tilde{\Lambda}_\mu(t)$  defined in (5.10) displays a plateau. Note that two eigenvalues are clearly separated from the rest. These eigenvalues correspond to the two eigenvectors shown in Fig. 5.10 that clearly correspond to the dynamics near the walls. It is apparent that the friction with the walls has a strong damping effect on the fluid near

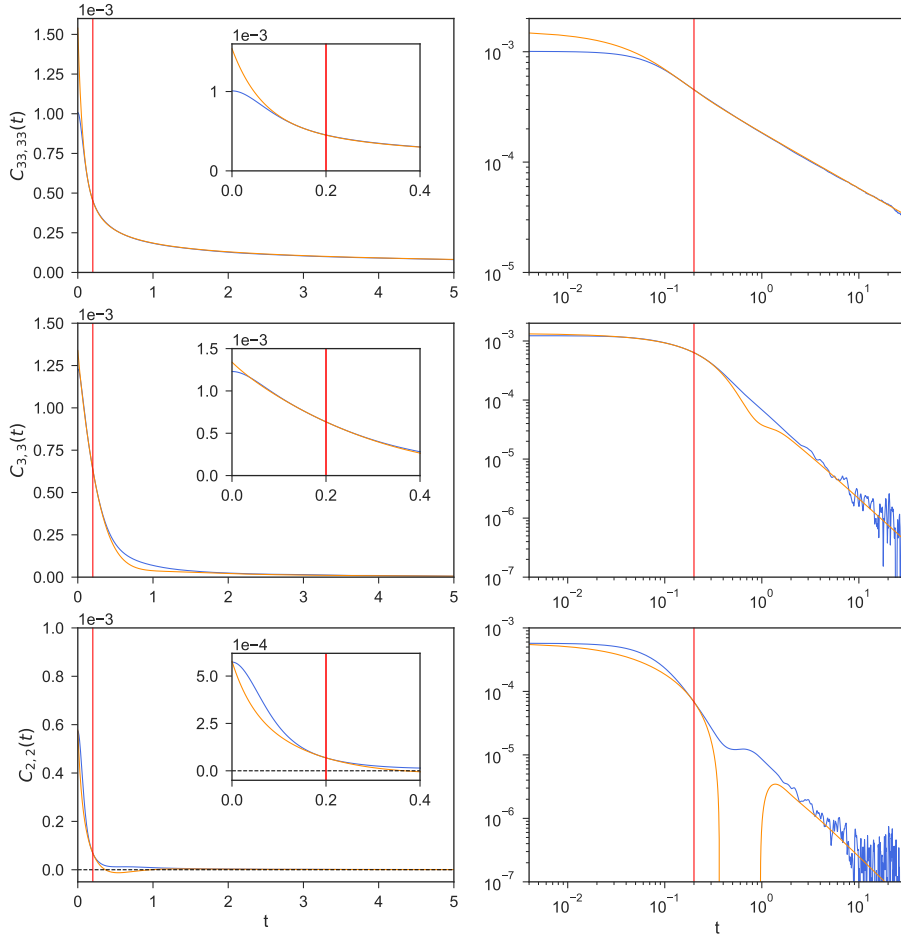


**Figure 5.7:** The predicted (orange) and the measured (blue) values of the autocorrelation  $C_{\mu\mu}(t)$  at different values of  $\mu$  (top  $\mu = 33$ , middle  $\mu = 3$  and bottom  $\mu = 2$ ). The predicted and measured correlations coincide by construction at  $t = \tau = 0.2$ , where the vertical red line is. The inset shows a zoom at short times. The right panel is the same in logscale, where the correlations extends up to time  $t = 30$ .

the wall. From Fig. 5.9 we select the plateau time  $\tau = 0.3$ . This time is larger than the one selected for thinner bins because now the statistical errors are not so pronounced. We measure the relaxation matrix  $\Lambda^*$  as the Fourier transform of the diagonal matrix

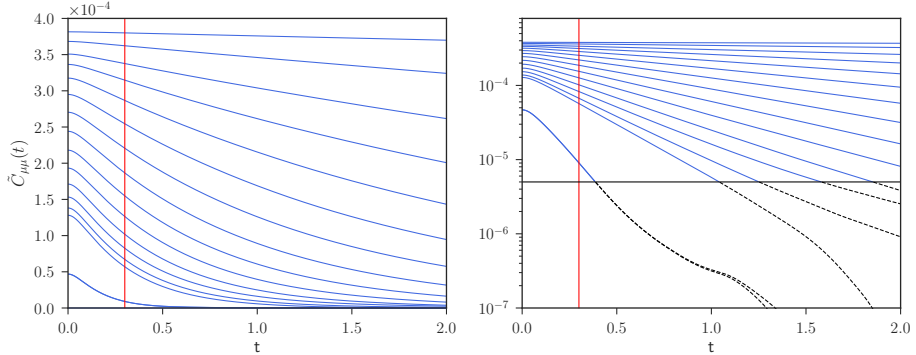


**Figure 5.8:** The evolution of the different eigenvalues  $\tilde{C}_{\mu\mu}(t)$  of the correlation matrix of momentum as a function of time in a lin-lin plot (left) and log-lin plot (right). Also plotted are a vertical line at  $t = \tau = 0.3$  and a horizontal line at the value  $5 \times 10^{-6}$ , signaling the threshold below which statistical errors give spurious results.

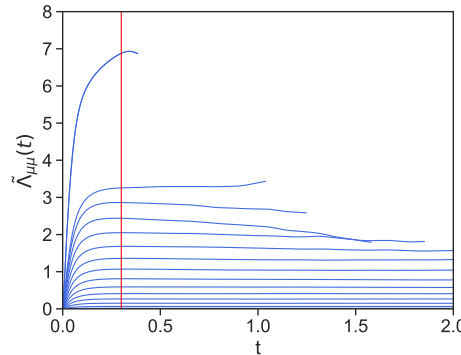


**Figure 5.9:** The diagonal elements  $\tilde{\Lambda}_{\mu\mu}(t)$  of the  $\Lambda(t)$  in the reciprocal space defined in (5.10), as a function of  $t$ .

$\tilde{\Lambda}_\mu^*(\tau)$ . In this way, we can now construct the prediction (5.4) for the correlation matrix  $C(t)$  in real space. We plot in Fig. 5.11 some selected autocorrelations corresponding to bins  $\mu = 7$  in the middle of the channel,  $\mu = 4$  which is a quarter distance from the wall, and  $\mu = 1$  the first bin with fluid (bin  $\mu = 0$  has no fluid contribution). We observe an excellent agreement between the predicted and measured correlations. This agreement is also very good for the cross-correlations, as shown in Fig. 5.12. Note that

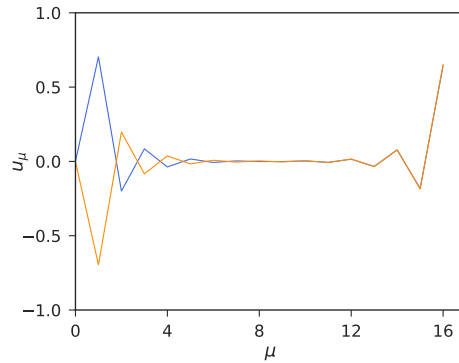


**Figure 5.10:** The eigenvectors correspondings to the two largest eigenvalues of  $\Lambda(t)$

the cross-correlation  $C_{8,7}(t)$  is non-zero at  $t = 0$  because the momentum at a given node is defined in terms of a finite element basis function. For neighbouring nodes, the finite element basis overlap and this gives rise to the non-zero value of the cross correlation. On the other hand, for nodes separated by two units, where the finite elements no longer overlap, the cross correlation at  $t = 0$  vanishes, as it is clear for  $C_{3,5}(t)$ .

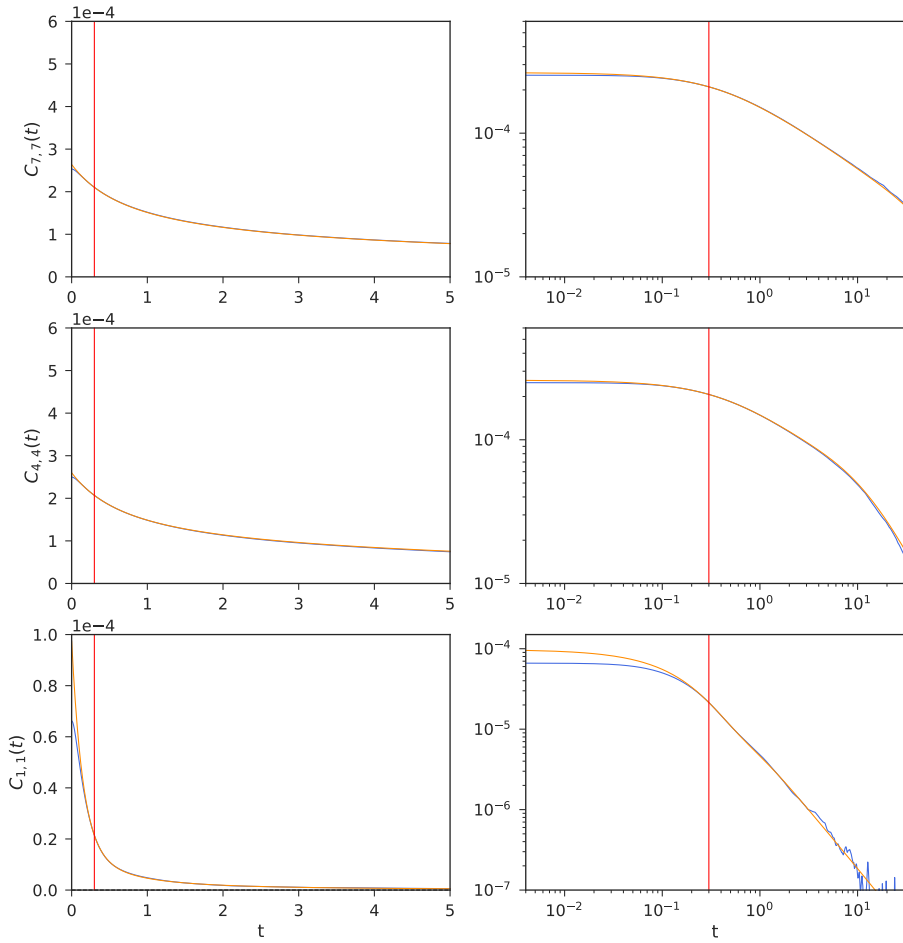


**Figure 5.11:** Autocorrelations  $C_{\mu\mu}(t)$  for different bins  $\mu = 1$  (bottom),  $\mu = 4$  (middle), and  $\mu = 7$  (top). The right panel is in logscale with a support up to  $t = 30$ . The red line is plot at  $t = 0.3$

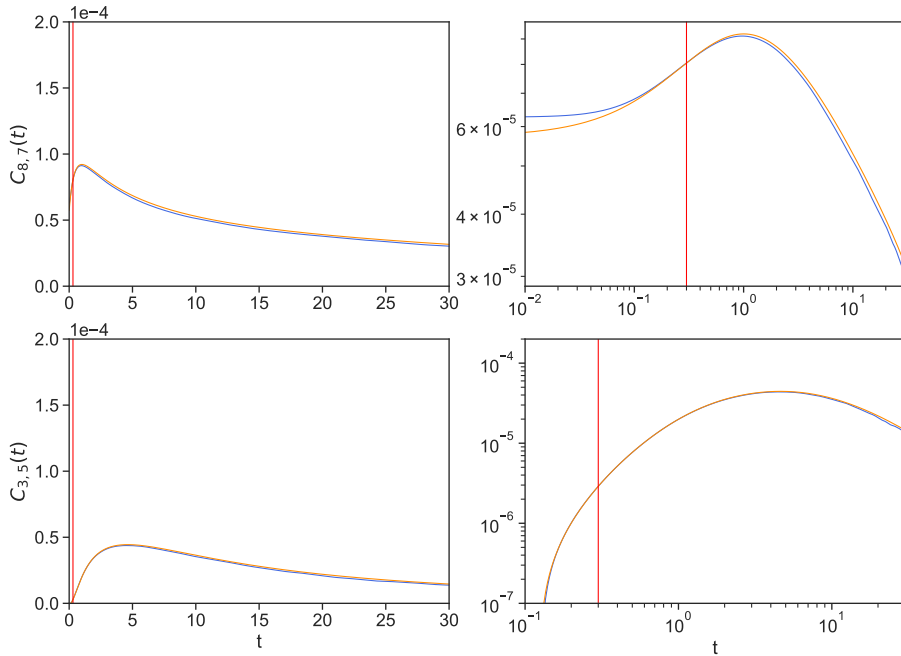


**Figure 5.12:** The crosscorrelations between nodes  $\mu = 3, \nu = 5$  (bottom) and  $\mu = 8, \nu = 7$  (top). The right panel is in logscale, and the red line is plot at  $t = 0.3$ .

## 5.4 Summary

In this chapter we have considered the discrete hydrodynamics of a LJ fluid confined between two rigid parallel walls of fixed LJ particles. We measure the correlation matrix  $C(t)$  of the component parallel to the wall of the discrete momentum density. According to Mori theory, under the Markovian approximation this correlation should decay in a matrix exponential form with a relaxation matrix  $\Lambda^*$  that can be obtained from the plateau region where the decay of  $C(t)$  is exponential. By looking at the eigenvalues  $\tilde{C}_\mu(t)$  of the correlation matrix, the Markov property translates into an exponential decay of all the eigenvalues. We have observed that for bins smaller than molecular dimensions  $\Delta z \leq \sigma$ , where  $\sigma$  is the LJ diameter, some of the eigenvalues do not decay as an exponential and become negative. Even though we can estimate a relaxation matrix from the plateau that gives good predictions away from the wall, the

correlations near the walls are poorly described by the Markovian theory.

When we increase the size of the bins, up to  $\Delta z = 2\sigma$ , a Markovian theory gives excellent results, where all the eigenvalues of the correlation function decay exponentially, a well-defined relaxation matrix  $\Lambda^*$  can be measured, and the resulting predictions with this relaxation matrix reproduce very well the measured correlation matrix.

The present chapter follows the methodology of Chapter 4 where we have discussed the correlation matrix of the discrete momentum parallel to the bins in an *unconfined* system with periodic boundary conditions. We have observed there that the correlation matrix for the discrete momentum defined in thin bins of size  $\Delta z = 0.5\sigma$  behaves in a Markovian way. Of course, this behaviour is observed only beyond certain time  $\tau$ , as observed also in the present chapter. It is clear that the breaking of the Markov assumption for thin bins is due to the presence of the walls, which is consistent with the observation that the eigenvectors of the non-Markov eigenvalues are different from zero only near the walls. The physics behind this non-Markov behaviour for thin bins is not entirely clear but we note that for thin bins, we are resolving scales that are comparable to the “roughness” of the lattice of the walls. Therefore, it is plausible that the bump in the autocorrelation of the bin close to the lattice shown in the bottom panel of Fig. 5.7 is due to a “caging effect” of the fluid particles due to the lattice. Such a caging would be undetectable for much wider bins, as it appears to be the case.

In the present chapter, we have only discussed the dynamics of transverse momentum. With the same methodology, we can discuss the coupled dynamics of the density and the normal component of the momentum. It is not yet clear to us whether the highly resolved hydrodynamics near the wall, that reproduce the density layering as shown in Fig. 5.13 is Markovian or not. In any case, we expect that the study of perpendicular sound waves confined in between parallel walls deserves further study.

The fact that hydrodynamics near walls is non-Markovian at highly resolved scales has a number of implications. For example, in Chapter 2 the delta function introduced in the hydrodynamic fields can not be a Dirac  $\delta$  functions. The continuum theory described in Chapter 2 can only make sense if the hydrodynamic fields are defined not with the Dirac  $\delta$  function, but rather with coarse delta functions with an intrinsic length scale larger than molecular dimensions as, for example a normalized Gaussian of width  $\sigma$ . As a consequence, the free energy functional that emerges from such a coarsely defined density field is not directly given by the usual free energy density in equilibrium Density Functional Theory, which is, in fact, the one particle distribution function. In fact, a local model for the free energy is expected for the former. The resulting free energy functional for coarsely defined density cannot resolve the density layering near walls. It is obvious now that in order to describe the resolved dynamics of the density layering near a wall requires a non-Markovian theory or, alternatively, a Markovian theory with additional non-hydrodynamic variables. Perhaps the stress

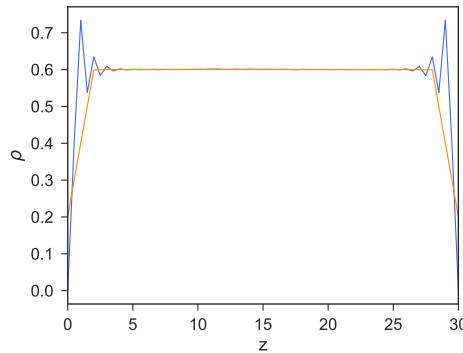


**Figure 5.13:** The equilibrium average discrete density for thin bins (blue) and thick bins (orange). The thick bins do not capture the layering of the density field.

tensor is a candidate to capture the apparent viscoelasticity of the density layering.

Note that it only make sense to speak of transport *coefficients* (or matrices of) in theories that are Markovian, otherwise one needs transport *memory kernels*. Another implication of non-Markovianity of highly resolved hydrodynamics is that in order to speak about the the nonlocal friction coefficients as the ones described by Camargo et al. in [84] one has to ensure that the bins are larger than the molecular size. In the following chapter we will measure the nonlocal viscosity and nonlocal friction matrices that are buried in the relaxation matrix  $\Lambda^*$  and that have not been considered in this chapter. These transport matrices will enter into the microscopic definition of the slip length.



# Chapter 6

## The slip boundary condition

*It is remarkable how long men will believe in  
the bottomlessness of a pond without taking the  
trouble to sound it.*

---

Walden  
HENRY DAVID THOREAU

### 6.1 Introduction

In this chapter, we compute explicitly the viscosity and friction kernels that appear in the discrete hydrodynamic theory presented in Chapter 3 for shear flows in between confining parallel solid walls. We show that the usual Green-Kubo formulas suffer dramatically from the plateau problem and cannot be used for the unambiguous determination of transport coefficients. This includes the solid-fluid friction coefficient which, as shown in Ref. [84], is equivalent to the expression given by Bocquet and Barrat [2]. We use the corrected Green-Kubo expressions, as formulated in Chapter 4, in order to determine unambiguously the transport kernels (which are matrices for the nonlocal viscosity and nonlocal frictions). With these transport matrices, we are able to predict correctly the evolution of the *correlation* matrix of the discrete hydrodynamic variables. We also validate Onsager's hypothesis by predicting, with the same transport matrices, the evolution of the *average* of the discrete momentum field. By looking at the equations for the averages of hydrodynamic variables we may reproduce the pillbox argument of Ref. [84] and re-derive the Navier slip boundary condition. This provides

an explicit microscopic expression for the slip length that involves the corrected transport kernels. The present formulation with corrected Green-Kubo formulas predicts the boundary conditions that should be imposed on the evolution equations for the average hydrodynamic variables. We observe in nonequilibrium MD simulations that the plug flow considered in this chapter violates the Navier slip boundary condition at short times, while it is very well satisfied at later stages of the flow. This violation is due to the unbalance between the solid friction and shear force, which is at the base of the derivation of the Navier slip boundary condition  $\delta \frac{\partial v}{\partial z} = v_{\text{slip}}$  derived in the Introduction. Finally, we also show that the corrected Green-Kubo transport kernels do describe intrinsic surface properties by observing that the slip length is independent on the channel width.

## 6.2 The CG variables

Although some of the expressions and mathematical derivations in this section and the following one have been obtained in the previous chapters, it is convenient to include them in order to make this chapter self-contained.

We consider a monoatomic fluid confined in between two parallel solid walls in the  $x, y$  directions while the normal axis  $z$  to the walls is divided in  $N_{\text{bin}}$  bins separated by nodal planes. In Chapter 3 we have obtained a set of evolution equations for the discrete mass and momentum densities of a fluid moving in between parallel walls and under the assumption that the flow is itself translationally invariant along the directions parallel to the solid walls. When the flow field is parallel to the walls like in shear flows (excluding the case of sound waves normal to the walls), the CG variable is the parallel component  $\mathbf{g}_\mu^x$  of the discrete momentum field defined on each nodal plane  $\mu = 0, \dots, N_{\text{bin}} - 1$ . The microscopic definition of the discrete momentum is

$$\hat{\mathbf{g}}_\mu = \sum_i^N \mathbf{p}_i \delta_\mu(\mathbf{r}_i), \quad (6.1)$$

where  $\mathbf{r}_i, \mathbf{p}_i$  are the position and momentum of the  $i$ -th atom and  $\delta_\mu(\mathbf{r})$  is proportional to a finite element basis function, as described in detail in Chapter 3. We will collect the CG variable (6.1) into an  $N_{\text{bin}}$ -dimensional column vector  $\hat{g}$  that contains as components the parallel component of the momentum density of bin  $\mu$ , this is  $\hat{g}^T = (\hat{\mathbf{g}}_1^x, \dots, \hat{\mathbf{g}}_{\text{bin}}^x)$ , where the superscript  $T$  denotes the transpose.

### 6.2.1 Time derivatives

As shown in Chapter 3 the momentum density changes due to the discrete force density  $\hat{\mathbf{F}}_\mu$  that the solid exerts on the fluid at node  $\mu$  and to the discrete gradient of the stress tensor  $\hat{\sigma}_\mu$  of bin  $\mu$ , this is

$$i\mathcal{L}\hat{\mathbf{g}}_\mu(z) = \hat{\mathbf{F}}_\mu(z) - \frac{\hat{\sigma}_\mu(z) - \hat{\sigma}_{\mu-1}(z)}{\Delta z} \cdot \mathbf{e}_z, \quad (6.2)$$

where the force density and the stress tensor are given, respectively, by the equations 3.26 and 4.20.

The stress tensor  $\hat{\sigma}_\mu$  of bin  $\mu$  contains only coordinates and velocities of fluid particles  $i = 1, \dots, N$ , while the force density  $\hat{\mathbf{F}}_\mu$  of node  $\mu$  contains the force  $\hat{\mathbf{F}}_{ij'}$  that a wall particle  $j' = 1, \dots, N'$  exerts on a liquid particle  $i$ . For the parallel component of the momentum, equation (6.2) becomes

$$i\mathcal{L}\hat{g}_\mu(z) = \hat{F}_\mu(z) - \frac{\hat{\sigma}_\mu(z) - \hat{\sigma}_{\mu-1}(z)}{\Delta z}, \quad (6.3)$$

where we have collected into vectors the forces and stresses,  $\hat{F}_\mu = \hat{\mathbf{F}}_\mu^x$  and  $\hat{\sigma}_\mu = \hat{\sigma}_\mu^{xz}$ . We may write equation (6.3) in matrix form as

$$i\mathcal{L}\hat{g} = \hat{F} + F^T \cdot \hat{\sigma}, \quad (6.4)$$

where  $\hat{F}$  and  $\hat{\sigma}$  are  $N_{\text{bin}}$ -dimensional column vectors and the matrix  $F$  is the bi-diagonal forward finite difference operator introduced in equation 4.22.

### 6.2.2 Correlation matrices

The equilibrium time-correlation matrix of the transverse momentum is denoted by

$$C(t) = \langle \hat{g}(t)\hat{g}^T \rangle \quad (6.5)$$

At time  $t = 0$  the time-correlation matrix is the covariance matrix

$$C(0) = \langle \hat{g}\hat{g}^T \rangle \quad (6.6)$$

We may now use the decomposition (6.4) in order to relate correlations of momenta, stresses, and forces. First, write the time derivative of the correlation matrix of the transverse momentum in the following form

$$\begin{aligned} \frac{d}{dt}C(t) &= - \int_0^t dt' \frac{d}{dt'} \langle \hat{g}(t') i \mathcal{L} \hat{g}^T \rangle = - \int_0^t dt' \langle i \mathcal{L} \hat{g}(t') i \mathcal{L} \hat{g}^T \rangle \\ &= -k_B T M(t), \end{aligned} \quad (6.7)$$

where we have used Green-Kubo running integral (4.18), i.e.

$$M(t) = \frac{1}{k_B T} \int_0^t dt' \langle i \mathcal{L} \hat{g}(t') i \mathcal{L} \hat{g}^T \rangle \quad (6.8)$$

By substituting (6.4) in the Green-Kubo integral (6.8) we have

$$M(t) = F^T \cdot \eta(t) \cdot F + G(t) \cdot F + F^T \cdot H(t) + \gamma(t), \quad (6.9)$$

where the  $N_{\text{bin}} \times N_{\text{bin}}$  matrices  $\eta(t), G(t), H(t), \gamma(t)$  have as components the following Green-Kubo running integrals

$$\begin{aligned} \eta_{\mu\nu}(t) &= \frac{1}{k_B T} \int_0^t dt' \langle \hat{\sigma}_\mu^{xz}(t') \hat{\sigma}_\nu^{xz} \rangle \\ G_{\mu\nu}(t) &= \frac{1}{k_B T} \int_0^t dt' \langle \hat{\mathbf{F}}_\mu^x(t') \hat{\sigma}_\nu^{xz} \rangle \\ H_{\mu\nu}(t) &= \frac{1}{k_B T} \int_0^t dt' \langle \hat{\sigma}_\mu^{xz}(t') \hat{\mathbf{F}}_\nu^x \rangle \\ \gamma_{\mu\nu}(t) &= \frac{1}{k_B T} \int_0^t dt' \langle \hat{\mathbf{F}}_\mu^x(t') \hat{\mathbf{F}}_\nu^x \rangle \end{aligned} \quad (6.10)$$

We have thus expressed the matrix  $M(t)$  in terms of Green-Kubo formula that involve the nonlocal transport matrices  $\eta(t), G(t), H(t), \gamma(t)$ . The matrix  $\eta_{\mu\nu}$  is a nonlocal viscosity kernel, while the matrices  $G_{\mu\nu}, H_{\mu\nu}, \gamma_{\mu\nu}$  describe the friction of the fluid with the walls.

Equations (6.7) and (6.9) lead to the following mathematical identity

$$\frac{d}{dt} C(t) = -k_B T [F^T \cdot \eta(t) \cdot F + G(t) \cdot F + F^T \cdot H(t) + \gamma(t)] \quad (6.11)$$

This mathematical identity relates correlations of momenta with correlations of stresses and forces. It is a useful identity to check for errors in coding the algorithms that compute these quantities. It also suggests that the Green-Kubo formulae (6.10) must decay to zero because the left hand side of (6.11) certainly decays to zero. In other words, the Green-Kubo formulae (6.10) suffer from the plateau problem and cannot be used as an unambiguous method to measure transport coefficients.

### 6.3 The dynamics of the discrete transverse momentum

Mori theory, as it was introduced in Chapter 1, allows one to obtain exact closed equations for both, the averages of the CG variables and their correlations. The exact

equations give the value of these quantities in terms of their past history. If there exists a separation of time scales, the Markovian approximation allows one to approximate the exact integro-differential equations with simple ordinary differential equations with no memory (see equation (4.17)). When we apply Mori's theory with the Markovian approximation to the particular CG variable given by the transverse discrete momentum  $\hat{g}(z)$ , we obtain the dynamic equation for the evolution of its nonequilibrium average  $g(t)$

$$\frac{d}{dt}g(t) = -k_B T M^* \cdot C^{-1}(0) \cdot g(t), \quad (6.12)$$

and the evolution equation for the equilibrium time correlation matrix

$$\frac{d}{dt}C(t) = -k_B T M^* \cdot C^{-1}(0) C(t) \quad (6.13)$$

Note that the transverse momentum does not have any reversible contribution. This is, the reversible matrix vanishes ( $L = \langle \hat{g} i \mathcal{L} \hat{g} \rangle = 0$ ) and the evolution of the transverse momentum is purely dissipative.

As discussed in Chapter 4, the dissipative matrix  $M^*$  is related to the Green-Kubo matrix  $M(t)$  defined in (6.9) through the *corrected* Green-Kubo formula

$$M^* = M(\tau) \cdot c^{-1}(\tau) \quad (6.14)$$

In equation (6.14),  $\tau$  is a time where the right hand side reaches a plateau. Note that the Green-Kubo matrix  $M(t)$  does not display a plateau and decays, precisely, as the correlations themselves, as observed in Chapter 4. Therefore, the matrix  $M^*$  does indeed have a well-defined plateau for which the value of  $\tau$  is irrelevant once the plateau is reached. In practice, because the inverse of the correlation matrix amplifies exponentially any statistical error, the value of  $\tau$  should be chosen as the smallest one that is already in the plateau region.

By using (6.14) and (6.9) in the dynamics of correlations (6.13) we obtain

$$\frac{d}{dt}C(t) = -k_B T [F^T \eta(\tau) \cdot F + G(\tau) \cdot F + F^T \cdot H(\tau) + \gamma(\tau)] \cdot C^{-1}(\tau) \cdot C(t) \quad (6.15)$$

Observe that the use of the corrected starred Green-Kubo expressions in (6.13) is entirely equivalent to use the usual Green-Kubo formula  $M(\tau)$  but with a redefinition of the normalization of the correlation, from  $C^{-1}(0)$  to  $C^{-1}(\tau)$  as in (6.15). Observe also that for  $t = \tau$  the dynamic equation (6.15) becomes an identity, as it complies with the theorem (6.11). The actual value of  $\tau$  is irrelevant in (6.15) provided that we are in

the plateau region of  $M^*$  but, as mentioned, cannot be taken too large in order to have controlled statistical errors.

In a similar way, by inserting (6.14) in (6.12) we obtain the following equation for the average of the discrete momentum field

$$\frac{d}{dt}g(t) = -k_B T [F^T \eta(\tau) \cdot F + G(\tau) \cdot F + F^T \cdot H(\tau) + \gamma(\tau)] \cdot C^{-1}(\tau) \cdot g(t) \quad (6.16)$$

This matrix equation is best described in terms of the velocity field. By following the discussion in Chapters 3 and 4, we define the discrete velocity field according to

$$\mathbf{v}_\mu = \sum_v \rho_{\mu v}^{-1} \mathbf{g}_v, \quad (6.17)$$

where the mass density matrix is defined as

$$\rho_{\mu v} = \frac{C_{\mu v}(0)}{k_B T} \mathcal{V}_v \quad (6.18)$$

Therefore, we may introduce the vector of velocities  $v^T = (v_0, \dots, v_{N_{\text{bin}-1}})$  as

$$v(t) \equiv k_B T \mathcal{V}^{-1} C^{-1}(0) \cdot g(t), \quad (6.19)$$

where the diagonal matrix  $\mathcal{V}$  contains the volume elements of each bin. For bins of equal volume, the matrix  $\mathcal{V}$  is just the identity matrix times the volume  $L_x L_y \Delta z$  of a bin. For momentum profiles that are smooth, the definition (6.17) of the velocity gives a result that is very similar to  $\mathbf{v}_\mu = \mathbf{g}_\mu / \rho_\mu$ , where  $\rho_\mu$  is the average density profile.

In terms of the velocity (6.19) the evolution equation (6.16) is

$$\frac{d}{dt}g(t) = -[F^T \eta(\tau) \cdot F + G(\tau) \cdot F + F^T \cdot H(\tau) + \gamma(\tau)] \cdot \mathcal{V} \cdot c^{-1}(\tau) \cdot v(t) \quad (6.20)$$

In this way, the transport equation (6.12) becomes

$$\frac{d}{dt}g(t) = -\mathcal{V} \cdot M^* \cdot v(t) \quad (6.21)$$

that can be expressed in the equivalent form

$$\frac{d}{dt}g(t) = -\mathcal{V} \cdot M(\tau) \cdot \bar{v}(t), \quad (6.22)$$

where we have introduced the scaled velocity field  $\bar{v} = c^{-1}(\tau) \cdot v$ . The components  $\bar{v}_\mu^x$  of  $\bar{v}$  are

$$\bar{v}_\mu^x = \sum_v \bar{\rho}_{\mu v}^{-1} \mathbf{g}_v^x, \quad (6.23)$$

where the rescaled mass density is

$$\bar{\rho}_{\mu\nu} = \frac{C_{\mu\nu}(\tau)}{k_B T} \mathcal{V}_\mu \quad (6.24)$$

to be compared with (6.18). Because in general  $C_{\mu\nu}(\tau) < C_{\mu\nu}(0)$  we expect that the scaled velocity field  $\bar{\mathbf{v}}_\mu(t)$  is larger than the velocity field  $\mathbf{v}_\mu(t)$ .

In explicit component form, equation (6.20) takes the form

$$\begin{aligned} \frac{d}{dt} \mathbf{g}_\mu^x(t) = & - \sum_\nu \mathcal{V}_\nu \frac{[\eta_{\mu\nu} - \eta_{\mu-1\nu} - \eta_{\mu\nu-1} + \eta_{\mu-1\nu-1}]}{\Delta z^2} \bar{\mathbf{v}}_\nu^x + \sum_\nu \mathcal{V}_\nu \frac{[G_{\mu\nu} - G_{\mu\nu-1}]}{\Delta z} \bar{\mathbf{v}}_\nu^x \\ & + \sum_\nu \mathcal{V}_\nu \frac{[H_{\mu\nu} - H_{\mu-1\nu}]}{\Delta z} \bar{\mathbf{v}}_\nu^x - \sum_\nu \mathcal{V}_\nu \gamma_{\mu\nu} \bar{\mathbf{v}}_\nu^x, \end{aligned} \quad (6.25)$$

where here, in order to ease the notation, we have not plotted the dependence of the matrices  $\eta_{\mu\nu}, G_{\mu\nu}, H_{\mu\nu}, \gamma_{\mu\nu}$  on the upper limit of integration  $\tau$ . Similar discrete equations have been obtained in Chapter 3 by using the Kawasaki-Gunton projector that gives state dependent transport coefficients in general. Under the assumption that these state dependent transport coefficients are evaluated at equilibrium, one obtains (6.25) from the equations in Chapter 3.

As discussed in Chapter 3 the discrete equation (6.25) can be also obtained from a finite element discretization of a continuum equation of the form

$$\begin{aligned} \partial_t \mathbf{g}(\mathbf{r}, t) = & \nabla \int d\mathbf{r}' \eta_{\mathbf{r}\mathbf{r}'} \nabla' \mathbf{v}(\mathbf{r}') - \nabla \int d\mathbf{r}' G_{\mathbf{r}\mathbf{r}'} \mathbf{v}(\mathbf{r}') \\ & - \int d\mathbf{r}' H_{\mathbf{r}\mathbf{r}'} \nabla' \mathbf{v}(\mathbf{r}') - \int d\mathbf{r}' \gamma_{\mathbf{r}\mathbf{r}'} \mathbf{v}(\mathbf{r}') \end{aligned} \quad (6.26)$$

The first term in the right hand side involving second derivatives is a nonlocal viscosity term, while the other three terms reflect the irreversible force that the solid wall exerts on the fluid. Equation (6.26) can also be obtained under the assumption of planar flow in planar geometries of the general continuum hydrodynamic equations presented in Ref. [84].

Note, however, that the present derivation of the equations (6.25) for the discrete hydrodynamics take into account the solution given in Chapter 4 of the plateau problem which is inherent to the Green-Kubo expressions in general. In that sense, note that the transport kernels decay with  $\tau$  while the scaled velocity field  $\bar{\mathbf{v}}$  increases with  $\tau$  thus compensating for the plateau problem.

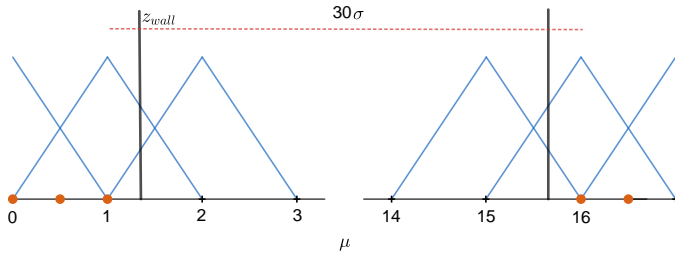


**Figure 6.1:** Scheme of the location of the nodal planes in the system, labeled with  $\mu = 0, 1, \dots, 16$ , and the corresponding finite element basis functions (linear tent functions). Orange circles indicate the location of the crystalline planes of the solid walls, with a lattice spacing of  $\sigma$ . The distance between nodal planes is  $\Delta z = 2\sigma$ , and the distance between the nodes  $\mu = 1$  and  $\mu = 16$  where the first crystalline planes are is  $30\sigma$ . Nodes  $\mu = 1$  and  $\mu = 16$  play a symmetrical role. The two vertical lines define the location of the hydrodynamic position of the walls, as defined from the friction in equation (6.37). For the lower wall  $z_{\text{wall}} = 2.65\sigma$ .

## 6.4 Simulation setup

We conduct MD simulations at equilibrium for a LJ fluid with parameters  $\sigma, \epsilon$  in between two crystalline walls made of fixed identical LJ particles. The geometry, thermodynamic point, and simulation are exactly the same as that studied in Chapter 5, giving a density in the bulk of  $\rho = 0.6$  and a temperature  $T = 2$  in reduced LJ units.

In Fig. 6.1 we show a detailed scheme of the location of the nodal planes in the system. The horizontal line is the  $z$  axis which is normal to the walls. The fixed atom walls (orange circles) are in a simple cubic lattice with a lattice spacing  $\sigma$ . Periodic boundary conditions are given in all directions but because we have a crystal with five lattice planes separated a distance of  $1\sigma$ , the atoms of fluid near the left wall do not interact with the atoms of fluid near the right wall, as the cutoff radius in the LJ potential is  $2.5\sigma$ . We choose a rather large distance  $\Delta z = 2\sigma$  between nodal planes. The reason for choosing this large bin size is that, as shown in Chapter 5, for smaller bin sizes with  $\Delta z = 0.5\sigma$  the dynamics is clearly non-Markovian near the walls, and the theory predictions break down near the walls. A bin size of  $\Delta z = 1\sigma$  still displays signs of non-Markovianity.

Also shown in Fig. 6.1 are the finite element basis functions (blue lines) centered at the nodal planes that define the discrete momentum. Note that due to the presence of the solid lattice there are no fluid particles contributing to the nodal plane  $\mu = 0$  and its mass and momentum densities are zero. Nodes  $\mu = 1, 16$ , which play a symmetrical role, receive contribution from the particles of the fluid. Note that the density profile, when resolved with a bin size of  $\Delta z = 0.1\sigma$  displays the typical layering near the wall,

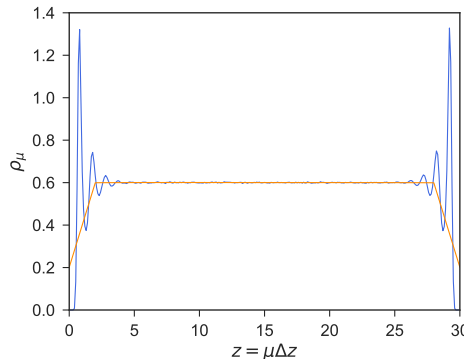


**Figure 6.2:** The average density profile for two resolutions  $\Delta z = 0.1\sigma$  (blue) and  $\Delta z = 2\sigma$  (orange).

as shown in Fig. 6.2. For the bin size of  $\Delta z = 2\sigma$  the density profile does not show the layering, which is buried inside the bin.

For future reference, we also show in Fig. 6.1 the hydrodynamic position  $z_{\text{wall}}$  of the wall as defined in microscopic terms in equation (6.37). It is at this wall position, within the fluid region, where boundary conditions will apply.

In order to see if the results are sensitive to the channel width, we have considered two cases, where the distance between the crystalline planes facing the fluid of the top and bottom walls are at a distance of  $30\sigma$  and  $60\sigma$ .

## 6.5 The transport matrices

From a typical equilibrium trajectory of the microscopic state generated by the MD simulation, we measure the forces on the nodes and stress on the bins defined in equation (4.20). We then compute the Green-Kubo running integrals (6.10). These matrices are observed to have no plateau in a way analogous to what we found in periodic boundary conditions in Chapter 4. For example, in Fig 6.3 we plot some elements of the matrices  $\eta_{\mu\nu}(t), \gamma_{\mu\nu}(t)$  as a function of time and they are seen to decay towards zero, in a quasi-algebraic way.

Given that the Green-Kubo formula for the transport matrices does not have a plateau, we resort to the methodology introduced in Chapter 4 and that essentially amounts to extract  $M^*$  defined in (6.14) from  $M(t)$  defined in (6.9). Once the matrix  $M(\tau) \cdot c^{-1}(\tau)$  is constructed, it is possible to obtain the value of  $\tau$  at which this matrix do has a plateau. The existence of the plateau is best observed in the eigenvalues of

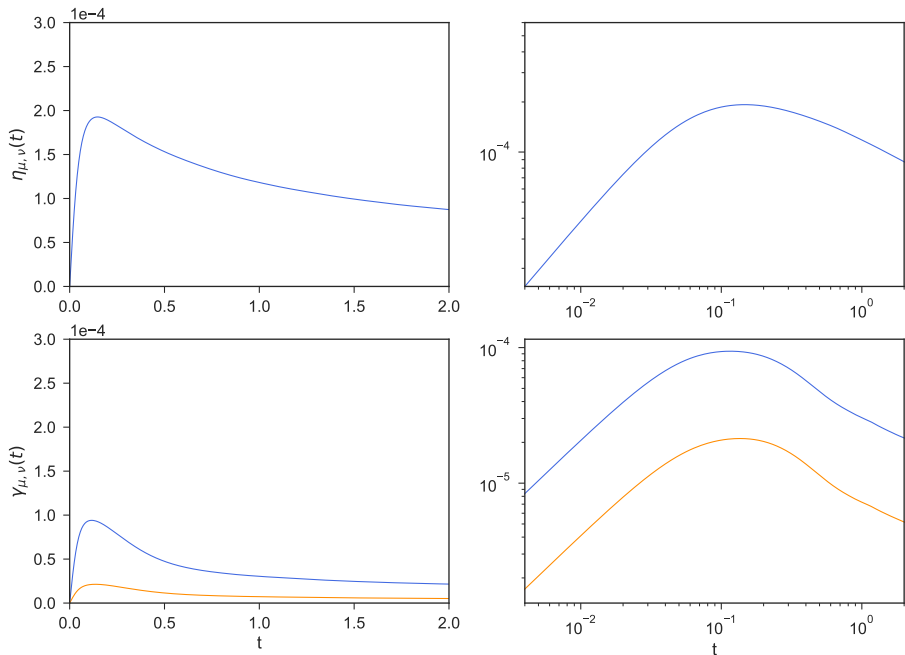


**Figure 6.3:** Top: Time evolution of the matrix element  $\eta_{\mu\nu}(t)$  for  $\mu = 10, \nu = 10$  that corresponds to a node in the center of the channel. Bottom:  $\gamma_{\mu\nu}(t)$  for  $\mu = 1, \nu = 1$  (blue) and  $\mu = 2, \nu = 2$  (orange). The right panel in both top and bottom is in log-log scale and shows that the decay is algebraic. No plateau is observed.

$M(\tau) \cdot c^{-1}(\tau)$ . We have followed this procedure in Chapter 5 and have shown that the matrix  $M^*$  defined in (6.14) reaches a clear plateau after a time  $\tau = 0.3$  in reduced units. This time is sufficiently large for being at the plateau and sufficiently small to not have substantial statistical errors due to the explosive inverse of the correlation matrix in (6.14). The transport matrices given in terms of the Green-Kubo running integrals (6.10) evaluated at  $\tau = 0.3$  are plotted in Fig. 6.4. The nonlocal viscosity is concentrated along the diagonal for which the only non-zero terms are  $\eta_{\mu\mu}$  and  $\eta_{\mu\mu+1}$ . As the nonlocal viscosity kernel  $\eta_{\mu\nu}$  involves the correlation of stress, and the stress is defined for pairs of particles interacting within the cutoff distance of  $2.5\sigma$ , the relatively large support of the nonlocal viscosity is explained by the fact that, typically, we should expect correlations between pairs of particles with a common particle to extend to  $5\sigma$ . As not all pairs are of this form, we observe stress correlations on a length scale of  $\sim 3 - 4\sigma$ . This is a large distance in molecular terms. The matrices  $G, H, \gamma$  are localized near the nodes close to the walls. The matrix  $H$  is the transpose of the matrix  $G$ , i.e.  $H_{\mu\nu}(\tau) = G_{\nu\mu}(\tau)$  as a reflection of Onsager's reciprocity. In the right panel of Fig. 6.4 we plot a zoom of the plots of the left panel where we observe the structure of the transport matrices near the walls. Observe that the nonlocal viscosity kernel  $\eta_{\mu\nu}(\tau)$  takes the bulk value at the node  $\mu = 2, \nu = 2$ . The elements that are different from zero in the matrix  $G_{\mu\nu}(\tau)$  are those corresponding to  $\mu = 1, \nu = 1, 2$  while in the matrix  $\gamma_{\mu\nu}(\tau)$  the non-vanishing elements are  $\mu = 1, 2, \nu = 1, 2$ . Therefore, the irreversible forces that the wall exert on the fluid extend over distances of the order of two bins, i.e around  $4\sigma$ . Note that this is a rather large distance in molecular terms.

Although impossible to distinguish in the plots, in Fig. 6.4 we have superimposed the results for the wide channel of size  $60\sigma$  and the smaller channel of size  $30\sigma$ . Therefore, the structure of the transport matrix near the walls is unaffected by the size of the channel.

## 6.6 Evolution of the flow in NEMD simulations

Mori theory for the averages describes the decay of an initial non-equilibrium profile towards the equilibrium state. Once we have measured the transport matrix  $M^*$  or, alternatively, the transport matrices  $\eta^*, G^*, H^*, \gamma^*$  we may predict the evolution of a nonequilibrium average where the initial nonequilibrium ensemble describes a particular flow profile. By measuring independently the actual nonequilibrium evolution we are able to validate the present theory.

We run microcanonical MD simulations in which the initial state is not an equilibrium state. In this chapter, we focus on an initial plug flow which is prepared as follows. From an equilibrated microscopic configuration, we add to the thermal velocity of each

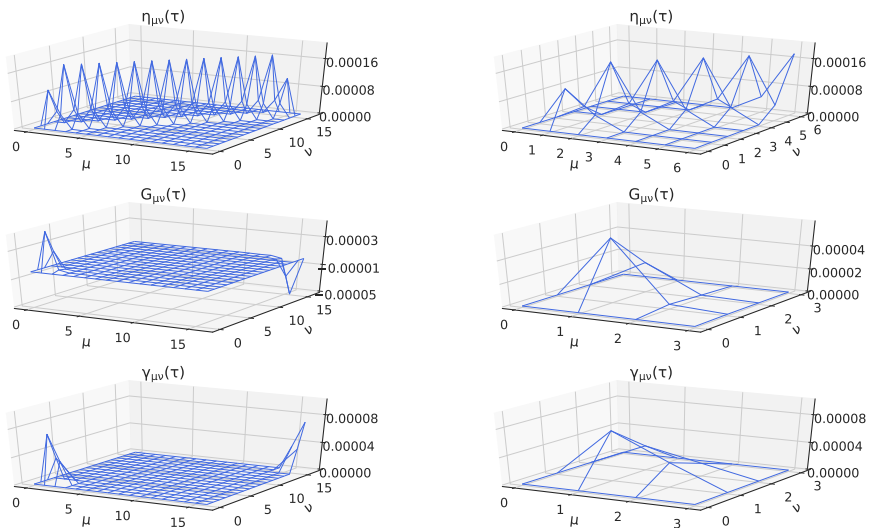


**Figure 6.4:** Left column: The transport matrices  $\eta_{\mu\nu}(\tau), G_{\mu\nu}(\tau), \gamma_{\mu\nu}(\tau)$  evaluated from the Green-Kubo running integrals at the plateau value time  $\tau$ . Right column: Zoom of the corresponding left plots. Results for two channels with interplane distance of  $30\sigma$  and  $60\sigma$ , and the same bin size  $\Delta z = 2\sigma$ , are plotted. The results are hard to distinguish implying that the structure of the transport kernels near the walls is unchanged with the channel width.

fluid atom the same velocity  $\mathbf{V} = (v_0, 0, 0)$ . This has two consequences. The first is to generate a nonequilibrium plug flow in a direction parallel to the wall. The second is to increase the kinetic energy and hence the temperature of the system. In order to remain at the same thermodynamic point, we rescale the resulting velocities in order to remain at the same temperature. We repeat many times this procedure with different initial configurations and look at the average over initial conditions of the mass and momentum density fields. The initial plug flow decays towards the equilibrium state of the system. We have observed in the simulations that at the initial stages of this plug flow, the density field becomes time-dependent. In fact, we observe that after the initial kick the fluid develops a component of the velocity normal to the walls. This is associated to a excitation of a sound wave which would need to be described, strictly speaking, with the full set of equations detailed in Chapter 3. However, these effects are small when we use a small initial value of the plug flow velocity and we assume that only the transverse momentum is necessary to describe the dynamics of the system.

The prediction within Mori theory of the evolution of the average of the momentum field is given in (6.12) that we write in a compact form as

$$\frac{d}{dt}g(t) = -\Lambda^* \cdot g(t), \quad (6.27)$$

where the relaxation matrix is  $\Lambda^* = k_B T M^* \cdot C^{-1}(0)$ . This equation has the following matrix exponential solution

$$g(t) = \exp\{-\Lambda^*(t - \tau)\} \cdot g(\tau), \quad (6.28)$$

where we choose as initial condition the profile at the time  $\tau$ . As we will see, for times shorter than  $\tau$ , the Markovian equation (6.27) gives wrong predictions. We have made a similar observation in Chapter 4 when we discussed the dynamics of an unconfined fluid.

The solution (6.28) represents a discrete version of the numerical solution of the integro-differential equation (6.26) which is solved, therefore, *without using any boundary condition*. The periodic boundary conditions in the normal direction  $z$  to the walls are irrelevant because the transport kernels vanish inside the solid walls as there is no fluid particles there. In the present theory boundary conditions are not needed in order to solve hydrodynamics, because the interaction with the solid is taken explicitly into account through the transport matrices  $G(\tau), H(\tau), \gamma(\tau)$  as shown in (6.16).

In the left panel of Fig. 6.5 we show the measured discrete momentum density profile at different times of the evolution for an initial plug flow. The times are  $t = 1, 3, \dots, 21$ . Also shown in that figure is the prediction given by equation (6.28). Excellent agreement is observed, implying that the proposed equations (6.16) and (6.25) describe adequately

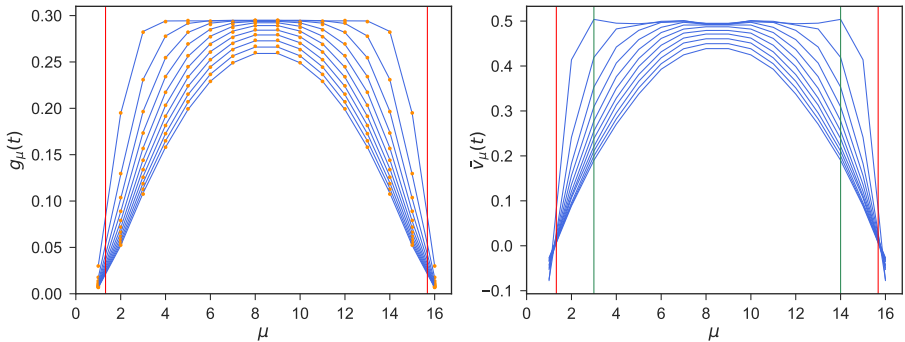


**Figure 6.5:** Left panel: the measured average momentum profile  $g(t)$  at different times ( $t = 1, 3, \dots, 21$ ), in descending order. The two vertical lines denotes the position of the wall  $z_{\text{wall}}$  as defined microscopically from the friction matrix in equation (6.37). Also plot (orange points) is the prediction given by (6.28), which is undistinguishable from the measured profile. Right panel panel: the velocity profile obtained from the momentum through (6.23). The green vertical lines delimit the region of the fluid that takes part in the boundary slab with  $B = 2$  used to define the mechanical balance.

the flow. The agreement between predicted and measured profiles at longer times is appreciated in the Fig. 6.6 where the momentum at nodes  $\mu = 1, 2, 4$  as a function of time is shown. Observe the very fast decay of the momentum near the wall due to the friction due to the wall. In the right panel we plot a zoom at short times of the evolution of the momentum. It is quite noticeable that the predictions of the Markovian theory are not correct at times smaller than  $t < \tau \simeq 0.2$ . This is another signal that at very short times from the initial preparation of the system in the plug flow configuration the Markovian approximation breaks down. Only after the time in which the transport matrix reaches a plateau, and hence a Markovian theory holds, it is expected that we get correct predictions, as observed. The comparison (not shown) of the Markovian prediction (6.15) of the correlation matrix  $C(t)$  with the actual measured correlation matrix also shows perfect agreement beyond  $t \simeq 0.2$  but incorrect results at shorter times.

In the right panel of Fig. 6.5 we show the velocity profile, defined according to (6.23). Note that the velocity shows some irregularities as compared with the smooth momentum density profiles in the left panel of the same figure. This is due to the fact that the velocity is defined in terms of the inverse density matrix which, for discontinuous momentum fields like the initial plug flow displays a strong structure. Only for smooth and continuous momentum fields one obtain smooth velocity fields.

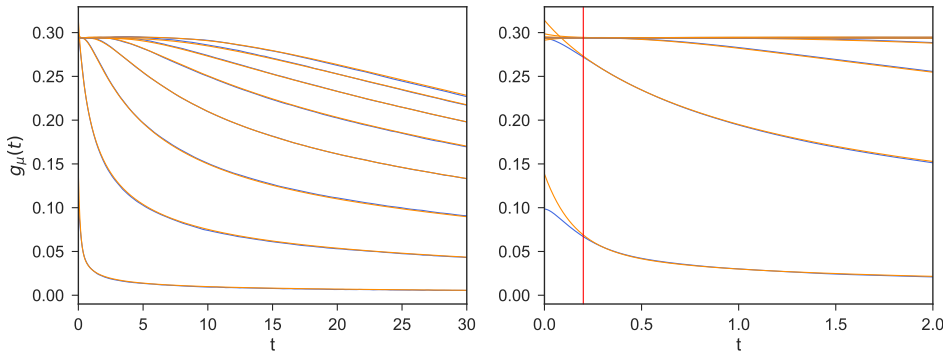


**Figure 6.6:** Left panel: the momentum  $g(t)$  profile for nodes  $\mu = 1, 2\dots 8$  (in ascending order) as a function of time (blue), and the predictions given by (6.28) (orange). Right panel: zoom of the left panel at short times. The red line is plotted at  $t = 0.2$ .

## 6.7 The slip boundary condition

In the previous section, we have solved the discrete version (6.25) of the nonlocal hydrodynamic equations (6.26) without any reference to boundary conditions. As it is manifest in equation (6.26), the interaction with the walls is not described with boundary conditions but rather in terms of irreversible friction forces that appear directly in the hydrodynamic equations. This was suggested in the continuum theory presented in Chapter 2. Later on in Ref. [84], Camargo et al. show how one can recover the Navier slip boundary conditions from the continuum theory presented in Chapter 2 by using a pillbox argument that allows to obtain a mechanical balance.

In subsection 6.7.1, we adapt the pillbox mechanical balance argument given in Ref. [84] for the case of a planar geometry of a fluid described with a *discrete* hydrodynamic field. This is the first step towards the derivation in subsection 6.7.2 of a boundary condition from the dynamics of the discrete field given by (6.20).

### 6.7.1 Mechanical balance on a slab near wall

We introduce the concept of *boundary slab* of fluid which is made of  $B$  bins near one of the walls. Hansen et al. [34] have used also a boundary slab to formulate a generalized Langevin equation on which to base a formulation of boundary conditions. The total

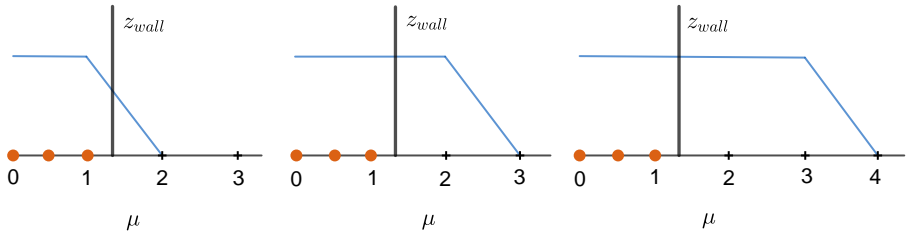


**Figure 6.7:** Scheme of the definition of the boundary slab of fluid. The blue line defines the function  $U_B(z)$ , for  $B = 1$  (left),  $B = 2$  (middle), and  $B = 3$  (right).

momentum  $\mathbf{P}_B^x$  of this slab is defined as

$$\mathbf{P}_B^x \equiv \sum_{\mu=0}^B \mathcal{V}_\mu \hat{\mathbf{g}}_\mu^x = \sum_i^N \mathbf{p}_i U_B(z_i), \quad (6.29)$$

where we have introduced the function

$$U_B(z) = \sum_{\mu}^B \mathcal{V}_\mu \delta_\mu(z) \quad (6.30)$$

This function is plotted in Fig. 6.7 for different values of  $B$  and basically counts the particles that are near the wall.

We consider the rate of change of the momentum of this boundary slab. The total force on the slab is given by

$$\mathbf{F}_B^x(t) = \frac{d}{dt} \sum_{\mu=0}^B \mathcal{V}_\mu \mathbf{g}_\mu^x(t) \quad (6.31)$$

We show in the Appendix H that once we use the equation of motion (6.25) in this expression we may write the force (per unit area) on the slab due to the combined action

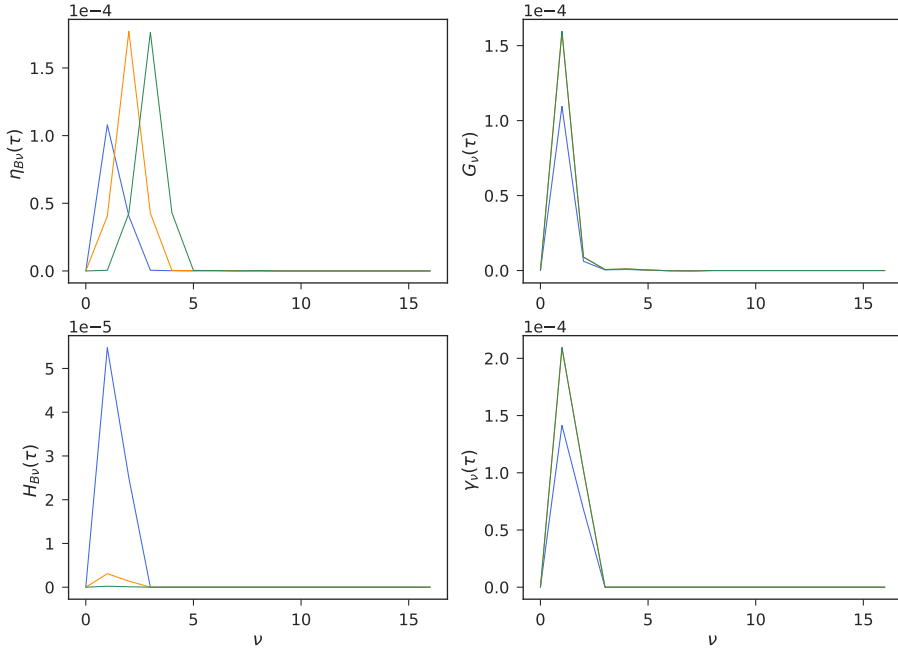


**Figure 6.8:** Top-left: The viscosity matrix  $\eta_{B\nu}$  for different values of  $\nu$ , for three values of  $B = 1$  (blue),  $B = 2$  (orange),  $B = 3$  (green). Observe that the last two quantities are identical except that are simply translated one node. Top-right and bottom-right: The local transport coefficients defined in (6.33). Three values of  $B = 1$  (blue),  $B = 2$  (orange),  $B = 3$  (green) are plotted, but the last two lay on top of each other. Also is plotted in bottom-left  $H_{B\nu}$  which has small value for  $B = 1$  and negligible values for  $B = 2$  and  $B = 3$ .

of the fluid outside the slab and the solid wall as

$$\frac{1}{S} \mathbf{F}_B^x = \sum_{\nu} \mathcal{V}_{\nu} [\eta_{B\nu} - G_{\nu}] \frac{\bar{\mathbf{v}}_{\nu+1}^x - \bar{\mathbf{v}}_{\nu}^x}{\Delta z} - \sum_{\nu=0} \mathcal{V}_{\nu} [\gamma_{\nu} - H_{B\nu}] \bar{\mathbf{v}}_{\nu}^x, \quad (6.32)$$

where the following local transport coefficients have been defined

$$G_{\nu} \equiv \frac{1}{S} \sum_{\mu=1}^B \mathcal{V}_{\mu} G_{\mu\nu}, \quad \gamma_{\nu} \equiv \frac{1}{S} \sum_{\mu=1}^B \mathcal{V}_{\mu} \gamma_{\mu\nu} \quad (6.33)$$

The different quantities appearing on the mechanical balance equation (6.32) on the boundary slab depend, obviously, on the number  $B$  of boundary bins that make the

slab. We plot in Fig. 6.8 the quantities  $\eta_{B\nu}, G_\nu, H_\nu, \gamma_\nu$  for different values of  $B = 1, 2, 3$ . In the top-left panel of Fig. 6.8 we plot  $\eta_{B\nu}$  where we see that the shape of  $\eta_{2\nu}$  and  $\eta_{3\nu}$  is the same but displaced one node from each other. In the top-right panel of Fig. 6.8 we plot  $G_\nu$  defined in (6.33) for the different values of  $B$ . We observe that the values for  $B = 2$  and  $B = 3$  coincide. This is a signature that beyond three bins, there are no further contributions to the local transport coefficient  $G_\nu$ . A similar behaviour is observed in the bottom-right panel where we plot the local coefficient  $\gamma_\mu$ . For reasons the will become clear later, we want to have the smaller possible slab that already does not change results. For this reason we choose  $B = 2$  from now on as a good definition of the boundary slab width. Note that the boundary slab contains fluid particles that are within a distance of  $4\sigma$  from the wall, which is a large distance in molecular terms.

The mechanical balance equation (6.32) is a direct consequence of the equation of motion (6.25) given by Mori theory. To the extent that (6.25) predicts correctly the average behaviour of the discrete momentum density, equation (6.32) should predict correctly the force on the fluid slab. However, as we have already noticed when comparing the predictions with the measurements of the discrete momentum profiles in Fig. 6.6, at very short times the Markovian assumption breaks down. In Fig. 6.9 we plot both sides of (6.32) and show that only after a time larger than  $t \simeq 0.3$  a very good agreement is found. After this time, the momentum profile obeys very well the proposed dynamic equation (6.25) and the difference (orange curve in Fig. 6.9) between the measured force on the boundary slab and the prediction (6.32) goes to zero.

### 6.7.2 The boundary condition

A boundary condition is a condition on the velocity of the fluid flow, in the region of the fluid, that somehow captures the influence of the solid wall on the fluid. It is a way to bypass the presence of the solid in the description of the fluid. As Camargo et al. described in [84] the boundary condition emerges from a mechanical balance condition like the one formulated in the previous section. The idea is to assume a parametric model for the fluid velocity profile. Then, the mechanical balance (6.32) implies a condition on the parameters of the model. For the case of a linear model, it implies a linear relationship between the velocity and the gradient at the wall position, leading to the slip boundary condition.

Assume that the velocity field in nodes  $\mu = 1, \dots, B$  inside the boundary slab is strictly linear

$$\bar{v}_\mu^x = \bar{v}_{\text{wall}}^x + \dot{\bar{\gamma}}_{\text{wall}}(\mu\Delta z - z_{\text{wall}}), \quad (6.34)$$

where  $\bar{v}_{\text{wall}}^x$  is the velocity at the wall position  $z_{\text{wall}}$ , to be defined below, and  $\dot{\bar{\gamma}}_{\text{wall}}$  is the shear rate.

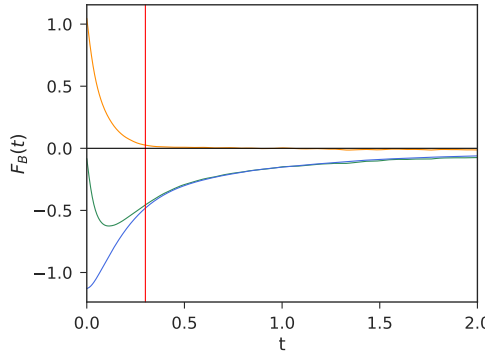


**Figure 6.9:** Check of equation (6.32) for  $B = 2$ . Green is the measured force  $F_B(t) = \mathbf{F}_B^x(t)$ , blue is the right hand side of (6.32), and orange is the difference between both quantities, and a reflection of the failure of the Markovian equation (6.27) at very short times. The vertical line is at the plateau time  $\tau = 0.3$ . Beyond this time the Markovian equation is valid but the force is not zero. For times larger than approximately  $t = 2$ , the force on the boundary slab vanishes.

When we choose  $B = 2$  as the width of the boundary slab, and observe the range of the values for  $\eta_{B\nu}, H_{B\nu}, G_\nu, \gamma_\nu$  in Fig. 6.8, we realize that the values of the velocity that actually contribute to the boundary force are those of nodes  $\mu = 1, 2, 3, 4$ . Therefore, the force on the boundary is actually given by

$$\frac{1}{S} \mathbf{F}_B^x = \sum_{\nu=1}^{B+1} \mathcal{V}_\nu [\eta_{B\nu} - G_\nu] \frac{\bar{\mathbf{v}}_{\nu+1}^x - \bar{\mathbf{v}}_\nu^x}{\Delta z} - \sum_{\nu=1}^B \mathcal{V}_\nu [\gamma_\nu - H_{B\nu}] \bar{\mathbf{v}}_\nu^x \quad (6.35)$$

If we insert the velocity field (6.34) in equation (6.35) we obtain

$$\frac{1}{S} \mathbf{F}_B^x = \eta' \dot{\bar{\gamma}}_{\text{wall}} - \gamma' \bar{\mathbf{v}}_{\text{wall}}^x \quad (6.36)$$

In order to obtain equation (6.36) we must define the wall position  $z_{\text{wall}}$  according to

$$z_{\text{wall}} = \frac{\sum_\nu^B \mathcal{V}_\nu (\gamma_\nu - H_{B\nu}) \nu \Delta z}{\sum_\nu^B \mathcal{V}_\nu (\gamma_\nu - H_{B\nu})} \quad (6.37)$$

This wall position is defined unambiguously from the friction properties of the wall and is, by construction, inside the fluid region, slightly away from the solid wall. Note that from a microscopic point of view, the solid does not have a prescribed “surface” as it is made by a collection of centers of force located at the fixed atoms positions.

In equation (6.36) we have introduced the following transport coefficients

$$\eta' = \eta - G, \quad \gamma' = \gamma - H \quad (6.38)$$

with the following definitions

$$\begin{aligned} \eta &= \sum_{\nu=1}^{N_{\text{bin}}} \mathcal{V}_\nu \eta_{B\nu} \\ G &= \frac{1}{S} \sum_{\nu=1}^{N_{\text{bin}}} \mathcal{V}_\nu \sum_{\mu=1}^B \mathcal{V}_\mu G_{\mu\nu} \\ \gamma &= \frac{1}{S} \sum_{\nu=1}^{N_{\text{bin}}} \mathcal{V}_\nu \sum_{\mu=1}^B \mathcal{V}_\mu \gamma_{\mu\nu} \\ H &= \sum_{\nu=1}^{N_{\text{bin}}} \mathcal{V}_\nu H_{B\nu} \end{aligned} \quad (6.39)$$

We have observed in Fig. 6.9 that after a time  $t \simeq 2$ , the force per unit area  $\frac{1}{S} \mathbf{F}_B^x(t)$  on the boundary slab is vanishingly small. In other flow situations like a steady state flow, the force, being a time derivative, that of the momentum, is also zero. When the force on the boundary slab vanishes,  $\mathbf{F}_B^x(t) \simeq 0$ , we obtain from (6.36) the Navier slip boundary condition [27],

$$\bar{\mathbf{v}}_{\text{wall}}^x = \delta \dot{\bar{\gamma}}_{\text{wall}} \quad (6.40)$$

with the slip length given by

$$\delta = \frac{\eta'}{\gamma'} \quad (6.41)$$

In summary, we have derived the Navier slip boundary condition from the assumptions that

- i) the discrete momentum obeys the dynamics (6.25).
- ii) the velocity field inside the boundary slab made of  $B$  bins is linear as in (6.34).
- iii) the force on the boundary slab is vanishingly small.

The hypothesis i) is true after the plateau time  $\tau$ , as verified in Fig. 6.9. Hypothesis ii) depends very much on the width of the boundary slab. As it is appreciated in the right panel of Fig. 6.5, the velocity profile has a parabolic curvature. An approximate linear profile is more accurate for smaller widths of the slab. That is the reason for choosing the smaller value of  $B = 2$  that already captures all the fluid-wall interaction (as shown in Fig. 6.8). Note that the linear velocity profile assumption becomes more and more accurate as time proceeds, but it is not satisfied at the initial stages of the plug flow, when there is a significative curvature of the velocity profile within the boundary slab.

For the hypothesis iii), note from Fig. 6.9 that the force  $\mathbf{F}_B(t)$  on the boundary slab is not zero until a time of the order of 2 in reduced units. Therefore, for this highly discontinuous plug flow, there is no balance between shear stress and friction force at short times, and the slip boundary condition cannot hold at times shorter than  $t = 2$ . Note that this time is at the very early stages of the decay of the plug flow velocity profile, as shown in Fig. 6.6.

In summary, we expect the slip boundary condition (6.40) to be satisfied only after a certain time in which the force on the boundary slab vanishes and the velocity profile inside the slab becomes linear. We will validate this conclusion in subsection 6.7.4.

One of the values of the present derivation of the Navier slip boundary condition is that the slip length is given in microscopic terms, through the transport coefficients (6.39). We next show that the microscopic expression for the slip length coincide with the one presented by Camargo et al. in Ref. [84], where they derived the Navier slip boundary condition from the continuum theory presented in Chapter 2. There it was also showed that the microscopic expression for the slip length coincides with Bocquet and Barrat under a suitable redefinition of the hydrodynamic wall position. Therefore, the expression given here coincides with the proposed one by Bocquet and Barrat.

### 6.7.3 The microscopic expression for the slip length

The strategy that has lead to (6.36) now provides the proper microscopic expressions for the two transport coefficients  $\eta', \gamma'$ . By using (6.39), and the explicit Green-Kubo

forms (6.10), we have

$$\begin{aligned}\eta &= \frac{1}{k_B T} \int_0^\tau dt \left\langle \hat{\sigma}_B^{xz}(t) \sum_{\nu=1}^{N_{\text{bin}}} \mathcal{V}_\nu \hat{\sigma}_\nu^{xz} \right\rangle^{\text{eq}} \\ G &= \frac{1}{S k_B T} \int_0^\tau dt \left\langle \sum_{\mu=1}^B \mathcal{V}_\mu \hat{\mathbf{F}}_\mu^x(t) \sum_{\nu=1}^{N_{\text{bin}}} \mathcal{V}_\nu \hat{\sigma}_\nu^{xz} \right\rangle^{\text{eq}} \\ H &= \frac{1}{k_B T} \int_0^\tau dt \left\langle \hat{\sigma}_B^{xz}(t) \sum_{\nu=1}^{N_{\text{bin}}} \mathcal{V}_\nu \hat{\mathbf{F}}_\nu^x(t) \right\rangle^{\text{eq}} \\ \gamma &= \frac{1}{S k_B T} \int_0^\tau dt \left\langle \sum_{\mu=1}^B \mathcal{V}_\mu \hat{\mathbf{F}}_\mu^x(t) \sum_{\nu=1}^{N_{\text{bin}}} \mathcal{V}_\nu \hat{\mathbf{F}}_\nu^x \right\rangle^{\text{eq}}\end{aligned}\quad (6.42)$$

Note that we have a partition of unity property that implies that

$$\sum_{\mu}^{N_{\text{bin}}} \psi_{\mu}(\mathbf{r}) = 1, \quad \sum_{\mu}^{N_{\text{bin}}} \chi_{\mu}(\mathbf{r}) = 1, \quad \sum_{\mu}^{N_{\text{bin}}} z_{\mu}(i, j) = 1 \quad (6.43)$$

Therefore, from (3.26) and (4.20) we have the microscopic forms of the total force and total stress tensor

$$\begin{aligned}\hat{\mathbf{F}} &\equiv \sum_{\mu} \mathcal{V}_{\mu} \hat{\mathbf{F}}_{\mu} = \sum_{ij'}^{NN'} \hat{\mathbf{F}}_{ij'} \\ \hat{\sigma} &\equiv \sum_{\mu} \mathcal{V}_{\mu} \hat{\sigma}_{\mu} = \sum_i^N \mathbf{p}_i \mathbf{v}_i + \frac{1}{2} \sum_{ij}^N \mathbf{r}_{ij} \hat{\mathbf{F}}_{ij},\end{aligned}\quad (6.44)$$

where  $\hat{\mathbf{F}}$  is the total force that the solid exerts on the fluid and  $\hat{\sigma}$  is the total stress tensor of the fluid. For  $B \geq 2$  the nodal plane at  $B$  is beyond the range of the solid-liquid interactions, and we have that summing the force density of node  $\mu$  over the bins up to  $\mu = B$  also gives the total force, this is

$$\hat{\mathbf{F}} \equiv \sum_{\mu}^B \mathcal{V}_{\mu} \hat{\mathbf{F}}_{\mu} \quad (6.45)$$

Therefore, the transport coefficients (6.42) are given by

$$\begin{aligned}\eta &= \frac{1}{k_B T} \int_0^\tau dt \langle \hat{\sigma}_B^{xz}(t) \hat{\sigma}^{xz} \rangle^{\text{eq}} \\ G &= \frac{1}{S k_B T} \int_0^\tau dt \langle \hat{\mathbf{F}}^x(t) \hat{\sigma}^{xz} \rangle^{\text{eq}} \\ H &= \frac{1}{k_B T} \int_0^\tau dt \langle \hat{\sigma}_B^{xz}(t) \hat{\mathbf{F}}^x \rangle^{\text{eq}} \\ \gamma &= \frac{1}{S k_B T} \int_0^\tau dt \langle \hat{\mathbf{F}}^x(t) \hat{\mathbf{F}}^x \rangle^{\text{eq}}\end{aligned}\quad (6.46)$$

These coefficients still depend on the value of  $B$  that determines the width of the boundary slab on which we are predicated the mechanical balance condition. In Table 6.1 we plot the values of these quantities as a function of the width of the boundary slab. We observe that the results for  $\eta, G, \gamma$  and  $z_{\text{wall}}$  for  $B = 2$  and for  $B = 3$  are very similar. The coefficient  $\eta$  is given in terms of the correlation of the stress tensor of bin  $B$  with the total stress tensor of the fluid. Because beyond  $B = 2$  this quantity does not change by increasing  $B$ , we may simply take an average over the bulk region

$$\begin{aligned}\eta &= \frac{1}{V} \sum_{\mu \in \text{bulk}} \mathcal{V}_\mu \frac{1}{k_B T} \int_0^\tau dt \langle \hat{\sigma}_\mu^{xz}(t) \hat{\sigma}^{xz} \rangle^{\text{eq}} \\ &\simeq \frac{1}{V} \frac{1}{k_B T} \int_0^\tau dt \langle \hat{\sigma}^{xz}(t) \hat{\sigma}^{xz} \rangle^{\text{eq}}\end{aligned}\quad (6.47)$$

This is, the coefficient  $\eta$  is given in terms of the correlation of the off-diagonal components of the total stress tensor. We recognize in  $\eta$  the usual expression for the shear viscosity of the fluid.

Observe in Table 6.1 that the value of  $H$  is two orders of magnitude smaller than the value of  $\gamma$  for  $B = 2$ , and three orders smaller for  $B = 3$ . We will neglect consistently the contribution of  $H \simeq 0$  in (6.41), leading to the following microscopic expression for the slip length (6.41)

$$\delta = \frac{\eta - G}{\gamma} \quad (6.48)$$

This result is identical to the one obtained in Ref. [84] by Camargo et al., and it coincides, after a suitable redefinition of the wall position, with the one provided by Bocquet and Barrat [2].

Even though we recover the results obtained from the continuum theory, the derivation of the slip length in terms of Green-Kubo expressions that we have derived here

	$B = 1$	$B = 2$	$B = 3$
$\eta$	0.479	0.836	0.843
$\nu_0 = \frac{\eta}{\rho^{\text{eq}}}$	0.792	1.388	1.400
$H$	0.25	0.014	0.001
$G$	0.374	0.544	0.544
$\gamma$	0.669	0.996	0.996
$z_{\text{wall}}$	2.662	2.655	2.655

**Table 6.1:** Values of the transport coefficients (6.46) for  $\tau = 0.3$  and for different widths  $B$  of the boundary slab. Note that the coefficient  $H_B$  is very small as it contains the correlation of the local stress tensor at the position  $\mu = B$  with the force.

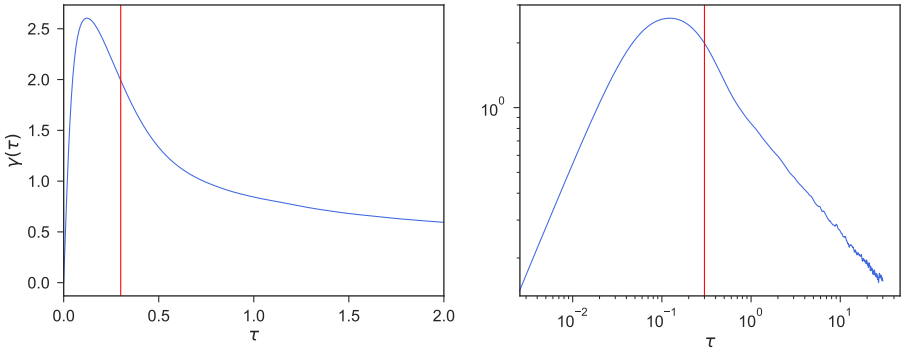


**Figure 6.10:** The total friction  $\gamma(\tau)$  as a function of the upper limit of integration of the running Green-Kubo integral (6.46). Inset is in logscale. The vertical line is at  $\tau = 0.3$  which is the time at which the corrected Green-Kubo expression displays a well-defined plateau.

from the discrete hydrodynamics gives an additional information that it was not evident in the continuum derivation presented by Camargo et al. in [84] or even in Bocquet and Barrat's derivation [2]. As it becomes apparent from the discussion, the transport coefficients defined in (6.46) depend on the upper limit of integration  $\tau$  and they do not show a well defined plateau. For example, we plot in Fig. 6.10 the friction coefficient  $\gamma(\tau)$  defined in (6.46) as a function of the upper limit of integration  $\tau$ . The absence of a plateau is obvious and concomitant to the absence of a plateau for the transport matrix  $\gamma_{\mu\nu}(t)$  in Fig. 6.3. Bocquet and Barrat [28] assumed that the thermodynamic limit would provide a cure for the plateau problem in the friction coefficient, but this is not correct. The solid-liquid friction coefficient  $\gamma(\tau)$  decays and does not display a plateau even in the thermodynamic limit. For example, as shown in Fig. 6.4, by doubling the

size of the channel does not modify the structure of the friction matrix  $\gamma_{\mu\nu}(\tau)$ , and hence of  $\gamma(\tau)$ . The strategy followed by Bocquet and Barrat of choosing the upper limit of the Green-Kubo running integral at the maximum of the friction coefficient may be a good first guess but clearly overestimates the actual friction coefficient.

The way to solve the plateau problem is to correct the Green-Kubo formula with the prescription in equation (6.14), as suggested in Chapter 4. This allows one to identify a well defined plateau in the matrix  $M^*$  and select a particular value  $\tau$  in the plateau region. With that value of the plateau time  $\tau$  we may use the usual uncorrected Green-Kubo formulae (6.46) but with the caveat of using the scaled velocity  $\bar{v}_\mu$  that contains information about  $\tau$  in its definition, as we have done in (6.22). Only in this way, one expects to have results that are independent of the actual value of  $\tau$ . It should be remarked that the slip boundary condition with slip length given by (6.48) should be applied to the scaled velocity field  $\bar{v}_\mu^x$  defined in equation (6.23), which depends on  $\tau$ .

Finally, we show in Fig. 6.11 the values of  $\eta'$ ,  $\gamma'$ ,  $\delta$  defined in (6.46) as a function of  $\tau$ . We observe that the coefficients  $\eta'$ ,  $\gamma'$  depend on  $\tau$ , but its ratio given by  $\delta$  is very insensitive to the value of  $\tau$ . We have also checked that  $z_{\text{wall}}$ , being a ratio between plateau problematic quantities, is also quite insensitive to the actual value of  $\tau$ . Note that, even though the range of  $\tau$  considered is small and limited by the explosive amplification of statistical errors involved in the inverse of the correlation matrix, it is sufficiently large to appreciate the decay of  $\eta'$ ,  $\gamma'$  due to the plateau problem, as shown in Fig. 6.11.

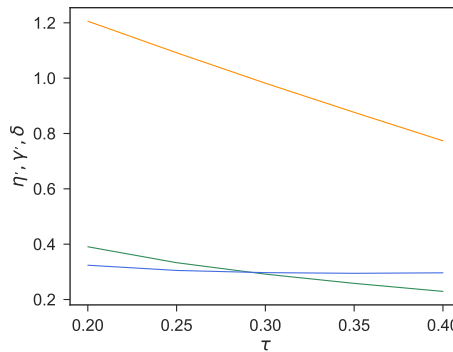


**Figure 6.11:** Dependence on the time  $\tau$  in the plateau region of  $\eta'$  (green),  $\gamma'$  (orange), and the slip length  $\delta$  (blue). Note that while  $\eta'$ ,  $\gamma'$  decay with  $\tau$  due to the plateau problem, its ratio given by the predicted slip length  $\delta$  in (6.48) is roughly constant.

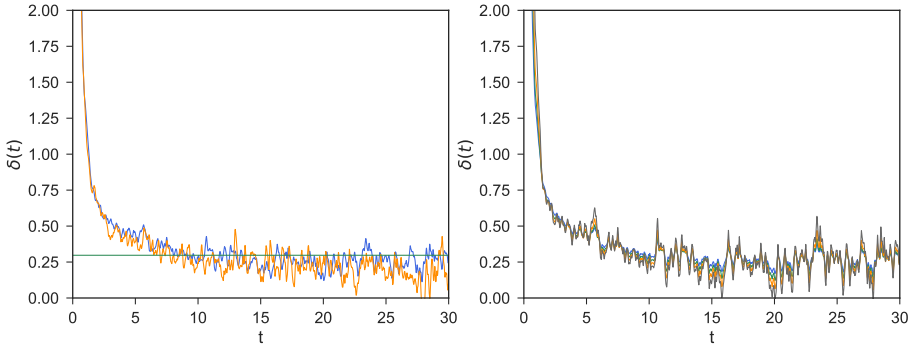


**Figure 6.12:** Left panel: The slip length  $\delta(t)$  as a function of time for the two channel widths considered. Note that only after a time  $\sim 2$  in reduced units, the total force  $F_B(t) \simeq 0$  (see Fig. 6.9) and we have a real balance between viscous and friction forces, leading to a constant nonzero slip length of  $\eta'/\gamma' = 0.29$  in reduced units (horizontal line). Right panel: The measured slip length (6.49) is obtained by adjusting  $\bar{v}_{\text{wall}}$  and  $\dot{\gamma}_{\text{wall}}$  to the scaled velocity profile  $\bar{v}_\mu$  in the boundary slab. For this reason it depends on the value of  $\tau$ . There are four curves superimposed, corresponding to  $\tau = 0.3, 0.4, 0.5, 0.6$ . Clearly, the measured slip length is roughly independent of the actual value of  $\tau$ .

#### 6.7.4 Validation of the slip boundary condition

We have obtained the slip boundary condition with a microscopic expression for the slip length but we have to see whether it is really satisfied in actual simulations. In order to see if the Navier slip boundary condition is satisfied by the nonequilibrium average initial plug flow considered in this chapter, we define the following time-dependent slip length

$$\delta(t) = \frac{\bar{v}_{\text{wall}}^x(t)}{\dot{\gamma}_{\text{wall}}(t)}, \quad (6.49)$$

where  $\bar{v}_{\text{wall}}^x(t)$  and  $\dot{\gamma}_{\text{wall}}(t)$  are measured from the actual velocity profiles. The way we have measured this flow parameters is as follows. First, note from Fig. 6.5 that the velocity field at short times is clearly not linear within the boundary slab. The discontinuous plug flow takes a while until an almost parabolic decaying profile is achieved. For this reason, we aim at using the smallest possible size  $B$  for the boundary slab that minimizes the non-linearity of the velocity within the boundary slab. The optimal choice is  $B = 2$ . Next, note from Fig. 6.8 that the nonlocal viscosity kernel  $\eta_{B\nu}$  is not zero for  $B = 2$  and  $\nu = 1, 2, 3$ . This implies that the force  $\mathbf{F}_B^x(t)$  in (6.32) depends on the values of the velocity  $\mathbf{v}_\mu^x$  at the nodes  $\mu = 1, 2, 3, 4$ . For this reason, we measure

$\bar{v}_{\text{wall}}^x(t)$  and  $\dot{\gamma}_{\text{wall}}(t)$  by adjusting a linear profile to the velocity at the four nodes near the wall. Note that the region where the velocity of the fluid affects the force on the boundary slab is rather large, around one quarter of the channel width. Note also that only at very long times, we expect the profile to be approximately linear within the boundary slab.

According to the slip boundary condition (6.41) the function  $\delta(t)$  should be given by the constant  $\eta'/\gamma'$ . We plot in Fig. 6.12 the measured  $\delta(t)$  as well as the constant value  $\eta'/\gamma'$ . We observe that the slip length decays towards  $\eta'/\gamma'$  after a time  $\approx 5$  in reduced units. This implies that the Navier slip boundary condition is *not* satisfied for the plug flow in the very initial stages of the flow field. This indicates that some of three assumptions i)-iii) used to derive the slip boundary conditions fail. As we know that i) is satisfied after a very short time around  $\tau = 0.3$  (see Fig. 6.6), the failure can only be attributed to ii) or iii). By observing Fig. 6.9 it is apparent that the force  $F_B(t)$  on the slab is non-zero at the early times  $0.3 < t < 2$  of the decay of the plug flow and this explains in part the violation of the slip boundary condition. However, even though the force has decayed to zero beyond  $t = 2$  the slip length  $\delta(t)$  still has not decayed to its predicted value. Therefore, we attribute the violation of the slip boundary condition for  $t < 5$  to the non-linear velocity profile within the boundary slab, as can be seen in the right panel of Fig. 6.5.

We have shown in Fig. 6.11 how the predicted slip length is insensitive to the value of  $\tau$ . In the right panel of Fig. 6.12 we show that the measured slip length is also insensitive to the value of  $\tau$ , even though the two parameters  $\bar{v}_{\text{wall}}^x(t)$  and  $\dot{\gamma}_{\text{wall}}(t)$  are obtained by a linear fitting of the scaled velocity  $\bar{v}^x$  that depends on  $\tau$  as shown in its definition (6.23). Together with the result that the predicted slip length given in (6.41) is independent of  $\tau$  this gives confidence on the correctness of the approach that we have taken.

Finally, Petracic and Harrowell [33] have raised the concern about the possible dependence of the friction coefficient  $\gamma$  defined in (6.46) on the channel width. If the solid-fluid friction coefficient would depend on the width of the channel, it could not be attributed to an intrinsic surface property. In order to answer to this question we have repeated the simulations for a channel with twice the width and twice the number of bins, in such a way that the bin width is the same in both simulations. As shown in Figs. 6.4 the transport matrices  $\eta_{\mu\nu}(\tau), G_{\mu\nu}(\tau), H_{\mu\nu}(\tau), \gamma_{\mu\nu}(\tau)$  take exactly the same values for the bins near to the walls in both channels. In the left panel of Fig. 6.12 the time-dependent slip length (6.49) for the two channel widths is plotted. Clearly, the slip length that we obtain is independent on the channel width.

## 6.8 A local hydrodynamic model with boundary conditions

In Sec. 6.7, we have predicted that the velocity and the velocity gradient at the wall position  $z_{\text{wall}}$  are proportional to each other, with the constant of proportionality given by the slip length  $\delta$ . Both  $\delta$  and  $z_{\text{wall}}$  have microscopic expressions. We have observed that this prediction is very good once the velocity field is well approximated by a linear profile inside the boundary layer and the total force on the boundary layer is vanishingly small. The fulfillment of this flow property is a nice phenomenological observation, and the theoretical prediction of the resulting slip length is an achievement, but the real interest lies in the possibility of formulating a boundary condition. A boundary condition is useful if one wants to solve the hydrodynamic equations *without having to take into account all the interactions of the fluid with the solid*.

In this section, we assess the prediction given by the local hydrodynamic equation described by the tangential component of the Navier-Stokes equation

$$\partial_t g(z, t) = \nu \frac{\partial^2}{\partial z^2} g(z, t) \quad (6.50)$$

with the slip boundary condition (6.40) applied at  $z_{\text{wall}}$ . The kinematic viscosity is given by  $\nu = \eta/\rho$ . As shown in Chapter 3, a Petrov-Galerkin discretization of the partial differential equation (6.50) takes the form

$$\frac{d}{dt} g_\mu(t) = \nu \frac{1}{\Delta z^2} (g_{\mu-1}(t) + g_{\mu+1}(t) - 2g_\mu(t)) \quad (6.51)$$

This equation is to be compared with the *nonlocal* hydrodynamic equation (6.25) that we know, from the results obtained so far, that describes very well the dynamics of the system. Therefore, a natural question is how one can obtain the discrete local hydrodynamic equation (6.51) from the nonlocal equation (6.25).

As we take the point of view that all the effects of the walls will be taken into account through the boundary condition, we neglect in (6.25) the terms containing  $G_{\mu\nu}, H_{\mu\nu}, \gamma_{\mu\nu}$  that represent the interaction of the fluid with the wall. In addition, we will assume that the nodes  $\mu = 2, \dots, 15$  are fluid nodes for which the fluid properties are those of the bulk fluid. We observed in Chapter 4 that the hydrodynamics of an unconfined fluid is reasonable local at long times, which amounts to approximate the viscosity matrix with a diagonal matrix of the form

$$\eta_{\mu\nu}(\tau) \simeq \frac{\delta_{\mu\nu}}{\mathcal{V}_\mu} \eta_\mu(\tau), \quad (6.52)$$

where the local viscosity is defined in a consistent way as

$$\eta_\mu(\tau) \equiv \sum_{\sigma} \mathcal{V}_{\sigma} \eta_{\mu\sigma}(\tau) \quad (6.53)$$

With this particular definition, if we sum both sides of (6.52) we get the same result. We further assume that  $\eta_\mu(\tau)$  is the same for all  $\mu$  in the fluid region, say equal to  $\eta_8(\tau)$  in the middle of the channel. We also assume a local approximation for the correlation matrix

$$C_{\mu\nu}(\tau) \simeq \frac{\delta_{\mu\nu}}{\mathcal{V}} k_B T \rho_\mu(\tau), \quad (6.54)$$

where we introduce the local scaled density as

$$\rho_\mu(\tau) = \sum_{\sigma} \frac{\mathcal{V} C_{\mu\sigma}(\tau)}{k_B T} \quad (6.55)$$

The momentum and the velocity are related through the matrix equation (6.23). In the local approximation (6.54) we have

$$g_\mu \simeq \rho_\mu(\tau) \bar{v}_\mu \quad (6.56)$$

We then insert in (6.25) the local approximations (6.52), (6.56) to obtain the equations (6.51) for the fluid nodes  $\mu = 2, \dots, 15$

$$\begin{aligned} \frac{dg_2}{dt} &= \nu \frac{g_3 + g_1 - 2g_2}{\Delta z^2} \\ \frac{dg_3}{dt} &= \nu \frac{g_4 + g_2 - 2g_3}{\Delta z^2} \\ &\vdots & \vdots \\ \frac{dg_{14}}{dt} &= \nu \frac{g_{15} + g_{13} - 2g_{14}}{\Delta z^2} \\ \frac{dg_{15}}{dt} &= \nu \frac{g_{16} + g_{14} - 2g_{15}}{\Delta z^2} \end{aligned} \quad (6.57)$$

We have introduce the kinematic viscosity as give by  $\nu = \eta_\mu(\tau)/\rho_\mu(\tau)$  that takes the value  $\nu = 1.41$ . Even though  $\eta_\mu(\tau)$  and  $\rho_\mu(\tau)$  depend on  $\tau$  and  $\mu$ , the kinematic viscosity is constant and does not depend on  $\tau$  and  $\mu$ . We see that (6.57) is a set of ODE for the variables  $g_\mu$  for  $\mu = 2, \dots, 15$  but it includes in the first and last equations

the values  $g_1, g_{16}$  that are undetermined. They should be fixed, of course, through the boundary condition, as follows.

If we define  $h$  as the distance between node 1, where the outer crystalline plane lies, and the position  $z_{\text{wall}}$  of the wall, the velocity at the wall is given by the linear interpolation

$$\begin{aligned}\bar{v}_{\text{wall}} &= \bar{v}_1 + \dot{\gamma}_{\text{wall}} h \\ \dot{\gamma}_{\text{wall}} &= \frac{\bar{v}_2 - \bar{v}_1}{\Delta z}\end{aligned}\quad (6.58)$$

Therefore, the slip boundary condition (6.40) takes the form, for the lower wall

$$\bar{v}_1 + \frac{\bar{v}_2 - \bar{v}_1}{\Delta z} h = \delta \frac{\bar{v}_2 - \bar{v}_1}{\Delta z} \quad (6.59)$$

This allows to infer the value of  $\bar{v}_1$  as a function of  $\bar{v}_2$

$$\bar{v}_1 = \frac{\epsilon}{\epsilon - 1} \bar{v}_2, \quad (6.60)$$

where  $\epsilon = (h - \delta)/\Delta z$  is a dimensionless number. A similar expression is obtained for the upper wall

$$\bar{v}_{16} = \frac{\epsilon}{\epsilon - 1} \bar{v}_{15} \quad (6.61)$$

In terms of the momentum we have

$$g_1 = \frac{\epsilon}{\epsilon - 1} g_2, \quad g_{16} = \frac{\epsilon}{\epsilon - 1} g_{15} \quad (6.62)$$

By inserting these expressions in (6.57) one obtains a closed ODE for the set of values  $g_\mu, \mu = 2, \dots, 15$ . This ODE can be expressed in matrix form as

$$\frac{d}{dt} g = \nu \Delta' g, \quad (6.63)$$

where the discrete Laplacian operator for slip boundary conditions is given by

$$\Delta' = \frac{1}{\Delta z^2} \begin{pmatrix} -\beta & 1 & 0 & \cdots & 0 \\ 1 & -2 & 1 & \cdots & 0 \\ \vdots & & \ddots & & \vdots \\ 0 & \cdots & 0 & 1 & -\beta \end{pmatrix}, \quad (6.64)$$

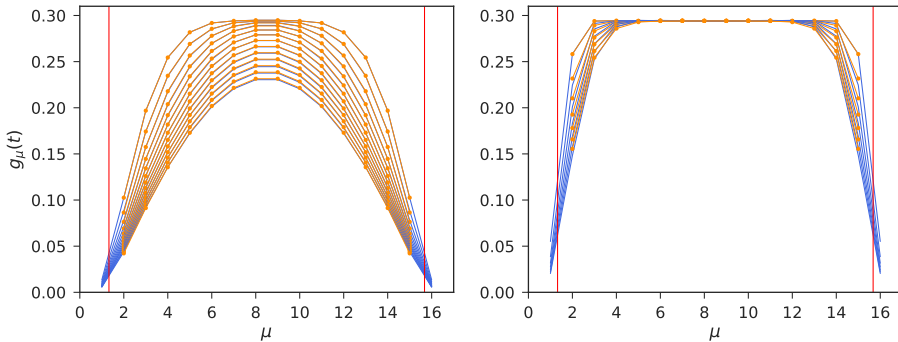


**Figure 6.13:** Left panel: Local prediction (6.67) with  $v = 1.41$  fixed from (6.53) and the slip boundary condition given in (6.41) (orange) compared with the measured momentum density profile (blue). There are no adjustable parameters in this comparison. Times are  $t = 5, 7, \dots, 29$  in descending order. The initial condition is the measured moment profile at time  $t = 5$ . Right panel: The same but with the initial condition given at  $t = 0.3$  and times  $t = 0.3, 0.6, \dots, 2.1$ .

where we have introduced the parameter

$$\beta = \frac{\epsilon - 2}{\epsilon - 1} \quad (6.65)$$

that contains the information about the slip boundary condition.

The solution of the linear equation (6.63) is given by the matrix exponential

$$g(t) = \exp\{\nu\Delta't\}g(0) \quad (6.66)$$

As we know that a Markovian description cannot hold at very short times, we will compare the MD results with the solution with initial condition at time  $\tau$ , this is

$$g(t) = \exp\{\nu\Delta'(t-\tau)\}g(\tau) \quad (6.67)$$

We then compare this prediction of local hydrodynamics plus microscopically derived slip boundary condition with the measurement of the discrete momentum. The comparison is given in Fig. 6.13, where we observe an excellent agreement. Note that there are no adjustable parameters in this prediction. Both the kinematic viscosity and the slip length which enter the local hydrodynamic equations are measured through well-defined Green-Kubo expressions.

A close inspection, however, reveals an appreciable discrepancy between measured and predicted values for the nodes near the wall and for times  $t < 5$ . In Fig. 6.14 in the

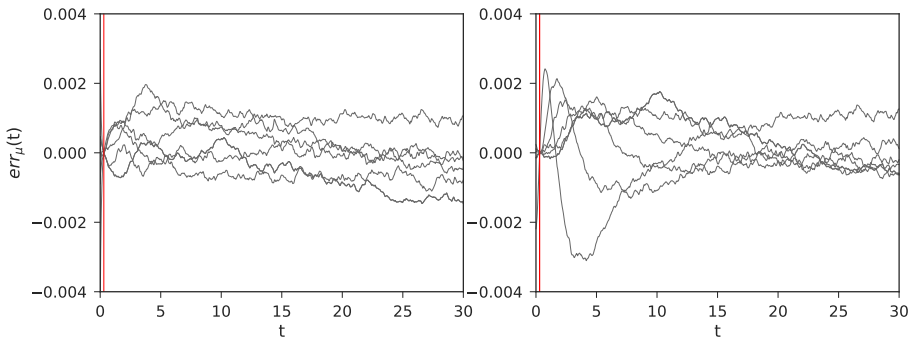


**Figure 6.14:** Comparison of the error between local and nonlocal theories. The error  $err_\mu(t) = g_\mu(t) - g_\mu^{\text{predict}}(t)$  between the real and predicted profiles as a function of time. Every curve corresponds to a different node  $\mu$ . Left panel is for the error with the nonlocal prediction corresponding to Fig. 6.6. The right panel is for the error with the local prediction corresponding to Fig. 6.13. Vertical red line is at  $t = \tau$  where the error is zero by construction.

right panel we plot the discrepancy  $err_\mu(t) = g_\mu(t) - g_\mu^{\text{predict}}(t)$  between the measured profile and the local prediction. A systematic error for the nodes close to the walls is clearly seen. This is attributed to the fact that at early times, neither the total force on the boundary slab is equilibrated, nor the velocity profile is linear inside the boundary slab. Therefore, the slip boundary condition used to predict the flow does not hold. This gives unaccurate predictions for the local theory for a highly discontinuous profile like the plug flow. To get better prediction it is necessary to consider the explicit interaction between the solid and the fluid through the surface irreversible forces containing the transport kernels  $G_{\mu\nu}, H_{\mu\nu}, \gamma_{\mu\nu}$ . The errors in using the nonlocal prediction are shown in the left panel of Fig 6.14. The conclusion is that while the local prediction with a slip boundary condition is acceptable, nonlocal effects are appreciable for a plug flow near the wall at short times.

## 6.9 Summary

In this chapter we have considered the discrete hydrodynamic equations of Chapter 3 for the case of flows along the parallel walls confining the fluid. The resulting discrete equations correspond to a Petrov-Galerkin finite element discretization of the continuum theory presented in Chapter 2 for parallel flows. We have computed from equilibrium MD simulations the transport matrices entering the discrete hydrodynamic

equations. Their continuum counterparts are nonlocal viscosity and nonlocal frictions. The friction forces in the hydrodynamic equations capture explicitly the interaction of the fluid with the solid. The transport matrices are defined in terms of Green-Kubo formulas that suffer dramatically from the plateau problem. Therefore, we have used the methodology presented in Chapter 4 in order to re-define the transport matrices in terms of corrected Green-Kubo formulas that exhibit a well-defined plateau. This amounts to using the plateau problematic transport matrices with an upper limit of integration  $\tau$  in the plateau region of the corrected Green-Kubo expressions, and using a scaled velocity field that compensates for the decaying transport matrices. With the input of the measured transport matrices in the hydrodynamic equations we are able to predict the decay of an initial plug flow. This flow is particularly challenging as it is unsteady and discontinuous near the wall at the initial time. By comparing with measurements of the average of the decay of the plug flow in MD simulations we observe that the nonlocal equations predict the evolution of this flow with great accuracy. Only at very short times (of molecular size) the prediction is inaccurate due the failure of the Markovian approximation at those short times.

We next consider the derivation of the slip boundary condition. We adapt the pillbox argument presented in Ref. [84] for the derivation of the slip boundary condition from the continuum hydrodynamic theory of Chapter 2 to the case of the present planar geometry and discrete hydrodynamics. The notion of pillbox is played in the present chapter by the concept of boundary slab, a portion of fluid near the wall on which a mechanical balance is satisfied provided that the discrete momentum field obeys the discrete hydrodynamic equations. Hansen et al. [34] used also the idea of a boundary slab, and they proposed a generalized Langevin equation for the motion of the slab in order to identify a friction. The derivation in the present chapter, which is based on the hydrodynamics in the full channel, gives not only the friction coefficient, but also the position of the wall where to apply the boundary condition, in microscopic terms.

In addition to the validity of the Markovian discrete hydrodynamics, two assumptions are required in order to obtain the slip boundary condition from the mechanical balance. The first is the assumption that the total force on the slab vanishes. This is not always true and, in particular, we observe that for the decay of the plug flow, the initial stages of evolution of the flow give a non-zero force on the slab. The second assumption required for the validity of the slip boundary condition is that the velocity profile is linear within the boundary layer. In this way, the mechanical balance imposes a restriction between the two parameters of the velocity field, which are the velocity at the wall and the shear rate at the wall position. The wall position is, in turn, defined microscopically from the friction matrix, giving an unambiguous definition of the wall position for a collection of points in a lattice that are centers of singular forces. The velocity profile is expected to be approximately linear if the boundary slab is not too

large. There is an optimal width of the boundary slab, around  $4\sigma$ , that is sufficiently large for capturing all the interactions with the wall but sufficiently small for a linear flow approximation to be valid. Nevertheless, we also observe that for the initial stages of the decay of the plug flow, the velocity field within the boundary slab is clearly non-linear. Therefore, at the initial stages the slip boundary condition is not satisfied by the plug flow because both, the force on the boundary slab does not vanish and the velocity field is not linear.

At later stages, we observe that the slip boundary condition is well satisfied for the decay of the plug flow and that the value of the slip length is very well predicted by our theory. The slip length that emerges from the mechanical balance argument is given in terms of microscopic expressions that involve Green-Kubo formulas for the viscosity and friction coefficients. The slip length predicted by the discrete hydrodynamic theory coincides with the slip length predicted from the continuum hydrodynamic theory obtained in [84]. As it was mentioned in the introduction to this chapter, the microscopic expressions for the slip boundary condition coincide with the ones proposed in the seminal paper by Bocquet and Barrat [2, 28] under a suitable redefinition of the wall position. Despite this nice match of theoretical results, we emphasize that the present derivation resolves the issue of the plateau problem that was overlooked in Refs. [2, 28] and also by Camargo et al. in [84]. In fact, we have shown that the Green-Kubo expressions for the viscosity  $\eta$ , the friction coefficient  $G$  and the friction coefficient  $\gamma$  entering the slip length all decay towards zero in an algebraic way, and one needs to correct these Green-Kubo integrals with the method presented in Chapter 4. Quite coincidentally, as the slip length is a ratio of two decaying transport coefficients, it is quite insensitive to the value of the upper limit of integration of the Green-Kubo running integrals. The same is true for the definition of the hydrodynamic position of the wall, where the boundary condition is to be applied. This is quite fortunate because it allows, in practical situation, to measure the slip length from plateau problematic Green-Kubo expressions.

The methodology that we have presented in order to derive the slip boundary condition is very different from either linear response theory [2, 33], the generalized Langevin equation [34], or the comparison of measured correlation functions with local predictions [39, 40]. As far as the controversy raised by Petracic and Harrowell about the validity of the friction coefficient obtained by Bocquet and Barrat we are still quite puzzled. The results of Petracic and Harrowell for the friction coefficient display a well defined plateau. This is very strange, as we know that such a friction coefficient *should* decay to zero at long times. We have not been able to track down the origin of this problem but a possible explanation lies in the use by Petracic and Harrowell of a thermostat applied to all fluid particles in the simulations, as this has been shown to have an effect [121].

The phenomenological observation of the validity of the slip boundary condition at the late stages of the plug flow, and the agreement with the theoretical prediction are nice interesting results. However, the usefulness of a boundary condition emerges from the fact that it can be used as a way to completely bypass the interactions of the fluid with the solid wall when solving the partial differential equations of a fluid contained by walls. For this reason, we solve the Navier-Stokes equations for these particular flow problem with the input of the microscopically derived slip boundary condition. As a first step, we derive the Navier-Stokes equation for parallel flow from the nonlocal equations. This is done by taking a local approximation for the viscosity kernel in the nonlocal discrete hydrodynamic equations. We also neglect the friction forces that appear in the discrete equations. The resulting discrete equations can be understood as a finite element discretization of the Navier-Stokes equations for a parallel flow. Of course, the equations are not closed for the set of velocities in the fluid region. The closure of the equations comes precisely from the boundary condition. We observe that the solution of the local Navier-Stokes equation with slip boundary condition gives accurate predictions for the decaying plug flow at late stages of the flow, precisely for those in which the slip boundary condition is valid. This implies that for this late stages, the hydrodynamics is local, an observation that is akin to what we observed for unconfined fluids in Chapter 4. However, at short times of the highly discontinuous plug flow the predictions of the Navier-Stokes equations are not accurate. One has to recourse in that case to the nonlocal theory with explicit account of the extended friction forces that the solid exerts on the fluid. Such a theory, as we have seen, gives excellent results even for the very early stages of the plug flow.

The size  $2\sigma$  of the bins that are used in the present work are pretty large in molecular terms. In particular, it blurs completely the density layering near the walls as it is shown in Fig. 5.13. The reason for using these large bins is the observation made in Chapter 5 that the dynamics for smaller bins is non-Markovian near the walls. As we are interested precisely in the derivation of boundary conditions near walls with a Markovian theory, we are forced to use large bins. However, even these large bins still display nonlocal effects. For example, the nonlocal viscosity transport matrix has a support of three bins or a length scale of  $\sim 5\sigma$  and the friction extend over two bins ( $4\sigma$ ). As mentioned above, such nonlocal effects are needed in order to describe the initial stage of a discontinuous plug flow. It is quite remarkable that the friction force on the optimal boundary slab that we have considered, and that has a size of  $4\sigma$ , depends on the velocity field at rather large distances of the order of  $8\sigma$ . This is due to the wide range of the viscosity kernel. The support of this viscosity kernel is determined by the length at which the stress tensor is correlated. As the microscopic stress tensor is defined in terms of pairs of particles, and the range of the interactions is determined by the cutoff  $2.5\sigma$  of the LJ potential, correlations are expected at a length scale of  $5\sigma$  for those pairs that have

a common particle. This explains the relatively large range of the viscosity kernel. Of course, for very smooth velocity fields, the nonlocality of the viscosity kernel may be approximated with a local viscosity.

# **Chapter 7**

## **Conclusions**

The present dissertation has addressed the formulation of hydrodynamics near solid walls in order to describe the phenomena of slip and its theoretical foundation. As a first step, we propose in Chapter 2 a continuum hydrodynamic theory derived with the Kawasaki-Gunton operator method that considers the interaction of a fluid with a solid sphere. In this theory the solid exerts both, reversible forces that forbid the penetration of the fluid inside the solid, and irreversible forces concentrated in the vicinity of the solid that describe the friction between the wall and the fluid. In principle, the equations are nonlocal in space and would describe the layering of the density field near the walls, thus generalizing Density Functional Theory for simple fluids to nonequilibrium situations. However, we have observed in Chapter 5 that in the strict continuum limit, the Markov assumption implicit in the derivation of the hydrodynamic equations breaks down near the walls. Only if one defines the hydrodynamic variables with an implicit length scale by using, for example, coarse  $\delta$  functions instead of Dirac  $\delta$  functions, one may expect the Markov assumption to hold.

One can reproduce step by step the procedure in Chapter 2 in order to obtain the hydrodynamic theory for these coarse hydrodynamic variables. The resulting hydrodynamic equations are formally identical to the hydrodynamic equations obtained in 2, but with a coarse-grained free energy functional which is different from the usual density functional of DFT. In particular, due to the coarser definition of the density, it does not allow one to describe the density layering near a wall.

In order to validate through MD simulations the hydrodynamic theory presented in Chapter 2, we have formulated a discrete hydrodynamic theory for planar flows between two solid walls. This theory can be understood as a finite element discretization of the continuum hydrodynamic theory of Chapter 2 when restricted to planar flows. The

discrete hydrodynamic theory introduces an intrinsic length scale given by the size of the bins in which space is discretized. In counterdistinction to the continuum theory presented in Chapter 2, the discrete theory of Chapter 3 allows for its validation through MD simulations.

In Chapter 4, we have considered the correlations of the discrete momentum of an unconfined fluid in periodic boundary conditions with no solid walls. This has allowed us to discuss the locality of hydrodynamics in time (i.e. the Markovian assumption) and how it is related to locality in space. Quite remarkably we show there that the Green-Kubo formula for the nonlocal viscosity kernel suffers dramatically from the plateau problem. In Sec. 4.2 of Chapter 4, we have shown that the plateau problem is due to the fact that the Green-Kubo formula defined in terms of the unprojected dynamics decays as the correlation of the CG variables. This suggest itself as a way to correct the Green-Kubo formula. The new corrected Green-Kubo formula has a well defined plateau that allows one to obtain unambiguously the transport coefficients. By using the corrected Green-Kubo expressions we obtain in Chapter 4 the explicit forms of the nonlocal viscosity. With this measured viscosity kernel, we predict correctly the evolution of the correlation matrix of the transverse momentum. We also show that for the times in which the hydrodynamics is well described by the Markovian approximation, i.e. locality in time, it is also well described with a local approximation in space.

In Chapter 5, we have shown that the shear flow dynamics in fluids confined between planar walls is not Markovian if the bins in which the fluid is divided are too thin, below the molecular scale dictated by  $\sigma$ . Non-Markovian effects are detected from the non-exponential decay of the eigenvalues of the correlation matrix. An important conclusion of this chapter is that the non-Markovian effects are clearly identified as originating near the walls. For bins larger than the molecular size, the dynamics becomes fully Markovian but the layering near the walls is lost.

Finally, in Chapter 6, we have measured, through equilibrium MD simulations, the nonlocal transport kernels that appear in the discrete hydrodynamic equations derived in Chapter 3. After observing that they suffer from the plateau problem, we have used the method presented in Chapter 4 for realibly extract the transport kernels out of the plateau-problematic Green-Kubo formula. We have obtained excellent predictions with these kernels for the decay of the average of the transverse momentum in a channel configuration when the initial velocity profile is a plug flow. We infered the slip boundary condition with a well-defined microscopic definition for the slip length and the location of the hydrodynamic position of the atomic wall. The microscopic expression for the slip length obtained coincides with the one originally proposed by Bocquet and Barrat [2]. We also have shown that the slip length does not depend on the channel width, thus demonstrating that the friction coefficient is an intrinsic surface

property. We have observed violations of the slip boundary condition for the initial stages of the plug flow. These are attributed to two effects. First, the force on the slab of fluid is not zero and, therefore, there is no exact balance between shear and friction forces, which is at the basis of the slip boundary condition. Second, the flow field is parabolic, not linear, within the slab of the fluid. Only when the flow has decayed sufficiently it is possible to approximate the parabolic profile with a linear one. Then the slip boundary condition holds very well.

A general final conclusion of this dissertation is that in order to talk about slip boundary conditions in nano-confined fluids, one should ensure that the hydrodynamic equations on which this boundary condition will be applied are valid at those scales. Only for supramolecularly resolved hydrodynamics one expects a Markovian hydrodynamic theory. Talking about slip in highly confined fluids like those in the interior of a carbon nanotube may not be entirely appropriate.



# Chapter 8

## Future Directions

In this dissertation we have presented an isothermal theory for a fluid in contact with a solid. In the MD simulations presented to validate the theory, the solid is treated as a frozen crystal where the atoms remain at fixed positions of space. One issue that needs to be addressed in the future is whether the non-Markovian effects observed may be related to the “hard” nature of the crystal. This issue may be addressed by using more realistic models for the solid wall in which the bonded atoms may still be subject to vibrations in such a way that transport of elastic energy may occur. The results in the present dissertation have been obtained at a particular thermodynamic point and we have not investigated what is the effect of changing the temperature or the density in the results. On the other hand, we have assumed that the parameters of the potential between crystal and the fluid atoms is the same as that of fluid and fluid atoms. Changing the strength of the former may allow to discuss how the attraction of the wall, related to the degree of hydrofobicity or hydrophilicity of the fluid, affects the conclusions reached so far. These issues, that are computationally very intensive, should be considered in the future.

Finally, a natural extension of this work is to derive a non-isothermal theory in which the CG relevant variables are, in addition to the mass and momentum densities presented in Chapter 2, the energy density of the fluid and the total energy of the solid, that is

$$\hat{e}_{\mathbf{r}}(z) = \sum_i^N e_i \delta(\mathbf{r} - \mathbf{q}_i) \quad \hat{E}(z) = \sum_{i'}^{N'} e_{i'}, \quad (8.1)$$

where  $e_i$  and  $e'_{i'}$  are the total energy of the fluid particle  $i$  and the total energy of the solid particle  $i'$ , respectively. With these new variables, we should be able to address

the problem of thermal boundary conditions and, in particular, the Kaptiza resistance. It is uncertain at these moment if the Kaptiza resistance, that plays the role of the solid-fluid friction coefficient for thermal effects, is also subject to the same issues (plateau problem and lack of Markovianicity at short scales) as the friction coefficient itself.

The interest behind the thermal aspects of the problem (and the original motivation of this dissertation) is to understand the heat transfer between solids and fluids, specifically between nanoparticles and molten salts. The industry has a high interest in the study of mixtures of molten salts with nanoparticles in order to use them as a storage thermal fluid in solar plants [122–126]. They have low toxicity and melting point, and high specific heat capacity which can be increased depending on the type and percentage by weight of the nanoparticles added. It has been observed an enhancement of 20% in the specific heat capacity of a solar salt<sup>i</sup> due to the introduction of silica and alumina nanoparticles [127].

There are a lot of experimental publications in which an enhancement in the specific heat of a molten salt due to the introduction of nanoparticles [123, 127, 128] is observed, but there is not a clear physical explanation for such an effect. This fascinating subject requires for its understanding a theoretical framework like the one proposed in the present dissertation, as well as a methodology similar to the one followed here.

---

<sup>i</sup>Molten salts consisting of 60-wt.% NaNO<sub>3</sub> and 40-wt.% KNO<sub>3</sub>.

# Bibliography

- [1] K. LLaneras. Los amigos se hacen antes de los treinta. *Jot Down*, 2018.
- [2] L. Bocquet and J. L. Barrat. Hydrodynamic boundary conditions, correlation functions, and Kubo relations for confined fluids. *Physical Review E*, 1994.
- [3] R. P. Feynman. There's Plenty of Room at the Bottom. *Engineering and Science*, XXIII(5):22–36, 1960.
- [4] Editorial: 'Plenty of room' revisited. *Nature Nanotechnology*, 4(12):781, 2009.
- [5] C. Tourney. Feynman into Nanotechnology: A text for a New Science. *Techné*, 13(3):133–168, 2008.
- [6] I. Asimov. *Fantastic vayage*. Houghton Mifflin, 1966.
- [7] J. Zheng. Layout of Nanotechnology Patents in Global Market. *Advanced Materials Research*, 889-890:1578–1584, 2014.
- [8] S. Nazir, T. Hussain, A. Ayub, U. Rashid, and A. J. MacRobert. Nanomaterials in combating cancer: Therapeutic applications and developments. *Nanomedicine: Nanotechnology, Biology, and Medicine*, 10(1):19–34, 2014.
- [9] E. C. Dreaden and M. A. El-sayed. than One Way with Noble Metals and Different Confinement Properties on the Nanoscale. *Accounts of chemical research*, 45(11):1854–1865, 2012.
- [10] F. M. Kievit and M. Zhang. Surface engineering of iron oxide nanoparticles for targeted cancer therapy. *Accounts of Chemical Research*, 44(10):853–862, 2011.
- [11] L. Bocquet and E. Charlaix. Nanofluidics, from bulk to interfaces. *Chemical Society Reviews*, 39(3):1073–1095, 2010.

- [12] G. Karniadakis, A. Beskok, and N. Aluru. *Microflows and Nanoflows, Fundamental and Simulation*. Springer Science + Business Media, Inc., 2005.
- [13] E. Lauga, M. P. Brenner, and H. A. Stone. *Handb. Exp. Fluid Dyn.* Springer, 2007.
- [14] L. Bocquet and E. Lauga. A smooth future? *Nature Materials*, 10:334, apr 2011.
- [15] J. Koplik and J. R. Banavar. Continuum Deductions from Molecular Hydrodynamics. *Annual review of Fluid Mechanics*, 27:257–292, 1995.
- [16] G.J. Wang and Ni. G. Hadjiconstantinou. Molecular mechanics and structure of the fluid-solid interface in simple fluids. *Physical Review Fluids*, 2(9):1–18, 2017.
- [17] R Evans. The nature of the liquid-vapour interface and other topics in the statistical mechanics of non-uniform , classical fluids. 1979.
- [18] H Lowen. Density functional theory : from statics to dynamics. *Journal of Physics: Condensed Matter*, 15:V1–V3, 2003.
- [19] R. Evans, M. Oettel, R. Roth, and G. Kahl. New developments in classical density functional theory. *Journal of Physics: Condensed Matter*, 28(24):240401, 2016.
- [20] U. Marconi and P. Tarazona. Dynamic density functional theory of fluids. *J. Phys. Condens. Matter*, 12(A413), 2000.
- [21] Z. Guo, T. S. Zhao, and Y. Shi. Generalized hydrodynamic model for fluid flows: From nanoscale to macroscale. *Physics of Fluids*, 18(6), 2006.
- [22] P. Espa  ol and H. L  wen. Derivation of dynamical density functional theory using the projection operator technique. *Journal of Chemical Physics*, 131(24), 2009.
- [23] Matthias Schmidt and Joseph M. Brader. Power functional theory for Brownian dynamics. *Journal of Chemical Physics*, 138(21), 2013.
- [24] B. D. Goddard, A. Nold, N. Savva, G. A. Pavliotis, and S. Kalliadasis. General dynamical density functional theory for classical fluids. *Physical Review Letters*, 109(12):1–5, 2012.
- [25] J. P. Hansen and I. R. McDonald. *Theory of simple liquids*. Academic Press, 2013.

- [26] G. Batchelor. *An introduction to Fluid Dynamics*. Cambridge University Press, 1967.
- [27] M. Navier. Mémoire sur les lois du Mouvement des Fluides. *Mémoires de l'Académie Royale des Sciences de l'Institut de France*, pages 389–440, 1823.
- [28] Lydéric Bocquet and Jean Louis Barrat. On the Green-Kubo relationship for the liquid-solid friction coefficient. *Journal of Chemical Physics*, 139(4), 2013.
- [29] L. Bocquet and J. Barrat. Large Slip Effect at a Nonwetting Fluid-Solid Interface. *Phys. Rev. Lett.*, 82(23), 1999.
- [30] L. Bocquet and J. L. Barrat. Flow boundary conditions from nano- to micro-scales. *Soft Matter*, 3(6):685–693, 2007.
- [31] Alexander E. Kobryn and Andriy Kovalenko. Molecular theory of hydrodynamic boundary conditions in nanofluidics. *Journal of Chemical Physics*, 129(13), 2008.
- [32] A. E. Kobryn and A. Kovalenko. Slip boundary conditions in nanofluidics from the molecular theory of solvation. *Molecular Simulation*, 37(8):733–737, 2011.
- [33] J. Petracic and P. Harrowell. On the equilibrium calculation of the friction coefficient for liquid slip against a wall. *Journal of Chemical Physics*, 127(17), 2007.
- [34] J. S. Hansen, B. D. Todd, and Peter J. Daivis. Prediction of fluid velocity slip at solid surfaces. *Physical Review E - Statistical, Nonlinear, and Soft Matter Physics*, 84(1):1–8, 2011.
- [35] K. Huang and I. Szlufarska. Green-Kubo relation for friction at liquid-solid interfaces. *Physical Review E - Statistical, Nonlinear, and Soft Matter Physics*, 2014.
- [36] B. Ramos-Alvarado, S. Kumar, and G. P. Peterson. Hydrodynamic slip in silicon nanochannels. *Physical Review E*, 93(3):1–8, 2016.
- [37] S. K. Kannam, B.D. Todd, J . S. Hansen, and J. Daivis. Slip length of water on graphene: Limitations of non-equilibrium molecular dynamics simulations. *The Journal of Chemical Physics*, 136, 2012.
- [38] R. Bhaduria, T. Sanghi, and N. R. Aluru. Interfacial friction based quasi-continuum hydrodynamical model for nanofluidic transport of water. *Journal of Chemical Physics*, 143(17), 2015.

- [39] S. Chen, H. Wang, T. Qian, and P. Sheng. Determining hydrodynamic boundary conditions from equilibrium fluctuations. *Physical Review E - Statistical, Nonlinear, and Soft Matter Physics*, 92(4):1–11, 2015.
- [40] L. Bocquet and J. L. Barrat. Hydrodynamic boundary conditions and correlation functions of confined fluids. *Physical Review Letters*, 70(18):2726–2729, 1993.
- [41] B. Robertson. Equations of motion in nonequilibrium statistical mechanics. *Physical Review*, 144(1):151–161, 1966.
- [42] R. A. Piccirelli. Theory of the dynamics of simple fluids for large spatial gradients and long memory. *Physical Review*, 175(1):77–98, 1968.
- [43] K. Kawasaki and J. Gunton. Theory of Nonlinear Transport Processes: Nonlinear Shear Viscosity and Normal Stress Effects. *Physical Review A*, 8(4):2048–2064, 1973.
- [44] H. Mori. Transport, Collective Motion, and Brownian Motion. 33(3), 1965.
- [45] D. Rickles. *The Philosophy of Physics*. Wiley, 2016.
- [46] A. Einstein. Über die von der molekularkinetischen Theorie der Wärme geforderte Bewegung von in ruhenden Flüssigkeiten suspendierten Teilchen. *Annalen der Physik*, 322(8):549–560, 1905.
- [47] L. Onsager. Reciprocal relations in irreversible processes. II. *Physical Review*, 405:2265, 1931.
- [48] J. G. Kirkwood. The statistical mechanical theory of transport processes I. General theory. *The Journal of Chemical Physics*, 14(3):180–201, 1946.
- [49] M. S. Green. Markoff Random Processes and the Statistical Mechanics of Time-Dependent Phenomena. *The Journal of Chemical Physics*, 20(8):1281–1295, 1952.
- [50] M.S. Green. Markoff random processes and the statistical mechanics of time-dependent phenomena. II. Irreversible processes in fluids. *The Journal of Chemical Physics*, 22(3):398–413, 1954.
- [51] R. Zwanzig. Memory effects in irreversible thermodynamics. *Physical Review*, 124(4):983–992, 1961.
- [52] H. Grabert. *Projection Operator Techniques in Nonequilibrium Statistical Mechanics*. Springer, 1982.

- [53] M. Karttunen, I. Vattulainen, and A. Lukkarinen, editors. *Novel Methods in soft Matter Simulations*. Springer-Verlag Berlin Heidelberg, 1 edition, 2004.
- [54] P.S. de Laplace. *A Philosophical Essay on Probabilities*. Dover, New York, 1951.
- [55] C. Delaunay. *Théorie du mouvement de la lune*. 1860.
- [56] J. A. de la Torre. *Top-down and Bottom-up Approaches to Discrete Diffusion Models*. PhD thesis, National University of Distance Education, 2015.
- [57] B. J. Alder and T. E. Wainwright. Phase Transition for a Hard Sphere System. *The Journal of Chemical Physics*, 27(5):1208–1209, 1957.
- [58] J. B. Gibson, A. N. Goland, M. Milgram, and G. H. Vineyard. Dynamics of radiation damage. *Physical Review*, 120(4):1229–1253, 1960.
- [59] A. Rahman. Correlations in the motion of atoms in liquid silicon. *Physical Review*, 136, 1964.
- [60] D.C. Rapaport. *The Art Of Molecular Dynamics Simulation*. Cambridge University Press, 2004.
- [61] E. T. Jaynes. Information theory and statistical mechanics. *Physical Review*, 1957.
- [62] H. B. Callen. *Thermodynamics*. John Wiley & Sons, New York, 1960.
- [63] R. Kubo, M. Toda, N. Hashitsume, and N. Saito. *Statistical Physics II: Nonequilibrium Statistical Mechanics*. Springer, Berlin, 1991.
- [64] D. Kauzlaric, P. Espaol, A. Greiner, and S. Succi. Macromol. Theory Simul. 7/2011. *Macromolecular Theory and Simulations*, 20(7).
- [65] K. Ryogo. Statistical-Mechanical Theory of Irreversible Processes. I. General Theory and Simple Applications to Magnetic and Conduction Problems. *Journal of the Physical Society of Japan*, 12(6):570–586, 1957.
- [66] K. Kawasaki and J. Gunton. Theory of Nonlinear Transport Processes: Nonlinear Shear Viscosity and Normal Stress Effects. *Physical Review A*, 1973.
- [67] R. Zwanzig. *Nonequilibrium Statistical Mechanics*. Oxford University Press, 2001.

- [68] I Oppenheim. Generalized the application. 54:195–222, 1971.
- [69] P. Mazur and I. Oppenheim. Molecular theory of Brownian motion. *Physica*, 50(2):241–258, 1970.
- [70] J. G. Kirkwood, Frank P. Buff, and M. S. Green. The Statistical Mechanical Theory of Transport Processes. III. The Coefficients of Shear and Bulk Viscosity of Liquids. *The Journal of Chemical Physics*, 17(10):988–994, oct 1949.
- [71] P. Espa  ol and I. Z  niga. Force autocorrelation function in Brownian motion theory. *The Journal of Chemical Physics*, 98(1):574–580, jan 1993.
- [72] Xiao Guang Wu and Raymond Kapral. Projected dynamics: Analysis of a chemical reaction model. *The Journal of Chemical Physics*, 91(9):5528–5543, 1989.
- [73] J. S. Hansen, P. J. Daivis, and B. D. Todd. Viscous properties of isotropic fluids composed of linear molecules: Departure from the classical Navier-Stokes theory in nano-confined geometries. *Physical Review E - Statistical, Nonlinear, and Soft Matter Physics*, 80(4):1–9, 2009.
- [74] J. S. Hansen, J. C. Dyre, P. J. Daivis, B. D. Todd, and H. Bruus. Nanoflow hydrodynamics. *Physical Review E - Statistical, Nonlinear, and Soft Matter Physics*, 84(3):1–6, 2011.
- [75] S. Grossmann. Nonlinear and nonlocal transport effects in simple fluids. *Zeitschrift f  r Physik*, 233(1):74–83, 1970.
- [76] J. Zhang, B. D. Todd, and K. P. Travis. Viscosity of confined inhomogeneous nonequilibrium fluids. *Journal of Chemical Physics*, 121(21):10778–10786, 2004.
- [77] J. S. Hansen, P. J. Daivis, K. P. Travis, and B. D. Todd. Parameterization of the nonlocal viscosity kernel for an atomic fluid. *Physical Review E - Statistical, Nonlinear, and Soft Matter Physics*, 76(4):1–8, 2007.
- [78] B. D. Todd, J. S. Hansen, and Peter J. Daivis. Nonlocal shear stress for homogeneous fluids. *Physical Review Letters*, 100(19):1–4, 2008.
- [79] P. Mazur, D. Bedeaux, A. M. Albano, R. Leiden, and B. Mawr. Boundary conditions and non-equilibrium thermodynamics. pages 438–462, 1976.

- [80] D. Bedeaux, A. M. Albano, and P. Mazur. Brownian motion and fluctuating hydrodynamics II; A fluctuation-dissipation theorem for the slip coefficient. *Physica A: Statistical Mechanics and its Applications*, 88(3):574–582, 1977.
- [81] J. Barrat and F. Chiaruttini. Kapitza resistance at the liquid-solid interface. *Mol. Physics*, 37, 2003.
- [82] S. K. Kannam, B. D. Todd, J. S. Hansen, and P. J. Daivis. Slip flow in graphene nanochannels. *Journal of Chemical Physics*, 135(14), 2011.
- [83] V. P. Sokhan, D. Nicholson, and N. Quirke. Fluid flow in nanopores: Accurate boundary conditions for carbon nanotubes. *Journal of Chemical Physics*, 117(18):8531–8539, 2002.
- [84] D. Camargo, J. A. de la Torre, R. Delgado-Buscalioni, F. Chejne, and P. Español. Boundary conditions derived from a microscopic theory of hydrodynamics near solids.
- [85] R. I. Cukier, R. Kapral, J. R. Lehenhaft, and J. R. Mehaffey. On the microscopic origin of Stokes' law. *The Journal of Chemical Physics*, 73(10):5244–5253, 1980.
- [86] P.J. Cadusch, B. D. Todd, J. Zhang, and P. J. Daivis. A non-local hydrodynamic model for the shear viscosity of confined fluids: Analysis of a homogeneous kernel. *Journal of Physics A: Mathematical and Theoretical*, 41(3), 2008.
- [87] P. Español, R. Delgado-Buscalioni, R. Everaers, R. Potestio, D. Donadio, and K. Kremer. Statistical mechanics of Hamiltonian adaptive resolution simulations. *The Journal of Chemical Physics*, 142(6):064115, 2015.
- [88] P. Schofield and J. R. Henderson. Statistical Mechanics of Inhomogeneous Fluids. *Proc. R. Soc. Lond. A*, 14(379):231–246, 1982.
- [89] I. Bitsanis, J. J. Magda, M. Tirrell, and H. T. Davis. Molecular dynamics of flow in micropores. *The Journal of Chemical Physics*, 87(3):1733–1750, 1987.
- [90] T. Qian, C. Qiu, and P. Sheng. *A scaling approach to the derivation of hydrodynamic boundary conditions*, volume 611. 2008.
- [91] H. C. Öttinger. Thermodynamic formulation of wall slip. *Journal of Non-Newtonian Fluid Mechanics*, 152(1-3):66–75, 2008.

- [92] L. M.C. Sagis. Dynamic properties of interfaces in soft matter: Experiments and theory. *Reviews of Modern Physics*, 83(4):1367–1403, 2011.
- [93] P. Español and I. Zúñiga. On the definition of discrete hydrodynamic variables. *Journal of Chemical Physics*, 131(16), 2009.
- [94] P. Español, J. G. Anero, and I. Zúñiga. Microscopic derivation of discrete hydrodynamics. *Journal of Chemical Physics*, 131(24), 2009.
- [95] J. A. de la Torre, Pep Español, and Aleksandar Donev. Finite element discretization of non-linear diffusion equations with thermal fluctuations. *Journal of Chemical Physics*, 142(9), 2015.
- [96] P. Español and A. Donev. Coupling a nano-particle with isothermal fluctuating hydrodynamics: Coarse-graining from microscopic to mesoscopic dynamics. *Journal of Chemical Physics*, 143(23), 2015.
- [97] A. Donev. *Chemical Reactions: notes*. Tech. Rep.
- [98] R. B. Bird, R. C. Armstrong, and O. Hassager. *Dynamics of Polymeric Liquids*. Wiley, New York, 1987.
- [99] C. Clarke and R. Carswell. *Principles of Astrophysical Fluid Dynamics*. Cambridge University Press, Cambridge, England.
- [100] P. E. Rubbert and G. R. Saaris. A General Three-Dimensional Potential-Flow Method Applied to V/STOL Aerodynamics. *SAE Transactions*, 77(2):945–957, 1968.
- [101] J. P. Boon and S. Yip. *Molecular hydrodynamics*. McGraw- Hill, New York, 1980.
- [102] R. D. Mountain. Generalized hydrodynamics. *Advances in Molecular Relaxation Processes*, 9(3):225–291, 1977.
- [103] B. J. Alder and W. E. Alley. Generalized hydrodynamics. *Physics Today*, 37, 1984.
- [104] C. H. Chung and S. Yip. Generalized Hydrodynamics and Time Correlation Functions. *Physical Review*, 182(1), 1969.
- [105] I. M. Schepper, E. G. D. Cohen, C. Bruin, J. C. van Rijs, W. Montfrooij, and L. A. de Graaf. Hydrodynamic time correlation functions for a Lennard-Jones fluid. *Physical Review A*, 38(1), 1988.

- [106] R. E. Khayat and B. C. Eu. Generalized hydrodynamics, normal-stress effects, and velocity slips in the cylindrical Couette flow of Lennard-Jones fluids. *Physical Review A*, 39(2):728–744, 1989.
- [107] H. T. Davis. *Statistical Mechanics of Phases, Interfaces and Thin Films*. Wiley-VCH, New York, 1996.
- [108] K. P. Travis. and K. E. Gubbins. Poiseuille flow of Lennard-Jones fluids in narrow slit pores. *Journal of Chemical Physics*, 112(4):1984–1994, 2000.
- [109] J. A. de la Torre and P. Espa  ol. Coarse-graining Brownian motion: From particles to a discrete diffusion equation. *Journal of Chemical Physics*, 135(11), 2011.
- [110] L. A. Pozhar and K. E. Gubbins. Dense inhomogeneous fluids: Functional perturbation theory, the generalized Langevin equation, and kinetic theory. *The Journal of Chemical Physics*, 94(2):1367–1384, 1991.
- [111] H. Hoang and G. Galliero. Local viscosity of a fluid confined in a narrow pore. *Physical Review E - Statistical, Nonlinear, and Soft Matter Physics*, 86(2):1–10, 2012.
- [112] H. Hoang and G. Galliero. Shear viscosity of inhomogeneous fluids. *Journal of Chemical Physics*, 136(12), 2012.
- [113] D. J. Evans and G. Morriss. *Statistical Mechanics of Nonequilibrium Liquids*. Cambridge University Press, 2 edition, 2008.
- [114] B. D. Todd and J. S. Hansen. Nonlocal viscous transport and the effect on fluid stress. *Physical Review E - Statistical, Nonlinear, and Soft Matter Physics*, 78(5):1–6, 2008.
- [115] P. Espa  ol and F. J. de la Rubia. Mixing and equilibrium probability densities in classical statistical mechanics. *Physica A: Statistical Mechanics and its Applications*, 187(3-4):589–602, 1992.
- [116] S. Plimpton. Fast Parallel Algorithms for Short-Range Molecular Dynamics. *Journal of Computational Physics*, 117:1–19, 1995.
- [117] L. V. Woodcock. Equation of state for the viscosity of lennard-jones fluids. *AIChE Journal*, 52(2):438–446, 2006.

- [118] I. M. Mryglod, I. P. Omelyan, and M. V. Tokarchuk. Generalized collective modes for the Lennard-Jones fluid. *Molecular Physics*, 84(2):235–259, 1995.
- [119] T. Bryk, I. Mryglod, T. Scopigno, G. Ruocco, F. Gorelli, and M. Santoro. Collective excitations in supercritical fluids: Analytical and molecular dynamics study of "positive" and "negative" dispersion. *Journal of Chemical Physics*, 133(2), 2010.
- [120] D. Camargo, J. A. De La Torre, D. Duque-Zumajo, P. Español, R. Delgado-Buscalioni, and F. Chejne. Nanoscale hydrodynamics near solids. *Journal of Chemical Physics*, 148(6), 2018.
- [121] A. Alizadeh Pahlavan and J. B. Freund. Effect of solid properties on slip at a fluid-solid interface. *Physical Review E - Statistical, Nonlinear, and Soft Matter Physics*, 83(2):1–7, 2011.
- [122] O. Mahian, A. Kianifar, S. A. Kalogirou, I. Pop, and S. Wongwises. A review of the applications of nanofluids in solar energy, 2013.
- [123] M. Schuller, Q. Shao, and T. Lalk. Experimental investigation of the specific heat of a nitrate-alumina nanofluid for solar thermal energy storage systems. *International Journal of Thermal Sciences*, 91:142–145, 2015.
- [124] I. M. Shahrul, I. M. Mahbubul, S. S. Khaleduzzaman, R. Saidur, and M. F M Sabri. A comparative review on the specific heat of nanofluids for energy perspective, 2014.
- [125] E. K. Goharshadi, H. Ahmadzadeh, S. Samiee, and M. Hadadian. Nanofluids for Heat Transfer Enhancement-A Review. *Physical Chemistry Research*, 1:1–33, 2013.
- [126] R. Serrano-López, J. Fradera, and S. Cuesta-López. Molten salts database for energy applications, 2013.
- [127] M. Chieruzzi, G. F. Cerritelli, A. Miliozzi, and J. M. Kenny. Effect of nanoparticles on heat capacity of nanofluids based on molten salts as PCM for thermal energy storage. *Nanoscale research letters*, 8(1):448, 2013.
- [128] K. Khanafer, F. Tavakkoli, K. Vafai, and A. AlAmiri. A critical investigation of the anomalous behavior of molten salt-based nanofluids. *International Communications in Heat and Mass Transfer*, 69:51–58, 2015.

- [129] P. Español, J. A. de la Torre, and D. Duque-Zumajo. Solution to the plateau problem in the Green-Kubo formula. *Physical Review E*, 99(2), 2019.
- [130] D. Duque-Zumajo, D. Camargo, J.A. de la Torre, F. Chejne, and Pep Español. Discrete hydrodynamics near solid planar walls. *Physical Review E*, 2019.
- [131] Pep Español Duque-Zumajo, D., J. A. de la Torre. Slip and non-Markovian effects in nanohydrodynamics (in preparation). *Physical Review Letters*.
- [132] Pep Español Duque-Zumajo, D. Camargo, D., J. A. de la Torre, Farid Chejne. Discrete hydrodynamics near solid walls: non-Markovian effects and slip (in preparation). *Physical Review E*, 2019.
- [133] D. Duque-Zumajo, J.A. de la Torre, and P. Español. Nanoscale hydrodynamics in periodic and confined geometries. In *22th Workshop on Statistical Physics*, Madrid, 2018.
- [134] D. Duque-Zumajo, J.A. de la Torre, and P. Español. Nanoscale hydrodynamics in periodic boundary conditions. In *International Workshop on Nonequilibrium Thermodynamics*, Sint-Michielsgestel, 2018.
- [135] D. Duque-Zumajo, J.A. de la Torre, and P. Español. Nanoscale heat transport in fluids near solids. In *Ulam Computer Simulation Workshop*, Lviv, 2017.
- [136] D. Duque-Zumajo, J.A. de la Torre, and P. Español. Thermal hydrodynamics transport between fluids and solids. In *21th Workshop on Statistical Physics*, Seville, 2017.



## Appendix A

# Contributions

The following articles and posters are related with this dissertation.

1. [120] D. Camargo, J. A. De La Torre, D. Duque-Zumajo, P. Español, R. Delgado-Buscalioni, and F. Chejne. Nanoscale hydrodynamics near solids. *Journal of Chemical Physics*, 148(6), 2018.
2. [129] P. Español, J. A. de la Torre, and D. Duque-Zumajo. Solution to the plateau problem in the Green-Kubo formula. *Physical Review E*, 99(2), 2019.
3. [130] D. Duque-Zumajo, D. Camargo, J. A. de la Torre, F. Chejne, and Pep Español. Discrete hydrodynamics for planar flows with confining walls. *Physical Review E*, 2019.
4. [131] D. Duque-Zumajo, J. A. de la Torre, and Pep Español. Slip and non-Markovian effects in nanohydrodynamics (in preparation). *Physical Review Letters*, 2019.
5. [132] D. Duque-Zumajo, D. Camargo, J. A. de la Torre, Farid Chejne, and Pep Español. Discrete hydrodynamics near solid walls: non-Markovian effects and slip (in preparation). *Physical Review E*, 2019.
6. [133] Nanoscale hydrodynamics in periodic and confined geometries. Poster presented at 22th Workshop on Statistical Physics (FISES18), Madrid (Spain) 2018.

7. [134] Nanoscale hydrodynamics in periodic boundary conditions. Poster presented at 8th International Workshop on Nonequilibrium Thermodynamics, Sint-Michielsgestel (The Netherlands) 2018.
8. [135] Nanoscale heat transport in fluids near solids. Poster presented at Ulam Computer Simulation Workshop, Lviv (Ukraine) 2017.
9. [136] Thermal hydrodynamics transport between fluids and solids. Poster presented at 21th Workshop on Statistical Physics (FISES17), Seville (Spain) 2017.

Furthermore, I presented part of this work in two seminars at Universidad Nacional de Educación a Distancia.

1. Nanoscale hydrodynamics nears solids. Universidad Nacional de Educación a Distancia, Madrid (Spain) 2017.
2. Simulación de procesos térmicos en la dinámica de nanofluidos. Universidad Nacional de Educación a Distancia, Madrid (Spain) 2016.

## Appendix B

# Forces

In this appendix we summarize the different forces and force densities introduced so far, and present some results concerning its averages with the relevant ensemble. The force densities that the fluid or the solid exert on a fluid molecule located at the point  $\mathbf{r}$  are introduced in (2.7),

$$\begin{aligned}\hat{\mathbf{F}}_{\mathbf{r}}^{l \rightarrow l}(z) &\equiv \sum_{ij}^{NN} \hat{\mathbf{F}}_{ij} \delta(\mathbf{r} - \mathbf{q}_i) \\ \hat{\mathbf{F}}_{\mathbf{r}}^{s \rightarrow l}(z) &\equiv \sum_{ij'}^{NN'} \hat{\mathbf{F}}_{ij'} \delta(\mathbf{r} - \mathbf{q}_i),\end{aligned}\quad (\text{B.1})$$

where  $\hat{\mathbf{F}}_{ij'}$  is the force that atom  $j'$  of the solid exerts on atom  $i$  of the liquid. This is,  $\hat{\mathbf{F}}_{\mathbf{r}}^{l \rightarrow l}(z)$  is the force density that the liquid exerts on the liquid molecules that are around the point  $\mathbf{r}$ , while  $\hat{\mathbf{F}}_{\mathbf{r}}^{s \rightarrow l}(z)$  is the force density that the solid exerts on the liquid at the point  $\mathbf{r}$ .

The total force density on the fluid is

$$\hat{\mathbf{F}}_{\mathbf{r}}^l = \hat{\mathbf{F}}_{\mathbf{r}}^{l \rightarrow l} + \hat{\mathbf{F}}_{\mathbf{r}}^{s \rightarrow l} = \sum_j^N -\frac{\partial U}{\partial \mathbf{q}_j} \delta(\mathbf{r} - \mathbf{q}_j) \quad (\text{B.2})$$

The total force on the fluid and on the solid are

$$\hat{\mathbf{F}}^l = \int d\mathbf{r} \hat{\mathbf{F}}_{\mathbf{r}}^l \quad \hat{\mathbf{F}}^s = -\hat{\mathbf{F}}^l, \quad (\text{B.3})$$

where we have used that the total force

$$\hat{\mathbf{F}} = - \sum_i^N \frac{\partial U}{\partial \mathbf{q}_i} - \sum_{i'}^{N'} \frac{\partial U}{\partial \mathbf{q}_{i'}} = \hat{\mathbf{F}}^l + \hat{\mathbf{F}}^s \quad (\text{B.4})$$

vanishes because the potentials are translational invariant (and therefore, Newton's third law holds).

Note that we have the result

$$\hat{\mathbf{F}}^s = - \int d\mathbf{r} \hat{\mathbf{F}}_{\mathbf{r}}^{\text{s} \rightarrow \text{l}} \quad (\text{B.5})$$

Now, let us consider the average of the total force density on the liquid, equation (2.6)

$$\begin{aligned} \mathbf{F}_{\mathbf{r}}^l &\equiv \text{Tr}[\bar{\rho}_t \hat{\mathbf{F}}_{\mathbf{r}}^l] = \langle \hat{\mathbf{F}}_{\mathbf{r}}^l \rangle^{\mu, \lambda_R} \\ &= \frac{1}{\Xi[\mu, \lambda_R]} \sum_{N=0}^{\infty} \frac{1}{N!} \int \frac{dq}{\Lambda^{3N}} \frac{dq'}{\Lambda^{3N'}} \left[ \sum_j^N - \frac{\partial U}{\partial \mathbf{q}_j} \delta(\mathbf{r} - \mathbf{q}_j) \right] \\ &\quad \times e^{-\beta U} \exp \left\{ -\beta \left( \lambda_R \cdot \hat{\mathbf{R}} - \sum_{i=1}^N m\mu(\mathbf{q}_i) \right) \right\}, \end{aligned} \quad (\text{B.6})$$

where we have used the definition of the average with respect to the relevant ensemble, after performing the momentum integrals. Next, we realize that the derivative of the Boltzmann factor is the potential times the Boltzmann factor itself, that is,

$$\begin{aligned} \mathbf{F}_{\mathbf{r}}^l &= \frac{1}{\Xi[\mu, \lambda_R]} \sum_{N=0}^{\infty} \frac{1}{N!} \int \frac{dq}{\Lambda^{3N}} \frac{dq'}{\Lambda^{3N'}} \\ &\quad \times \exp \left\{ -\beta \left( \lambda_R \cdot \hat{\mathbf{R}} - \sum_{i=1}^N m\mu(\mathbf{q}_i) \right) \right\} k_B T \sum_j^N \delta(\mathbf{r} - \mathbf{q}_j) \frac{\partial}{\partial \mathbf{q}_j} e^{-\beta U} \end{aligned} \quad (\text{B.7})$$

Integrate by parts to obtain

$$\begin{aligned}
\mathbf{F}_r^l &= \frac{1}{\Xi[\mu, \lambda_R]} \sum_{N=0}^{\infty} \frac{1}{N!} \int \frac{dq}{\Lambda^{3N}} \frac{dq'}{\Lambda^{3N'}} \\
&\quad \times e^{-\beta U} k_B T \sum_j^N -\frac{\partial}{\partial \mathbf{q}_j} \left[ \delta(\mathbf{r} - \mathbf{q}_j) \exp \left\{ -\beta \left( \lambda_R \cdot \hat{\mathbf{R}} - \sum_{i=1}^N m\mu(\mathbf{q}_i) \right) \right\} \right] \\
&= \frac{1}{\Xi[\mu, \lambda_R]} \sum_{N=0}^{\infty} \frac{1}{N!} \int \frac{dq}{\Lambda^{3N}} \frac{dq'}{\Lambda^{3N'}} e^{-\beta U} \sum_j^N \exp \left\{ -\beta \left( \lambda_R \cdot \hat{\mathbf{R}} - \sum_{i \neq j}^N m\mu(\mathbf{q}_i) \right) \right\} \\
&\quad \times k_B T \left[ -\frac{\partial}{\partial \mathbf{q}_j} \delta(\mathbf{r} - \mathbf{q}_j) \exp \left\{ \beta m\mu(\mathbf{q}_j) \right\} \right] \\
&= \frac{k_B T}{m} \nabla \rho(\mathbf{r}) - \rho(\mathbf{r}) \nabla \mu(\mathbf{r})
\end{aligned} \tag{B.8}$$

By following identical steps, we may compute the average of the total force on the solid  $\mathbf{F}^s$  and obtain

$$\begin{aligned}
\mathbf{F}^s &= \text{Tr}[\bar{\rho}_t \hat{\mathbf{F}}^s] = \langle \hat{\mathbf{F}}^s \rangle^{\mu, \lambda_R} \\
&= \frac{1}{\Xi[\mu, \lambda_R]} \sum_{N=0}^{\infty} \frac{1}{N!} \int \frac{dq}{\Lambda^{3N}} \frac{dq'}{\Lambda^{3N'}} \left[ -\sum_{i'}^{N'} \frac{\partial U}{\partial \mathbf{q}_{i'}} \right] e^{-\beta U} \exp \left\{ -\beta \left( \sum_{i=1}^N m\mu(\mathbf{q}_i) + \lambda_R \cdot \hat{\mathbf{R}} \right) \right\} \\
&= \frac{1}{\Xi[\mu, \lambda_R]} \sum_{N=0}^{\infty} \frac{1}{N!} \int \frac{dq}{\Lambda^{3N}} \frac{dq'}{\Lambda^{3N'}} \exp \left\{ -\beta \left( \sum_{i=1}^N m\mu(\mathbf{q}_i) + \lambda_R \cdot \hat{\mathbf{R}} \right) \right\} k_B T \left[ \sum_{i'}^{N'} \frac{\partial}{\partial \mathbf{q}_{i'}} \right] e^{-\beta U} \\
&= \frac{1}{\Xi[\mu, \lambda_R]} \sum_{N=0}^{\infty} \frac{1}{N!} \int \frac{dq}{\Lambda^{3N}} \frac{dq'}{\Lambda^{3N'}} e^{-\beta U} k_B T \left[ -\sum_{i'}^{N'} \frac{\partial}{\partial \mathbf{q}_{i'}} \right] \exp \left\{ -\beta \left( \sum_{i=1}^N m\mu(\mathbf{q}_i) + \lambda_R \cdot \hat{\mathbf{R}} \right) \right\} \\
&= \frac{1}{\Xi[\mu, \lambda_R]} \sum_{N=0}^{\infty} \frac{1}{N!} \int \frac{dq}{\Lambda^{3N}} \frac{dq'}{\Lambda^{3N'}} e^{-\beta U} \exp \left\{ -\beta \left( \sum_{i=1}^N m\mu(\mathbf{q}_i) + \lambda_R \cdot \hat{\mathbf{R}} \right) \right\} \left[ \sum_{i'}^{N'} \frac{\partial}{\partial \mathbf{q}_{i'}} \right] \lambda_R \cdot \hat{\mathbf{R}} \\
&= \lambda_R
\end{aligned} \tag{B.9}$$

This identity allows one to interpret physically the Lagrange multiplier  $\lambda_R$  as the force on the solid sphere. By using (2.38) we obtain that the total force on the solid sphere is due to the gradient of the free energy functional

$$\mathbf{F}^s = -\frac{\partial \mathcal{F}}{\partial \mathbf{R}} [\rho, \mathbf{R}] \tag{B.10}$$



## Appendix C

# The projected currents

In this appendix we consider the explicit form of the projected currents  $Q_t i \mathcal{L} \hat{A}$  for the present selection of relevant variables. The projector defined in (1.38) gives rise to the following two projected currents  $Q_t \hat{\mathbf{F}}_{\mathbf{r}}^{s \rightarrow l}, Q_t \hat{\sigma}_{\mathbf{r}}$  given explicitly by

$$\begin{aligned} Q_t \hat{\mathbf{F}}_{\mathbf{r}}^{s \rightarrow l} = & \hat{\mathbf{F}}_{\mathbf{r}}^{s \rightarrow l} - \text{Tr} [\bar{\rho}_t \hat{\mathbf{F}}_{\mathbf{r}}^{s \rightarrow l}] - (\hat{\mathbf{R}} - \mathbf{R}(t)) \cdot \frac{\partial}{\partial \mathbf{R}(t)} \text{Tr} [\bar{\rho}_t \hat{\mathbf{F}}_{\mathbf{r}}^{s \rightarrow l}] \\ & - (\hat{\mathbf{P}} - \mathbf{P}(t)) \cdot \frac{\partial}{\partial \mathbf{P}(t)} \text{Tr} [\bar{\rho}_t \hat{\mathbf{F}}_{\mathbf{r}}^{s \rightarrow l}] - \int d\mathbf{r}' (\hat{\rho}_{\mathbf{r}'} - \rho(\mathbf{r}', t)) \frac{\delta}{\delta \rho(\mathbf{r}', t)} \text{Tr} [\bar{\rho}_{t'} \hat{\mathbf{F}}_{\mathbf{r}}^{s \rightarrow l}] \\ & - \int d\mathbf{r}' (\hat{\mathbf{g}}_{\mathbf{r}'} - \mathbf{g}(\mathbf{r}', t)) \cdot \frac{\delta}{\delta \mathbf{g}(\mathbf{r}', t)} \text{Tr} [\bar{\rho}_{t'} \hat{\mathbf{F}}_{\mathbf{r}}^{s \rightarrow l}] \end{aligned} \quad (C.1)$$

and

$$\begin{aligned} Q_t \hat{\sigma}_{\mathbf{r}} = & \hat{\sigma}_{\mathbf{r}} - \text{Tr} [\bar{\rho}_t \hat{\sigma}_{\mathbf{r}}] - (\hat{\mathbf{R}} - \mathbf{R}(t)) \cdot \frac{\partial}{\partial \mathbf{R}(t)} \text{Tr} [\bar{\rho}_t \hat{\sigma}_{\mathbf{r}}] - (\hat{\mathbf{P}} - \mathbf{P}(t)) \cdot \frac{\partial}{\partial \mathbf{P}(t)} \text{Tr} [\bar{\rho}_t \hat{\sigma}_{\mathbf{r}}] \\ & - \int d\mathbf{r}' (\hat{\rho}_{\mathbf{r}'} - \rho(\mathbf{r}', t)) \frac{\delta}{\delta \rho(\mathbf{r}', t)} \text{Tr} [\bar{\rho}_{t'} \hat{\sigma}_{\mathbf{r}}] - \int d\mathbf{r}' (\hat{\mathbf{g}}_{\mathbf{r}'} - \mathbf{g}(\mathbf{r}', t)) \cdot \frac{\delta}{\delta \mathbf{g}(\mathbf{r}', t)} \text{Tr} [\bar{\rho}_{t'} \hat{\sigma}_{\mathbf{r}}] \end{aligned} \quad (C.2)$$

Under the assumption that the solid particle is sufficiently large, the actual values  $\hat{\mathbf{R}}, \hat{\mathbf{P}}$  of the microscopic functions will not differ too much from its average values, and the

corresponding terms in (C.1), (C.2) may be neglected. The projected currents become

$$\begin{aligned} Q_t \hat{\mathbf{F}}_{\mathbf{r}}^{\text{s}\rightarrow\text{l}} &= \hat{\mathbf{F}}_{\mathbf{r}}^{\text{s}\rightarrow\text{l}} - \text{Tr} [\bar{\rho}_t \hat{\mathbf{F}}_{\mathbf{r}}^{\text{s}\rightarrow\text{l}}] - \int d\mathbf{r}' (\hat{\rho}_{\mathbf{r}'} - \rho(\mathbf{r}', t)) \frac{\delta}{\delta \rho(\mathbf{r}', t)} \text{Tr} [\bar{\rho}_{t'} \hat{\mathbf{F}}_{\mathbf{r}}^{\text{s}\rightarrow\text{l}}] \\ &\quad - \int d\mathbf{r}' (\hat{\mathbf{g}}_{\mathbf{r}'} - \mathbf{g}(\mathbf{r}', t)) \cdot \frac{\delta}{\delta \mathbf{g}(\mathbf{r}', t)} \text{Tr} [\bar{\rho}_{t'} \hat{\mathbf{F}}_{\mathbf{r}}^{\text{s}\rightarrow\text{l}}] \end{aligned} \quad (\text{C.3})$$

and

$$\begin{aligned} Q_t \hat{\sigma}_{\mathbf{r}} &= \hat{\sigma}_{\mathbf{r}} - \text{Tr} [\bar{\rho}_t \hat{\sigma}_{\mathbf{r}}] - \int d\mathbf{r}' (\hat{\rho}_{\mathbf{r}'} - \rho(\mathbf{r}', t)) \frac{\delta}{\delta \rho(\mathbf{r}', t)} \text{Tr} [\bar{\rho}_{t'} \hat{\sigma}_{\mathbf{r}}] \\ &\quad - \int d\mathbf{r}' (\hat{\mathbf{g}}_{\mathbf{r}'} - \mathbf{g}(\mathbf{r}', t)) \cdot \frac{\delta}{\delta \mathbf{g}(\mathbf{r}', t)} \text{Tr} [\bar{\rho}_{t'} \hat{\sigma}_{\mathbf{r}}] \end{aligned} \quad (\text{C.4})$$

Let us start with the projected current (C.3), that requires the average with the relevant ensemble of the force density that the solid exerts on the fluid

$$\text{Tr} [\bar{\rho}_{t'} \hat{\mathbf{F}}_{\mathbf{r}}^{\text{s}\rightarrow\text{l}}] = \text{Tr} [\mathcal{G} \bar{\rho}_{t'} \mathcal{G} \hat{\mathbf{F}}_{\mathbf{r}}^{\text{s}\rightarrow\text{l}}] \quad (\text{C.5})$$

Because the force does not depend on velocities, the Galilean operator does nothing on it. Therefore, we need to compute

$$\text{Tr} [\bar{\rho}_{t'} \hat{\mathbf{F}}_{\mathbf{r}}^{\text{s}\rightarrow\text{l}}] = \frac{1}{\Xi[\lambda(t)]} \text{Tr} \left[ \rho^{\text{eq}}(z) \exp \left\{ \beta \int d\mathbf{r} \mu(\mathbf{r}) \hat{\rho}_{\mathbf{r}}(z) - \beta \lambda_R(t) \cdot \hat{\mathbf{R}} - \beta \lambda_P(t) \cdot \hat{\mathbf{P}} \right\} \hat{\mathbf{F}}_{\mathbf{r}}^{\text{s}\rightarrow\text{l}} \right] \quad (\text{C.6})$$

which does not depend on the momentum of the fluid (because none of the conjugate variables does). Note that the average of the force density that the solid exerts on the fluid does not depend on the momentum variable, and the last term in (C.3) vanishes. We end up, therefore, with the following result

$$Q_t \hat{\mathbf{F}}_{\mathbf{r}}^{\text{s}\rightarrow\text{l}} = \hat{\mathbf{F}}_{\mathbf{r}}^{\text{s}\rightarrow\text{l}} - \text{Tr} [\bar{\rho}_t \hat{\mathbf{F}}_{\mathbf{r}}^{\text{s}\rightarrow\text{l}}] - \int d\mathbf{r}' (\hat{\rho}_{\mathbf{r}'} - \rho(\mathbf{r}', t)) \frac{\delta}{\delta \rho(\mathbf{r}', t)} \text{Tr} [\bar{\rho}_t \hat{\mathbf{F}}_{\mathbf{r}}^{\text{s}\rightarrow\text{l}}] \quad (\text{C.7})$$

Note that the functional derivative of the relevant ensemble is

$$\begin{aligned} \frac{\delta}{\delta \rho(\mathbf{r}', t)} \bar{\rho}_t &= \frac{\delta}{\delta \rho(\mathbf{r}', t)} \frac{1}{\Xi[\lambda(t)]} \rho^{\text{eq}}(z) \exp \left\{ \beta \int d\mathbf{r} \mu(\mathbf{r}) \hat{\rho}_{\mathbf{r}}(z) - \beta \lambda_R(t) \cdot \hat{\mathbf{R}} - \beta \lambda_P(t) \cdot \hat{\mathbf{P}} \right\} \\ &= \bar{\rho}_t \left[ \frac{\delta}{\delta \rho(\mathbf{r}', t)} \beta \int d\mathbf{r} \mu(\mathbf{r}) \hat{\rho}_{\mathbf{r}}(z) - \frac{\delta}{\delta \rho(\mathbf{r}', t)} \ln \Xi[\lambda(t)] \right] \\ &= \bar{\rho}_t \beta \int d\mathbf{r}' \frac{\delta \mu(\mathbf{r}'')}{\delta \rho(\mathbf{r}', t)} \delta \hat{\rho}_{\mathbf{r}''}(z), \end{aligned} \quad (\text{C.8})$$

where  $\delta\hat{\rho}_{\mathbf{r}''}(z) = \hat{\rho}_{\mathbf{r}''}(z) - \rho(\mathbf{r}'', t)$ . We have neglected terms that involve the functional derivative of  $\lambda_{\mathbf{R}}$  and  $\lambda_{\mathbf{P}}$  because they accompany fluctuations of  $\mathbf{R}$  and  $\mathbf{P}$  which are assumed to be negligible.

We need to evaluate the functional derivative of the chemical potential with respect to the number density field. This can be achieved by noting that

$$\begin{aligned}\frac{\delta}{\delta\mu(\mathbf{r})}\ln\Xi[\lambda] &= \beta\rho(\mathbf{r}) \\ \frac{\delta^2}{\delta\mu(\mathbf{r})\delta\mu(\mathbf{r}')}\ln\Xi[\lambda] &= \beta^2\langle\delta\hat{\rho}(\mathbf{r})\delta\hat{\rho}(\mathbf{r}')\rangle\end{aligned}\quad (\text{C.9})$$

which both imply

$$\frac{\delta\rho(\mathbf{r}')}{\delta\mu(\mathbf{r})} = \beta\langle\delta\hat{\rho}_{\mathbf{r}}\delta\hat{\rho}_{\mathbf{r}'}\rangle\quad (\text{C.10})$$

The functional derivative appearing in (C.8) is, therefore, the inverse of the density correlation matrix, that is,

$$\frac{\delta\mu(\mathbf{r})}{\delta\rho(\mathbf{r}')} = \beta^{-1}\langle\delta\hat{\rho}_{\mathbf{r}}\delta\hat{\rho}_{\mathbf{r}'}\rangle^{-1}\quad (\text{C.11})$$

Therefore, the projected current (C.7) is

$$Q_t\hat{\mathbf{F}}_{\mathbf{r}}^{s\rightarrow l} = \hat{\mathbf{F}}_{\mathbf{r}}^{s\rightarrow l} - \text{Tr}[\bar{\rho}_t\hat{\mathbf{F}}_{\mathbf{r}}^{s\rightarrow l}] - \int d\mathbf{r}' \int d\mathbf{r}'' (\hat{\rho}_{\mathbf{r}'} - \rho(\mathbf{r}', t)) \langle\delta\hat{\rho}_{\mathbf{r}'}\delta\hat{\rho}_{\mathbf{r}''}\rangle^{-1} \langle\delta\hat{\rho}_{\mathbf{r}''}\hat{\mathbf{F}}_{\mathbf{r}}^{s\rightarrow l}\rangle\quad (\text{C.12})$$

Let us now move to the projected current  $Q_t \hat{\sigma}_r$ .

$$\begin{aligned}
Q_t \hat{\sigma}_r &= \hat{\sigma}_r - \text{Tr} [\bar{\rho}_t \hat{\sigma}_r] \\
&- \int d\mathbf{r}' (\hat{\rho}_{\mathbf{r}'} - \rho(\mathbf{r}', t)) \frac{\delta}{\delta \rho(\mathbf{r}', t)} \text{Tr} [\bar{\rho}_{t'} \hat{\sigma}_r] \\
&- \int d\mathbf{r}' (\hat{\mathbf{g}}_{\mathbf{r}'} - \mathbf{g}(\mathbf{r}', t)) \frac{\delta}{\delta \mathbf{g}(\mathbf{r}', t)} \text{Tr} [\bar{\rho}_{t'} \hat{\sigma}_r] \\
&= \hat{\sigma}_r - \text{Tr} [\bar{\rho}_t \hat{\sigma}_r] \\
&- \int d\mathbf{r}' (\hat{\rho}_{\mathbf{r}'} - \rho(\mathbf{r}', t)) \frac{\delta}{\delta \rho(\mathbf{r}', t)} [\text{Tr} [\bar{\rho}_t \hat{\mathbf{K}}_r] + \text{Tr} [\bar{\rho}_t \hat{\mathbf{\Pi}}_r]] \\
&- \int d\mathbf{r}' (\hat{\mathbf{g}}_{\mathbf{r}'} - \mathbf{g}(\mathbf{r}', t)) \frac{\delta}{\delta \mathbf{g}(\mathbf{r}', t)} [\text{Tr} [\bar{\rho}_t \hat{\mathbf{K}}_r] + \text{Tr} [\bar{\rho}_t \hat{\mathbf{\Pi}}_r]] \\
&= \hat{\sigma}_r - \text{Tr} [\bar{\rho}_t \hat{\sigma}_r] \\
&- \int d\mathbf{r}' (\hat{\rho}_{\mathbf{r}'} - \rho(\mathbf{r}', t)) \frac{\delta}{\delta \rho(\mathbf{r}', t)} \left[ \frac{k_B T}{m} \rho(\mathbf{r}) \delta + \frac{\mathbf{g}(\mathbf{r}) \mathbf{g}(\mathbf{r})}{\rho(\mathbf{r})} + \text{Tr} [\bar{\rho}_t \hat{\mathbf{\Pi}}_r] \right] \\
&- \int d\mathbf{r}' (\hat{\mathbf{g}}_{\mathbf{r}'} - \mathbf{g}(\mathbf{r}', t)) \frac{\delta}{\delta \mathbf{g}(\mathbf{r}', t)} \left[ \frac{k_B T}{m} \rho(\mathbf{r}) \delta + \frac{\mathbf{g}(\mathbf{r}) \mathbf{g}(\mathbf{r})}{\rho(\mathbf{r})} + \text{Tr} [\bar{\rho}_t \hat{\mathbf{\Pi}}_r] \right], \quad (\text{C.13})
\end{aligned}$$

where we have decomposed the kinetic and virial parts of the stress tensor and used (2.55). The ideal part and the virial part are independent of momentum variables, the latter because the virial stress tensor  $\hat{\mathbf{\Pi}}_r$  does not depend on velocities of the particles. The only term that depends on momentum is the convective term. Therefore,

$$\begin{aligned}
Q_t \hat{\sigma}_r^{\alpha\beta} &= \hat{\sigma}_r^{\alpha\beta} - \text{Tr} [\bar{\rho}_t \hat{\sigma}_r^{\alpha\beta}] \\
&- \int d\mathbf{r}' (\hat{\rho}_{\mathbf{r}'} - \rho(\mathbf{r}', t)) \frac{\delta}{\delta \rho(\mathbf{r}', t)} \left[ \frac{k_B T}{m} \rho(\mathbf{r}) \delta^{\alpha\beta} + \frac{\mathbf{g}^\alpha(\mathbf{r}) \mathbf{g}^\beta(\mathbf{r})}{\rho(\mathbf{r})} + \text{Tr} [\bar{\rho}_t \hat{\mathbf{\Pi}}_r^{\alpha\beta}] \right] \\
&- \int d\mathbf{r}' (\hat{\mathbf{g}}_{\mathbf{r}'}^\gamma - \mathbf{g}^\gamma(\mathbf{r}', t)) \frac{\delta}{\delta \mathbf{g}^\gamma(\mathbf{r}', t)} \frac{\mathbf{g}^\alpha(\mathbf{r}) \mathbf{g}^\beta(\mathbf{r})}{\rho(\mathbf{r})} \\
&= \hat{\sigma}_r^{\alpha\beta} - \text{Tr} [\bar{\rho}_t \hat{\sigma}_r^{\alpha\beta}] \\
&- \int d\mathbf{r}' (\hat{\rho}_{\mathbf{r}'} - \rho(\mathbf{r}', t)) \delta(\mathbf{r} - \mathbf{r}') \left[ \frac{k_B T}{m} \delta^{\alpha\beta} - \mathbf{v}^\alpha(\mathbf{r}) \mathbf{v}^\beta(\mathbf{r}) \right] \\
&- \int d\mathbf{r}' (\hat{\rho}_{\mathbf{r}'} - \rho(\mathbf{r}', t)) \frac{\delta}{\delta \rho(\mathbf{r}', t)} \text{Tr} [\bar{\rho}_t \hat{\mathbf{\Pi}}_r^{\alpha\beta}] \\
&- \int d\mathbf{r}' (\hat{\mathbf{g}}_{\mathbf{r}'}^\gamma - \mathbf{g}^\gamma(\mathbf{r}', t)) \delta(\mathbf{r} - \mathbf{r}') [\delta^{\gamma\beta} \mathbf{v}^\alpha(\mathbf{r}) + \delta^{\alpha\gamma} \mathbf{v}^\beta(\mathbf{r})] \quad (\text{C.14})
\end{aligned}$$

Simplifying

$$\begin{aligned} Q_t \hat{\sigma}_r^{\alpha\beta} &= \hat{\sigma}_r^{\alpha\beta} - \text{Tr} \left[ \bar{\rho}_t \hat{\sigma}_r^{\alpha\beta} \right] - (\hat{\mathbf{g}}_r^\beta - \mathbf{g}^\beta(\mathbf{r}, t)) \mathbf{v}^\alpha(\mathbf{r}) + (\hat{\mathbf{g}}_r^\alpha - \mathbf{g}^\alpha(\mathbf{r}, t)) \mathbf{v}^\beta(\mathbf{r}) \\ &\quad - \int d\mathbf{r}' (\hat{\rho}_{\mathbf{r}'} - \rho(\mathbf{r}', t)) \frac{\delta}{\delta \rho(\mathbf{r}', t)} \text{Tr} \left[ \bar{\rho}_t \hat{\Pi}_r^{\alpha\beta} \right] - (\hat{\rho}_{\mathbf{r}'} - \rho(\mathbf{r}', t)) \frac{k_B T}{m} \delta^{\alpha\beta} \end{aligned} \quad (\text{C.15})$$

We may use now the same argument as in the case of the projected force for computing the last functional derivative. The final result for the projected currents is

$$\begin{aligned} Q_t \hat{\mathbf{F}}_r^{s \rightarrow l} &= \hat{\mathbf{F}}_r^{s \rightarrow l} - \text{Tr} \left[ \bar{\rho}_t \hat{\mathbf{F}}_r^{s \rightarrow l} \right] - \int d\mathbf{r}' \int d\mathbf{r}'' (\hat{\rho}_{\mathbf{r}'} - \rho(\mathbf{r}', t)) \langle \delta \hat{\rho}_{\mathbf{r}'} \delta \hat{\rho}_{\mathbf{r}''} \rangle^{-1} \langle \delta \hat{\rho}_{\mathbf{r}'} \hat{\mathbf{F}}_r^{s \rightarrow l} \rangle \\ Q_t \hat{\sigma}_r^{\alpha\beta} &= \hat{\sigma}_r^{\alpha\beta} - \text{Tr} \left[ \bar{\rho}_t \hat{\sigma}_r^{\alpha\beta} \right] - (\hat{\mathbf{g}}_r^\beta - \mathbf{g}^\beta(\mathbf{r}, t)) \mathbf{v}^\alpha(\mathbf{r}) + (\hat{\mathbf{g}}_r^\alpha - \mathbf{g}^\alpha(\mathbf{r}, t)) \mathbf{v}^\beta(\mathbf{r}) \\ &\quad - \int d\mathbf{r}' \int d\mathbf{r}'' (\hat{\rho}_{\mathbf{r}'} - \rho(\mathbf{r}', t)) \langle \delta \hat{\rho}_{\mathbf{r}'} \delta \hat{\rho}_{\mathbf{r}''} \rangle^{-1} \langle \delta \hat{\rho}_{\mathbf{r}''} \hat{\Pi}_r^{\alpha\beta} \rangle - (\hat{\rho}_{\mathbf{r}'} - \rho(\mathbf{r}', t)) \frac{k_B T}{m} \delta^{\alpha\beta} \end{aligned} \quad (\text{C.16})$$

Under the approximation that the system is close to equilibrium, the relevant ensemble is very similar to the equilibrium ensemble, and we may take  $\mathbf{v}(\mathbf{r}, t) \simeq 0$  and  $\rho(\mathbf{r}, t) \simeq \rho^{\text{eq}}(\mathbf{r})$ . This gives the final result for the projected currents

$$\begin{aligned} Q_t \hat{\mathbf{F}}_r^{s \rightarrow l} &= \hat{\mathbf{F}}_r^{s \rightarrow l} - \text{Tr} \left[ \rho^{\text{eq}} \hat{\mathbf{F}}_r^{s \rightarrow l} \right] - \int d\mathbf{r}' \int d\mathbf{r}'' (\hat{\rho}_{\mathbf{r}'} - \rho^{\text{eq}}(\mathbf{r}')) \langle \delta \hat{\rho}_{\mathbf{r}'} \delta \hat{\rho}_{\mathbf{r}''} \rangle_{\text{eq}}^{-1} \langle \delta \hat{\rho}_{\mathbf{r}'} \hat{\mathbf{F}}_r^{s \rightarrow l} \rangle^{\text{eq}} \\ Q_t \hat{\sigma}_r^{\alpha\beta} &= \hat{\sigma}_r^{\alpha\beta} - \text{Tr} \left[ \bar{\rho}_t \hat{\sigma}_r^{\alpha\beta} \right] - \int d\mathbf{r}' \int d\mathbf{r}'' (\hat{\rho}_{\mathbf{r}'} - \rho^{\text{eq}}(\mathbf{r}')) \langle \delta \hat{\rho}_{\mathbf{r}'} \delta \hat{\rho}_{\mathbf{r}''} \rangle^{-1} \langle \delta \hat{\rho}_{\mathbf{r}''} \hat{\sigma}_r^{\alpha\beta} \rangle^{\text{eq}} \end{aligned} \quad (\text{C.17})$$

Physically, the last integral terms are the responsible to subtract from the equilibrium fluctuations of the force density and stress tensor that part that may still have a systematic dependence on the fluctuations of the density.



## Appendix D

# Details of the derivation of discrete hydrodynamics

In this appendix we give the details needed to obtain the dynamic equations of the discrete hydrodynamic variables using the projection operator method. We refer to the textbook by Grabert [52] and to the Chapters 1 and 2 to set the notation.

### D.1 The relevant ensemble and the entropy

As we saw in Chapter 1 the relevant ensemble is at the core of the projection operator formalism [52]. It is an approximation to the real time dependent ensemble obeying Liouville's equation, and it allows to express the real ensemble in terms of the CG variables at the present time and in the past, leading to closed equations for the CG variables. The relevant ensemble is obtained by maximizing the Gibbs-Jaynes functional

$$\mathcal{S}[\rho] = -k_B \text{Tr} \left[ \rho \ln \frac{\rho}{\rho_0} \right], \quad (\text{D.1})$$

where  $\rho_0 = \frac{1}{N!h^{3N}}$  is a constant that renders dimensionless the argument of the logarithm. The trace denotes a macrocanonical sum over particles and an integration over phase space.

The maximization is done subject to provide the correct averages of the CG variables (3.22) (plus the total energy). This result in a generalized canonical ensemble of the

form

$$\bar{\rho} = \frac{1}{\Xi(\lambda, \mathbf{v})} \exp \left\{ -\beta \hat{H} - \beta \left( M_{\mu\nu}^{\psi} \lambda_{\nu} \hat{\rho}_{\mu} - M_{\mu\nu}^{\psi} \mathbf{v}_{\nu} \cdot \hat{\mathbf{g}}_{\mu} \right) \right\} \quad (\text{D.2})$$

Here, the Lagrange multipliers are  $\beta, \beta M_{\mu\nu}^{\psi} \lambda_{\nu}, -\beta M_{\mu\nu}^{\psi} \mathbf{v}_{\nu}$  where  $\beta, \lambda_{\nu}, \mathbf{v}_{\nu}$  will be interpreted as the inverse temperature, chemical potential per unit mass and the velocity, respectively. The introduction of the matrix  $M^{\psi}$  in the definition of the Lagrange multipliers is justified a posteriori. The resulting equations of motion have, with this definition, a direct counterpart with a discretization equations of the continuum hydrodynamic theory as presented in Sec. 3.5. We use Einstein's convention stating that sums over repeated indices is implied. The normalization factor is the generalized grand-canonical partition function defined as

$$\Xi(\lambda, \mathbf{v}) \equiv \sum_{N=0}^{\infty} \frac{1}{N! h^{3N}} \int d\hat{z} d\hat{z}' \exp \left\{ -\beta \hat{H}(z) - \beta \left( M_{\mu\nu}^{\psi} \lambda_{\nu} \hat{\rho}_{\mu} - M_{\mu\nu}^{\psi} \mathbf{v}_{\nu} \cdot \hat{\mathbf{g}}_{\mu} \right) \right\} \quad (\text{D.3})$$

From the partition function one defines the generalized thermodynamic potential

$$\Phi(\lambda, \mathbf{v}) \equiv -k_B T \ln \Xi(\lambda, \mathbf{v}) \quad (\text{D.4})$$

The conjugate fields  $\lambda_{\nu}, \mathbf{v}_{\nu}$  are fixed by the condition that the averages of the CG variables (3.22) with the relevant ensemble (D.2) coincide with the averages  $\rho_{\mu}, \mathbf{g}_{\mu}$  computed with the real ensemble (i.e. the solution of the Liouville equation). This condition can be expressed in terms of the generalized grand-canonical potential (D.4) in the form

$$\begin{aligned} \rho_{\mu} &= M_{\mu\nu}^{\delta} \frac{\partial \Phi(\lambda, \mathbf{v})}{\partial \lambda_{\nu}} \\ \mathbf{g}_{\mu} &= -M_{\mu\nu}^{\delta} \frac{\partial \Phi(\lambda, \mathbf{v})}{\partial \mathbf{v}_{\nu}}, \end{aligned} \quad (\text{D.5})$$

where we have used that the matrices  $M^{\delta}, M^{\psi}$ , defined in (3.20), are inverse of each other.

Because the function  $\Phi(\lambda, \mathbf{v})$  is convex, the conjugate variables  $\lambda, \mathbf{v}$  are in one to one connection with  $\rho, \mathbf{g}$ . Therefore, the functions  $\lambda(\rho, \mathbf{g}), \mathbf{v}(\rho, \mathbf{g})$ , exist and are unique. We can therefore switch from the conjugate variables  $\lambda, \mathbf{v}$  to the CG variables  $\rho, \mathbf{g}$ . One way to do it is through a Legendre transform. In an alternative and complementary way, in the Kawasaki-Gunton method, one defines the entropy of the present level of description as the result of evaluating the Gibbs-Jaynes entropy at the maximum, which

is given by the relevant ensemble (D.2). The result is

$$S(\rho, \mathbf{g}) = k_B \beta \left[ E - \Phi(\lambda, \mathbf{v}) + \rho_\mu M_{\mu\nu}^\psi \lambda_\nu - \mathbf{g}_\mu \cdot M_{\mu\nu}^\psi \mathbf{v}_\nu \right], \quad (\text{D.6})$$

where here the conjugate variables  $\lambda, \mathbf{v}$  are to be understood as functions of the averages  $\rho, \mathbf{g}$ . This allows one to define the following coarse-grained Hamiltonian

$$\mathcal{H}(\rho, \mathbf{g}) = \Phi(\lambda, \mathbf{v}) - M_{\mu\nu}^\psi \lambda_\nu \rho_\mu + M_{\mu\nu}^\psi \mathbf{v}_\nu \cdot \mathbf{g}_\mu \quad (\text{D.7})$$

as the free energy of the level of description determined by  $\rho_\mu, \mathbf{g}_\mu$ . The derivatives of the entropy are given by

$$\begin{aligned} \frac{\partial S}{\partial \rho_\mu}(\rho, \mathbf{g}) &= \beta M_{\mu\nu}^\psi \lambda_\nu \\ \frac{\partial S}{\partial \mathbf{g}_\mu}(\rho, \mathbf{g}) &= -\beta M_{\mu\nu}^\psi \mathbf{v}_\nu \end{aligned} \quad (\text{D.8})$$

This gives the form of the conjugate variables in terms of the CG variables.

## D.2 Momentum integration

We next consider the explicit evaluation of the momentum integrals in the grand partition function (D.3). We may integrate over the solid degrees of freedom  $\hat{z}'$ , with the result

$$\Xi(\lambda, \mathbf{v}) \equiv \sum_{N=0}^{\infty} \frac{1}{N! h^{3N}} \int d\hat{z} \exp \left\{ -\beta(\hat{H}^l + \hat{V}^{\text{sl}}) - \beta \left( M_{\mu\nu}^\psi \lambda_\nu \hat{\rho}_\mu - M_{\mu\nu}^\psi \mathbf{v}_\nu \cdot \hat{\mathbf{g}}_\mu \right) \right\}, \quad (\text{D.9})$$

where the CG effective potential  $\hat{V}^{\text{sl}}(z)$  captures, in a CG way, the interaction of the fluid atoms with the solid walls. It is defined as

$$\exp \{-\beta \hat{V}^{\text{sl}}(\hat{z})\} = \int d\hat{z}' \exp \{-\beta \hat{H}^s(\hat{z}') + \hat{V}(\hat{z}, \hat{z}')\} \quad (\text{D.10})$$

We may separate the integrals over position and momenta explicitly in the partition function (D.9)

$$\begin{aligned} \Xi(\lambda, \mathbf{v}) &\equiv \sum_{N=0}^{\infty} \frac{1}{N! h^{3N}} \int d\hat{q} \exp \left\{ -\beta \hat{V}(\hat{z}) - \beta M_{\mu\nu}^\psi \lambda_\nu \hat{\rho}_\mu(\hat{z}) \right\} \times \\ &\quad \int d\hat{p} \exp \left\{ -\beta \sum_i \frac{\mathbf{p}_i^2}{2m_i} + \beta M_{\mu\nu}^\psi \mathbf{v}_\nu \cdot \sum_i \mathbf{p}_i \delta_\mu(\mathbf{q}_i) \right\}, \end{aligned} \quad (\text{D.11})$$

where  $\hat{V}(\hat{z}) = \hat{V}^{ll}(\hat{z}) + \hat{V}^{sl}(\hat{z})$  is the potential energy of the fluid.

The integral over momenta is just a Gaussian integral. In the calculations that follow we will need the following integrals over momenta

$$\begin{aligned}\Omega_0 &\equiv \int d\hat{p} \exp \left\{ -\beta \sum_i \frac{\mathbf{p}_i^2}{2m_i} + \beta M_{\mu\nu}^\psi \mathbf{v}_\nu \cdot \sum_i \mathbf{p}_i \delta_\mu(\mathbf{q}_i) \right\} \\ \Omega_1 &\equiv \int d\hat{p} \mathbf{p}_i \exp \left\{ -\beta \sum_i \frac{\mathbf{p}_i^2}{2m_i} + \beta M_{\mu\nu}^\psi \mathbf{v}_\nu \cdot \sum_i \mathbf{p}_i \delta_\mu(\mathbf{q}_i) \right\} \\ \Omega_2 &\equiv \int d\hat{p} \mathbf{p}_i \mathbf{p}_i \exp \left\{ -\beta \sum_i \frac{\mathbf{p}_i^2}{2m_i} + \beta M_{\mu\nu}^\psi \mathbf{v}_\nu \cdot \sum_i \mathbf{p}_i \delta_\mu(\mathbf{q}_i) \right\}\end{aligned}\quad (\text{D.12})$$

The first integral  $\Omega_0$  is a particular example of the following Gaussian integral

$$\Omega_0(J) = \int dp \exp \left\{ -\frac{1}{2} p^T A p + J^T p \right\} = \frac{(2\pi)^{N/2}}{\det A^{1/2}} \exp \left\{ \frac{1}{2} J^T A^{-1} J \right\}\quad (\text{D.13})$$

for the particular form

$$\begin{aligned}A_{ij} &\rightarrow \frac{\beta}{m_i} \delta_{ij} \mathbf{1} \\ J_i &\rightarrow \beta M_{\mu\nu}^\psi \mathbf{v}_\nu \delta_\mu(\mathbf{r}_i) = \beta \mathbf{v}_\mu \psi_\mu(\mathbf{r}_i) \\ A_{ij}^{-1} J_j &\rightarrow \mathbf{v}_\mu \psi_\mu(\mathbf{r}_i) m_i\end{aligned}\quad (\text{D.14})$$

The other integrals can be obtained from the derivatives of the Gaussian integral (D.13)

$$\begin{aligned}\frac{\partial \Omega_0}{\partial J}(J) &= \int dp p \exp \left\{ -\frac{1}{2} p^T A p + J^T p \right\} = \Omega_0(J) A^{-1} J \\ \frac{\partial^2 \Omega_0}{\partial J \partial J}(J) &= \int dp p p \exp \left\{ -\frac{1}{2} p^T A p + J^T p \right\} = \Omega_0(J) [A^{-1} + (A^{-1} J)(A^{-1} J)]\end{aligned}\quad (\text{D.15})$$

leading to the following results

$$\begin{aligned}\Omega_0 &= (2\pi k_B T m)^{3N/2} \exp \left\{ \frac{\beta}{2} \sum_i \mathbf{v}_\mu \psi_\mu(\mathbf{q}_i) m_i \psi_\nu(\mathbf{q}_i) \mathbf{v}_\nu \right\} = (2\pi k_B T m)^{3N/2} \exp \left\{ \frac{\beta}{2} \hat{M}_{\mu\nu}(q) \mathbf{v}_\mu \mathbf{v}_\nu \right\} \\ \Omega_1 &= \Omega_0 \mathbf{v}_\mu \psi_\mu(\mathbf{r}_i) m_i \\ \Omega_2 &= \Omega_0 [k_B T m_i \delta_{ij} \mathbf{1} + m_i^2 \mathbf{v}_\mu \psi_\mu(\mathbf{r}_i) \mathbf{v}_\nu \psi_\nu(\mathbf{r}_i)],\end{aligned}\quad (\text{D.16})$$

where we have introduced the following matrix with dimensions of mass

$$\hat{\mathcal{M}}_{\mu\nu}(z) = \sum_i m_i \psi_\mu(\mathbf{q}_i) \psi_\nu(\mathbf{q}_i) = (\psi_\mu \psi_\nu \hat{\rho}) \quad (\text{D.17})$$

This matrix is a function of the coordinates of the particles.

By using the result for  $\Omega_0$  in (D.16), the grand partition function (D.11) becomes

$$\Xi(\lambda, \mathbf{v}) \equiv \sum_{N=0}^{\infty} \frac{1}{N!} \int \frac{dq}{\Lambda^{3N}} \exp \left\{ -\beta V(q) - \beta M_{\mu\nu}^\psi \lambda_\nu \hat{\rho}_\mu(z) + \frac{\beta}{2} \hat{\mathcal{M}}_{\mu\nu}(q) \mathbf{v}_\mu \cdot \mathbf{v}_\nu \right\}, \quad (\text{D.18})$$

where the thermal wavelength  $\Lambda$  is defined in (2.28).

It is possible to find the explicit expression for the velocity  $\mathbf{v}_\mu$  as a function of the CG variables  $\rho_\mu, \mathbf{g}_\mu$ . The velocity and momentum density field are related through (D.5). By using (D.4) and (2.27) one is lead directly to the explicit form of the conjugate variables

$$\mathbf{g}_\mu = M_{\mu\mu'}^\delta \left\langle \hat{\mathcal{M}}_{\mu'\nu} \right\rangle^{\lambda\mathbf{v}} \mathbf{v}_\nu = \rho_{\mu\nu} \mathbf{v}_\nu, \quad (\text{D.19})$$

where the matrix  $\hat{\mathcal{M}}_{\mu'\nu}$  is defined in (D.17) and we have introduced the density matrix defined by

$$\rho_{\mu\nu} = \int d\mathbf{r} \delta_\mu(\mathbf{r}) \psi_\nu(\mathbf{r}) \langle \hat{\rho}_\mathbf{r} \rangle^{\lambda\mathbf{v}}, \quad (\text{D.20})$$

where  $\langle \dots \rangle^{\lambda\mathbf{v}}$  is the average with respect to the relevant ensemble (D.2).

### D.3 The exact reversible part of the dynamics

The reversible part of the dynamics is given by the relevant ensemble average of the time derivatives (3.24), that is,

$$\begin{aligned} \langle i \mathcal{L} \hat{\rho}_\mu \rangle^{\lambda\mathbf{v}} &= \left\langle \sum_{i=1}^N \mathbf{p}_i \cdot \nabla \delta_\mu(\mathbf{q}_i) \right\rangle^{\lambda\mathbf{v}} \\ \langle i \mathcal{L} \hat{\mathbf{g}}_\mu \rangle^{\lambda\mathbf{v}} &= \left\langle \sum_{i=1}^N \mathbf{F}_i \delta_\mu(\mathbf{q}_i) \right\rangle^{\lambda\mathbf{v}} + \left\langle \sum_{i=1}^N \mathbf{p}_i \mathbf{v}_i \cdot \nabla \delta_\mu(\mathbf{q}_i) \right\rangle^{\lambda\mathbf{v}} \end{aligned} \quad (\text{D.21})$$

In all their glory, the averages over the relevant ensemble appearing in these expressions have the form

$$\begin{aligned}
\langle i \mathcal{L} \hat{\rho}_\mu \rangle^{\lambda v} &= \frac{1}{\Xi} \sum_{N=0}^{\infty} \frac{1}{N! h^{3N}} \\
&\times \int dq dp \exp \left\{ -\beta V(q) - \beta \sum_i \frac{\mathbf{p}_i^2}{2m_i} - \beta M_{\mu'v'}^\psi \lambda_{v'} \hat{\rho}_\mu + \beta M_{\mu'v'}^\psi \mathbf{v}_{v'} \cdot \hat{\mathbf{g}}_{\mu'} \right\} \sum_{i=1}^N \mathbf{p}_i \cdot \nabla \delta_\mu(\mathbf{q}_i) \\
&= \frac{1}{\Xi} \sum_{N=0}^{\infty} \frac{1}{N! h^{3N}} \int dq \exp \left\{ -\beta V(q) - \beta M_{\mu'v'}^\psi \lambda_{v'} \hat{\rho}_{\mu'} \right\} \sum_{i=1}^N \nabla \delta_\mu(\mathbf{q}_i) \\
&\times \int dp \mathbf{p}_i \exp \left\{ -\beta \sum_i \frac{\mathbf{p}_i^2}{2m_i} + \beta M_{\mu'v'}^\psi \mathbf{v}_{v'} \cdot \hat{\mathbf{g}}_{\mu'} \right\} \\
\langle i \mathcal{L} \hat{\mathbf{g}}_\mu \rangle^{\lambda v} &= \left\langle \sum_{i=1}^N \mathbf{F}_i \delta_\mu(\mathbf{q}_i) \right\rangle^{\lambda v} + \frac{1}{\Xi} \sum_{N=0}^{\infty} \frac{1}{N! h^{3N}} \int dq \exp \left\{ -\beta V(q) - \beta M_{\mu'v'}^\psi \lambda_{v'} \hat{\rho}_{\mu'} \right\} \sum_{i=1}^N \nabla \delta_\mu(\mathbf{q}_i) \\
&\times \frac{1}{m_i} \int dp \mathbf{p}_i \mathbf{p}_i \exp \left\{ -\beta \sum_i \frac{\mathbf{p}_i^2}{2m_i} + \beta M_{\mu'v'}^\psi \mathbf{v}_{v'} \cdot \hat{\mathbf{g}}_{\mu'} \right\} \tag{D.22}
\end{aligned}$$

and we recognize the momentum integrals  $\Omega_0, \Omega_1$  in (D.16). By substituting these results (D.16) in (D.22) we obtain

$$\begin{aligned}
\langle i \mathcal{L} \hat{\rho}_\mu \rangle^{\lambda v} &= \frac{1}{\Xi} \sum_{N=0}^{\infty} \frac{1}{N! h^{3N}} \\
&\times \int dq \exp \left\{ -\beta V(q) - \beta M_{\mu'v'}^\psi \lambda_{v'} \hat{\rho}_{\mu'} + \frac{\beta}{2} \hat{\mathcal{M}}_{\mu'v'}(q) \mathbf{v}_{\mu'} \cdot \mathbf{v}_{v'} \right\} \sum_{i=1}^N \nabla \delta_\mu(\mathbf{q}_i) \cdot m_i \mathbf{v}_\mu \psi_\mu(\mathbf{q}_i) \\
\langle i \mathcal{L} \hat{\mathbf{g}}_\mu \rangle^{\lambda v} &= \left\langle \sum_{i=1}^N \mathbf{F}_i \delta_\mu(\mathbf{q}_i) \right\rangle^{\lambda v} \\
&+ \frac{1}{\Xi} \sum_{N=0}^{\infty} \frac{1}{N! h^{3N}} \int dq \exp \left\{ -\beta V(q) - \beta M_{\mu'v'}^\psi \lambda_{v'} \hat{\rho}_{\mu'} + \frac{\beta}{2} \hat{\mathcal{M}}_{\mu'v'}(q) \mathbf{v}_{\mu'} \cdot \mathbf{v}_{v'} \right\} \\
&\times \sum_{i=1}^N [k_B T \mathbf{1} + m_i \mathbf{v}_\mu \psi_\mu(\mathbf{q}_i) \mathbf{v}_v \psi_v(\mathbf{q}_i)] \cdot \nabla \delta_\mu(\mathbf{q}_i) \tag{D.23}
\end{aligned}$$

By introducing the identity  $\int d\mathbf{r} \delta(\mathbf{r} - \mathbf{q}_i) = 1$  inside these expressions and using the definition of the microscopic mass density (3.22) we arrive at the final expression for

the reversible part of the dynamics

$$\begin{aligned}\langle i\mathcal{L}\hat{\rho}_\mu \rangle^{\lambda v} &= (\langle \hat{\rho} \rangle^{\lambda v} \psi_\nu \nabla \delta_\mu) \cdot \mathbf{v}_\nu = (\langle \hat{\rho} \rangle^{\lambda v} \bar{\mathbf{v}} \cdot \nabla \delta_\mu) \\ \langle i\mathcal{L}\hat{\mathbf{g}}_\mu \rangle^{\lambda v} &= \mathbf{F}_\mu(\rho, \mathbf{g}) + \frac{k_B T}{m} (\langle \hat{\rho} \rangle^{\lambda v} \nabla \delta_\mu) + (\langle \hat{\rho} \rangle^{\lambda v} \bar{\mathbf{v}} \cdot \nabla \delta_\mu),\end{aligned}\quad (\text{D.24})$$

where we have used the notation (3.10) and introduced the discrete force density

$$\mathbf{F}_\mu(\rho, \mathbf{g}) = \left\langle \sum_{i=1}^N \mathbf{F}_i \delta_\mu(\mathbf{q}_i) \right\rangle^{\lambda v} \quad (\text{D.25})$$

We consider now a more explicit form of this force density. By using Hamilton's equation  $\mathbf{F}_i = -\frac{\partial \hat{H}}{\partial \dot{\mathbf{q}}_i}$  we have

$$\begin{aligned}\mathbf{F}_\mu(\rho, \mathbf{g}) &= \text{Tr} \left[ \frac{1}{\Xi} \exp\{-\beta \hat{H}\} \sum_i \hat{\mathbf{F}}_i \delta_\mu(\mathbf{r}_i) \exp\left\{-\beta M_{\mu'\nu'}^\psi (\lambda_{\nu'} \hat{\rho}_{\mu'} - \mathbf{v}_{\nu'} \cdot \hat{\mathbf{g}}_{\mu'})\right\} \right] \\ &= \text{Tr} \left[ \frac{1}{\Xi} \exp\{-\beta \hat{H}\} \sum_i -\frac{\partial \hat{H}}{\partial \mathbf{r}_i} \delta_\mu(\mathbf{r}_i) \exp\left\{-\beta M_{\mu'\nu'}^\psi (\lambda_{\nu'} \hat{\rho}_{\mu'} - \mathbf{v}_{\nu'} \cdot \hat{\mathbf{g}}_{\mu'})\right\} \right] \\ &= k_B T \text{Tr} \left[ \frac{1}{\Xi} \sum_i \frac{\partial \exp\{-\beta \hat{H}\}}{\partial \mathbf{r}_i} \delta_\mu(\mathbf{r}_i) \exp\left\{-\beta M_{\mu'\nu'}^\psi (\lambda_{\nu'} \hat{\rho}_{\mu'} - \mathbf{v}_{\nu'} \cdot \hat{\mathbf{g}}_{\mu'})\right\} \right]\end{aligned}\quad (\text{D.26})$$

An integration by parts allows to write this force in the form

$$\begin{aligned}\mathbf{F}_\mu(\rho, \mathbf{g}) &= -k_B T \text{Tr} \left[ \frac{1}{\Xi} \exp\{-\beta \hat{H}\} \sum_i \frac{\partial}{\partial \mathbf{r}_i} \left( \delta_\mu(\mathbf{r}_i) \exp\left\{-\beta M_{\mu'\nu'}^\psi (\lambda_{\nu'} \hat{\rho}_{\mu'} - \mathbf{v}_{\nu'} \cdot \hat{\mathbf{g}}_{\mu'})\right\} \right) \right] \\ &= -k_B T \text{Tr} \left[ \frac{1}{\Xi} \exp\{-\beta \hat{H}\} \sum_i \nabla \delta_\mu(\mathbf{r}_i) \exp\left\{-\beta M_{\mu'\nu'}^\psi (\lambda_{\nu'} \hat{\rho}_{\mu'} - \mathbf{v}_{\nu'} \cdot \hat{\mathbf{g}}_{\mu'})\right\} \right] \\ &\quad - k_B T \text{Tr} \left[ \frac{1}{\Xi} \exp\{-\beta \hat{H}\} \sum_i \delta_\mu(\mathbf{r}_i) \frac{\partial}{\partial \mathbf{r}_i} \exp\left\{-\beta M_{\mu'\nu'}^\psi (\lambda_{\nu'} \hat{\rho}_{\mu'} - \mathbf{v}_{\nu'} \cdot \hat{\mathbf{g}}_{\mu'})\right\} \right] \\ &= -\frac{k_B T}{m} \int d\mathbf{r} \langle \hat{\rho}_\mathbf{r} \rangle^{\lambda v} \nabla \delta_\mu(\mathbf{r}) + \text{Tr} \left[ \bar{\rho} \sum_i \delta_\mu(\mathbf{r}_i) \frac{\partial}{\partial \mathbf{r}_i} M_{\mu'\nu'}^\psi (\lambda_{\nu'} \hat{\rho}_{\mu'} - \mathbf{v}_{\nu'} \cdot \hat{\mathbf{g}}_{\mu'}) \right]\end{aligned}\quad (\text{D.27})$$

Let us compute the last term in the right hand side of (D.27)

$$\begin{aligned}
& \text{Tr} \left[ \bar{\rho} \sum_i \delta_\mu(\mathbf{r}_i) \frac{\partial}{\partial \mathbf{r}_i} M_{\mu'\nu'}^\psi (\lambda_{\nu'} \hat{\rho}_{\mu'} - \mathbf{v}_{\nu'} \cdot \hat{\mathbf{g}}_{\mu'}) \right] \\
&= \text{Tr} \left[ \bar{\rho} \sum_i \delta_\mu(\mathbf{r}_i) M_{\mu'\nu'}^\psi (\lambda_{\nu'} m_i \nabla \delta_{\mu'}(\mathbf{r}_i) - \mathbf{v}_{\nu'} \cdot \mathbf{p}_i \nabla \delta_{\mu'}(\mathbf{r}_i)) \right] \\
&= \text{Tr} \left[ \bar{\rho} \sum_i \delta_\mu(\mathbf{r}_i) (m_i \nabla \bar{\lambda}(\mathbf{r}_i) - \mathbf{p}_i^\alpha \nabla \bar{\mathbf{v}}^\alpha(\mathbf{r}_i)) \right] \\
&= \int d\mathbf{r} \langle \hat{\rho}_\mathbf{r} \rangle^{\lambda v} \delta_\mu(\mathbf{r}) \nabla \bar{\lambda}(\mathbf{r}) - \int d\mathbf{r} \delta_\mu(\mathbf{r}) \langle \hat{\mathbf{g}}_\mathbf{r}^\alpha \rangle^{\lambda v} \nabla \bar{\mathbf{v}}^\alpha(\mathbf{r}) \\
&= \left( \delta_\mu \langle \hat{\rho}_\mathbf{r} \rangle^{\lambda v} \nabla \bar{\lambda} \right) - \left( \delta_\mu \langle \hat{\rho}_\mathbf{r} \rangle^{\lambda v} \nabla \frac{\bar{\mathbf{v}}^2}{2} \right), \tag{D.28}
\end{aligned}$$

where we have used that the relevant ensemble average of the microscopic momentum density  $\hat{\mathbf{g}}_\mathbf{r}$  is obtained from the result for  $\Omega_1$  in (D.16) in the form

$$\langle \hat{\mathbf{g}}_\mathbf{r} \rangle^{\lambda v} = \mathbf{v}_{\mu'} \psi_{\mu'}(\mathbf{r}) \langle \hat{\rho}_\mathbf{r} \rangle^{\lambda v} = \bar{\mathbf{v}}(\mathbf{r}) \langle \hat{\rho}_\mathbf{r} \rangle^{\lambda v} \tag{D.29}$$

The final form of the force density is

$$\mathbf{F}_\mu(\rho, \mathbf{g}) = -\frac{k_B T}{m} \left( \langle \hat{\rho}_\mathbf{r} \rangle^{\lambda v} \nabla \delta_\mu \right) - \left( \delta_\mu \langle \hat{\rho}_\mathbf{r} \rangle^{\lambda v} \nabla \bar{\mu} \right), \tag{D.30}$$

where we have introduced the interpolated chemical potential per unit mass field

$$\bar{\mu}(\mathbf{r}) = \frac{1}{2} \bar{\mathbf{v}}^2(\mathbf{r}) - \bar{\lambda}(\mathbf{r}) \tag{D.31}$$

In summary, by collecting results, the *exact* reversible part of the mass and momentum evolution is given by

$$\begin{aligned}
\langle i \mathcal{L} \hat{\rho}_\mu \rangle^{\lambda v} &= \left( \langle \hat{\rho}_\mathbf{r} \rangle^{\lambda v} \bar{\mathbf{v}} \cdot \nabla \delta_\mu \right) \\
\langle i \mathcal{L} \hat{\mathbf{g}}_\mu \rangle^{\lambda v} &= \left( \langle \hat{\rho}_\mathbf{r} \rangle^{\lambda v} \bar{\mathbf{v}} \bar{\mathbf{v}} \cdot \nabla \delta_\mu \right) + \left( \delta_\mu \langle \hat{\rho}_\mathbf{r} \rangle^{\lambda v} \nabla \bar{\mu} \right) \tag{D.32}
\end{aligned}$$

## D.4 The approximate form of the reversible part of the dynamics

We consider now several approximations that allow one to obtain more explicit expressions for the reversible dynamics. We start with the partition function (D.18), that

contains in its definition the matrix  $\hat{\mathcal{M}}_{\mu\nu}(z)$  defined in (D.17). Under the LFSAs (3.43), this matrix becomes

$$\hat{\mathcal{M}}_{\mu\nu}(z) \simeq \hat{\rho}_\sigma(z) (\psi_\sigma \psi_\mu \psi_\nu) \quad (\text{D.33})$$

and the partition function (D.18) becomes

$$\Xi(\lambda, \mathbf{v}) \equiv \sum_{N=0}^{\infty} \frac{1}{N!} \int \frac{dq}{\Lambda^{3N}} \exp \{-\beta V(q) + \beta \mu_\sigma \hat{\rho}_\sigma(q)\}, \quad (\text{D.34})$$

where we have introduced the discrete chemical potential per unit mass as

$$\mu_\sigma = \frac{1}{2} (\psi_\sigma \bar{\mathbf{v}}^2) - M_{\sigma\sigma'}^\psi \lambda_{\sigma'} \quad (\text{D.35})$$

Note that, under the LFSAs, the partition function depends on the conjugate variables  $\lambda_\sigma, \mathbf{v}_\sigma$  only through the combination  $\mu_\sigma$ . It makes sense to introduce the grand potential depending only on the variables  $\mu$

$$\Phi^{\text{pos}}(\mu) = -k_B T \ln \Xi(\lambda, \mathbf{v}) \quad (\text{D.36})$$

that satisfies

$$-\frac{\partial \Phi^{\text{pos}}}{\partial \mu_\sigma} = \langle \hat{\rho}_\sigma \rangle^{\lambda \mathbf{v}} \quad (\text{D.37})$$

We introduce the free energy function  $F(\rho)$  as the Legendre transform

$$F(\rho) \equiv \Phi^{\text{pos}}(\mu) + \mu_\sigma \rho_\sigma \quad (\text{D.38})$$

This is the free energy of a level of description that considers the discrete mass density  $\rho_\mu$  as the only CG variable in the system. The continuum counterpart of this free energy is the usual free energy functional of DFT, which in the present case contains also the effects of the solid walls.

The derivatives of the free energy  $F(\rho)$  are given by

$$\frac{\partial F}{\partial \rho_\sigma}(\rho) = \mu_\sigma \quad (\text{D.39})$$

We may now express the CG Hamiltonian (D.7) as

$$\mathcal{H}(\rho, \mathbf{g}) = \frac{1}{2} \mathcal{M}_{\mu\nu} \mathbf{v}_\mu \cdot \mathbf{v}_\nu + F(\rho), \quad (\text{D.40})$$

where we introduce the matrix

$$\mathcal{M}_{\mu\nu} = \rho_\sigma (\psi_\sigma \psi_\mu \psi_\nu) \quad (\text{D.41})$$

with dimensions of mass. The CG Hamiltonian  $\mathcal{H}$  in (D.40), which is the free energy function of the level of description given by  $\rho_\mu, \mathbf{g}_\mu$  is expressed as the sum of a kinetic part and a “potential” part given in terms of a free energy function of the level of description given by  $\rho_\mu$  alone. Note that we may also express the CG Hamiltonian (D.40) in the form

$$\mathcal{H}(\rho, \mathbf{g}) = \frac{1}{2} (\bar{\rho} \bar{\mathbf{v}}^2) + F(\rho) \quad (\text{D.42})$$

This expression (D.42) is identical to the result of evaluating the continuum CG Hamiltonian functional

$$\mathcal{H}[\rho, \mathbf{g}] = \frac{1}{2} \int d\mathbf{r} \rho(\mathbf{r}) \mathbf{v}^2(\mathbf{r}) + \mathcal{F}[\rho] \quad (\text{D.43})$$

at the interpolated fields  $\bar{\rho}(\mathbf{r}), \bar{\mathbf{v}}(\mathbf{r})$ , provided that the microscopically defined free energy functional  $\mathcal{F}[\rho]$  and free energy function  $F(\rho)$  are related according to (3.74).

In the LFSAs the chemical potential term in the reversible part of the momentum evolution (D.32) is given by

$$(\delta_\mu \langle \hat{\rho} \rangle^{\lambda\mathbf{v}} \nabla \bar{\mu}) \simeq (\delta_\mu \bar{\rho} \nabla \bar{\mu}) \quad (\text{D.44})$$

We now show that in the LFSAs we have the following approximate expression

$$(\delta_\mu \bar{\rho} \nabla \bar{\mu}) \simeq (\bar{\rho} \delta_\mu \nabla \delta_\nu) \frac{\partial F}{\partial \rho_\nu}(\rho) \quad (\text{D.45})$$

This can be shown by using (D.31) and (D.35)

$$\left( \delta_\mu \bar{\rho} \nabla \left[ \frac{1}{2} \bar{\mathbf{v}}^2(\mathbf{r}) - \bar{\lambda}(\mathbf{r}) \right] \right) = (\bar{\rho} \delta_\mu \nabla \delta_\nu) \left[ \frac{1}{2} (\psi_\nu \bar{\mathbf{v}}^2) - M_{\nu\nu'}^\psi \lambda_{\nu'} \right] \quad (\text{D.46})$$

The terms involving the Lagrange multiplier  $\lambda_\mu$  cancel each other and we are left with

$$(\bar{\rho} \delta_\mu \nabla \bar{\mathbf{v}}^2(\mathbf{r})) \simeq (\bar{\rho} \delta_\mu \nabla \delta_\nu) (\psi_\nu \bar{\mathbf{v}}^2) = (\bar{\rho} \delta_\mu \nabla \delta_\nu (\psi_\nu \bar{\mathbf{v}}^2)) \quad (\text{D.47})$$

But, this is approximately true provided that the velocity field is sufficiently smooth in the length scale of the cell. Indeed, we have that

$$\delta_\nu(\mathbf{r}) (\psi_\nu \bar{\mathbf{v}}^2) = \int d\mathbf{r}' \delta_\nu(\mathbf{r}) \psi_\nu(\mathbf{r}') \bar{\mathbf{v}}^2(\mathbf{r}') = \int d\mathbf{r}' \Delta(\mathbf{r}, \mathbf{r}') \bar{\mathbf{v}}^2(\mathbf{r}'), \quad (\text{D.48})$$

where we have introduced the fat Dirac  $\delta$  function (3.77). When the velocity field is sufficiently smooth on the lattice scale, we may approximate

$$\int d\mathbf{r}' \Delta(\mathbf{r}, \mathbf{r}') \bar{\mathbf{v}}^2(\mathbf{r}') \simeq \bar{\mathbf{v}}^2(\mathbf{r}) \quad (\text{D.49})$$

and, therefore, (D.47) and (D.45) are approximately true.

In summary, the exact reversible part of the mass and momentum evolution in equation. (D.32) can be approximated in the LFSA and for sufficiently smooth fields as

$$\begin{aligned} \langle i\mathcal{L}\hat{\rho}_\mu \rangle^{\lambda\mathbf{v}} &= (\bar{\rho} \bar{\mathbf{v}} \cdot \nabla \delta_\mu) \\ \langle i\mathcal{L}\hat{\mathbf{g}}_\mu \rangle^{\lambda\mathbf{v}} &= (\bar{\rho} \bar{\mathbf{v}} \bar{\mathbf{v}} \cdot \nabla \delta_\mu) + (\bar{\rho} \delta_\mu \nabla \delta_\nu) \frac{\partial F}{\partial \rho_\nu}(\rho) \end{aligned} \quad (\text{D.50})$$

## D.5 The connection between the free energy functional and the free energy function

First we address the connection between the thermodynamic potentials of the two levels of description given by the continuum CG variables  $\hat{A}_\mathbf{r} = \hat{\rho}_\mathbf{r}, \hat{\mathbf{g}}_\mathbf{r}$  and the discrete CG variables  $\hat{A}_\mu = \hat{\rho}_\mu, \hat{\mathbf{g}}_\mu$ . The continuum and discrete CG variables are related according to (3.23) that we write in a compact form as

$$\hat{A}_\mu(z) = \int d\mathbf{r} \delta_\mu(\mathbf{r}) \hat{A}_\mathbf{r}(z) \quad (\text{D.51})$$

At the continuum level we have a thermodynamic potential  $\Phi[\lambda]$  which is a *functional* of the conjugate fields  $\lambda_\mathbf{r}$ , denoted with square parenthesis. At the discrete level the thermodynamic potential  $\Phi(\lambda)$  is a *function*, denoted with rounded parenthesis, of  $\lambda_\mu$ . The microscopic definition of both potentials is given as the logarithm of a partition function. At the continuum level the thermodynamic potential is

$$\Phi[\lambda] = -k_B T \ln \text{Tr} \left[ \rho^{\text{eq}} \exp \left\{ -\beta \int d\mathbf{r} \lambda_\mathbf{r} \hat{A}_\mathbf{r} \right\} \right] \quad (\text{D.52})$$

and at the discrete level it is

$$\Phi(\lambda) = -k_B T \ln \text{Tr} \left[ \rho^{\text{eq}} \exp \left\{ -\beta \lambda_\mu M_{\mu\nu}^\psi \hat{A}_\nu \right\} \right] \quad (\text{D.53})$$

Note that the conjugate variables in the discrete are conveniently defined as  $\lambda_\mu M_{\mu\nu}^\psi$  for reasons that will become apparent soon. The matrix  $M_{\mu\nu}^\psi$  defined in (3.20) has

dimensions of volume and plays the role of the “volume element”  $d\mathbf{r}$  at the discrete level. With this definition of the conjugate variables at the discrete level it is straightforward to show that the connection between the two thermodynamic potentials is given by

$$\Phi[\bar{\lambda}] = \Phi(\lambda), \quad (\text{D.54})$$

where we have evaluated the thermodynamic potential of the continuum level at the interpolated conjugate field  $\bar{\lambda}_{\mathbf{r}}$  defined as

$$\bar{\lambda}_{\mathbf{r}} \equiv \lambda_{\mu} \psi_{\mu}(\mathbf{r}) \quad (\text{D.55})$$

Because the thermodynamic potential is convex, there is a one to one connection between the conjugate variables and the averages of the CG variables, that is,

$$\lambda_{\mu} \leftrightarrow a_{\mu}(\lambda), \quad \lambda_{\mathbf{r}} \leftrightarrow a_{\mathbf{r}}[\lambda] \quad (\text{D.56})$$

In particular, we denote by  $a_{\mathbf{r}}[\bar{\lambda}]$  the field which is conjugate to the interpolated  $\bar{\lambda}_{\mathbf{r}}$ . This field is, in general, different from the interpolated field

$$\bar{a}_{\mathbf{r}} = a_{\mu}(\lambda) \psi_{\mu}(\mathbf{r}) \quad (\text{D.57})$$

The interpolated field can be understood as a smoothing operation because

$$\begin{aligned} \bar{a}_{\mathbf{r}} &= a_{\mu} \psi_{\mu}(\mathbf{r}) = \int d\mathbf{r}' a_{\mathbf{r}} \delta_{\mu}(\mathbf{r}') \psi_{\mu}(\mathbf{r}) \\ &= \int d\mathbf{r}' a_{\mathbf{r}} \Delta(\mathbf{r}', \mathbf{r}) \end{aligned} \quad (\text{D.58})$$

We will assume that the fields are *sufficiently smooth* on the scale of the lattice spacing, in such a way that we have

$$\begin{aligned} a_{\mathbf{r}}[\bar{\lambda}] &= \bar{a}_{\mathbf{r}} \\ a_{\mathbf{r}}[\bar{\lambda}] &= a_{\mu}(\lambda) \psi_{\mu}(\mathbf{r}) \end{aligned} \quad (\text{D.59})$$

The mathematical identity (D.54) relating the two thermodynamic potentials may suggest that a similar connection exists between the free energies, which are defined at both levels by the Legendre transforms

$$\begin{aligned} \mathcal{F}[a] &= \Phi[\lambda] - \int d\mathbf{r} \lambda_{\mathbf{r}} a_{\mathbf{r}} \\ F(a) &= \Phi(\lambda) - \lambda_{\mu} M_{\mu\nu}^{\psi} a_{\nu} \end{aligned} \quad (\text{D.60})$$

Here  $\mathcal{F}[a]$  is a functional (denoted with square parenthesis) of the fields  $a_{\mathbf{r}}$  while  $F(a)$  is a function (denoted with rounded parenthesis) of the discrete values  $a_{\mu}$ .

Note that the free energy function can be written in the form

$$\begin{aligned} F(a) &= \Phi[\bar{\lambda}] - \int d\mathbf{r} \lambda_{\mu} \psi_{\mu}(\mathbf{r}) \psi_{\nu}(\mathbf{r}) a_{\nu} \\ &= \Phi[\bar{\lambda}] - \int d\mathbf{r} \bar{\lambda}_{\mathbf{r}} \bar{a}_{\mathbf{r}} \\ &= \Phi[\bar{\lambda}] - \int d\mathbf{r} \bar{\lambda}_{\mathbf{r}} a_{\mathbf{r}}[\bar{\lambda}] - \int d\mathbf{r} \bar{\lambda}_{\mathbf{r}} (\bar{a}_{\mathbf{r}} - a_{\mathbf{r}}[\bar{\lambda}]) \\ &= \mathcal{F}[a_{\mathbf{r}}[\bar{\lambda}]] - \int d\mathbf{r} \bar{\lambda}_{\mathbf{r}} (\bar{a}_{\mathbf{r}} - a_{\mathbf{r}}[\bar{\lambda}]) \end{aligned} \quad (\text{D.61})$$

This result is rigorous. Under the smoothness assumption (D.59) the two free energies are related according to

$$\mathcal{F}[\bar{a}] = F(a) \quad (\text{D.62})$$

Therefore, for realizations of the fields that are “sufficiently smooth” on the length scale of the bin, the *definition* of the discrete free energy  $F(a)$  with the prescription (3.74) gives the correct statistical mechanics definition (D.60) of the discrete free energy  $F(a)$ .

The relationship (D.62) is very useful because it allows one to obtain the discrete free energy  $F(a)$  at the discrete level once we know the free energy functional  $\mathcal{F}[a]$  at the continuum. As we have a vast amount of knowledge in equilibrium DFT about useful models for the free energy functional  $\mathcal{F}[\rho]$  this allows one to readily obtain the free energy function at the discrete level  $F(\rho)$ .



## Appendix E

# Isotropic fourth order tensors

In the Appendix of Ref. [84], Camargo et al. consider the second and third order tensors that are invariant under a rotation around an axis with unit vector  $\mathbf{n}$  and a reflection around any plane containing  $\mathbf{n}$ . In this chapter we consider the general form of a fourth order tensor satisfying these symmetries following the same route as in [84]. We introduce the following two symmetric second order tensors, that we call tangential and normal projectors, respectively

$$\mathbf{T}^{\alpha\beta} \equiv \delta^{\alpha\beta} - \mathbf{n}^\alpha \mathbf{n}^\beta, \quad \mathbf{N}^{\alpha\beta} \equiv \mathbf{n}^\alpha \mathbf{n}^\beta \quad (\text{E.1})$$

The unit tensor may be written as

$$\boldsymbol{\delta} = \mathbf{t}_1 \mathbf{t}_1^T + \mathbf{t}_2 \mathbf{t}_2^T + \mathbf{n} \mathbf{n}^T, \quad (\text{E.2})$$

where  $\mathbf{t}_1, \mathbf{t}_2$  are unit vectors tangent to the surface and mutually orthonormal. We take the convention that  $\mathbf{t}_1 \times \mathbf{t}_2 = \mathbf{n}, \mathbf{t}_2 \times \mathbf{n} = \mathbf{t}_1, \mathbf{n} \times \mathbf{t}_1 = \mathbf{t}_2$ . Therefore, the tangential projector  $\mathbf{T}$  becomes

$$\mathbf{T}^{\alpha\beta} = \mathbf{t}_1^\alpha \mathbf{t}_1^\beta + \mathbf{t}_2^\alpha \mathbf{t}_2^\beta \quad (\text{E.3})$$

This projector satisfies

$$\begin{aligned} \mathbf{T}^{\alpha\beta} \mathbf{T}^{\beta\gamma} &= \mathbf{T}^{\alpha\gamma} \\ \mathbf{T}^{\alpha\beta} \mathbf{n}^\alpha &= 0 \\ \mathbf{T}^{\alpha\beta} \mathbf{n}^\beta &= 0 \\ \mathbf{T}^{\alpha\alpha} &= 2 \\ \mathbf{T}^{\alpha\beta} \mathbf{T}^{\alpha\beta} &= 2 \end{aligned} \quad (\text{E.4})$$

where repeated indices are summed over.

The general form is a linear combinations of the tensor products of fourth rank of  $\mathbf{n}^\alpha$  and  $\mathbf{T}^{\alpha\beta} = \delta^{\alpha\beta} - \mathbf{n}^\alpha \mathbf{n}^\beta$  which are

$$\begin{array}{cccccc} \mathbf{n}^\alpha \mathbf{n}^\beta \mathbf{n}^\gamma \mathbf{n}^\delta & & & & & \\ \mathbf{n}^\alpha \mathbf{n}^\beta \mathbf{T}^{\gamma\delta} & \mathbf{n}^\alpha \mathbf{n}^\gamma \mathbf{T}^{\beta\delta} & \mathbf{n}^\alpha \mathbf{n}^\delta \mathbf{T}^{\beta\gamma} & \mathbf{n}^\beta \mathbf{n}^\gamma \mathbf{T}^{\alpha\delta} & \mathbf{n}^\beta \mathbf{n}^\delta \mathbf{T}^{\alpha\gamma} & \mathbf{n}^\gamma \mathbf{n}^\delta \mathbf{T}^{\alpha\beta} \\ \mathbf{T}^{\alpha\beta} \mathbf{T}^{\gamma\delta} & \mathbf{T}^{\alpha\gamma} \mathbf{T}^{\beta\delta} & \mathbf{T}^{\alpha\delta} \mathbf{T}^{\beta\gamma} & & & \end{array} \quad (\text{E.5})$$

The only allowed linear combination of the tensors that ensure that the fourth order tensor is symmetric with respect to its first two indices and symmetric with respect to its last two indices is given by

$$\begin{aligned} \eta_{rr'}^{\alpha\beta\gamma\delta} = & \eta_{rr'}^{(1)} \mathbf{T}^{\alpha\beta} \mathbf{T}^{\gamma\delta} + \eta_{rr'}^{(2)} (\mathbf{T}^{\alpha\gamma} \mathbf{T}^{\beta\delta} + \mathbf{T}^{\alpha\delta} \mathbf{T}^{\beta\gamma}) + \eta_{rr'}^{(3)} \mathbf{n}^\alpha \mathbf{n}^\beta \mathbf{n}^\gamma \mathbf{n}^\delta \\ & + \eta_{rr'}^{(4)} (\mathbf{n}^\alpha \mathbf{n}^\gamma \mathbf{T}^{\beta\delta} + \mathbf{n}^\beta \mathbf{n}^\gamma \mathbf{T}^{\alpha\delta} + \mathbf{n}^\alpha \mathbf{n}^\delta \mathbf{T}^{\beta\gamma} + \mathbf{n}^\beta \mathbf{n}^\delta \mathbf{T}^{\alpha\gamma}) \\ & + \eta_{rr'}^{(5)} \mathbf{n}^\alpha \mathbf{n}^\beta \mathbf{T}^{\gamma\delta} + \eta_{rr'}^{(6)} \mathbf{T}^{\alpha\beta} \mathbf{n}^\gamma \mathbf{n}^\delta \end{aligned} \quad (\text{E.6})$$

## Appendix F

### The covariance

In this appendix, we compute explicitly the covariance of the transverse momentum density which is given by the molecular ensemble average

$$C_{\mu\nu}^E = \langle \hat{g}_\mu^x \hat{g}_\nu^x \rangle = \frac{1}{\Omega(E)} \int dr dp \delta(\hat{H}(z) - E) \delta \left( \sum_i^N \mathbf{p}_i \right) \sum_{ij}^N \mathbf{p}_i^x \mathbf{p}_j^x \delta_\mu(\mathbf{r}_i) \delta_\nu(\mathbf{r}_j) \quad (\text{F.1})$$

The molecular ensemble is microcanonical in the total energy and total momentum, where we have chosen the reference frame of the center of mass of the system, where total momentum vanishes. Although this microcanonical average can be computed explicitly, it is much simpler to compute the following canonical average

$$C_{\mu\nu}^\beta = \langle \hat{g}_\mu^1 \hat{g}_\nu^1 \rangle = \frac{1}{Z(\beta)} \int dr dp \exp\{-\beta \hat{H}(z)\} \delta \left( \sum_i^N \mathbf{p}_i \right) \sum_{ij}^N \mathbf{p}_i^x \mathbf{p}_j^x \delta_\mu(\mathbf{r}_i) \delta_\nu(\mathbf{r}_j), \quad (\text{F.2})$$

where the Dirac  $\delta$  function on the Hamiltonian is substituted by a Gibbs factor. We keep, however the momentum conservation Dirac  $\delta$  function as this has observable consequences. The two covariances are related by

$$C_{\mu\nu}^\beta = \int dE P_\beta(E) C_{\mu\nu}^E, \quad (\text{F.3})$$

where the probability distribution of the energy in the canonical ensemble is

$$P_\beta(E) = \frac{1}{Z(\beta)} e^{-\beta E} \Omega(E) \quad (\text{F.4})$$

In the thermodynamic limit, the probability distribution is highly peaked at the average energy  $E^*$  corresponding to the particular value  $\beta$ . In this case, we may approximate the molecular ensemble average with the canonical average

$$C_{\mu\nu}^\beta = C_{\mu\nu}^{E^*} \quad (\text{F.5})$$

The momentum integral of the canonical average involves a Gaussian and the Dirac  $\delta$  function on total momentum. This integral may be computed by using the Fourier representation of the Dirac  $\delta$  function. The result is

$$\frac{\int d\mathbf{p}_i \mathbf{p}_j e^{-\beta \sum_i p_i^2 / 2m_i} \delta(\sum_k \mathbf{p}_k)}{\int dp e^{-\beta \sum_i p_i^2 / 2m_i} \delta(\sum_k \mathbf{p}_k)} = k_B T m_i \left( \delta_{ij} - \frac{1}{N} \right) \mathbf{1} \quad (\text{F.6})$$

This expression satisfies that if we sum both sides of this equation over the total number of particles we obtain  $0 = 0$  as it should, on momentum conservation considerations.

After performing the momentum integrations with the result (F.6) we obtain

$$C_{\mu\nu}^\beta = k_B T m n \int d\mathbf{r} \delta_\mu(\mathbf{r}) \delta_\nu(\mathbf{r}) - \frac{k_B T m}{N} \langle \hat{n}_\mu \hat{n}_\nu \rangle^\beta \quad (\text{F.7})$$

In this expression  $\hat{n}_\mu = \sum_i \delta_\mu(\mathbf{r}_i)$  is the discrete number density of node  $\mu$  and  $n = \langle \hat{n}_\mu \rangle$  is the average number density, which for an homogeneous system is independent of the bin, and given by  $n = N/V$ .

Note that the covariance satisfies

$$\sum_\mu \mathcal{V}_\mu C_{\mu\nu}^\beta = 0 \quad (\text{F.8})$$

which is a reflection of momentum conservation. For nodes that are more than, roughly, a couple of bins apart, the first term in (F.7) is very small, and the covariance takes the value

$$C_{\mu\nu}^\beta \simeq -\frac{k_B T m n^2}{N} \quad (\text{F.9})$$

This value, although vanishingly small in the thermodynamic limit  $N \rightarrow \infty$ , is consistently detectable in our simulations. From a physical point of view it means that if a bin has a positive momentum, the rest of the bins should have a negative momentum in order to comply with a zero total momentum, resulting into the negative covariance (F.9).

## Appendix G

# The continuum and thermodynamic limits

In this appendix, we consider the continuum and thermodynamic limits of the exponential matrix (4.67) governing the decay of the correlation (4.66). Note that, according to Onsager's regression hypothesis, the evolution of the average profile is given by

$$g_\mu(t) = \exp\{\Delta \cdot \nu t\}_{\mu\nu} g_\nu(0) \quad (\text{G.1})$$

The matrix exponential may be understood as the Green's function of the problem. We choose as initial profile a Dirac  $\delta$  like function at the origin, suitably displaced to have a zero value of total momentum, this is

$$g_\mu(0) = \frac{\delta_{\mu 0}}{\Delta z} g_0 - \frac{1}{N_{\text{bin}} \Delta z} g_0 \quad (\text{G.2})$$

that satisfies  $\sum_{\mu=0}^{N_{\text{bin}}-1} g_\mu(0) = 0$ . If we insert this initial profile into (G.1), we have

$$g_\mu(t) = g_0 \frac{1}{N_{\text{bin}} \Delta z} \sum_{\mu'=1}^{N_{\text{bin}}-1} \exp\left\{i \frac{2\pi}{N_{\text{bin}}} (\mu - \nu)\mu'\right\} \exp\left\{-\tilde{\nu}_{\mu'} \frac{2}{\Delta z^2} \left(1 - \cos \frac{2\pi}{N_{\text{bin}}} \mu'\right) t\right\}, \quad (\text{G.3})$$

where note that the term  $\mu' = 0$  is now absent. Note that total momentum is conserved at all times  $\sum_{\mu=0}^{N_{\text{bin}}-1} g_\mu(t) = 0$ . Therefore, we may visualize the matrix exponential through the evolution of an initial profile of the form (G.2). For simplicity, we consider the local

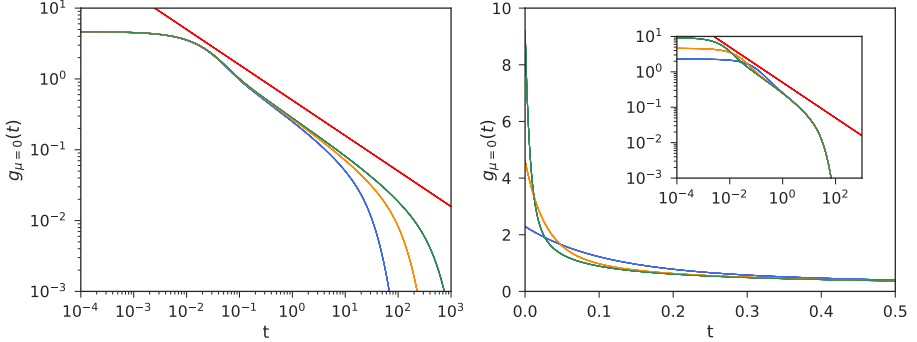


**Figure G.1:** Left panel: Value of  $g_{\mu=0}(t)$  for an initial Dirac delta like initial profile (G.2). The length of the box is  $L_z = 24, 48, 96$ , and the number of nodes is  $N_{\text{bin}} = 112, 224, 448$  thus keeping the size of the bins fixed, for increasing curves. This leads to the thermodynamic limit. This shows that the shoulder is due to the size of the box. As we approach the thermodynamic limit, the decay seems to approach  $t^{-1/2}$ , as plotted. Right panel: Value of  $g_{\mu=0}(t)$  for an initial Dirac delta like initial profile (G.2). The length of the box is  $L_z = 24$ , and the number of nodes is  $N_{\text{bin}} = 112, 224, 448$  for increasing curves (leading to the continuum limit). This shows that as we increase the resolution, we converge towards a singular function at  $t = 0$ , related to the divergence with  $\Delta z^{-1}$ . At large times, all curves behave in the same way. The line corresponds to  $\propto t^{-1/2}$ . Only in both limits (thermodynamic and continuum limits) we approach an algebraic decay with  $t^{-1/2}$ .

approximation  $\tilde{\nu}_\mu = \nu_0$ . We plot in Fig. G.1 this evolution by suitably changing the size of the box or the size of the bins. We recognize that the algebraic prediction  $t^{-1/2}$  is only attained in the thermodynamic and continuum limit.

## Appendix H

# Force on the boundary slab

In this appendix we derive the expression (6.32) for the force on the boundary slab made of  $B$  bins.

By multiplying (6.25) with the bin volume  $\mathcal{V}_\mu$ , and summing over the  $B$  layers of the slab we have

$$\begin{aligned} \mathbf{F}_B^x = & - \sum_{\mu=1}^B \mathcal{V}_\mu \sum_{\nu=1}^{N_{\text{bin}}} \mathcal{V}_\nu \frac{[\eta_{\mu\nu} - \eta_{\mu-1\nu} - \eta_{\mu\nu-1} + \eta_{\mu-1\nu-1}]}{\Delta z^2} \bar{\mathbf{v}}_\nu^x + \sum_{\mu=1}^B \mathcal{V}_\mu \sum_{\nu=1}^{N_{\text{bin}}} \mathcal{V}_\nu \frac{[G_{\mu\nu} - G_{\mu\nu-1}]}{\Delta z} \bar{\mathbf{v}}_\nu^x \\ & + \sum_{\mu=1}^B \mathcal{V}_\mu \sum_{\nu=1}^{N_{\text{bin}}} \mathcal{V}_\nu \frac{[H_{\mu\nu} - H_{\mu-1\nu}]}{\Delta z} \bar{\mathbf{v}}_\nu^x - \sum_{\mu=1}^B \mathcal{V}_\mu \sum_{\nu=1}^{N_{\text{bin}}} \mathcal{V}_\nu \gamma_{\mu\nu} \bar{\mathbf{v}}_\nu^x \end{aligned} \quad (\text{H.1})$$

Consider the term

$$\begin{aligned} \sum_{\mu=1}^B \mathcal{V}_\mu \sum_{\nu=1}^{N_{\text{bin}}} \mathcal{V}_\nu \frac{[H_{\mu\nu} - H_{\mu-1\nu}]}{\Delta z} \bar{\mathbf{v}}_\nu^x &= \sum_{\nu=1}^{N_{\text{bin}}} \mathcal{V}_\nu \bar{\mathbf{v}}_\nu^x \sum_{\mu=1}^B \mathcal{V}_\mu \frac{[H_{\mu\nu} - H_{\mu-1\nu}]}{\Delta z} = \sum_{\nu=1}^{N_{\text{bin}}} \mathcal{V}_\nu \mathcal{V}_\mu \bar{\mathbf{v}}_\nu^x \frac{[H_{B\nu} - H_{0\nu}]}{\Delta z} \\ &= S \sum_{\nu=1}^{N_{\text{bin}}} \mathcal{V}_\nu H_{B\nu} \bar{\mathbf{v}}_\nu^x, \end{aligned} \quad (\text{H.2})$$

where  $S = \mathcal{V}_\mu / \Delta z$  coincides with the area of the wall and we have used the fact that  $H_{0\nu} = 0$  because the node  $\mu = 0$  is inside the solid and the fluid stress tensor vanishes

there. In a similar way, the viscosity term becomes

$$\begin{aligned}
& - \sum_{\mu=1}^B \mathcal{V}_\mu \sum_{\nu=1}^{N_{\text{bin}}} \mathcal{V}_\nu \frac{[\eta_{\mu\nu} - \eta_{\mu-1\nu} - \eta_{\mu\nu-1} + \eta_{\mu-1\nu-1}]}{\Delta z^2} \bar{\mathbf{v}}_\nu^x \\
& = - \sum_{\nu=1}^{N_{\text{bin}}} \mathcal{V}_\nu \bar{\mathbf{v}}_\nu^x \sum_{\mu=1}^B \mathcal{V}_\mu \frac{[\eta_{\mu\nu} - \eta_{\mu-1\nu} - \eta_{\mu\nu-1} + \eta_{\mu-1\nu-1}]}{\Delta z^2} \\
& = - \sum_{\nu=1}^{N_{\text{bin}}} \mathcal{V}_\nu \bar{\mathbf{v}}_\nu^x \mathcal{V}_\mu \frac{[\eta_{B\nu} - \eta_{0\nu} - \eta_{B\nu-1} + \eta_{0\nu-1}]}{\Delta z^2} = - \mathcal{V}_B \sum_{\nu=1}^{N_{\text{bin}}} \mathcal{V}_\nu \bar{\mathbf{v}}_\nu^x \frac{[\eta_{B\nu} - \eta_{B\nu-1}]}{\Delta z^2} \\
& = - S \sum_{\nu=1}^{N_{\text{bin}}} \mathcal{V}_\nu \eta_{B\nu} \frac{\bar{\mathbf{v}}_\nu^x - \bar{\mathbf{v}}_{\nu+1}^x}{\Delta z}
\end{aligned} \tag{H.3}$$

Note that  $\eta_{0\nu} = 0$  because inside the solid the stress tensor vanish.

By using these results, equation (H.1) becomes

$$\begin{aligned}
\mathbf{F}_B^x & = S \sum_{\nu=1}^{N_{\text{bin}}} \mathcal{V}_\nu \eta_{B\nu} \frac{\bar{\mathbf{v}}_{\nu+1}^x - \bar{\mathbf{v}}_\nu^x}{\Delta z} - \sum_{\mu=1}^B \mathcal{V}_\mu \sum_{\nu=1}^{N_{\text{bin}}} \mathcal{V}_\nu G_{\mu\nu} \frac{\bar{\mathbf{v}}_{\nu+1}^x - \bar{\mathbf{v}}_\nu^x}{\Delta z} \\
& \quad + S \sum_{\nu=1}^{N_{\text{bin}}} \mathcal{V}_\nu H_{B\nu} \bar{\mathbf{v}}_\nu^x - \sum_{\mu=1}^B \mathcal{V}_\mu \sum_{\nu=1}^{N_{\text{bin}}} \mathcal{V}_\nu \gamma_{\mu\nu} \bar{\mathbf{v}}_\nu^x
\end{aligned} \tag{H.4}$$

The final expression for the force (per unit area) on the slab due to the combined action of the fluid outside the slab and the solid wall is given by

$$\frac{1}{S} \mathbf{F}_B^x = \sum_{\nu=1}^{N_{\text{bin}}} \mathcal{V}_\nu [\eta_{B\nu} - G_\nu] \frac{\bar{\mathbf{v}}_{\nu+1}^x - \bar{\mathbf{v}}_\nu^x}{\Delta z} - \sum_{\nu=1}^{N_{\text{bin}}} \mathcal{V}_\nu (\gamma_\nu - H_{B\nu}) \bar{\mathbf{v}}_\nu^x \tag{H.5}$$

# **Appendix I**

## **List of Acronyms**

DFT	Density Functional Theory
DDFT	Dynamic Density Functional Theory
GLE	Generalized Langevin equation
LADM	Local Average Density Model
LFSA	Linear For Spiky Approximation
LJ	Lennard-Jones
MD	Molecular Dynamics
NEMD	Nonequilibrium Molecular Dynamics
NESM	Nonequilibrium Statistical Mechanics
PBC	Periodic Boundary Conditions
SDE	Stochastic Differential Equation
ToCG	Theory of Coarse-Graining



## Appendix J

# List of symbols and variables

$B$	Backward difference operator
$\beta$	$(k_B T)^{-1}$
$\delta_{\mu\nu}$	Kronecker delta
$\Delta z$	Distance between two nodal planes
$\Delta$	Laplacian matrix
$\mathcal{F}[]$	Free energy functional
$F()$	Free energy function
$F$	Fordward difference operator
$\mathcal{G}$	Galilean operator
$G_{tt'}$	Time ordered projected propagator
$\Gamma(t - t')$	Memory kernel
$h$	Planck's constant
$\mathcal{H}[]$	Hydrodynamic functional
$i\mathcal{L}$	Liouville operator
$k_B$	Boltzmann's constant
$L_x, L_y, L_Z$	Dimensions of the simulation box
$\lambda(\mathbf{z}), \mu$	Lagrange multipliers
$\Lambda$	Relaxation matrix
$m$	Mass of the particles
$M'$	Mass solid sphere

$M$	Mass solid walls
$M^\Phi$	Mass matrix
$M^*$	Friction matrix
$N$	Number of fluid particles
$N'$	Number of solid particles
$N_{\text{bins}}$	Number of bins
$\mathcal{P}, Q$	Projection operators
$\Phi_\mu(\mathbf{r})$	Finite element basis functions
$\Phi[\lambda]$	Grand-canonical potential
$\rho_{\mu\nu}$	Mass density matrix
$\rho(\mathbf{z})$	Microscopic probability density
$\bar{\rho}(\mathbf{z}, t)$	Microscopic relevant ensemble
$\rho^{\text{eq}} \mathbf{z}$	Equilibrium stationary microscopic probability density
$S[\rho]$	Gibbs-Jaynes functional
$T$	Temperature
$V_T$	Volume of the simulation box
$V_\mu$	Volume of the bin $\mu$
$\chi_\mu(z)$	Characteristic function of bin $\mu$
$\hat{\mathbf{z}}$	Microscopic state
$\hat{\mathbf{z}}_0$	Initial microscopic state
$\langle \dots \rangle^c$	Conditional expectation

# List of Figures

1	Visual representation of a MD simulation with a sketch of the binning used . . . . .	7
3.1	Basis function $\Phi_\mu(z)$ and the characteristic function $\chi_\mu(z)$ . . . . .	63
3.2	Visual representation of the “spiky” approximation . . . . .	71
4.1	Visual representation of the MD simulation of an unconfined fluid . . . . .	89
4.2	Correlation matrix $C(t)$ at $t = 0$ and $t = 0.6$ for an unconfined fluid . . . . .	102
4.3	$C_{30\nu}(t)$ for an unconfined fluid . . . . .	103
4.4	Autocorrelation for an unconfined fluid . . . . .	103
4.5	Diagonal $\tilde{C}_{\mu\nu}(t)$ for an unconfined fluid . . . . .	104
4.6	Evolution of different eigenvalues $\tilde{C}_{\mu\nu}(t)$ for an unconfined fluid . . . . .	104
4.7	Diagonal elements $\tilde{\Lambda}_{\mu\mu}(t)$ of the Fourier transform of $\Lambda(t)$ for an unconfined fluid . . . . .	105
4.8	Comparison $\tilde{\Lambda}_{\mu\mu}^*$ and $\tilde{\Lambda}_{\mu\mu}(\tau)$ for an unconfined fluid . . . . .	107
4.9	Comparison of autocorrelation $C_{\mu\mu}$ with the predictions for an unconfined fluid . . . . .	107
4.10	Comparison of cross correlation $C_{\mu\mu+1}$ with the predictions for an unconfined fluid . . . . .	108
4.11	The nonlocal viscosity as a function of time for an unconfined fluid . . . . .	109
4.12	The local kinematic viscosity for an unconfined fluid . . . . .	110
4.13	The nonlocal shear viscosity kernel for an unconfined fluid . . . . .	110
4.14	Comparison $\eta_{30,\nu}^*$ and $\eta_{30,\nu}$ for an unconfined fluid . . . . .	111
4.15	The eigenvalues of the nonlocal kinematic viscosity matrix for an unconfined fluid . . . . .	112

5.1	Visual representation of the MD simulation of a confined fluid between two solid slabs . . . . .	120
5.2	Correlation matrix $C(t)$ at $t = 0$ and $t = 0.6$ for a confined fluid - Thin bins	121
5.3	Diagonal elements $\tilde{\Lambda}_{\mu\mu}(t)$ of $\Lambda(t)$ in three different basis for a confined fluid - Thin bins . . . . .	122
5.4	Evolution of different eigenvalues $\tilde{C}_{\mu\nu}(t)$ for a confined fluid - Thin bins	122
5.5	Diagonal elements $\tilde{\Lambda}_{\mu\mu}(t)$ of $\Lambda(t)$ in the reciprocal space for a confined fluid - Thin bins . . . . .	123
5.6	Eigenvalues and eigenvectors near the walls for a confined fluid - Thin bins . . . . .	123
5.7	Predicted autocorrelations of $C(t)$ for a confined fluid - Thin bins . . . .	125
5.8	Evolution of different eigenvalues $\tilde{C}_{\mu\nu}(t)$ for a confined fluid - Thick bins	126
5.9	Diagonal elements $\tilde{\Lambda}_{\mu\mu}(t)$ of $\Lambda(t)$ in the reciprocal space for a confined fluid - Thick bins . . . . .	126
5.10	The igenvectors correspondings to the two largest eigenvalues of $\Lambda(t)$ for a confined fluid - Thick bins . . . . .	127
5.11	Predicted autocorrelations of $C(t)$ for a confined fluid - Thick bins . . . .	128
5.12	Predicted crosscorrelations of $C(t)$ for a confined fluid - Thick bins . . . .	129
5.13	Comparison between the fluid density profile for thin and thick bins . . . . .	131
6.1	Scheme of the location of the nodal planes in the system . . . . .	140
6.2	The average density profile for two resolutions . . . . .	141
6.3	Time evolution of the matrix element $\eta_{\mu\nu}$ for a confined fluid - Thick bins	142
6.4	The transport matrices evaluated from the Green-Kubo running integrals at the plateau value time for a confined fluid - Thick bins . . . . .	144
6.5	The momentum profile at different times and the velocity profile obtained from the momentum for a confined fluid - Thick bins . . . . .	146
6.6	The momentum profile as a function of time for a confined fluid - Thick bins . . . . .	147
6.7	Scheme of the definition of the boundary slab of fluid . . . . .	148
6.8	The viscosity matrix for different values of $\nu$ , for three values of $B$ . . . .	149
6.9	Check mechanical balance . . . . .	151
6.10	The total friction as a funtion of the upper limit of integration of the running Green-Kubo integral for a confined fluid - Thick bins . . . . .	156
6.11	Dependence on time $\tau$ in the plateau region of $\eta', \gamma'$ and the slip length $\delta$	157
6.12	The slip length for two channel with different width . . . . .	158
6.13	Local prediction from local viscosity and slip boundary condition . . . .	163
6.14	Comparison of the error between local and nonlocal theories . . . . .	164

G.1 Visualization of the algebraic prediction of $g_\mu(t)$ in the thermodynamic and continuum limit . . . . .	218
---	-----



# List of Tables

6.1	Transport coefficients for different widths of the boundary slab . . . .	156
-----	--	-----



*The runner runs truly to the end.*

Once a runner

JOHN L. PARKER

This dissertation was finished in May 2019.